Interdisciplinary perspectives in TRPV5 & TRPV6 physiology

Een wetenschappelijke proeve op het gebied van de Medische Wetenschappen

Proefschrift

ter verkrijging van de graad van doctor
aan de Radboud Universiteit Nijmegen
op gezag van de Rector Magnificus, prof. dr. C.W.P.M. Blom,
volgens besluit van het College van Decanen
in het openbaar te verdedigen op maandag 5 maart 2007
om 15.30 uur precies

door

Teartse Tim Lambers
geboren op 25 augustus 1978
te Arnhem

Promotor:

Prof. dr. R.J.M. Bindels

Copromotor:

Dr. J.G.J. Hoenderop

Manuscriptcommissie:

Prof. dr. F.P.M. Cremers (voorzitter)

Prof. dr. B. Wieringa

Dr. K. Jalink (het Nederlands Kankerinstituut, Amsterdam)

Table of contents

CHAPTER I

GENERAL INTRODUCTION

Lambers T.T., Bindels R.J., Hoenderop J.G.

Department of Physiology, Nijmegen Centre for Molecular Life Sciences,
Radboud University Nijmegen Medical Centre, The Netherlands

1. TRP channels: a remarkable family of ion channels

Ion channels are pore-forming integral membrane proteins that allow ions to cross the biological membrane barrier upon channel activation. Once activated, channels utilize an electrochemical gradient across cellular membranes generated by pumps and co-transporters. This gradient determines the so-called membrane potential and enables the entering of ions with rates up to millions of ions per second until inactivation of the channel complex that can be independent of the chemical equilibrium. Based upon their structure, function and biophysical properties several ion channel families can be distinguished. Transient Receptor Potential (TRP) channels constitute a large and functionally versatile superfamily of cation channel proteins that are expressed in many cell types from yeast to mammals (1). Here these channels fulfill critical functions in processes ranging from sensory physiology, male fertility, vasorelaxation and epithelial ion transport. Based on structure homology mammalian TRP channels are comprised of six related subfamilies defined as *Classical or Canonical* (TRPC); *Vanilloid receptor related* (TRPV); *Melastin related* (TRPM); *Polycystins* (TRPP); *Mucolipins* (TRPML) and *ANKTM1 related* (TRPA) **(Fig. 1)** (2). A seventh family, *NOMPC related* (TRPN), has so far only been detected in worm, fly, frog and zebra fish and is proposed to form a mechanosensing channel (3-6). All TRP channels are postulated to share a topology of six transmembrane domains (TM), with a cytoplasmic amino- and carboxyl-terminus and a cation-permeable pore between TM5 and TM6 that come together in functional (hetero) tetramers. Most TRP channels are nonselective cation channels with the exception of the monovalent-selective TRPM4 and TRPM5, and the Ca^{2+}-selective TRPV5 and TRPV6.

2. TRPV5 and TRPV6 as key players in Ca^{2+} homeostasis

Ion homeostasis in our body is tightly maintained and disturbances in its balance may lead to pathogenesis. The kidney plays a vital role in this process by harmonizing the dietary ion intake by the intestine with ion reabsorption from the pro-urine. One of these ions is Ca^{2+} that plays a key role in many physiological processes like hormone secretion, muscle contraction, bone formation, nerve conduction, exocytosis and (in)activation of enzymes. The body, therefore, carefully regulates the plasma concentration of Ca^{2+} within a narrow range by the concerted action of intestinal Ca^{2+} absorption, exchange of Ca^{2+} from bone and renal Ca^{2+} reabsorption. In kidney, Ca^{2+} can re-enter the blood from the prourine by paracellular (passive) as well as transcellular (active) Ca^{2+} reabsorption. The latter is the main target for the calciotropic hormones that are released upon a demand for Ca^{2+} and subsequently increase the renal Ca^{2+} reabsorption.
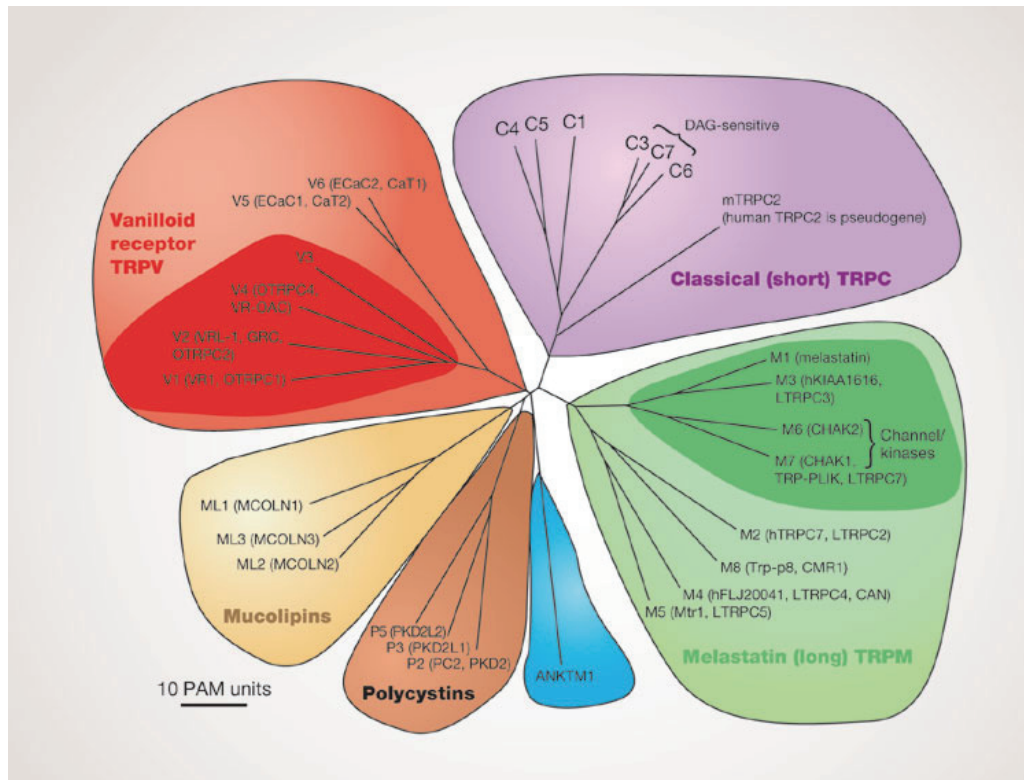
Fig. 1. Mammalian TRP channel phylogeny

The mammalian TRP families consist of six related subfamilies defined as *Classical or Canonical* (TRPC); *Vanilloid receptor related* (TRPV); *Melastin related* (TRPM); *Polycystins* (TRPP); *Mucolipins* (TRPML) and *ANKTM1 related* (TRPA). The evolutionary distance between individual TRP family members is indicated by the total branch lengths in point accepted mutations (PAM) units, which resembles the mean number of amino acid substitutions per 100 residues (from Clapham (1)).

Paracellular Ca^{2+} transport is localized in the proximal part of the nephron, whereas active Ca^{2+} reabsorption comprises a sequence of processes restricted to the distal convoluted tubule (DCT) and the connecting tubule (CNT). At the cellular level, Ca^{2+} enters the renal epithelial cell via the highly Ca^{2+}-selective channel TRPV5 due to the steep inward electrochemical gradient across the apical membrane (7). In the cell, Ca^{2+} is bound to calbindin-D_{28K} that ferries Ca^{2+} from the apical to the basolateral side where the high affinity / low capacity plasma membrane ATPase (PMCA1b) and the low affinity / high capacity Na^+/Ca^{2+}-exchanger (NCX1) extrude Ca^{2+} into the blood compartment **(Fig. 2)**. In kidney, TRPV5 is abundantly expressed compared to other tissues, whereas TRPV6 localization and regulation has been largely confined to the small intestine. In the intestine a similar mechanism for transcellular Ca^{2+} absorption occurs with TRPV6 as the gatekeeper, calbindin-D_{9K} for intracellular Ca^{2+} handling and PMCA1b as the extrusion mechanism. In addition, immunohistochemistry revealed that TRPV6 localizes at the apical domain of the DCT and

CNT in kidney were it might contribute to Ca^{2+} reabsorption. However, TRPV6 was also found at the apical domain of principal and intercalated cells in cortical and medullar collecting ducts (CCD, MCD), which are not generally implicated in active Ca^{2+} reabsorption (8).
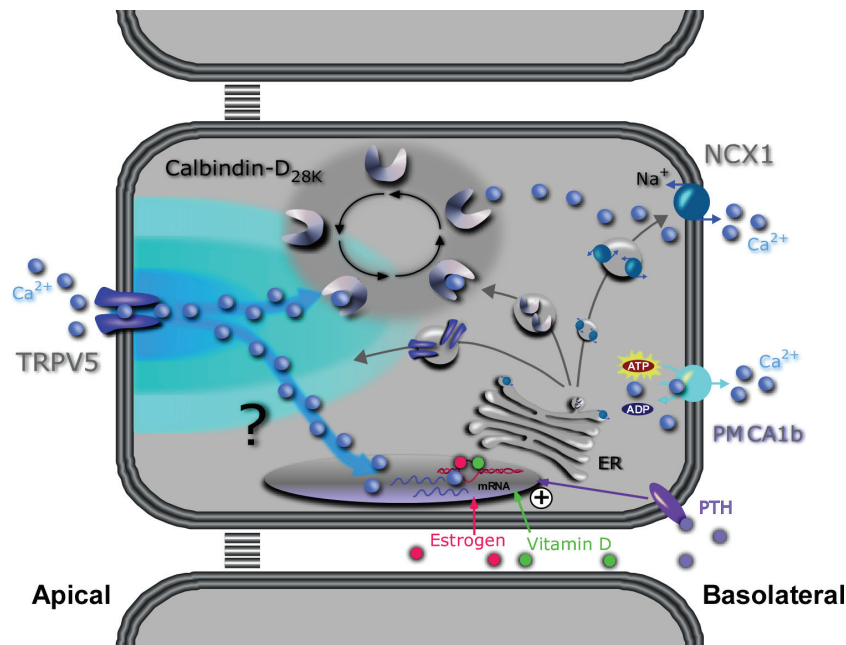

Fig. 2. Transcellular Ca^{2+} transport
Integrated model of active transcellular Ca^{2+} transport in kidney consisting of TRPV5 as the apical entry gate for Ca^{2+}, calbindin-D_{28K} as an intracellular ferry protein for Ca^{2+} and, NCX1 and PMCA1b as Ca^{2+} extrusion systems across the basolateral membrane to the blood compartment. These proteins are under the control of the calciotropic hormones that are released upon a demand for Ca^{2+}. PTH stimulates renal Ca^{2+} handling by regulating active Ca^{2+} reabsorption on both the genomic and non-genomic level. The active form of vitamin D, $1,25(OH)_2D_3$ contributes to the overall Ca^{2+} balance by enhancing the expression of the Ca^{2+} transport machinery. Estrogens harbor calciotropic hormone characteristics positively regulating the expression of TRPV5, independently of $1,25(OH)_2D_3$. The magnitude of Ca^{2+} entry via TRPV5 controls the expression of the other Ca^{2+} transport proteins.

Bone is the major Ca^{2+} store of the body in which osteoblasts deposit Ca^{2+} from blood into bone during bone formation and osteoclasts resorb Ca^{2+} from bone during bone mineralization. In both osteoblasts and osteoclasts transcellular Ca^{2+} transport is crucial during bone formation and absorption. In osteoclasts TRPV5, calbindin-D_{28K}, NCX1 and PMCA1b are present (9). Moreover, the predominant localization of TRPV5 to the ruffled border membranes facing bone and the finding that bone resorption in osteoclast cultures from mice that lack TRPV5 (TRPV5$^{-/-}$) is impaired led to the conclusion that TRPV5-mediated transcellular Ca^{2+} transport in osteoclastic bone resorption is comparable to that of the kidney (9). Importantly, osteoclastic ruffled border membranes are strongly acidified by an active mechanism which is mediated by a specialized H^+ pump (V-ATPase) located on the plasma membrane (10). This V-ATPase mediates H^+ transport into the resorption pits where a low pH is essential for dissolution of bone crystals. At acidified extracellular conditions TRPV5 is not active which will result in the absence of ruffled border membrane Ca^{2+} influx

(11-13) (see below). In total, the results until now demonstrate that TRPV5 is present in bone and that osteoclastic bone resorption in TRPV5$^{-/-}$ mice is impaired. However, if TRPV5 constitutes the ruffled border membrane Ca^{2+} gate essential for the maintenance of a normal Ca^{2+} balance remains to be elucidated.

3. Expression of TRPV5 and TRPV6 in other tissues

3.1 Stomach

Although TRPV5 and TRPV6 are mainly expressed in Ca^{2+}-transporting organs, including kidney, intestine, and bone, both channels are detected in several other tissues. Along the gastro-intestinal tract, the stomach is generally not considered to play a major role in Ca^{2+} absorption, however, functional measurements demonstrated a luminal to blood transport of Ca^{2+} (14). Interestingly, TRPV6 and, to a lesser extent, TRPV5 have been detected in the stomach (15, 16). At least for TRPV6 it was suggested that in mucus-secreting cells this channel plays an important role in maintaining $[Ca^{2+}]_i$ by refilling the depleted Ca^{2+} stores after hormone-controlled mucus secretion (17). Thus, in these latter cells TRPV6 potentially acts as a kind of store-operated Ca^{2+} channel. However, functional characterization of mucus-secreting cells from stomach isolated from TRPV5$^{-/-}$ and TRPV6$^{-/-}$ mice is needed to completely understand the role of these Ca^{2+} channels in the stomach.

3.2 Placenta

During pregnancy, Ca^{2+} absorption in the placenta is solely responsible for the Ca^{2+} supply to the developing fetus. In line with this function, transcellular Ca^{2+} transport takes place in placental syncytiotrophoblasts that separate maternal and fetal circulation (18). Similar as in the intestine and kidney, the Ca^{2+} transport machinery in these cells is suggested to comprise of apical influx followed by subsequent intracellular transport by calbindin-D$_{9K}$ and -D$_{28K}$ and basolateral extrusion by Ca^{2+}-ATPases and Na^{+}/Ca^{2+} exchangers (19). Among the candidates for apical Ca^{2+} influx channels are TRPV5 and TRPV6 which both are expressed in the placenta, although the expression of TRPV6 appears to be dominating (20, 21). Moreover, the expression level of TRPV5 and TRPV6 correlates with the differences in Ca^{2+} uptake during the differentiation of cultured human trophoblasts isolated from placenta providing circumstantial evidence for a role of these channels in Ca^{2+} uptake by the syncytiotrophoblast (21).

3.3 Exocrine tissues

In exocrine tissues such as pancreas, testis, prostate, mammary-, sweat- and salivary-gland epithelial Ca^{2+} channels are expressed (22). Although the function of TRPV5 and TRPV6 in these tissues remains elusive several studies indicated that they are essential components of Ca^{2+} handling in these tissues. TRPV5 and TRPV6 possibly fulfill an critical role in the

pancreas were they are part of the signaling complex leading to excretion of insulin from β-cells (23). In prostate, TRPV6 is correlated with the progression of prostate carcinoma and here TRPV6 is involved in Ca^{2+} signaling (24, 25). In conclusion, the differences in the localization of these channels throughout the organism may reflect diverse physiological functions.

4. TRPV5 and TRPV6; biophysically unique channels

TRPV channels are Ca^{2+} permeable, however TRPV5 and TRPV6 discriminate much higher between divalent and monovalent cations. They are, however, permeable for monovalents in the absence of divalents (e.g. the relative selectivity for Ca^{2+} over Na^+ P_{ca}/P_{Na} = 1-10 (TRPV1-TRPV4) and P_{ca}/P_{Na} >100 (TRPV5 and TRPV6)) (26-29). For both TRPV5 and TRPV6 a divalent cation permeation sequence of $Ca^{2+} > Ba^{2+} > Sr^{2+} > Mn^{2+}$ has been reported (30-32). In the physiological context, this selectivity makes TRPV5 and TRPV6 particularly suited for Ca^{2+} transport in the presence of other cations, fitting the basic requisites for luminal Ca^{2+} influx channels in Ca^{2+}-transporting epithelia. Differences in selectivity and permeation within the TRPV subfamily are explained by structural variations residing in the selectivity filter (a stretch of negatively charged residues in the pore structure that selectively enables the entering of cations). For TRPV5 and TRPV6 the high Ca^{2+} selectivity is pinpointed to a single aspartate residue within the selectivity filter (TRPV5-D542 and TRPV6-D541) and mutation of this residue completely abolished Ca^{2+} permeability without affecting Na^+ permeability (33, 34) **(Table 1)**. In addition, apartate-542 within the selectivity filter of TRPV5 is essential for its Mg^{2+} sensitivity since mutation of this residue (D542A) abolished the Mg^{2+}-induced inhibition (35). Single channel measurements of Na^+ currents for TRPV5 and TRPV6 indicated a similar conductance of 40-70 pS and corresponding current-voltage relationships show inward rectification. Whereas other TRP channels are activated upon a rise in $[Ca^{2+}]_i$, TRPV5 and TRPV6 display a negative feedback regulation of channel activity by Ca^{2+}, even in the presence of high affinity Ca^{2+} buffers and a negative membrane potential (36) **(Fig. 3)**. It could be envisaged that such channel regulation is of physiological importance in Ca^{2+}-transporting cells to reduce the entering of Ca^{2+} when $[Ca^{2+}]_i$ becomes detrimental. The subsequent recovery after Ca^{2+}-dependent inactivation of TRPV5 and TRPV6 is not directly linked to $[Ca^{2+}]_i$ (e.g. unbinding of Ca^{2+} from the channel complex). This originated from the observations that the recovery from the Ca^{2+}-induced inhibited state is much slower than the inhibition and does not correlate with the restoration of the basal Ca^{2+} level after Ca^{2+} influx (36). The complex kinetics of Ca^{2+} inhibition and subsequent recovery of channel activity thus suggest that processes other than rapid binding of Ca^{2+} to the channel and slow dissociation are involved in coupling the Ca^{2+} current and coherent $[Ca^{2+}]_i$ to TRPV5 and TRPV6 activity.

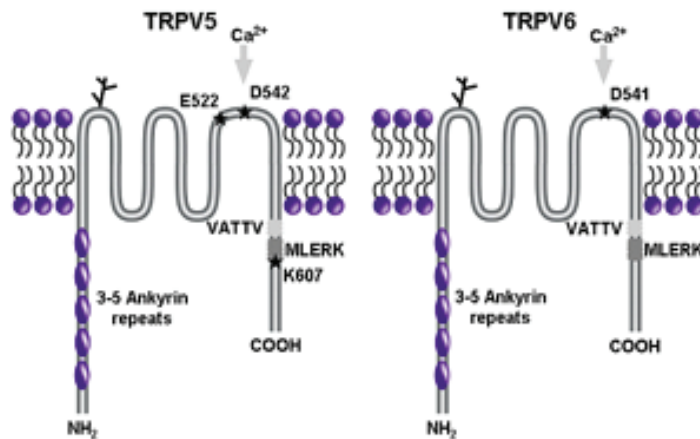| Stimulus	TRPV5	TRPV6	REF
[Ca^{2+}]	Inhibition	Inhibition	38
Extracellular pH	>pH 7.4 stimulation by affecting the pore helix orientation	Unknown	11 - 13
Intracellular pH	>pH 7.4 stimulation by affecting the pore helix orientation	Unknown	11 - 13
PIP$_2$	Stimulation due to removal of inhibition by extracellular Mg^{2+}	Unknown	35
Klotho	Stimulation due to hydrolysis of extracellular N-glycosylation	Stimulation by hydrolysis of extracellular N-glycosylation	79
Associated proteins			
S100A10-Annexin 2	Involved in cell surface expression	Involved in cell surface expression	62
Rab11A	Regulation of cell surface expression by a GTP / GDP-dependent recycling mechanism	Regulation of cell surface expression by a GTP / GDP-dependent recycling mechanism	69
80K-H	Regulation of Ca^{2+}-dependent activity	Unknown	71
BSPRY	Stimulation independent from altered cell surface expression	Unknown	72
NHERF2	In combination with SGK1 stimulation	Unknown	74

Table 1. TRPV5 and TRPV6 topology and regulation

Like all TRP channels TRPV5 and TRPV6 are comprised of six transmembrane domains with a predicted pore structure between TM5 and TM6 and an intracellular amino- and carboxyl-terminus. TRPV5 and TRPV6 contain 3-5 conserved ankyrin repeats in their amino-terminus involved in channel multimerization. Indicated are the suggested extra- and intracellular pH sensors E522 and K607 determining the pH sensitivity of TRPV5. For TRPV5 and TRPV6 the high Ca^{2+} selectivity is pinpointed to a single aspartate residue within the selectivity filter (TRPV5-D542 and TRPV6-D541). A number of factors and associated proteins were previously identified to affect the activity of TRPV5 and TRPV6 (see text for details). VATTV and MLERK are important residues for associated proteins.

Detailed electrophysiological analysis of TRPV5 and TRPV6 currents revealed that both channels display constitutive activity at physiological membrane potentials with similar characteristics. However, differences concern divalent cation permeability, pharmacology, the kinetics of Ca^{2+}-dependent inactivation and recovery from inactivation **(Fig. 3)**. In the absence of other cations TRPV5 is more permeable for Ba^{2+} than TRPV6 (37). Furthermore, the Ca^{2+}-dependent inactivation kinetics of TRPV5 are initially, after hyperpolarization, less pronounced than for TRPV6 although total inactivation is not significantly different (37). Subsequent recovery of TRPV6 activity after Ca^{2+}-dependent inactivation is twice as slow as for TRPV5. In addition, TRPV5 sensitivity for the potent Ca^{2+} channel blocker ruthenium red is 100-fold higher ($IC_{50} \sim 121 \pm 13$ nM) than TRPV6 ($IC_{50} \sim 9 \pm 1$ μM). In total these differences should allow dissection of individual TRPV5 and TRPV6 currents in tissues where both channels are expressed and operate independently from each other.
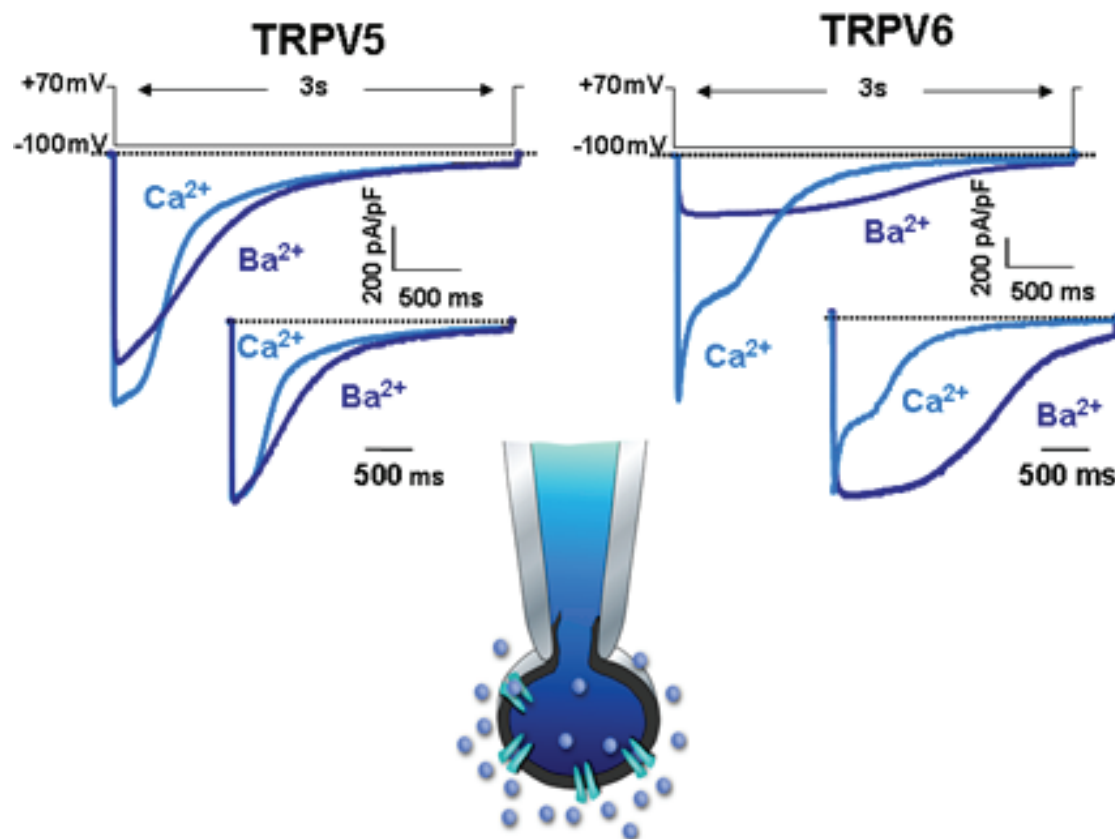
Fig. 3. Negative feedback inhibition of TRPV5 and TRPV6 activity by intracellular Ca^{2+}
Currents through TRPV5 and TRPV6 during a voltage step from +70 to -100 mV. Charge carrier is either Ca^{2+} (30 mM) or Ba^{2+} (30 mM). All of the other cations are substituted by 150 mM $NMDG^+$. Cells were loaded with 10 mM BAPTA. *Insets* show currents normalized to the peak current. Upon opening of these channels, as evident from the immediate rise in current after hyperpolarization, channel activity decreases as reflected by inactivation of the current.

Like the majority of the TRP channels, TRPV5 and TRPV6 form functional hetero tetramers that posses distinctive properties than that of either channel alone (38). TRP channel multimerization appears to be restricted to members within relatively narrow confines of phylogenetic subfamilies, although several TRP channels form functional multimers with other non-TRP ion channels underlying a direct coupling of TRP channels mediated signaling with other process (39-43). The tetrameric stoichiometry of TRP channels resembles that of KscA K^+ channels where the four subunits cluster together to form a central pore such that the pore selectivity filters are central in determining ion permeation **(Fig. 4)**. Within the TRPV6 amino-terminus an ankyrin repeat at position 116 - 191 was identified as a stringent requirement for physical assembly of TRPV6 subunits. It was proposed that this repeat initiates a molecular zippering process that proceeds past the last ankyrin repeat, thereby creating an intracellular anchor essential for functional TRPV6 subunit assembly (44). The regions that determine TRPV5 subunit assembly reside within both the N- (64-77) and carboxyl-terminus (596-601) (45). Recently the crystal structure of the TRPV2 ankyrin repeats has been elucidated and detailed analyses revealed that, although TRPV2 form functional tetramers, the six ankyrin repeat domains do not associate during multimerization (46). Translating these results to the epithelial Ca^{2+} channels suggests that the ankyrin repeats in TRPV5 and TRPV6 are distantly related to those in TRPV2 and directly tertramerize to promote channel assembly. Another possibility is that the TRPV5 and TRPV6 ankyrin repeats promote channel assembly by interacting with associated proteins or other regions of these channels. Additional studies with the isolated TRPV5 and/or TRPV6 ankyrin repeat domains could discriminate between these hypotheses.

5. TRP channel regulation

Regulation of TRP channels has recently gained profound interest due to the diverse cellular functions they fulfill. The various mechanisms adapted by cells to control channel activity basically operate at four distinct levels. First, channel activity can be affected on the genomic level via (hormone-mediated) signaling of messengers to the nucleus to regulate gene transcription. Second, after synthesis and controlled assembly of (hetero)multimeric channel complexes in the ER/Golgi trafficking of these channels towards the cell surface is under the control of several systems. Trafficking of TRP channels is of special interest since many channels (including TRPV5 and TRPV6) are not clearly localized at the plasma membrane, but merely reside in intracellular vesicles. Third, channel activity at the cell surface can be affected by structural modifications of the channel complex and/or binding and release of intra- and extracellular compounds affecting channel (in)activation. Fourth, recycling and degradation of plasma membrane inserted channels via distinct pathways enables tight and spatiotemporal control of TRP channels. Regulation of TRPV5 and TRPV6 is a pivotal

process in the maintenance of a normal Ca^{2+} balance. In this way the organism is able to respond to fluctuations in the demand for Ca^{2+}.
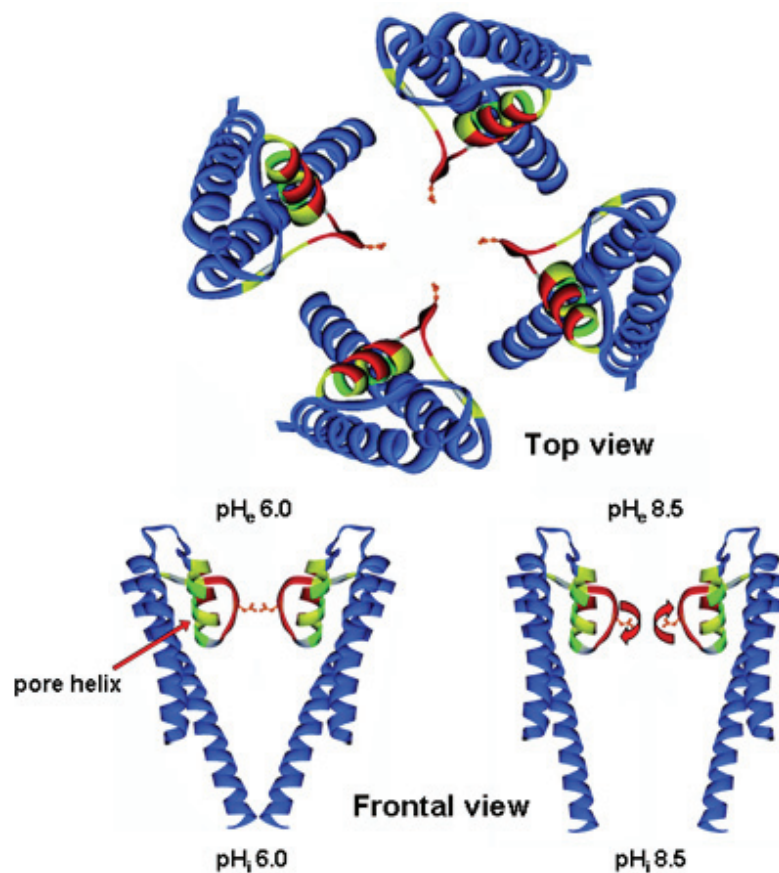

Fig. 4. TRPV5 pore structure

Model for the TRPV5 pore region, based on the K^+ channel KscA structure. Views of the structure are shown, looking down from the external solution to the complete homotertrameric channel (top) or looking sideways (below). Blue residues correspond to the residues in TM5 and TM6. Amino acids that were subjected to SCAM analysis to determine their position to the extracellular compartment (47), are colored in green, yellow, red or gray. Intra- and extracellular protons determine the position of the TRPV5 pore helix position leading to opening and closing of the TRPV5 pore such that protons cause the pore helix to rotate in the clockwise direction, leading to closing (narrowing) of the pore, whereas in the absence of protons (alkalinization) the pore opens. The model is partly adapted from Voets *et al* (48).

5.1 Hormonal regulation of TRPV5- and TRPV6-mediated transcellular Ca^{2+} transport

An intrinsic physiological mechanism is sensing the Ca^{2+} demand by a specialized Ca^{2+}-sensing receptor (CaSR) that couples the blood Ca^{2+} levels to the secretion and production of the Calciotropic hormones including 1,25-dihydroxyvitamin D_3 (1,25$(OH)_2D_3$), parathyroid hormone (PTH) and calcitonin. At a blood ionized [Ca^{2+}] below 1.25 mM the parathyroid CaSR is inactivated, which enables a cascade of signaling pathways to increase the secretion of PTH. PTH in turn stimulates the production of 1,25-dihydroxyvitamin D_3 (1,25$(OH)_2D_3$) and calcitonin that increase Ca^{2+} uptake in the intestine, Ca^{2+} reabsorption in kidney and Ca^{2+} uptake from bone. Upon a subsequent rise in blood ionized [Ca^{2+}] the CaSR is activated which suppresses the release of PTH and thus maintains plasma Ca^{2+} levels within a narrow

physiologic range by efficiently regulating Ca^{2+} transport processes in kidney, intestine and bone **(Fig. 2)**.

5.1.1 Transcellular Ca^{2+} transport and PTH

Primary hyperparathyroidism is characterized by PTH levels that are inappropriate to the level of plasma Ca^{2+} and is one of the endocrine disorders that underline the importance of PTH in maintaining the overall Ca^{2+} balance. In addition, mutations in the CaSR, which couples plasma Ca^{2+} levels to the production and secretion of PTH from the thyroid glands, were identified in patients with familial hypocalciuric hypercalcemia, neonatal severe hyperparathyroidism (inactivating mutations) (49) and autosomal-dominant hypocalcemia (activating mutations) (50). From the clinical symptoms of these PTH-related disorders, including hypo- or hypercalciuria and renal stone formation, it is evident that also renal Ca^{2+} handling is affected. PTH receptors have been detected throughout the nephron including DCT and CNT, thus enabling the body to directly control active Ca^{2+} reabsorption in kidney via PTH (22). In addition, genetic ablation of CaSR resulted in hyperparathyroidism and hypercalcemia, accompanied by an up-regulation of TRPV5 and TRPV6 in kidney and intestine, respectively (51). To understand the molecular regulation of the Ca^{2+} transport proteins by PTH, parathyroidectomy was performed in rats (52). The effectiveness of this treatment was evident from the marked reduction of PTH levels and hyperphosphatemia, a well-known symptom of hypoparathyroidism. Moreover, parathyroidectomy reduced the expression of TRPV5, calbindin-D_{28K} and NCX1 in kidney. This decline in expression of the renal Ca^{2+} transport proteins was accompanied by reduced active Ca^{2+} reabsorption and the development of hypocalcemia. PTH supplementation in these parathyroidectomized rats normalized the renal Ca^{2+} transport protein expression levels and increased the plasma Ca^{2+} concentration (52). In addition, the regulation by PTH was investigated in primary cultures of rabbit CNT and cortical collecting duct (CCD) cells (52). Long-term stimulation of PTH resulted in an elevated expression of the Ca^{2+} transport proteins TRPV5, calbindin-D_{28K}, NCX1 and PMCA1b in these renal cell cultures. Taken together, these studies indicated that PTH stimulates renal Ca^{2+} handling by co-regulating the expression of the Ca^{2+} transport proteins.

Regulation of expression of the Ca^{2+} transport proteins, however, is a relatively slow process, while a fast non-genomic response operates on a time scale that is sufficient for an immediate increase of Ca^{2+} reabsorption. An established pathway for short-term PTH-stimulated active Ca^{2+} reabsorption in kidney is activation of adenylyl cyclase, accumulation of cAMP and subsequent activation of protein kinase A (PKA). Addition of PTH to perfused rabbit CNT or primary cultures of rabbit CNT and CCD resulted in a rise of cytosolic cAMP levels accompanied by an increase in transcellular Ca^{2+} transport (53, 54). Moreover, PKA inhibitors

reduced this PTH stimulation, which suggests that cAMP-dependent phosphorylation is an essential step in short-term PTH stimulation. In addition to cAMP, a prominent role for protein kinase C (PKC) was demonstrated in the short-term PTH response (55). However, it remains to be established if this short-term PTH stimulation of transcellular Ca^{2+} transport is mediated by direct activation of TRPV5. Thus, besides a genomic effect, PTH can stimulate Ca^{2+} reabsorption directly via a short-term mechanism involving PKA and PKC.

Taken together, these studies revealed that PTH-dependent stimulation of transcellular Ca^{2+} reabsorption in kidney occurs via both genomic and non-genomic pathways.

5.1.2 Transcellular Ca^{2+} transport and estrogens

The increased risk for osteoporosis in postmenopausal women is associated with estrogen deficiency. Furthermore, estrogen deficiency is associated with renal Ca^{2+} wasting and intestinal Ca^{2+} malabsorption that can be restored by estrogen replacement therapy (56). From these findings the physiological relevance of estrogens in maintaining the Ca^{2+} balance is feasible. In addition, this suggests that estrogens can comply with the action of the calciotropic hormones, regulating the expression of the renal Ca^{2+} transport proteins. Estrogen receptors have been detected in DCT and CNT, thus enabling the body to directly regulate active Ca^{2+} reabsorption in kidney by estrogen (22). Estrogen replacement therapy in ovariectomized rats revealed an increase in the renal expression of TRPV5, calbindin-D_{28K}, NCX1 and PMCA1b suggesting an important role for this hormone in regulating Ca^{2+} reabsorption (22). In addition, genetic ablation of the estrogen receptor-α in mice decreased the expression of the aforementioned renal Ca^{2+} transport proteins. In principle these effects could be explained by estrogen-dependent vitamin D activation. This possibility was investigated in vitamin D-deficient animal models. Estrogen supplementation in 25-hydroxyvitamin D_3-1α-hydroxylase (1α-OHase) knockout mice increased the expression of TRPV5 in kidney, while the expression of the other Ca^{2+} proteins remained unaltered (22). In the intestine estrogens regulate the expression of TRPV6 in a vitamin D-independent manner that became clear from estrogen supplementation in vitamin D receptor (VDR) and 1α-OHase knockout mice. This resulted in an up-regulation of duodenal TRPV6, whereas the expression of calbindin-D_{9K} and PMCA1b was not altered (22). Thus, estrogens harbor calciotropic hormone characteristics regulating the expression of TRPV5 and TRPV6 in kidney and intestine, respectively.

5.1.3 Transcellular Ca^{2+} transport and vitamin D

The active form of vitamin D, 1,25$(OH)_2D_3$, is an important steroid hormone in the body Ca^{2+} homeostasis. This is reflected by several vitamin D-related disorders with symptoms like rickets and hypercalciuria. Inactivating mutations in 1α-OHase are associated with vitamin D-

deficiency rickets type 1 (57) and mutations in the VDR are associated with hypocalcemic rickets (58). Active Ca^{2+} (re)absorption is a main target for $1,25(OH)_2D_3$, as illustrated by $1,25(OH)_2D_3$-stimulated Ca^{2+} transport in primary cultures of rabbit CNT and CCD cells and human intestinal Caco-2 cells (53, 59). Strikingly, microarray analysis of $1,25(OH)_2D_3$-stimulated carcinoma cells revealed TRPV6 as one of the most highly vitamin D-responsive genes underlining the ability of vitamin D to regulate TRPV6 expression (60).

Evidence for $1,25(OH)_2D_3$-controlled expression of the renal Ca^{2+} transport proteins came from rats that were raised on a vitamin D-deficient diet. This diet decreased the renal expression of TRPV5, which was accompanied by a marked drop in plasma Ca^{2+} levels. In addition, genetic ablation of 1α-OHase in mice resulted in severe hypocalcemia, hyperparathyroidism, bone abnormalities and retarded growth (61). In line with the development of hypocalcemia is the diminished Ca^{2+} reabsorption in kidney, presumably as a result of the down-regulated expression of the Ca^{2+} transport proteins TRPV5, calbindin-D_{28K} and NCX1 (22). Supplementation of $1,25(OH)_2D_3$ restored the expression of the renal Ca^{2+} transport proteins and normalized the hypocalcemia (22). Thus, vitamin D is of fundamental importance for the regulation of renal Ca^{2+} transport proteins and the maintenance of a normal Ca^{2+} balance.

Mice lacking TRPV5 display robust renal Ca^{2+} wasting due to impaired Ca^{2+} reabsorption in DCT and CNT (62). In addition, elevated $1,25(OH)_2D_3$ plasma levels, intestinal Ca^{2+} hyperabsorption and reduced bone thickness were demonstrated. Besides the decreased storage of Ca^{2+} in bone, compensatory hyperabsorption of Ca^{2+} in the intestine prevented the development of hypocalcemia in these knockout mice. The underlying mechanism of this compensatory hyperabsorption is hypervitaminosis D which increases the expression of the intestinal Ca^{2+} transport proteins TRPV6, calbindin-D_{9K} and PMCA1b (62). This finding indicates that a renal Ca^{2+} leak due to the absence of TRPV5 triggers a rescue mechanism resulting in an increased production of vitamin D-stimulated intestinal Ca^{2+} absorption. The absence of hypervitaminosis D in the recently developed 1α-OHase and TRPV5 double knockout (1α-OHase$^{-/-}$/TRPV5$^{-/-}$) mice, resulted in hypocalcemia and thus suggests that the elevated levels of $1,25(OH)_2D_3$ in TRPV5$^{-/-}$ mice are responsible for the up-regulation of intestinal Ca^{2+} transport proteins and the coherent Ca^{2+} hyperabsorption (63). The absence of hyperabsorption in 1α-OHase$^{-/-}$/TRPV5$^{-/-}$ mice resulted in a more aggravated phenotype compared to TRPV5 ablation. Thus, $1,25(OH)_2D_3$ is crucial to compensate for the renal Ca^{2+} leak and to maintain normal plasma Ca^{2+} levels in TRPV5$^{-/-}$ mice. Importantly, PTH levels in these knockout models are comparable to wild-type littermates, indicating that the observed regulation is not due to altered PTH levels.

5.2 Regulation of TRPV5 and TRPV6 activity by associated protein complexes

Non-genomic regulation of TRPV5 and TRPV6 activity is under the control of associated protein partners that affect channel trafficking and, activity or stability at the cell surface **(Table 1)**. The Ca^{2+}-dependent activity of TRPV5 and TRPV6 is under special interest since the biophysical properties of these channels cannot explain this phenomenon and sequences analysis revealed that both TRPV5 and TRPV6 do not contain known sequences involved in Ca^{2+}-sensing. Both channels are, however, highly regulated by Ca^{2+} suggesting the involvement of Ca^{2+}-binding proteins that translate the local Ca^{2+} concentration to TRPV5 and TRPV6 activity.

5.2.1 Cell surface expression of TRPV5 and TRPV6: role of S100A10-annexin 2 and Rab11

Using yeast two-hybrid, GST pull-down analyses and co-immunoprecipitations the Ca^{2+}-binding protein S100A10 was identified as an associated protein of TRPV5. S100A10 forms a well-defined heterotetrameric complex with annexin 2 and specifically binds the conserved sequence VATTV in the carboxyl-terminus of TRPV5 and TRPV6 (64). Importantly, both S100A10 and annexin 2 co-localize with TRPV5 in kidney and with TRPV6 in the intestine. Disruption of the first threonine of the VATTV motif in the carboxyl-terminus (TRPV5 T599A and TRPV6 T600A) resulted in a diminished S100A10 binding, localization of TRPV5 to a sub-plasma membrane area in *Xenopus leavis* oocytes and disruption of channel activity. In addition, downregulation of annexin 2 using annexin 2-specific small interference RNA inhibited TRPV5 and TRPV6 activity as assessed by electrophysiological recordings in HEK293 cells. In total, these findings revealed that the S100A10-annexin 2 complex is essential for TRPV5 and TRPV6 trafficking towards the cell surface. S100A10 is a member of the Ca^{2+}-binding proteins and annexin 2 is a phosphoinositide binding protein (65). Since both Ca^{2+} and phosphoinositides affect the activity of TRPV5 and TRPV6 (7, 35, 66, 67) (see below), it could be envisaged that the S100A10-annexin 2 complex is involved in Ca^{2+}- and/or phosphoinositide-dependent channel activity. The binding of S100A10 to TRPV5 and TRPV6 is, however, independent of Ca^{2+} as reflected by the lack of Ca^{2+} dependence in GST pull-down experiments suggesting that the S100A10-annexin 2 dependent regulation does not involve Ca^{2+}-sensing. It remains, however, to be elucidated if S100A10 is involved in phosphoinositide-dependent activity of TRPV5 and TRPV6.

The family of Rab GTPases consists of important factors in vesicular cargo delivery (68). The ability to cycle between GTP- and GDP-bound states enables Rab proteins to act as molecular switches determining protein delivery to their targets. Rab11a was found to directly associate with TRPV5 and TRPV6 (69). Detailed analysis of this association revealed that the interaction was specific for GDP-bound Rab11a. Co-expression of a GDP-locked Rab11a

mutant resulted in an inhibition of TRPV5-mediated Ca^{2+} uptake in oocytes and transcellular Ca^{2+} transport in primary rabbit CNT/CCD cultures. This inhibition is caused by a diminished cell surface expression of TRPV5 that substantiated the conclusion that Rab11a is an essential factor in TRPV5 trafficking. In intracellular vesicles Rab11a-GDP and TRPV5 and/or TRPV6 directly associate and upon exchange of GDP for GTP, the channel is delivered to the plasma membrane. Subsequent GTP hydrolyzes will result in an internalization of the complex and inhibition of transcellular Ca^{2+} transport.

5.2.2 Activity of TRPV5 and TRPV6 at the cell surface: 80K-H and BSPRY

The widely expressed PKC substrate 80K-H was found to be concomitantly regulated with TRPV5 by $1,25(OH)_2D_3$ and dietary Ca^{2+} (70). Both proteins co-localize in kidney and directly associate independently of Ca^{2+} (71). 80K-H binds Ca^{2+} and inactivation of its Ca^{2+}-binding EF-hand structures eliminated Ca^{2+} binding. Co-expression of a Ca^{2+}-insensitive 80K-H mutant in TRPV5-expressing cells reduced TRPV5 currents which led to the conclusion that 80K-H acts as a Ca^{2+}-sensor controlling TRPV5 activity.

The biological function of BSPRY (B-box and SPRY-domain containing protein) remains to be established, however, yeast two-hybrid, GST pull-downs and co-immunoprecipitation experiments revealed that BSPRY associates with TRPV5 independently of Ca^{2+} (72). Both proteins co-localize in kidney and co-expression of BSPRY resulted in a significant reduction of TRPV5-mediated Ca^{2+} influx in confluent monolayers of Madine Darby Canine Kidney cells. BSPRY affects TRPV5 activity at the cell surface, which is evident from the biotinylation experiments showing that the BSPRY-mediated TRPV5 inhibition independent from altered plasma membrane expression. Together these findings demonstrated a role of BSPRY in the regulation of TRPV5-mediated epithelial Ca^{2+} transport and revealed the first physiological function of this novel protein.

5.2.3 TRPV5 and TRPV6 stability at the plasma membrane: NHERF and klotho

Molecular and cellular studies over the past decade showed that NHERF members (Na^+/H^+ Exchanger Regulating Factors) regulate the targeting and stability of ion transporters and other membrane proteins, and transduce (patho)physiological signals that determine ion homeostasis in mammals (73). NHERF2 specifically interacts with the TRPV5 carboxyl-terminus, whereas NHERF4 associates with both TRPV5 and TRPV6 (74, 75). Interestingly, in a large-scale proteomic analysis to unravel the TRPV5 interactome NHERF1 was found to associate with TRPV5 (Lambers *et al.*, unpublished results). Although NHERF4 binds to both TRPV5 and TRPV6, these proteins only co-localize in the intestine where NHERF4 could act as putative plasma membrane scaffolding protein. Upon co-expression of NHERF2 and serum and glucocorticoid inducible kinases (SGK1 and SGK3) the activity of TRPV5 was

upregulated (75). Similarly, co-expression of SGK1 with NHERF2 stimulates the activity of the K^+ channel ROMK1 as a result from stabilization of channels at the plasma membrane (76). To address whether TRPV5 stimulation by NHERF2, SGK1 and SGK3 is mediated by stabilization of the channel at the plasma membrane remains to be elucidated. In conclusion, NHERF proteins appear to be essential factors involved in controlling TRPV5 and TRPV6 activity.

The β-glucuronidase klotho is associated with human aging, however, the molecular function and the downstream targets of this enzyme are largely unknown (77). Detailed analysis revealed that the klotho gene also expresses a secreted form, lacking transmembrane and intracellular domains, due to alternative RNA splicing. Therefore, klotho could also act as a humoral factor (78). The expression of klotho in kidney was found to be downregulated in mice lacking TRPV5 (79). Moreover, the expression of klotho is tightly regulated by vitamin D, suggesting a functional link between TRPV5 and klotho in the maintenance of the Ca^{2+} balance. Furthermore, mice lacking klotho (klotho$^{-/-}$) displayed renal Ca^{2+} loss (77). In line with the detection of klotho in urine it was found that klotho regulates the activity of TRPV5 from the extracellular side via its glucuronidase activity. Further analysis revealed that klotho hydrolyzes the extracellular N-glycosylation of TRPV5 resulting in entrapment of TRPV5 at the plasma membrane. This study demonstrated the first molecular target of klotho providing insight in TRPV5-mediated Ca^{2+} reabsorption, Ca^{2+} deficits in klotho$^{-/-}$ mice and aging-related Ca^{2+} disorders.

5.3. Other factors that control TRPV5 and TRPV6 activity

Besides hormones and associated proteins several other physiological factors are involved in TRPV5 and TRPV6 regulation, thereby indirectly determining the overall Ca^{2+} balance **(Table 1)**.

5.3.1 Dietary Ca^{2+}

Hereditary hypocalcemic vitamin D-resistant rickets, which are caused by a genetic defect in the VDR gene, are treated with high dietary Ca^{2+} supplementation (80). This suggests that dietary Ca^{2+} can act as an additional regulatory mechanism of Ca^{2+} handling independent of vitamin D. From a molecular point of view, dietary Ca^{2+} affects the Ca^{2+} balance by regulation the expression of the renal and intestinal Ca^{2+} transport proteins. This is evident from high dietary Ca^{2+} supplementation in mice which, among others, resulted in a decreased TRPV5 and TRPV6 expression (22). This decline in expression is likely mediated by the accompanied decrease in $1,25(OH)_2D_3$ levels. In contrast, in 1α-Ohase$^{-/-}$ a high dietary Ca^{2+} load normalized the plasma Ca^{2+} concentration as well as the expression of TRPV5, calbindin-D_{28K}, NCX1 and PMCA1b (22). Likewise, in mice that lack VDR an increased

dietary Ca^{2+} intake upregulated the expression of TRPV5 in kidney and TRPV6 in the intestine (80). Taken together, dietary Ca^{2+} regulates the expression of the Ca^{2+} transport proteins, both independent and dependent of $1,25(OH)_2D_3$.

5.3.2 Phosphoinositides

Phosphoinositides are ubiquitously employed interconverting signaling molecules in eukaryotic cells that can affect a wide range of cellular process among others the activity of ion channels. Phosphatidylinositol 4,5-biphosphate (PIP_2) influences the activity of a diverse range of ion channels like, inward-rectifier and voltage-gated K^+ channels, the two-P domain K^+ channels, voltage-gated Ca^{2+} channels, cyclic nucleotide-gated channels, intracellular Ca^{2+} release channels and the epithelial Na^+ and Cl^- channels (81). How phosphoinositides alter channel function is an area of intense research interests. It has been shown for many ion channels that direct interaction with PIP_2 stabilizes channels in a particular conformation (81). By stabilization in one conformation, PIP_2 modulates the response of ion channels to regulators, such as GTP-binding proteins, intracellular pH, Na^+, ATP, etc. Likewise, several TRP channels have been shown to be affected by PIP_2 and recently a mechanism was proposed for PIP_2-mediated TRPM8 channel regulation via a carboxyl-terminal stretch of amino acids that is conserved in most TRP members (termed TRP domain). TRPV5 and TRPV6 do not contain a conserved TRP domain, however, TRPV5 is demonstrated to be regulated by PIP_2 (35). In this study PIP_2 was identified to stimulate TRPV5 activity by decreasing the sensitivity of the channel to extracellular Mg^{2+}-induced inhibition.

5.3.3 Extracellular pH

Acid-base homeostasis is known to affect the Ca^{2+} balance as evident from changes in renal Ca^{2+} handling during chronic metabolic acidosis or alkalosis (82, 83). Likely, renal Ca^{2+} loss during chronic acidosis is a result of downregulation of the Ca^{2+} transport proteins TRPV5, $CaBP_{28K}$ and NCX1, while renal Ca^{2+} sparing during chronic alkalosis is a result of an increased expression of the Ca^{2+} transport machinery (83). Besides genomic regulation, pH (both intra- and extracellular) was found to directly affect the activity of TRPV5 such that acidification inhibited TRPV5 activity and alkalinization increased channel activity (11-13). The intracellular lysine (K607) and the extracellular glutamic acid (E522) residues of TRPV5 have been postulated as pH sensors determining TRPV5 activity, although K607N and E522Q mutants still displayed pH-sensitivity (11, 13) **(Table 1)**. The activity of a diverse range of ion channels is regulated by extracellular factors and often structural rearrangements within the pore underlie biophysical changes that determine channel activity (84-86). Likewise, cellular pH was found to determine the position of the TRPV5 pore helix such that intra- and extracellular protons cause the pore helix to rotate in the clockwise direction, leading to

closing (narrowing) of the pore, whereas in the absence of protons the pore opens **(Fig. 4)** (13).

6. Scope of this thesis

The molecular regulation of TRPV5 and TRPV6 activity in kidney and intestine, respectively, is of fundamental importance to understand the Ca^{2+} homeostasis. Since the discovery of these channels, TRPV5 and TRPV6 regulation also gained interest from clinicians given the numerous symptoms involving malfunctioning of the Ca^{2+} balance. Although we can now pinpoint the effect of the calciotropic hormones to changes in the expression of the Ca^{2+} transport machinery including TRPV5 and TRPV6 as the luminal entry gates, the molecular regulation of these channels at the plasma membrane and their trafficking to the cell surface still remains elusive. As indicated, channel-associated protein complexes generally fulfill an important role in these processes. To date, a number of associated proteins are implicated in TRPV5 trafficking to the plasma membrane. However, physiological factors that initiate (rapid) recruitment of TRPV5 towards the cell surface and the precise mechanisms these factors employ to transport channels to the cell surface remain to be identified. To this end, several processes known to affect the activity of TRPV5 and TRPV6 have been studied for their ability to initiate TRPV5 trafficking.

The general aim of this thesis was to gain insight into the molecular regulation of TRPV5 and TRPV6 in Ca^{2+}-transporting epithelia. In **chapter 2** the influence of extracellular pH on the rapid insertion of TRPV5 is described. This study demonstrated that TRPV5 plasma membrane expression is under tight control of extracellular pH. TRPV5 accesses the extracellular compartment via transient openings of rapidly recruited vesicles, providing evidence that rapid activation of constitutive active ion channels in response to physiological stimuli relies on vesicular "kiss and linger" interactions with the plasma membrane. **Chapter 3, 4 and 5** focus on the intrinsic mechanism of Ca^{2+}-dependent regulation of TRPV5 and TRPV6, a mode of channel regulation still not understood. In **chapter 3** the regulation of TRPV5 and TRPV6 by the Ca^{2+}-sensor calmodulin is presented. Although both TRPV5 and TRPV6 interact with calmodulin, TRPV6 is specifically regulated by calmodulin. Calmodulin is constitutively bound to TRPV6 were it acts as a Ca^{2+}-sensor regulating TRPV6 channel activity. To identify novel TRPV5 and/or TRPV6 interacting protein partners that might affect channel activity, a large-scale proteomic approach has been performed. This resulted in the identification of calbinidin-D_{28K} as a TRPV5-interacting protein. In **Chapter 4**, the association and functional regulation of calbindin-D_{28K} is described. This study demonstrated that upon a decrease in $[Ca^{2+}]_i$ calbindin-D_{28K} translocates towards the plasma membrane where it associates with TRPV5 to regulate $[Ca^{2+}]$ in close proximity of the TRPV5 pore. To further implicate our experimental data on transcellular Ca^{2+} transport a mathematical model

of transcellular Ca^{2+} transport was established as given in **chapter 5**. In addition, Nipsnap1 was identified as novel TRPV5-interacting protein. **Chapter 6** highlighted that Nipsnap1 is a novel protein of which the physiological function is unknown. However, our study demonstrated the first function for this protein as regulator of the TRPV5 activity at the plasma membrane.

In the past years TRPV5 research has focused on the unraveling of its function and regulation in kidney, while its function in other tissues remains elusive. The results given in **chapter 7** provide evidence for localization of TRPV5 in the inner ear and elucidate a new physiological function of TRPV5 in sound perception. Finally, a general discussion and summary of the thesis work is presented in **chapter 8**.

7. References

1. Clapham, D. E. (2003) *Nature* **426,** 517-24.
2. Montell, C., Birnbaumer, L., Flockerzi, V., Bindels, R. J., Bruford, E. A., Caterina, M. J., Clapham, D. E., Harteneck, C., Heller, S., Julius, D., Kojima, I., Mori, Y., Penner, R., Prawitt, D., Scharenberg, A. M., Schultz, G., Shimizu, N. & Zhu, M. X. (2002) *Mol Cell* **9,** 229-31.
3. Sidi, S., Friedrich, R. W. & Nicolson, T. (2003) *Science* **301,** 96-9.
4. Walker, R. G., Willingham, A. T. & Zuker, C. S. (2000) *Science* **287,** 2229-34.
5. Li, W., Feng, Z., Sternberg, P. W. & Xu, X. Z. (2006) *Nature* **440,** 684-7.
6. Shin, J. B., Adams, D., Paukert, M., Siba, M., Sidi, S., Levin, M., Gillespie, P. G. & Grunder, S. (2005) *Proc Natl Acad Sci U S A* **102,** 12572-7.
7. Hoenderop, J. G., van der Kemp, A. W., Hartog, A., van de Graaf, S. F., van Os, C. H., Willems, P. H. & Bindels, R. J. (1999) *J Biol Chem* **274,** 8375-8.
8. Nijenhuis, T., Hoenderop, J. G., van der Kemp, A. W. & Bindels, R. J. (2003) *J Am Soc Nephrol* **14,** 2731-40.
9. van der Eerden, B. C., Hoenderop, J. G., de Vries, T. J., Schoenmaker, T., Buurman, C. J., Uitterlinden, A. G., Pols, H. A., Bindels, R. J. & van Leeuwen, J. P. (2005) *Proc Natl Acad Sci U S A* **102,** 17507-12.
10. Rousselle, A. V. & Heymann, D. (2002) *Bone* **30,** 533-40.
11. Yeh, B. I., Sun, T. J., Lee, J. Z., Chen, H. H. & Huang, C. L. (2003) *J Biol Chem* **278,** 51044-52.
12. Vennekens, R., Prenen, J., Hoenderop, J. G., Bindels, R. J., Droogmans, G. & Nilius, B. (2001) *Pflugers Arch* **442,** 237-42.
13. Yeh, B. I., Kim, Y. K., Jabbar, W. & Huang, C. L. (2005) *Embo J* **24,** 3224-34.
14. Schroder, B., Vossing, S. & Breves, G. (1999) *J Comp Physiol [B]* **169,** 487-94.
15. Nijenhuis, T., Hoenderop, J. G., van der Kemp, A. W. & Bindels, R. J. (2003) *J Am Soc Nephrol* **14,** 2731-2740.
16. Hoenderop, J. G., Vennekens, R., Muller, D., Prenen, J., Droogmans, G., Bindels, R. J. & Nilius, B. (2001) *J Physiol* **537,** 747-61.
17. Zhuang, L., Peng, J. B., Tou, L., Takanaga, H., Adam, R. M., Hediger, M. A. & Freeman, M. R. (2002) *Lab Invest* **82,** 1755-1764.
18. Faulk, W. P. & McIntyre, J. A. (1983) *Immunol Rev* **75,** 139-75.
19. Belkacemi, L., Bedard, I., Simoneau, L. & Lafond, J. (2005) *Cell Calcium* **37,** 1-8.
20. Peng, J. B., Brown, E. M. & Hediger, M. A. (2001) *Genomics* **76,** 99-109.
21. Moreau, R., Hamel, A., Daoud, G., Simoneau, L. & Lafond, J. (2002) *Biol Reprod* **67,** 1473-9.
22. Hoenderop, J. G., Nilius, B. & Bindels, R. J. (2005) *Physiol Rev* **85,** 373-422.
23. Janssen, S. W., Hoenderop, J. G., Hermus, A. R., Sweep, C. G., Martens, G. J. & Bindels, R. J. (2002) *J Histochem Cytochem* **50,** 789-798.
24. Peng, J. B., Zhuang, L., Berger, U. V., Adam, R. M., Williams, B. J., Brown, E. M., Hediger, M. A. & Freeman, M. R. (2001) *Biochem Biophys Res Commun* **282,** 729-34.
25. Wissenbach, U., Niemeyer, B. A., Fixemer, T., Schneidewind, A., Trost, C., Cavalie, A., Reus, K., Meese, E., Bonkhoff, H. & Flockerzi, V. (2001) *J Biol Chem* **276,** 19461-8.
26. Gunthorpe, M. J., Benham, C. D., Randall, A. & Davis, J. B. (2002) *Trends Pharmacol Sci* **23,** 183-91.
27. Nilius, B., Vriens, J., Prenen, J., Droogmans, G. & Voets, T. (2004) *Am J Physiol Cell Physiol* **286,** C195-205.
28. Voets, T., Prenen, J., Vriens, J., Watanabe, H., Janssens, A., Wissenbach, U., Bodding, M., Droogmans, G. & Nilius, B. (2002) *J Biol Chem* **277,** 33704-10.
29. Benham, C. D., Davis, J. B. & Randall, A. D. (2002) *Neuropharmacology* **42,** 873-88.
30. Vennekens, R., Hoenderop, J. G., Prenen, J., Stuiver, M., Willems, P. H., Droogmans, G., Nilius, B. & Bindels, R. J. (2000) *J Biol Chem* **275,** 3963-9.
31. Vennekens, R., Prenen, J., Hoenderop, J. G., Bindels, R. J., Droogmans, G. & Nilius, B. (2001) *J Physiol* **530,** 183-91.
32. Peng, J. B., Chen, X. Z., Berger, U. V., Weremowicz, S., Morton, C. C., Vassilev, P. M., Brown, E. M. & Hediger, M. A. (2000) *Biochem Biophys Res Commun* **278,** 326-32.
33. Voets, T., Janssens, A., Prenen, J., Droogmans, G. & Nilius, B. (2003) *J Gen Physiol* **121,** 245-60.
34. Nilius, B., Vennekens, R., Prenen, J., Hoenderop, J. G., Droogmans, G. & Bindels, R. J. (2001) *J Biol Chem* **276,** 1020-5.
35. Lee, J., Cha, S. K., Sun, T. J. & Huang, C. L. (2005) *J Gen Physiol* **126,** 439-51.

36. Nilius, B., Prenen, J., Vennekens, R., Hoenderop, J. G., Bindels, R. J. & Droogmans, G. (2001) *Cell Calcium* **29,** 417-28.
37. Hoenderop, J. G. J., Vennekens, R., Müller, D., Prenen, J., Droogmans, G., Bindels, R. J. M. & Nilius, B. (2001) *J Physiol (Lond)* **537,** 747-761.
38. Hoenderop, J. G., Voets, T., Hoefs, S., Weidema, F., Prenen, J., Nilius, B. & Bindels, R. J. (2003) *Embo J* **22,** 776-85.
39. Delmas, P. (2004) *Novartis Found Symp* **258,** 75-89; discussion 89-102, 263-6.
40. Hellwig, N., Albrecht, N., Harteneck, C., Schultz, G. & Schaefer, M. (2005) *J Cell Sci* **118,** 917-28.
41. Schaefer, M. (2005) *Pflugers Arch* **451,** 35-42.
42. Earley, S., Heppner, T. J., Nelson, M. T. & Brayden, J. E. (2005) *Circ Res* **97,** 1270-9.
43. Zhu, M. X. & Tang, J. (2004) *Novartis Found Symp* **258,** 44-58; discussion 58-62, 98-102, 263-6.
44. Erler, I., Hirnet, D., Wissenbach, U., Flockerzi, V. & Niemeyer, B. A. (2004) *J Biol Chem*.
45. Chang, Q., Gyftogianni, E., van de Graaf, S. F., Hoefs, S., Weidema, F. A., Bindels, R. J. & Hoenderop, J. G. (2004) *J Biol Chem* **279,** 54304-11.
46. Jin, X., Touhey, J. & Gaudet, R. (2006) *J Biol Chem*.
47. Dodier, Y., Banderali, U., Klein, H., Topalak, O., Dafi, O., Simoes, M., Bernatchez, G., Sauve, R. & Parent, L. (2004) *J Biol Chem* **279,** 6853-62.
48. Voets, T., Janssens, A., Droogmans, G. & Nilius, B. (2004) *J Biol Chem* **279,** 15223-30.
49. Pollak, M. R., Brown, E. M., Chou, Y. H., Hebert, S. C., Marx, S. J., Steinmann, B., Levi, T., Seidman, C. E. & Seidman, J. G. (1993) *Cell* **75,** 1297-303.
50. Pollak, M. R., Brown, E. M., Estep, H. L., McLaine, P. N., Kifor, O., Park, J., Hebert, S. C., Seidman, C. E. & Seidman, J. G. (1994) *Nat Genet* **8,** 303-7.
51. Kos, C. H., Karaplis, A. C., Peng, J. B., Hediger, M. A., Goltzman, D., Mohammad, K. S., Guise, T. A. & Pollak, M. R. (2003) *J Clin Invest* **111,** 1021-8.
52. van Abel, M., Hoenderop, J. G., van der Kemp, A. W., Friedlaender, M. M., van Leeuwen, J. P. & Bindels, R. J. (2005) *Kidney Int* **68,** 1708-21.
53. Bindels, R. J., Hartog, A., Timmermans, J. & Van Os, C. H. (1991) *Am J Physiol* **261,** F799-807.
54. Lau, K. & Bourdeau, J. E. (1989) *J Biol Chem* **264,** 4028-32.
55. Hoenderop, J. G., De Pont, J. J., Bindels, R. J. & Willems, P. H. (1999) *Kidney Int* **55,** 225-33.
56. Prince, R. L., Smith, M., Dick, I. M., Price, R. I., Webb, P. G., Henderson, N. K. & Harris, M. M. (1991) *N Engl J Med* **325,** 1189-95.
57. Kitanaka, S., Takeyama, K., Murayama, A., Sato, T., Okumura, K., Nogami, M., Hasegawa, Y., Niimi, H., Yanagisawa, J., Tanaka, T. & Kato, S. (1998) *N Engl J Med* **338,** 653-61.
58. Hughes, M. R., Malloy, P. J., Kieback, D. G., Kesterson, R. A., Pike, J. W., Feldman, D. & O'Malley, B. W. (1988) *Science* **242,** 1702-5.
59. Fleet, J. C., Eksir, F., Hance, K. W. & Wood, R. J. (2002) *Am J Physiol Gastrointest Liver Physiol* **283,** G618-25.
60. Wang, T. T., Tavera-Mendoza, L. E., Laperriere, D., Libby, E., MacLeod, N. B., Nagai, Y., Bourdeau, V., Konstorum, A., Lallemant, B., Zhang, R., Mader, S. & White, J. H. (2005) *Mol Endocrinol* **19,** 2685-95.
61. Dardenne, O., Prud'homme, J., Arabian, A., Glorieux, F. H. & St-Arnaud, R. (2001) *Endocrinology* **142,** 3135-41.
62. van de Graaf, S. F., Hoenderop, J. G., Gkika, D., Lamers, D., Prenen, J., Rescher, U., Gerke, V., Staub, O., Nilius, B. & Bindels, R. J. (2003) *Embo J* **22,** 1478-87.
63. Renkema, K. Y., Nijenhuis, T., van der Eerden, B. C., van der Kemp, A. W., Weinans, H., van Leeuwen, J. P., Bindels, R. J. & Hoenderop, J. G. (2005) *J Am Soc Nephrol*.
64. van de Graaf, S. F., Hoenderop, J. G., Gkika, D., Lamers, D., Prenen, J., Rescher, U., Gerke, V., Staub, O., Nilius, B. & Bindels, R. J. (2003) *Embo J* **22,** 1478-1487.
65. Gerke, V. & Moss, S. E. (2002) *Physiol Rev* **82,** 331-71.
66. Hoenderop, J. G., van der Kemp, A. W., Hartog, A., van Os, C. H., Willems, P. H. & Bindels, R. J. (1999) *Biochem Biophys Res Commun* **261,** 488-92.
67. Peng, J. B., Chen, X. Z., Berger, U. V., Vassilev, P. M., Tsukaguchi, H., Brown, E. M. & Hediger, M. A. (1999) *J Biol Chem* **274,** 22739-46.
68. Jordens, I., Marsman, M., Kuijl, C. & Neefjes, J. (2005) *Traffic* **6,** 1070-7.
69. van de Graaf, S. F., Chang, Q., Mensenkamp, A. R., Hoenderop, J. G. & Bindels, R. J. (2006) *Mol Cell Biol* **26,** 303-12.

70. Hoenderop, J. G., Dardenne, O., van Abel, M., van der Kemp, A. W., Van Os, C. H., St-Arnaud, R. & Bindels, R. J. (2002) *Faseb J* **16,** 1398-1406.
71. Gkika, D., Mahieu, F., Nilius, B., Hoenderop, J. G. & Bindels, R. J. (2004) *J Biol Chem* **279,** 26351-7.
72. van de Graaf, S. F., van der Kemp, A. W., van den Berg, D., van Oorschot, M., Hoenderop, J. G. & Bindels, R. J. (2006) *J Am Soc Nephrol* **17,** 26-30.
73. Shenolikar, S., Voltz, J. W., Cunningham, R. & Weinman, E. J. (2004) *Physiology (Bethesda)* **19,** 362-9.
74. Embark, H. M., Setiawan, I., Poppendieck, S., van de Graaf, S. F., Boehmer, C., Palmada, M., Wieder, T., Gerstberger, R., Cohen, P., Yun, C. C., Bindels, R. J. & Lang, F. (2004) *Cell Physiol Biochem* **14,** 203-12.
75. Palmada, M., Poppendieck, S., Embark, H., van de Graaf, S., Boehmer, C., Bindels, R. & Lang, F. (2005) *Cell Physiol Biochem* **15,** 175-82.
76. Palmada, M., Embark, H. M., Yun, C., Bohmer, C. & Lang, F. (2003) *Biochem Biophys Res Commun* **311,** 629-634.
77. Kuro-o, M., Matsumura, Y., Aizawa, H., Kawaguchi, H., Suga, T., Utsugi, T., Ohyama, Y., Kurabayashi, M., Kaname, T., Kume, E., Iwasaki, H., Iida, A., Shiraki-Iida, T., Nishikawa, S., Nagai, R. & Nabeshima, Y. I. (1997) *Nature* **390,** 45-51.
78. Matsumura, Y., Aizawa, H., Shiraki-Iida, T., Nagai, R., Kuro-o, M. & Nabeshima, Y. (1998) *Biochem Biophys Res Commun* **242,** 626-30.
79. Chang, Q., Hoefs, S., van der Kemp, A. W., Topala, C. N., Bindels, R. J. & Hoenderop, J. G. (2005) *Science* **310,** 490-3.
80. van Cromphaut, S., Dewerchin, M., Hoenderop, J. G., Stockmans, I., van Herck, E., Kato, S., Bindels, R. J., Collen, D., Carmeliet, P., Bouillon, R. & Carmeliet, G. (2001) *Proc Natl Acad Sci U S A* **98,** 13324-13329.
81. Suh, B. C. & Hille, B. (2005) *Curr Opin Neurobiol* **15,** 370-8.
82. Sutton, R. A., Wong, N. L. & Dirks, J. H. (1979) *Kidney Int* **15,** 520-33.
83. Nijenhuis, T., Renkema, K. Y., Hoenderop, J. G. & Bindels, R. J. (2006) *J Am Soc Nephrol* **17,** 617-26.
84. Flynn, G. E., Johnson, J. P., Jr. & Zagotta, W. N. (2001) *Nat Rev Neurosci* **2,** 643-51.
85. Yi, B. A., Minor, D. L., Jr., Lin, Y. F., Jan, Y. N. & Jan, L. Y. (2001) *Proc Natl Acad Sci U S A* **98,** 11016-23.
86. Perozo, E., Cortes, D. M. & Cuello, L. G. (1999) *Science* **285,** 73-8.

CHAPTER II

Extracellular pH Dynamically Controls Cell Surface Delivery of Functional TRPV5 Channels

[1]**Lambers T.T.**, [2]Oancea E., [1]Hoenderop J.G., [1]Bindels R.J.

[1]Department of Physiology, Nijmegen Centre for Molecular Life Sciences, Radboud University Nijmegen Medical Centre, The Netherlands
[2]Department of Cardiology, Howard Hughes Medical Institute, Children's Hospital Boston, Harvard Medical School, USA

Abstract

Extracellular pH has long been known to affect the rate and magnitude of ion transport processes among others via regulation of ion channel activity. The Ca^{2+}-selective Transient Receptor Potential Vanilloid 5 (TRPV5) channel constitutes the apical entry gate in Ca^{2+}-transporting cells contributing significantly to the overall Ca^{2+} balance. Here, we demonstrate that extracellular pH determines the cell surface expression of TRPV5 via a unique mechanism. By a comprehensive approach using total internal reflection fluorescence microscopy, cell surface protein labeling, electrophysiology, $^{45}Ca^{2+}$ uptake assays and functional channel recovery after chemobleaching this study shows that upon extracellular alkalinization a pool of TRPV5-containing vesicles is rapidly recruited to the cell surface without completely fusing with the plasma membrane. These vesicles contain functional TRPV5 channels since extracellular alkalinization is accompanied by an increased TRPV5 activity. Conversely, upon subsequent extracellular acidification vesicles are retrieved from the plasma membrane, simultaneously resulting in decreased TRPV5 activity. Thus, TRPV5 accesses the extracellular compartment via transient openings of vesicles suggesting that rapid responses of constitutive active TRP channels to physiological stimuli rely on vesicular "kiss and linger" interactions with the plasma membrane.

Introduction

The superfamily of transient receptor potential (TRP) channels is involved in diverse physiological processes ranging from sensory activity to fertility and epithelial ion transport (1). The highly Ca^{2+}-selective TRPV5 channel constitutes the apical entry gate in Ca^{2+}-transporting cells and facilitates renal Ca^{2+} influx from the pro-urine (2). Several lines of evidence indicate that TRPV5 activity is sensitive to pH. First, acid-base homeostasis is known to affect renal Ca^{2+} handling as reflected by altered Ca^{2+} excretion in kidneys during chronic acidosis or alkalosis, which is mediated at least in part by changes in TRPV5 gene expression (3). Second, *in vitro* studies indicated that intra- and extracellular pH directly regulate the activity of TRPV5. Acidification inhibited, whereas alkalinization stimulated TRPV5 activity, likely mediated by conformational changes of the channel pore helix (4-6).

An intrinsic physiological effect of extracellular pH is the regulation of trafficking processes like endo- and exocytosis and lysosomal trafficking (7-9). Since several TRP channels display constitutive activity, controlled recruitment of these channels towards the plasma membrane is important to translate physiological stimuli into an increased ion permeability of the plasma membrane. For instance, an essential process during insulin-like growth factor-I stimulation of cell growth is TRPV2 recruitment facilitating Ca^{2+} entry during progression through the cell cycle (10). In *Drosophila* photoreceptors, TRPL is shuttled between the plasma membrane and an intracellular compartment by a light-regulated mechanism to fine-tune

visual responses (11). Furthermore, rapid insertion of TRPC5 channels into the plasma membrane was recently identified as a mechanism underlying epidermal growth factor (EGF)-hormone-induced neurite extension in cultured hippocampal neurons (12). However, rapid plasma membrane recruitment of TRPV5 by extracellular physiological stimuli to control its activity in Ca^{2+}-transporting epithelia has not been studied.

The aim of the present study was to investigate the effect of extracellular pH on TRPV5 plasma membrane recruitment as a mechanism underlying pH-dependent channel activity. By using Total Internal Reflection Fluorescence (TIRF) microscopy, cell surface protein labeling, electrophysiology, $^{45}Ca^{2+}$ uptake assays and Functional Recovery After Chemobleaching (FRAC), this study revealed that plasma membrane expression of TRPV5 is under the control of extracellular pH and relies on TRPV5-containing vesicles that remain intact during recruitment and subsequent retrieval. Our results contribute to the concept of "kiss and linger" delivery of constitutive active TRP channels in response to physiological stimuli.

Materials and Methods

Molecular biology and cell culture

pCINEO/IRES-GFP-HA-TRPV5, pCINEO/IRES-GFP, EGFP-TRPV5 and EGFP-TRPM7 were constructed and transiently transfected in HEK293T cells as described previously (13, 14). MDCK cells were stably transfected with EGFP-TRPV5 as described (14).

$^{45}Ca^{2+}$ uptake assay and electrophysiology

$^{45}Ca^{2+}$ uptake was determined using EGFP, EGFP-TRPM7 and EGFP-TRPV5 transfected HEK293T cells and confluent layers of MDCK cells stably expressing EGFP-TRPV5. After 10 min incubation in KHB buffer (for TRPV5: 110 mM NaCl, 5 mM KCl, 1.2 mM $MgCl_2$, 0.1 mM $CaCl_2$, 10 mM Na-acetate, 2 mM NaH_2PO_4, 20 mM HEPES pH 6.0, 7.4 or 8.5 with HCl / NaOH; for TRPM7: 110 mM NaCl, 5 mM KCl, 10 mM Na-acetate, 20 mM HEPES pH 6.0, 7.4 or 8.5 with HCl / NaOH), cells were incubated for 6-10 min with $^{45}CaCl_2$ (1 µCi/ml) in KHB buffer with 4 mM L-lactate, 10 mM D-glucose, 1 mM L-alanine and voltage-gated Ca^{2+} channel inhibitors (10 µM felodipine, 10 µM verapamil). Cells were incubated with 10 µM ruthenium red to block TRPV5-mediated $^{45}Ca^{2+}$ uptake. After washing with ice-cold stop buffer (110 mM NaCl, 5 mM KCl, 1.2 mM $MgCl_2$, 10 mM Na-acetate, 20 mM HEPES, 0.5 mM $CaCl_2$, 1.5 mM $LaCl_3$ pH 6.0, 7.4 or 8.5) $^{45}Ca^{2+}$ uptake was measured. Whole cell currents of HEK293 cells, transiently transfected with pCINEO/IRES-GFP-HA-TRPV5, were measured using ramp protocols and standard extracellular divalent free solutions (adjusted to pH 6.0 and 8.5 with HCl and NaOH, respectively) as described previously (15). On line

alterations in extracellular pH were achieved by perfusion of the extracellular solution surrounding the clamped cell.

Functional recovery after chemobleaching

MDCK-EGFP-TRPV5 cells were incubated for 10 min with 5 mM MTSET in KHB pH 7.4 to nullify all TRPV5 channels on the cell surface. Cells were washed three times with KHB pH 7.4 before pre-incubation for 10 min in KHB pH 6.0, pH 7.4 or pH 8.5 and subsequent $^{45}Ca^{2+}$ uptake to investigate the recovery of TRPV5 channels on the functional level. Total block was investigated by adding 5 mM MTSET to all buffers and 10 μM ruthenium red was added to investigate ruthenium red sensitivity of the functional recovery.

Confocal microscopy, TIRF microscopy and image analysis

Live cell confocal images were taken on A Zeiss LSM510meta (Carl Zeiss GmbH, Jena, Germany) with a PlanApochromatic 63x 1.4 oil immersion DIC lens (Carl Zeiss GmbH) at room temperature. A custom-built objective-based TIRF microscope, as described in detail previously (12), was used to image EGFP-labeled proteins in close proximity to the cell surface. Cells grown on glass cover slips were placed in a custom made chamber with standard external solution (135 mM NaCl, 5 mM KCl, 1.5 mM $MgCl_2$, 1.5 mM $CaCl_2$, 20 mM HEPES 10 mM D-glucose, pH 6.0 or pH 8.5 with HCl / NaOH) and imaged at room temperature. Cells were analyzed for 100 s (1 frame/s) at pH 6.0 to establish a baseline in whole-cell TIRF measurements before switching to pH 8.5 by whole bath perfusion. After 150 s extracellular pH was reduced to pH 6.0 and images were taken for 150 s. To quantify changes in TIRF, intensities of the regions of interests (ROIs) of several (n = 5-6) cells, with areas between 5-10% of the footprint of the cell, were averaged and normalized according to the following equation: Relative change = I(t) – I(0). Where I(0) is the intensity at the beginning of the time series and I(t) is the intensity at time point t. Changes in the mean square displacement (MSD) and diffusion constant (D) were calculated as described (16).

Biotinylation

HEK293T cells were transfected with pCINEO/IRES-GFP-HA-TRPV5 or pCINEO/IRES-GFP. Cells were incubated at 37ºC with standard external solution pH 6.0 or pH 8.5 for 10 min before cells were placed on ice to inhibit endo- and exocytosis. Subsequent biotinylation was performed on ice as described previously (17). Thus, at the point of biotin incubation the pH of the solutions was equal in all conditions, thereby preventing differences in cell surface labeling due to pH sensitivity of biotinylation. The purified biotinylated surface proteins were probed for the presence of TRPV5 by immunoblotting using anti-TRPV5.

Statistical analysis

In all experiments, data are expressed as mean ± SEM. Overall statistical significance was determined by analysis of variance (ANOVA) followed by Bonferroni contrast analysis to investigate individual significance using Instat 3 software for Macintosh (San Diego, CA, USA). P values below 0.05 were considered significant.

Results

Extracellular pH determines TRPV5-mediated Ca^{2+} influx

In kidney, TRPV5 is exposed to pro-urine pH values ranging from 6 to 7 (2). Using electrophysiological recordings TRPV5 has been reported to be regulated by both intra- and extracellular pH (4, 5). To further assess the role of extracellular pH on TRPV5 activity ^{45}Ca^{2+} uptake in transiently transfected Human Embryonic Kidney (HEK293T) cells was investigated at different extracellular pH values. At pH 6.0, ^{45}Ca^{2+} uptake of TRPV5-expressing cells was not significantly different from mock (EGFP) transfected cells indicating a lack of functional TRPV5 channels at the cell surface. At pH 7.4, however, ^{45}Ca^{2+} uptake of TRPV5-expressing cells was significantly higher compared to mock transfected cells and extracellular alkalinization (pH 8.5) further increased ^{45}Ca^{2+} uptake of TRPV5-expressing cells **(Fig. 1A)**. Interestingly, extracellular pH had no significant effect on TRPM7-mediated ^{45}Ca^{2+} uptake in this pH range, showing the specificity of the pH effect on TRPV5 activity **(Fig. 1B)**. Furthermore, electrophysiological recordings of HEK293 cells transiently expressing TRPV5 were used to investigate the pH dependence of channel activity. Extracellular alkalinization from pH 6.0 to 8.5 resulted in a rapid increase in TRPV5 activity while extracellular acidification from pH 8.5 to pH 6.0 revealed a rapid decrease in TRPV5 activity **(Fig. 1C)**.

The intracellular lysine (K607) and the extracellular glutamic acid (E522) residues of TRPV5 have been postulated as pH sensors regulating TRPV5 activity, although K607N and E522Q mutants still displayed pH-sensitivity (4, 5). To further assess the pH dependence of these mutants ^{45}Ca^{2+} uptake measurements were performed with HEK293T cells transiently expressing these mutated channels **(Fig. 1D)**. Cells expressing EGFP-TRPV5 E522Q or EGFP-TRPV5 K607N exhibited pH-dependent ^{45}Ca^{2+} uptake activity that was not significantly different from wild-type EGFP-TRPV5. Importantly, expression levels of these mutants were equal to wild-type EGFP-TRPV5 **(Fig. 1E)**.
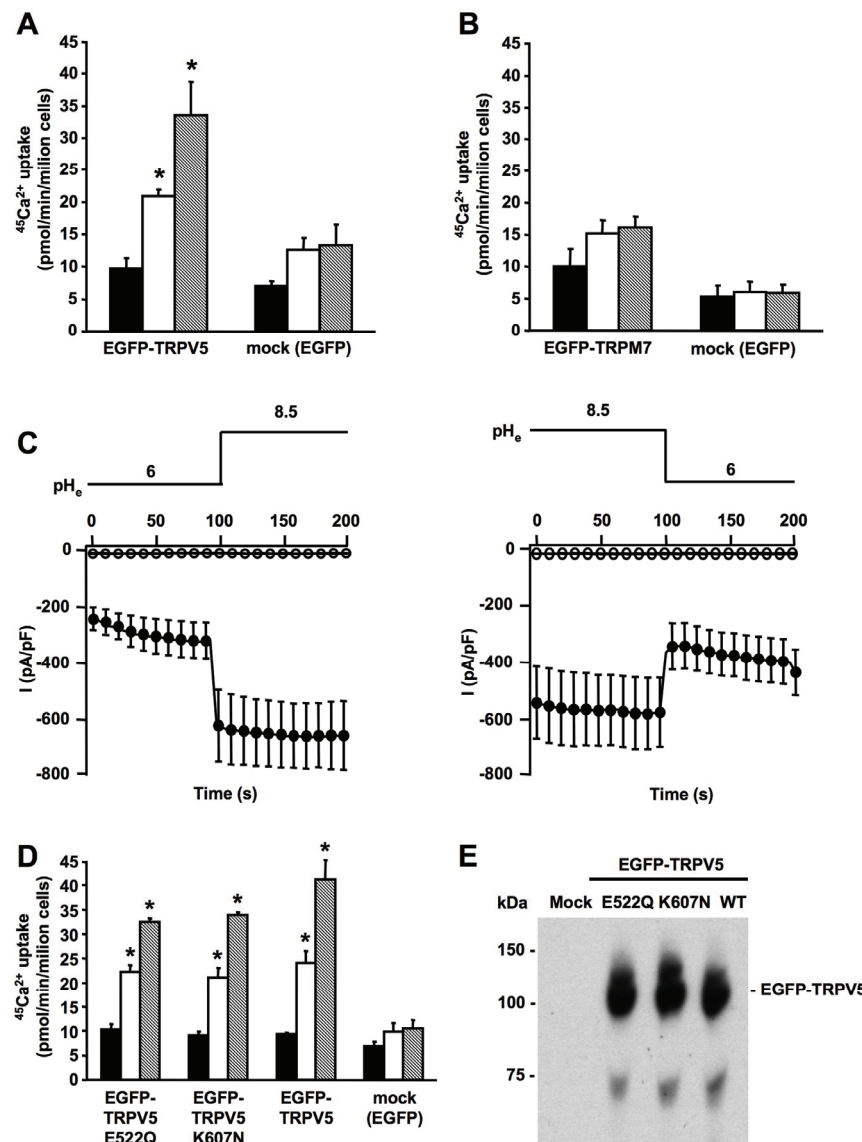
Fig. 1. Alkaline pH stimulates the activity of TRPV5 $^{45}Ca^{2+}$ uptake at different extracellular pH values of HEK293T cells expressing EGFP-TRPV5 (n=6) **(A)**, or EGFP-TRPM7 (n=6) **(B)** compared to $^{45}Ca^{2+}$ uptake of mock (EGFP) transfected cells (n=6). Black bars represent $^{45}Ca^{2+}$ uptake at pH 6.0, open bars at pH 7.4 and dashed at pH 8.5. **(C)** Whole cell current voltage relation measured from 400 ms voltage ramps (interval = 10 s) in nominally DVF solution in HEK293 cells transiently expressing TRPV5 (n = 10). Extracellular pH was switched at indicated time points. Open symbols represent traces of mock transfected HEK293 cells. **(D)** Comparison of alkaline pH-stimulated $^{45}Ca^{2+}$ uptake in HEK293T cells transfected with EGFP, EGFP-TRPV5 or EGFP-TRPV5 E522Q or EGFP-TRPV5 K607N. Black bars represent $^{45}Ca^{2+}$ uptake at pH 6.0, open bars at pH 7.4 and dashed at pH 8.5. **(E)** Expression of EGFP-TRPV5 and EGFP-TRPV5 mutants as analyzed by immunoblotting using the anti-GFP antibody. Significant differences in pH-dependent $^{45}Ca^{2+}$ uptake compared to mock transfected cells are indicated by an asterisk (p<0.05).

Extracellular alkalinization stimulates insertion of TRPV5 at the plasma membrane

pH-dependent $^{45}Ca^{2+}$ uptake in TRPV5-expressing cells can be explained by altered activity of TRPV5 present at the cell surface or changes in the number of functional TRPV5 channels at the plasma membrane. Because cellular trafficking processes, like endo- and exocytosis, are regulated by extracellular pH (7-9), the trafficking of TRPV5 was assessed by TIRF

microscopy. Detailed analysis of EGFP-labeled TRPV5 in transiently transfected HEK293T cells with live cell confocal and TIRF microscopy revealed a highly motile punctuate distribution pattern with no clear plasma membrane localization **(Fig. 2A, Movies IA and IB)**. Immunocytochemistry in fixed cells expressing TRPV5 showed no co-localization of the channel with markers for endosomes (EEA1), lipid rafts (Caveolin1), endoplasmic reticulum (58K) and lysosomes (LAMP1) **(data not shown)**. TIRF microscopy indicated that these EGFP-TRPV5-containing vesicles move in an undirected manner **(Movie IB)**. To investigate the influence of extracellular pH on these EGFP-TRPV5-containing vesicles, TIRF microscopy was applied to monitor the number and proximity of vesicles to the plasma membrane in response to changes in extracellular pH **(Fig. 2B/C, movie IIA)**. Alkalinization resulted in a rapid elevation of the overall EGFP-TRPV5 TIRF signal to a peak plateau level suggesting rapid recruitment and subsequent delivery of EGFP-TRPV5 to the plasma membrane **(Fig. 2C/D)**. Subsequent acidification decreased the overall EGFP-TRPV5 TIRF signal, even below the initial unstimulated level of fluorescence, suggesting retrieval of TRPV5 from the plasma membrane to a cytosolic compartment. Importantly, no significant changes in TIRF signal were observed in EGFP-TRPM7 or EGFP transfected HEK293T cells when switching the pH from 6.0 to 8.5 or from 8.5 to 6.0 **(Fig. 2C/D, Movies IIB/C)**. This indicates that recruitment of TRPM7 is independent of extracellular pH and fluorescent changes were not due to a pH sensitivity of EGFP. TIRF microscopy is a valuable method to study protein movements within the periplasmic space, but does not define plasma membrane expression. Therefore, cell surface biotinylation was applied to investigate the localization of TRPV5 in the plasma membrane at different extracellular pH values **(Fig. 2E)**. Importantly, at the point of incubation with biotin the pH of the solutions was equal in all conditions to prevent differences in cell surface labeling due to pH sensitivity of biotinylation (see methods for details). In line with the results obtained with TIRF microscopy, cell surface expression of TRPV5 was significantly increased (2.35 ± 0.75 fold) at pH 8.5 compared to pH 6.0.

Functional recovery after chemobleaching of TRPV5 activity is regulated by extracellular pH

Madin-Darby Canine Kidney type-I epithelial (MDCK) cells stably expressing TRPV5 were used to assess the pH dependence of TRPV5 trafficking by Functional Recovery After Chemobleaching (FRAC) (18). MDCK cells are convenient for imaging of EGFP-TRPV5-containing vesicles in contrast to transfected HEK293T cells that display a high density of EGFP-TRPV5-containing vesicles. In agreement with the observations in HEK293T cells, extracellular alkalinization of TRPV5-expressing MDCK cells resulted in rapid recruitment of EGFP-TRPV5 towards the plasma membrane, while subsequent acidification reduced cell surface EGFP-TRPV5 expression **(Supplemental data Fig. SI, Movie IIIA).** 2-(trimethylammonium)ethyl methanethiosulfonate bromide (MTSET) irreversibly binds to an

accessible cysteine in the channel pore of wild-type rabbit TRPV5 (19). This enabled us to study FRAC without introducing cysteine residues in the TRPV5 pore, which could potentially alter channel activity. Addition of MTSET to stably EGFP-TRPV5-expressing MDCK cells completely silenced $^{45}Ca^{2+}$ uptake at pH 6.0, 7.4 and 8.5 **(Fig. 3)**, confirming the accessibility of the cysteine in the TRPV5 pore and the blockade by MTSET. Cells only pre-incubated for 10 min with MTSET, showed a subsequent functional recovery of $^{45}Ca^{2+}$ uptake at pH 7.4 and 8.5, whereas no recovery was observed at pH 6.0. At pH 8.5 the recovery of $^{45}Ca^{2+}$ uptake was significantly increased compared to the recovery at pH 7.4 demonstrating that extracellular alkalinization amplified the insertion of active TRPV5 channels. Furthermore, incubation with the TRPV5 channel antagonist ruthenium red (10 μM) during the $^{45}Ca^{2+}$ uptake completely inhibited functional recovery after MTSET treatment, indicating that the recovery is mediated by TRPV5.

"Kiss and linger" plasma membrane delivery of TRPV5-containing vesicles

In MDCK cells stably expressing EGFP-TRPV5 TIRF single vesicle fluorescence rapidly increased after switching from pH 6.0 to 8.5 and reached a peak plateau level within 10-20 s, whereas subsequent extracellular acidification decreased the vesicle fluorescence **(Fig. 4A/B, Movie IIIB)**. These findings indicate that recruitment to and subsequent retrieval of single TRPV5-containing vesicles from the plasma membrane is affected by extracellular pH. Moreover, TRPV5-containing vesicles appeared to remain intact at the plasma membrane interface since the fluorescence intensity did not disperse after reaching the peak plateau level. In addition, the number of vesicles within the TIRF field did not increase, suggesting that the rise in fluorescence reflects rapid recruitment of TRPV5-containing vesicles just underneath the plasma membrane.
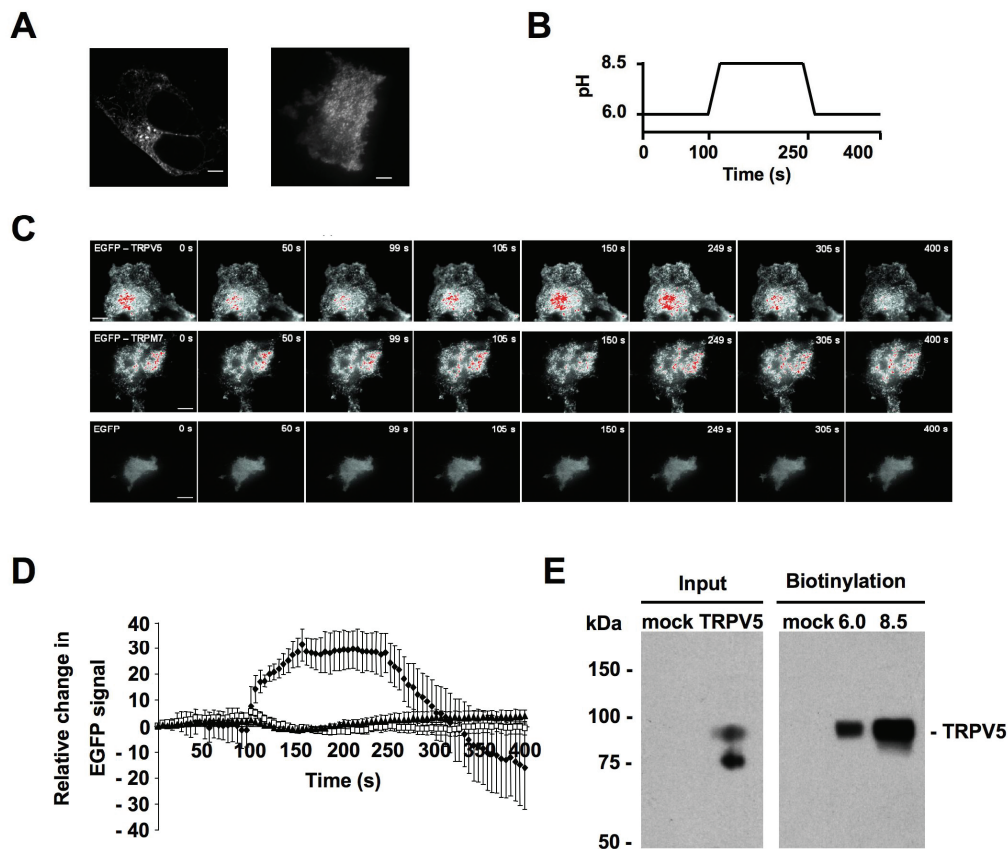
Fig. 2. Alkaline pH stimulates plasma membrane insertion of TRPV5 channels in HEK293T cells

Confocal (left) and TIRF (right) image of a single HEK293T cell expressing EGFP-TRPV5 **(A)** **(supplemental Movies IA/B)**. Scale bar = 5 μm. TIRF images of single HEK293T cells expressing EGFP-TRPV5, EGFP-TRPM7 or EGFP **(B/C) (supplemental Movies IIA/B/C)**. Scale bar = 10 μm. Cells were imaged as indicated in the figure and extracellular pH was switched at the indicated time points. Gradient filters were applied such that saturating levels turn red. Time course of the overall EGFP fluorescence signal in EGFP-TRPV5- (♦, n=5), EGFP-TRPM7- (□, n=5) or EGFP- (▲, n=5) expressing HEK293T cells **(D)**. Cell surface expression of TRPV5 at different extracellular pH values as measured by cell surface biotinylation of HA-TRPV5-expressing HEK293T cells **(E)**. Analysis of total TRPV5 expression revealed a non-glycosylated form (lower band) and a complex glycosylated form (upper) that is the band accessible to extracellular biotin. A representative blot of three independent experiments is shown.

To determine the vesicle motility upon consecutively extracellular alkalinization and acidification we calculated the Mean Square Displacement (MSD) **(Fig. 4C)**. Upon extracellular alkalinization TRPV5-containing vesicles were rapidly converted in lateral motility from a high to a more restricted velocity. The decrease in MSD occurred as the vesicle fluorescence increased, suggesting capture of TRPV5-containing vesicles at the plasma membrane as soon as they approach the cell surface. During subsequent decrease of vesicle fluorescence due to extracellular acidification, TRPV5-containing vesicles are rapidly

converted to a high lateral motility, suggesting retrieval from the plasma membrane to a cytosolic compartment. Note that the average diffusion constant as calculated from changes in MSD (16) of several vesicles from different cells before recruitment and after retrieval was identical **(Fig. 4D).** Because the diffusion constant is determined by the radius of the vesicle as reflected by the Stokes and Einstein equation (20) these findings further support that TRPV5-containing vesicles remain intact during the delivery of TRPV5 to the cell surface.
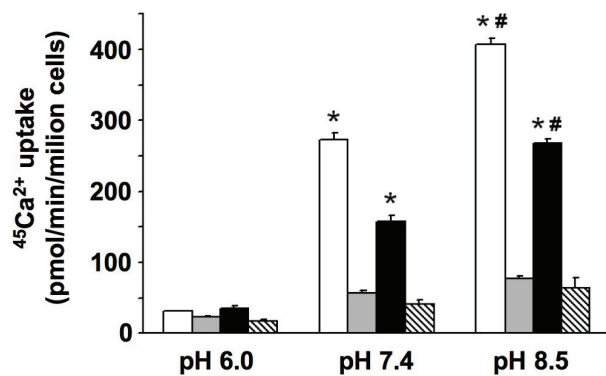

Fig. 3. Functional recovery of TRPV5 activity after chemobleaching is elevated at alkaline pH.
$^{45}Ca^{2+}$ uptake at different extracellular pH values of MDCK cells stably expressing EGFP-TRPV5 (n=6). To inhibit TRPV5-mediated $^{45}Ca^{2+}$ uptake 10 μM of ruthenium red was added. The irreversible blocker 2-(trimethylammonium)ethyl methanethiosulfonate bromide (MTSET) (5 mM) was applied to study the functional recovery of TRPV5 after MTSET treatment. Open bars represent $^{45}Ca^{2+}$ uptake under normal conditions, gray bars with continues presence of MTSET, black bars recovery after MTSET treatment and dashed bars recovery in the presence of ruthenium red. Significant differences in pH-dependent $^{45}Ca^{2+}$ uptake compared to MTSET or ruthenium red treated cells are indicated by an asterisk (p<0.05). Significant increases in $^{45}Ca^{2+}$ uptake as compared to $^{45}Ca^{2+}$ uptake at pH 7.4 are indicated by a hash (p<0.05).

Discussion

The present study identifies extracellular pH as a dynamic switch controlling TRPV5 cell surface expression and, thereby, TRPV5 activity. This conclusion is based on the following experimental observations. First, extracellular alkalinization increases, whereas acidification decreases TRPV5 channel activity. Second, extracellular alkalinization induces rapid recruitment of EGFP-TRPV5 containing vesicles that remain intact at the plasma membrane interface, whereas subsequent acidification results in retrieval of TRPV5-containing vesicles. Third, extracellular alkalinization augments the number of TRPV5 channels at the plasma membrane as analyzed by cell surface protein biotinylation. Fourth, functional recovery of TRPV5 activity after chemobleaching is dependent on extracellular pH. Fifth, TRPV5 vesicles undergo a rapid conversion in lateral motility from high to restricted as they approach the membrane and visa versa during manipulation of the extracellular pH.

Here, we showed that the activity of TRPV5 is directly controlled by the extracellular pH as measured by electrophysiological recordings and $^{45}Ca^{2+}$ uptake analysis. This is in line with our previous studies demonstrating that the current density of TRPV5-expressing HEK293 cells is significantly smaller at pH 6.0 compared to pH 7.4. At pH 8.5 they were slightly larger (4-6). Subsequently, Huang and coworkers further substantiated our findings by showing that both extracellular and intracellular acidification reduces TRPV5 channel activity (4-6). In addition, two pH-sensing residues were identified in TRPV5. Compared to wild-type TRPV5, mutation of these amino acids (K607N and E522Q) revealed a significantly diminished electrophysiological response to intra- and extracellular pH, although the overall pH sensitivity persisted. Our $^{45}Ca^{2+}$ uptake experiments indicated that mutation of these residues does not change the activity of TRPV5 in the pH range 6.0-8.5, suggesting that the role of these amino acids as pH sensors is less pronounced as previously assumed. Despite this controversy, all observations share an important physiological role of the extracellular pH in determining TRPV5 activity. Indeed, the pH of the pro-urine in the TRPV5-expressing tubule segments normally varies between 6 and 7, a range by which TRPV5 activity is significantly altered. Furthermore, early observations showed that urinary Ca^{2+} excretion increases during metabolic and respiratory acidosis (21, 22), which is in line with the observed pH-sensitivity of TRPV5.

To determine the molecular mechanism by which extracellular protons inhibit TRPV5 channel activity a comprehensive set of experiments was performed. TIRF analysis, biotinylation assays and functional recovery of TRPV5 activity after chemobleaching together demonstrated that extracellular pH determines the cell surface localization of TRPV5. Importantly, the increase in single vesicle recruitment upon alkalinization was accompanied by a rise in TRPV5 activity, suggesting capture of functional channels at the plasma membrane. Subsequent acidification decreased the TRPV5 activity that was accompanied by retrieval of TRPV5-containing vesicles from the plasma membrane to the cytosol. Previous data describing that conformational changes within the channel pore are coupled to inhibition of TRPV5 by protons (4), together with our results suggest that the extracellular pH affects the activity of TRPV5 via multiple mechanisms. Both TRPV5 trafficking to and activity at the cell surface are inhibited by extracellular protons indicating an efficient regulation of TRPV5 channel activity during changes in extracellular pH.
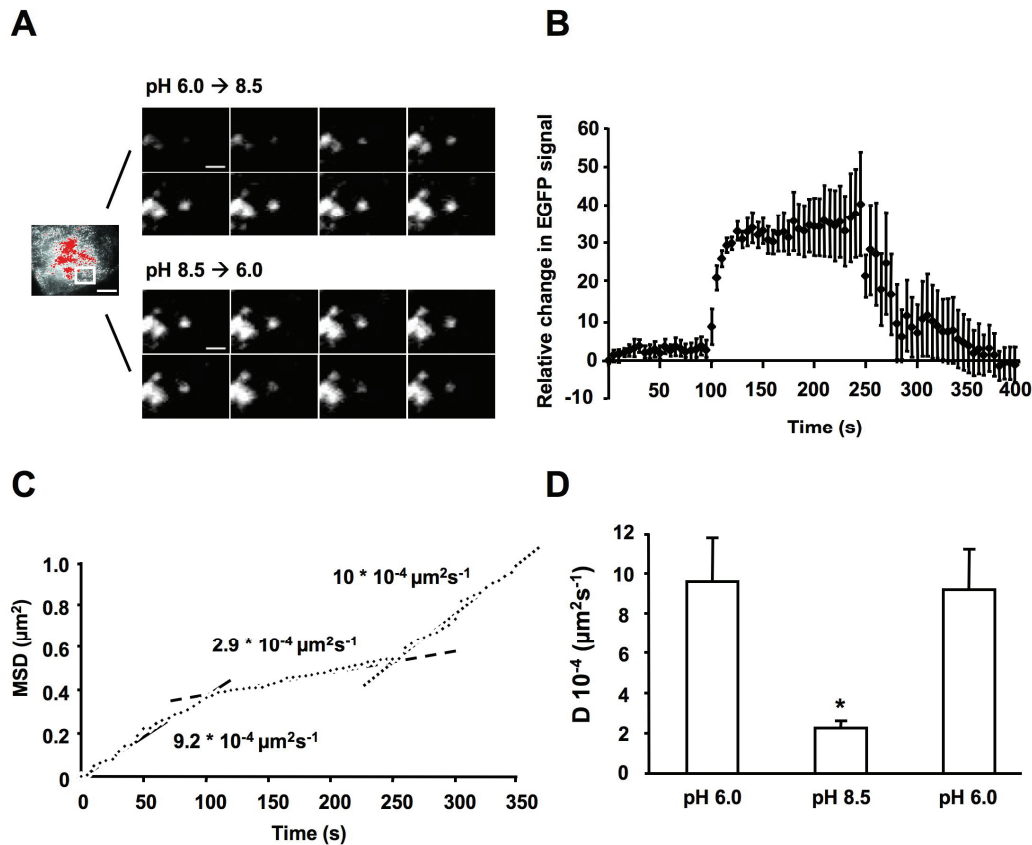
Fig. 4. Alkaline pH stimulates plasma membrane recruitment of TRPV5-containing vesicles in MDCK cells

TIRF images of a single vesicle in MDCK cells stably expressing EGFP-TRPV5 directly after extracellular alkalinization (upper panel) and subsequent acidification (lower panel) **(A)** **(supplemental Movie IIIB)**. Time interval between images is 3 s and scale bar = 2 μm. Average time course of single vesicle fluorescence in EGFP-TRPV5-expressing MDCK cells (n=5) **(B)**. The mean square displacement (plotted accumulative in time) of the vesicle shown in **(A)** reveals a rapid conversion from cytosolic diffusion at pH 6.0 (solid line) to a more restricted lateral motion at pH 8.5 (dashed line) and back to free cytosolic diffusion at pH 6.0 (dotted line) **(C)**. Averaged vesicle diffusion constant **(D)** (n=10 vesicles) during the protocol (pH 6.0 at time points 0-100 s, pH 8.5 at 125-250 s and subsequent pH 6.0 at 275-400 s). Significant difference in the diffusion constant compared with cells exposed to pH 6.0 is indicated by an asterisk (p<0.05).

TIRF analysis revealed that upon stimulation by extracellular alkalinization the EGFP-TRPV5 fluorescence of single vesicles rapidly reaches a peak plateau level. Importantly, this fluorescence signal did subsequently not disperse while the pH was maintained at 8.5, suggesting that the TRPV5-containing vesicles are not completely fused with the plasma membrane, but rather remain intact at the membrane interface. This finding is different from that observed with TIRF recordings of GLUT4-containing vesicles or synaptic vesicles (23, 24). Upon stimulation GLUT4-containing vesicles were recruited towards the cell surface where they completely fused with the membrane and GLUT4 diffused into the plasma

membrane as reflected by dispersion of the vesicle fluorescence. On the other hand, synaptic vesicles translocated towards the plasma membrane after stimulation where a transient opening with the plasma membrane is formed. Upon exocytosis of its cargo, these vesicles immediately relocated to the cytosol as measured by the sudden loss in fluorescence of intact vesicles (termed "kiss and run") (25). TRPV5 recruitment during extracellular alkalinization is, however, comparable with plasma membrane recruitment of TRPC5-containing vesicles by EGF stimulation (12). After initiation of plasma membrane recruitment both TRPV5- and TRPC5-containing vesicles did not clearly fuse with the membrane as reflected by the lack of fluorescence diffusion and disappearance of single vesicles after reaching the cell surface. These channels might access the extracellular solution from inside the vesicle membrane (referred to as "kiss and linger"), as supported by the accompanied increase in activity, enhanced accessibility to biotin and, for TRPV5, increased FRAC. Because several TRP channels, including TRPV5 and TRPC5, display constitutive activity, the suggested "kiss and linger" mechanism of channel delivery to the plasma membrane is attractive since this novel concept integrates a direct response to physiological stimuli by TRP channel insertion. The experiments with TRPC5 could not distinguish between actual vesicle fusion and subsequent diffusion of the channel into the plasma membrane or transient interaction of the vesicles with the plasma membrane (12). The performed experiments, however, enabled us to control TRPV5 plasma membrane expression by consecutive alkalinization and acidification of the extracellular solution. Our results indicate that single vesicles, located just underneath the plasma membrane, are rapidly recruited towards the plasma membrane upon extracellular alkalinization, linger at the plasma membrane without fusing, and are subsequently retrieved to the cytosol upon removal of the stimulus (i.e. extracellular acidification). Together with the increase in TRPV5 activity, enhanced accessibility to biotin and functional recovery of TRPV5 activity after chemobleaching, this suggests that upon extracellular alkalinization recruited TRPV5 accesses the extracellular environment via transient openings because the same vesicles are intact relocated upon extracellular acidification. Comparable with secretory vesicles in synapses, vesicles are recaptured largely intact after exocytosis (25, 26). Thus, recapturing non-fused vesicles from the plasma membrane might occur via uniform mechanisms.

In summary, these findings demonstrate recruitment of TRPV5 to the cell surface as a novel mechanism underlying pH-sensitive TRPV5-mediated Ca^{2+} transport. Thereby contributing to the concept that activation of constitutive active ion channels relies on "kiss and lingering" vesicles which remain intact during the process of plasma membrane recruitment and subsequent retrieval.

References

1. Montell, C., Birnbaumer, L., Flockerzi, V., Bindels, R. J., Bruford, E. A., Caterina, M. J., Clapham, D. E., Harteneck, C., Heller, S., Julius, D., Kojima, I., Mori, Y., Penner, R., Prawitt, D., Scharenberg, A. M., Schultz, G., Shimizu, N. & Zhu, M. X. (2002) *Mol Cell* **9,** 229-31.
2. Hoenderop, J. G., Nilius, B. & Bindels, R. J. (2005) *Physiol Rev* **85,** 373-422.
3. Nijenhuis, T., Renkema, K. Y., Hoenderop, J. G. & Bindels, R. J. (2006) *J Am Soc Nephrol* **17,** 617-26.
4. Yeh, B. I., Kim, Y. K., Jabbar, W. & Huang, C. L. (2005) *Embo J* **24,** 3224-34.
5. Yeh, B. I., Sun, T. J., Lee, J. Z., Chen, H. H. & Huang, C. L. (2003) *J Biol Chem* **278,** 51044-52.
6. Vennekens, R., Prenen, J., Hoenderop, J. G., Bindels, R. J., Droogmans, G. & Nilius, B. (2001) *Pflugers Arch* **442,** 237-42.
7. Glunde, K., Guggino, S. E., Solaiyappan, M., Pathak, A. P., Ichikawa, Y. & Bhujwalla, Z. M. (2003) *Neoplasia* **5,** 533-45.
8. Keyes, S. R. & Rudnick, G. (1982) *J Biol Chem* **257,** 1172-6.
9. Lindgren, C. A., Emery, D. G. & Haydon, P. G. (1997) *J Neurosci* **17,** 3074-84.
10. Kanzaki, M., Zhang, Y. Q., Mashima, H., Li, L., Shibata, H. & Kojima, I. (1999) *Nat Cell Biol* **1,** 165-70.
11. Bahner, M., Frechter, S., Da Silva, N., Minke, B., Paulsen, R. & Huber, A. (2002) *Neuron* **34,** 83-93.
12. Bezzerides, V. J., Ramsey, I. S., Kotecha, S., Greka, A. & Clapham, D. E. (2004) *Nat Cell Biol* **6,** 709-20.
13. Oancea, E., Wolfe, J. T. & Clapham, D. E. (2006) *Circ Res* **98,** 245-53.
14. den Dekker, E., Schoeber, J., Topala, C. N., van de Graaf, S. F., Hoenderop, J. G. & Bindels, R. J. (2005) *Pflugers Arch* **450,** 236-44.
15. van de Graaf, S. F., Hoenderop, J. G., Gkika, D., Lamers, D., Prenen, J., Rescher, U., Gerke, V., Staub, O., Nilius, B. & Bindels, R. J. (2003) *Embo J* **22,** 1478-87.
16. Steyer, J. A. & Almers, W. (1999) *Biophys J* **76,** 2262-71.
17. Chang, Q., Hoefs, S., van der Kemp, A. W., Topala, C. N., Bindels, R. J. & Hoenderop, J. G. (2005) *Science* **310,** 490-3.
18. Sun, H., Shikano, S., Xiong, Q. & Li, M. (2004) *Proc Natl Acad Sci U S A* **101,** 16964-9.
19. Dodier, Y., Banderali, U., Klein, H., Topalak, O., Dafi, O., Simoes, M., Bernatchez, G., Sauve, R. & Parent, L. (2004) *J Biol Chem* **279,** 6853-62.
20. Rusakov, D. A. & Kullmann, D. M. (1998) *Proc Natl Acad Sci U S A* **95,** 8975-80.
21. Sutton, R. A., Wong, N. L. & Dirks, J. H. (1979) *Kidney Int* **15,** 520-33.
22. Canzanello, V. J., Bodvarsson, M., Kraut, J. A., Johns, C. A., Slatopolsky, E. & Madias, N. E. (1990) *Kidney Int* **38,** 409-16.
23. Li, C. H., Bai, L., Li, D. D., Xia, S. & Xu, T. (2004) *Cell Res* **14,** 480-6.
24. Gundelfinger, E. D., Kessels, M. M. & Qualmann, B. (2003) *Nat Rev Mol Cell Biol* **4,** 127-39.
25. Gandhi, S. P. & Stevens, C. F. (2003) *Nature* **423,** 607-13.
26. Taraska, J. W., Perrais, D., Ohara-Imaizumi, M., Nagamatsu, S. & Almers, W. (2003) *Proc Natl Acad Sci U S A* **100,** 2070-5.

CHAPTER III

Regulation of the Epithelial Ca^{2+} Channel, TRPV6, by the Ca^{2+}-Sensor Calmodulin

[*]**Lambers T.T.**, [*]Weidema A.F., [#]Nilius B., [*]Hoenderop J.G., [*]Bindels R.J.

[*]Department of Physiology, Nijmegen Center for Molecular Life Sciences, University Medical Centre Nijmegen, The Netherlands.
[#]Department of Physiology, Campus Gasthuisberg, KU Leuven, Belgium.

Summary

TRPV5 and TRPV6 are members of the superfamily of transient receptor potential (TRP) channels and facilitate Ca^{2+} influx in a variety of epithelial cells. The activity of these Ca^{2+} channels is tightly controlled by the intracellular Ca^{2+} concentration in close vicinity to the channel mouth. The molecular mechanism underlying the Ca^{2+}-dependent activity of TRPV5/TRPV6 is, however, still unknown. Here, the putative role of calmodulin (CaM) as the Ca^{2+}-sensor mediating the regulation of channel activity was investigated. Overexpression of Ca^{2+}-insensitive CaM mutants (CaM_{1234} and CaM_{34}) significantly reduced the Ca^{2+} as well as Na^+ current of TRPV6, but not of TRPV5, expressing HEK293 cells. By combining pull-down assays and co-immunoprecipitations we demonstrated that CaM binds to both TRPV5 and TRPV6 in a Ca^{2+}-dependent fashion. The binding of CaM to TRPV6 was localized to the transmembrane domain ($TRPV6^{327-577}$) and consensus CaM-binding motifs located in the N-(1-5-10 motif, $TRPV6^{88-97}$) and C-terminus (1-8-14 motif, $TRPV6^{643-656}$) suggesting a mechanism of regulation involving multiple interaction sites. Subsequently, chimeric TRPV6/TRPV5 proteins, in which the N- and/or C- termini of TRPV6 were substituted by that of TRPV5, were co-expressed with CaM_{34} in HEK293 cells. Exchanging, the N- and/or C-terminus of TRPV6 by that of TRPV5 did not effect the CaM_{34}-induced reduction of the Ca^{2+} and Na^+ current. In conclusion, these results suggest that CaM positively affects TRPV6 activity upon Ca^{2+} binding to EF-hand 3 and 4 located in the high Ca^{2+} affinity CaM C-terminus, which involves the N- and C-terminus and the transmembrane domain of TRPV6.

Introduction

The superfamily of transient receptor potential (TRP) channels is involved in diverse processes ranging from sensory activity to fertility and epithelial Ca^{2+} transport (1). The submembers TRPV5 (formerly named ECaC1) and TRPV6 (formerly named CaT1) are postulated as gatekeepers facilitating epithelial Ca^{2+} influx in kidney and small intestine (2,3). Initial electrophysiological characterization of these channels revealed that TRPV5 and TRPV6 are homologous channels that display a Ca^{2+}-dependent feedback regulation of channel activity. Differences between these channels concern their divalent cation permeability, the kinetics of Ca^{2+}-dependent inactivation and subsequent recovery (4). Furthermore, it was shown that TRPV5 and TRPV6 form functional homo- and heterotetrameric channels displaying intermediate phenotypes (5). At present, the molecular mechanism underlying these differences in Ca^{2+}-dependent activity is unknown.

 Ca^{2+}-regulated channel activity is not restricted to TRPV5 and TRPV6 since a diverse range of voltage and non-voltage-dependent ion channels are regulated by the intracellular Ca^{2+} concentration. Ca^{2+}-dependent regulation of the L- and P/Q-type voltage-gated Ca^{2+} channels (Cav) is mediated by the ubiquitously expressed Ca^{2+}-sensor calmodulin (CaM) (6,7). CaM

consists of four Ca^{2+}-binding EF-hand structures, which are localized in the N- and C-terminus. Ca^{2+} binding to CaM is highly cooperative with Ca^{2+} binding first to the C-terminal EF-hands, which have the highest affinity for Ca^{2+}, followed by Ca^{2+} binding to lower affinity sites located in the N-terminus (8). The CaM termini can differentially regulate ion channel activity as shown by electrophysiological analysis of Ca^{2+}-dependent regulation of P/Q- and L-type Cav channels (6,7). Ca^{2+} binding to the high Ca^{2+}-affinity C-terminus of CaM selectively induces P/Q-type Cav channel facilitation, whereas Ca^{2+}-sensing by the low Ca^{2+}-affinity N-terminus induces channel inactivation. Thus, CaM acts as a Ca^{2+}-sensor translating the local Ca^{2+} signals that modulate these channels (7).

Consensus CaM binding motifs have been identified in associated proteins (9). CaM binding to Cav is localized to an IQ-like motif in the α1C- (L-type Cav) and α1A C-terminus (P/Q-type Cav). Although, TRPV5 and TRPV6 lack an IQ-related motif a previous study indicated that CaM binds to the TRPV6 C-terminus in a Ca^{2+}-dependent manner (4,10). The described mechanism of competitive regulation of TRPV6 by protein kinase C (PKC) and CaM is, however, restricted to human TRPV6 since this PKC site in the CaM–binding motif is not conserved between different species (10). Recently, the corresponding region in mouse TRPV6 was shown to bind CaM. Detailed analysis of this region predicted a caseine kinase motif, but no significant phosphorylation could be detected in this particular domain (11). Also other members of the TRP family are possibly regulated by CaM. CaM binding to TRPV1 was restricted to a 35 amino-acid segment in the C-terminus and deletion of this CaM binding segment prevented TRPV1 desensitization (12). Members of the TRPC family have been shown to bind CaM (13). Another study using CaM inhibitors described that TRPC6 can be regulated by CaM (14). Furthermore, CaM acts as a Ca^{2+}-sensor in the Ca^{2+}-dependent feedback inhibition of TRPC1 as demonstrated using Ca^{2+}-insensitive CaM mutants (15).

The aim of the present study was to investigate the potential role of CaM in Ca^{2+}-dependent regulation of TRPV5 and TRPV6 activity. To this end, we combined pull-down assays and co-immunoprecipitations with electrophysiological analysis of HEK293 cells heterologously expressing TRPV5, TRPV6 or TRPV5/6 chimeras in combination with Ca^{2+}-insensitive CaM mutants.

Experimental procedures

Construction of mammalian expression vectors

CaM, CaM_{1234}, CaM_{12}, and CaM_{34} were mutated (D --> A) in the EF-hand structures present in the N- and C-terminus resulting in (partial) Ca^{2+} insensitive mutants (16). CaM, CaM_{1234}, CaM_{12}, and CaM_{34} (kindly provided by Dr. Adelman) (16) used in the patch-clamp analysis were cloned by polymerase chain reaction (PCR) into the pCINeo/IRES-BFP vector (17)

using the sense primer (5' GGGACTAGT<u>ATG</u>GCTGACCAACTGACTGAA 3') and the antisense primer (5' GGGCTGGAG<u>TCA</u>CTTCGCTGTCATCATTTG 3'). CaM_{34} was cloned by PCR into pGEX6p-2 (Amhersham Pharmacia Biotech, Roosendaal, Netherlands) using the sense primer (5' CGCGGATCC<u>ATG</u>GCTGACCAACTGACTGAA 3') and the antisense primer (5' GGGGTCGAC<u>TCA</u>CTTCGCTGTCATCATTTG 3'). Mouse TRPV5-, rabbit TRPV6- and TRPV5/6 chimeras-pCINeo/IRES-GFP were constructed as described previously [18]. In short, TRPV5 and TRPV6 N-termini were exchanged in pCINeo/IRES-GFP constructs via an introduced unique *Bsp*EI site at amino acid position Ser^{221}-Tyr^{222} and C-termini were exchanged via an introduced unique *Bsi*WI site at amino acid position Arg^{615}-Ser^{616}. The fragment IQ-α1C ($\alpha1C^{1589-1708}$) containing the IQ-like motif from the L-type Ca^{2+}-channel α-subunit C-terminus (kindly provided by Dr. Birnbaumer) [19], the TRPV5 N- and C-terminus and truncated forms of the TRPV6 C-terminus were cloned into the oocyte-pT7Ts expression vector using PCR. Sense primers contained an EcoRV restriction site, a Kozak sequence, and ATG at the 5' end with ATG in frame with the triplet encoding the first amino acid. Antisense primers contained a SpeI restriction site at the 3' end with a stop codon in frame after the last amino acid. Truncated forms of the TRPV6 N-terminus were cloned into the pT7Ts expression vector (using a sense primer as described above). The antisense primer contained a BstEII restriction site at the 3' end with a stop codon in frame after the last amino acid. All pCINeo/IRES-BFP, pGEX6p-2 and pT7Ts constructs were verified by sequence analysis.

Cell culture and transfection

Human Embryonic Kidney (HEK293) cells were grown in DMEM (Bio Whittaker Europe, Vervier, Belgium) containing 10% (v/v) fetal calf serum (PAA, Linz, Austria), 13 mM $NaHCO_3$, 2 mM L-glutamine, 2 U/ml penicillin and 2 mg/ml streptomycin at 37 °C in a humidity controlled incubator with 5% CO_2. The cells were transiently transfected with the pCINeo/IRES-GFP and pCINeo/IRES-BFP vectors using lipofectamine 2000 (Invitrogen-Life Technologies, Breda, Netherlands) as described previously [17]. The GFP-containing vector was used for TRPV5, TRPV6 and TRPV5/6 chimeras, while the BFP-containing vector was used for CaM constructs. Transfected cells were identified visually by their green and/or blue appearance as described previously [17]. GFP/BFP-negative cells from the same batch of cells were used as controls.

Electrophysiology

Electrophysiological methods have been described previously in detail [17,20]. Whole cells currents were measured using an EPC-9 amplifier (HEKA, Lambrecht, Germany) using ruptured patches. Electrode resistances were 3-6 MΩ, and capacitance and access resistance

was monitored continuously. A ramp protocol, consisting of linear voltage-ramps from -100 to +100 mV within 450 ms, was applied every 2 s from a holding potential of +20 mV. Ca^{2+}-dependent inactivation was studied using a 3 second voltage step to –100 mV from a holding potential of +70 mV. Current densities, expressed per unit of membrane capacitance, were calculated from the current at –80 mV during the ramp protocols (21).

Solutions and experimental procedures

The standard extracellular solution ("Krebs") contained 150 mM NaCl, 6 mM CsCl, 1 mM $MgCl_2$, 10 mM HEPES/NaOH pH 7.4 and 10 mM Glucose. The concentration of Ca^{2+} was varied between 1 and 10 mM. Divalent free solutions did not contain added divalent cations, while trace amounts of divalent cations were removed with 100 μM EDTA. To inhibit monovalent cation currents, 150 mM NaCl was replaced with an equimolar amount of N-methyl-D-glucamine-Cl. The standard internal (pipette) solution contained 20 mM CsCl, 100 mM Cs-aspartate, 1 mM $MgCl_2$, 4 mM Na_2ATP, 10 mM BAPTA, 10 mM HEPES/CsOH pH 7.2. Cells were kept in nominal Ca^{2+}-free medium to prevent Ca^{2+} overload and exposed for maximal 5 min to a Krebs solution containing 1.5 mM Ca^{2+} before sealing the patch pipette to the cell. All experiments were performed at room temperature (RT).

CaM binding assays

pT7Ts constructs were linearized and cRNA was synthesized *in vitro* using T7-RNA polymerase as described previously (21). [^{35}S]Methionine labeled TRPV5 and TRPV6 proteins were prepared *in vitro* using a reticulocyte lysate system in the presence of canine microsomal membranes (Promega Madison, WI, USA). To investigate potential interactions [^{35}S]methionine labeled proteins were incubated for 2 h at RT either with CaM-coupled agarose beads or non-coupled agarose beads (Sigma-Aldrich, St. Louis MO, USA) in Tris buffered saline (TBS) pH 7.4 containing 1% (v/v) Triton X-100 and either 1 mM $CaCl_2$ or 5 mM EDTA. For pull-down experiments with CaM_{34} shown in Fig. 4B, GST-CaM_{34} and GST were expressed in and purified from transformed *Escherichia coli* BL21 according to the manufacturer's protocol (Amersham Pharmacia Biotech, Roosendaal, Netherlands). For pull-down experiments shown in Fig. 7 the indicated amount of free Ca^{2+} was buffered with EGTA as calculated with SLIDERS version 2.10 (www.stanford.edu/~cpatton/maxc.html). After extensive washing, bound proteins were subjected to SDS-polyacrylamide gel electrophoresis and binding was established by autoradiography.

Xenopus laevis oocytes were isolated as described previously (22) and subsequently co-injected with 5 ng Flag-tagged TRPV6 cRNA (23) and 15 ng CaM cRNA. For each immuno-precipitation 20 oocytes were lysed by incubation for 30 min on ice in buffer containing 150 mM NaCl, 20 mM Tris-HCl pH 7.5, 2 mM $CaCl_2$, 10% (v/v) glycerol, 1% (v/v) NP-40, 0.5%

(w/v) sodium desoxycholate and protease inhibitors leupeptine (0.01 mg/ml), pepstatine (0.05 mg/ml) and PMSF (1 mM). The lysates were centrifuged for 30 min at 16000 g and supernatants were incubated with protein A beads (Kem-En-Tec A/S, Kopenhagen, Denmark), coated o/n at 4 °C with either rabbit anti-TRPV6 antiserum (23) (1:3000) or monoclonal anti-CaM (Campro-scientific, Veenendaal, Netherlands) (1:2000). After extensive washing with lysis buffer, bound proteins were subjected to SDS-polyacrylamide gel electrophoresis. After immuno blotting co-immuno precipitation was investigated by incubating either with anti-CaM or peroxidase coupled anti-Flag (Sigma-Aldrich, St. Louis MO, USA).

Statistical analysis.

Data are expressed as mean ± SEM. Overall statistical significance was determined by analysis of variance. In case of significance ($p < 0.05$), individual groups were compared using Student t-test.
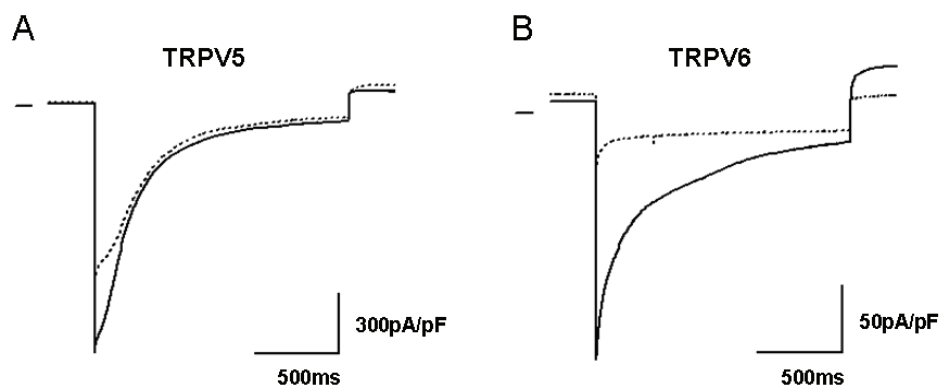

Figure 1. Effect of Ca^{2+} insensitive CaM (CaM$_{1234}$) on TRPV5 and TRPV6 Ca^{2+} current kinetics. Mean currents through TRPV5 **(A)** or TRPV6 **(B)** expressing HEK293 cells in response to a voltage step to -100 mV (V$_H$ = +70mV) in the presence of 10 mM [Ca^{2+}]$_e$. Other cations were substituted by 150 mM NMDG$^+$. Cells were loaded with 10 mM BAPTA. Control traces are shown as solid lines, while CaM$_{1234}$ traces are depicted as dotted lines. Zero current concentration is presented by a small bar at the left of each figure. n > 11 cells.

Results

Effect of CaM on TRPV5 and TRPV6 activity

To study the potential role of CaM in modulating TRPV5 and TRPV6, the activity of these channels was determined by whole-cell patch-clamp analysis in HEK293 cells transiently co-transfected with Ca^{2+}-insensitive CaM mutants and TRPV5 or TRPV6. The CaM mutant (CaM$_{1234}$) in which all four EF-hand structures were mutated, significantly reduced the inward

Ca^{2+} current in response to a hyperpolarizing voltage step in TRPV6 expressing HEK293 cells **(Fig. 1B)** (p_{peak} < 0.05, n > 11 cells), but had no significant effect on TRPV5 expressing HEK293 cells **(Fig. 1A)** (p_{peak} > 0.0.5, n > 11 cells). Likewise, the Na^+ current measured with a ramp protocol was reduced in TRPV6 and CaM_{1234} expressing cells, whereas in TRPV5 expressing cells no effect was observed **(Fig 2)**. Subsequently, partial Ca^{2+}-insensitive CaM mutants were co-transfected with TRPV5 or TRPV6 in HEK293 cells **(Fig. 2)**. CaM constructs were mutated (D --> A) in either the low Ca^{2+} affinity site present in the N-(CaM_{12}) or the high Ca^{2+} affinity site present in the C-terminus (CaM_{34}). Overexpression of CaM_{1234} or CaM_{34} significantly reduced the Ca^{2+} as well as the Na^+ current density in TRPV6 expressing HEK293 cells, but did not affect the currents of TRPV5 expressing cells. In contrast, the expression of CaM_{12} did not significantly affect the Ca^{2+} or Na^+ currents of TRPV5 or TRPV6 expressing HEK293 cells. Thus, the high affinity EF-hand Ca^{2+} binding sites contribute primarily to the observed CaM effect on TRPV6 activity.
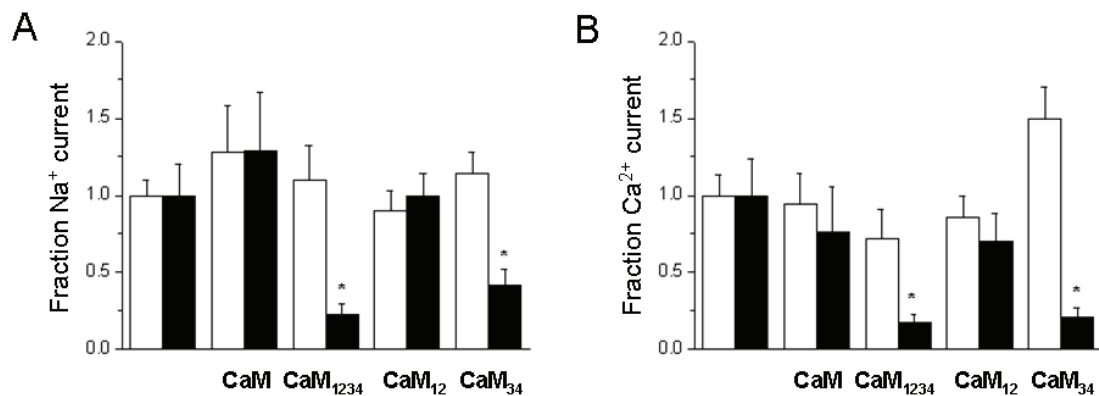

Figure 2. **Effect of CaM mutants on TRPV5 and TRPV6 activity.** Data obtained from linear ramps from +100 to −100 mV, holding potential was +20 mV. Currents were normalized to the density at −80 mV of controls. HEK293 cells heterologously expressing either TRPV5 or TRPV6 and CaM mutated in EF-hands in the N-terminus (CaM_{12}) or C-terminus (CaM_{34}) or both (CaM_{1234}) as indicated on the X-axis. **(A)** Effect of CaM and CaM mutants on Na^+ current densities (100 μM EDTA in bath) **(B)**. Effect of CaM_{WT} and CaM mutants on Ca^{2+} current densities in 10 mM $[Ca^{2+}]_e$ (Open bars, TRPV5; solid bars, TRPV6). Significant differences from controls are indicated by an asterisk (p < 0.05, n = 7-23 cells).

CaM binding to TRPV5 and TRPV6

Subsequently, CaM binding to TRPV5 and TRPV6 was investigated. Binding was determined using CaM coupled agarose beads and *in vitro* translated full-length TRPV5 or TRPV6. In the presence of Ca^{2+} (1 mM $CaCl_2$), CaM bound to TRPV6, whereas in the absence of Ca^{2+} (5 mM EDTA) binding was virtually abolished **(Fig. 3A)**. Likewise, TRPV5 bound CaM as determined for TRPV6, although CaM mutants do not affect currents in TRPV5-expressing

HEK293 cells. Binding experiments of *in vitro* translated full-length TRPV5 and TRPV6 to non-coupled and CaM-coupled agarose beads in the presence of Ca^{2+} indicated both TRPV5 and TRPV6 specifically bind CaM **(Fig. 3B)**. Subsequently, we tested the association of TRPV6 and CaM by co-immunoprecipitation studies. To this end, CaM and Flag-TRPV6 were co-expressed in *Xenopus laevis* oocytes and immunoprecipitated with the CaM or TRPV6 antibodies. Immunoblots containing the precipitated complexes were probed with a peroxidase-coupled Flag antibody or the CaM antibody, respectively. CaM (17 KDa) co-immunoprecipitated with the Flag-TRPV6 and vice versa, confirming the association of CaM and TRPV6 **(Fig. 3C-D)**.
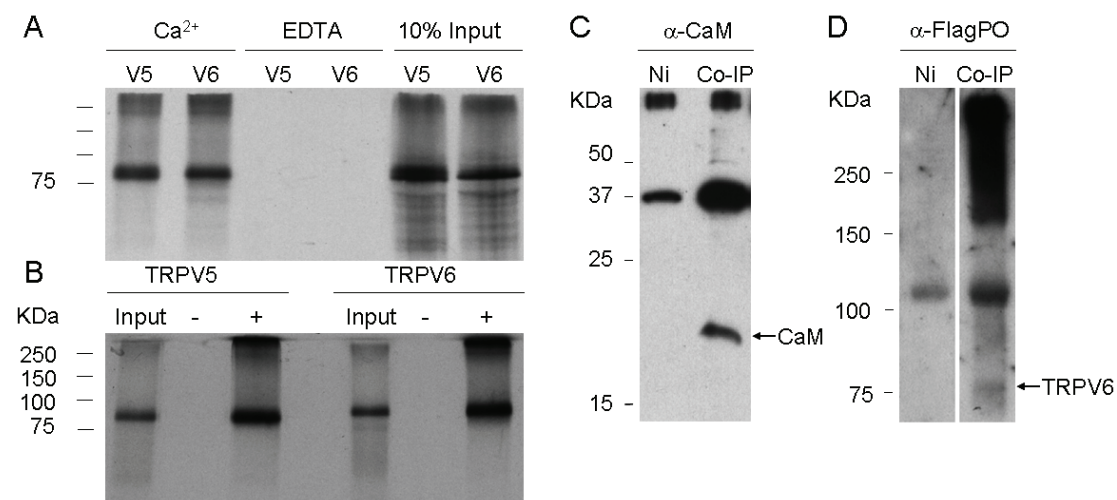

Figure 3. CaM binding to TRPV5 and TRPV6. [^{35}S]Methionine labeled, *in vitro* translated full-length TRPV5 or TRPV6 was incubated with CaM-coupled agarose beads either in the presence (1 mM $CaCl_2$) or absence (5 mM EDTA) of Ca^{2+} **(A)**. [^{35}S]Methionine labeled, *in vitro* translated full-length TRPV5 or TRPV6 was incubated with either CaM-coupled (+) or non-coupled (-) agarose beads in the presence (1 mM $CaCl_2$) of Ca^{2+} **(B)**. Input control is 10% of the pull-down input. *Xenopus laevis* oocytes were co-injected with 15 ng CaM_{WT} cRNA and 5 ng flag-tagged TRPV6 cRNA. Oocyte lysates were loaded to protein A beads coated either with anti-TRPV6 **(C)** or monoclonal anti-CaM **(D)**. Blots were incubated with monoclonal anti-CaM **(C)** or peroxidase-coupled monoclonal anti-flag

To further identify the CaM binding site in TRPV5 and TRPV6 the N-termini (TRPV5$^{1-327}$, TRPV6$^{1-326}$) and C-termini (TRPV5$^{578-730}$, TRPV6$^{577-727}$) were *in vitro* translated and subsequently CaM binding was determined **(Fig. 4A)**. The described IQ-like CaM-binding motif in the C-terminus of α1C (24) was used as a positive control, whereas TRPV5 transmembrane region TRPV5$^{421-512}$ was used as a negative control. Besides the positive control, the N- and C-terminus of both TRPV5 and TRPV6 bound CaM in the presence of Ca^{2+}, whereas no binding was observed with the negative control. In addition, it was

demonstrated that both TRPV5 and TRPV6 bind to GST-CaM$_{34}$ in a Ca^{2+}-independent manner **(Fig. 4B)**. Furthermore, the TRPV6 transmembrane domain (TRPV6$^{327-577}$) was *in vitro* translated and subsequently CaM binding was determined **(Fig. 4C)**. The TRPV6 transmembrane domain bound CaM only in the presence of Ca^{2+} although binding seems weaker than CaM binding to both TRPV6 tails.
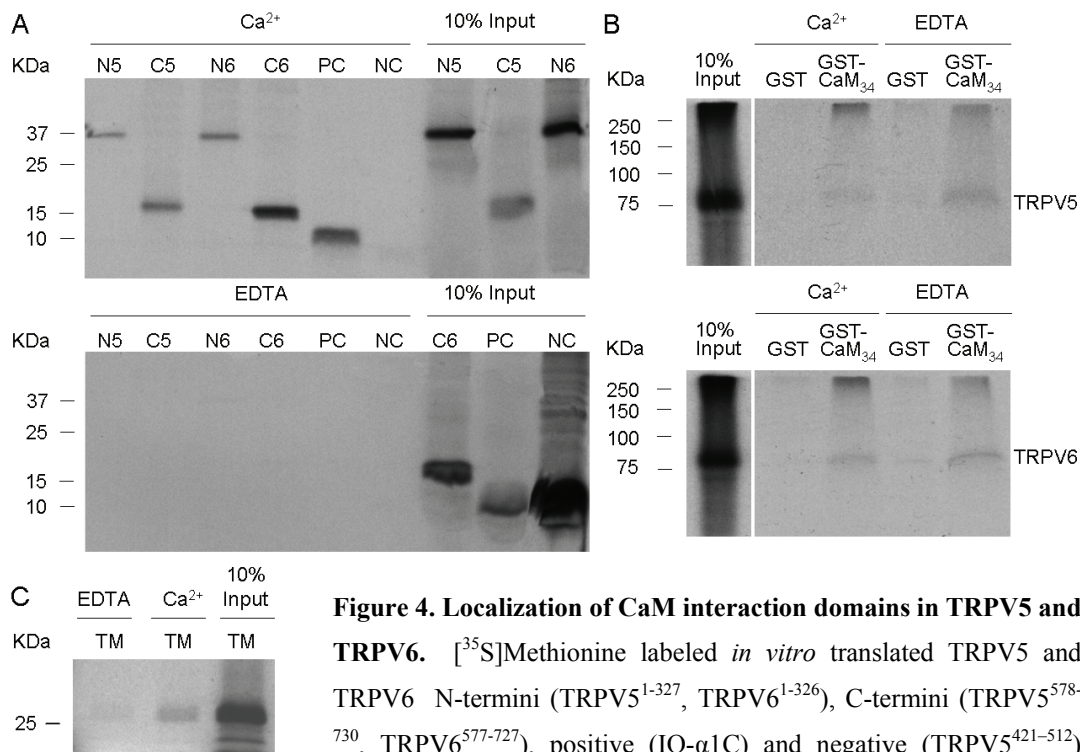

Figure 4. Localization of CaM interaction domains in TRPV5 and TRPV6. [^{35}S]Methionine labeled *in vitro* translated TRPV5 and TRPV6 N-termini (TRPV5$^{1-327}$, TRPV6$^{1-326}$), C-termini (TRPV5$^{578-730}$, TRPV6$^{577-727}$), positive (IQ-α1C) and negative (TRPV5$^{421-512}$) controls were incubated with CaM-coupled agarose beads in the presence of 5 mM EDTA or 1 mM CaCl$_2$ **(A)**. [^{35}S]Methionine labeled *in vitro* translated TRPV5 and TRPV6 were incubated with GST and GST-CaM$_{34}$ in the presence of 5 mM EDTA or 1 mM CaCl$_2$ **(B)**. [^{35}S]Methionine labeled *in vitro* translated TRPV6 transmembrane domain (TRPV6$^{327-577}$) was incubated with CaM-coupled agrose beads in the presence of 5 mM EDTA or 1 mM CaCl$_2$ **(C)**. Input control is 10% of the pull-down input.

Functional effect of CaM-binding domains in TRPV6

Subsequently, TRPV5/6 chimeras were used in order to identify the critical domains in TRPV6 for the inhibition by CaM$_{34}$. To this end, the effect of CaM$_{34}$ on the Ca^{2+} and Na$^+$ current density was examined in HEK293 cells expressing the TRPV5/6 chimera, in which the N- and/or C-termini were exchanged **(Fig. 5)**. Co-transfection of CaM$_{34}$ and TRPV6-C5, the chimera in which the TRPV6 C-terminus was substituted by that of TRPV5, revealed a reduction of both the Ca^{2+} and Na$^+$ current as observed with co-transfection of CaM$_{34}$ and wild-type TRPV6. Co-transfection of CaM$_{34}$ with TRPV6-N5, the chimera in which the N-terminus of TRPV6 was substituted by that of TRPV5, resulted in a reduction of the Ca^{2+} and Na$^+$ current as compared to currents in TRPV6-N5 expressing cells. Co-transfection of CaM$_{34}$

and TRPV6-N5C5 , the chimera in which both termini of TRPV6 were substituted by that of TRPV5, resulted in a reduction of the Ca^{2+} and Na^+ current as compared to currents measured in TRPV6-N5C5 expressing cells.
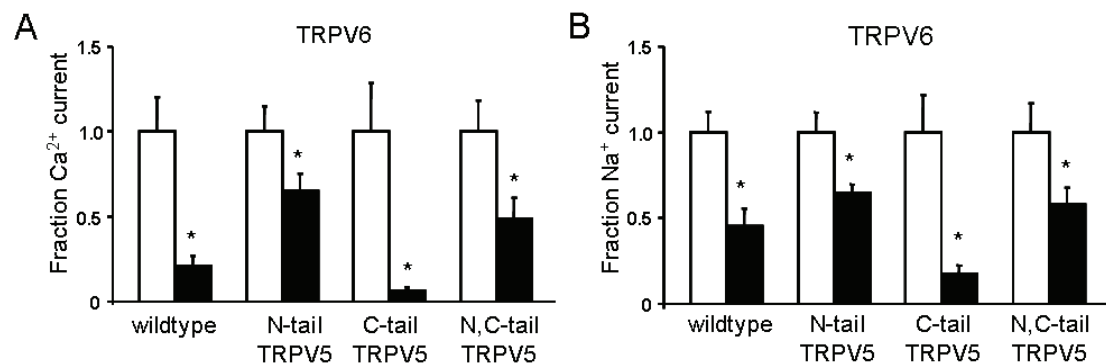

Figure 5. Effect of the N-, C-terminus and transmembrane domain of TRPV6 on the inhibitory effect of CaM_{34}. Effects of CaM_{34} on Na^+ current density of TRPV6 expressing HEK293 cells with 100 μM EDTA in the bath solution. Data obtained from linear ramps from +100 to −100 mV, holding potential was +20 mV. Currents were normalized to the density at −80 mV of controls. TRPV6 chimeras (TRPV6 N- and/or C-termini replaced by that of TRPV5) were used for the experiments. Open bars represent control currents; solid bars represent co-transfection with CaM_{34} (n > 12 cells).

Elucidation of the CaM binding sites in TRPV6

A series of TRPV6 N- and C-terminal deletion mutants were constructed as depicted in **Fig. 6**. Truncated forms of TRPV6 were *in vitro* translated and binding was determined as described above. The interaction between TRPV6 N-terminus and CaM was abolished when the N-terminus was truncated at position 93, whereas truncations at positions 103 up to 266 had no effect on the interaction with CaM **(Fig. 6A).** This indicates that CaM binds the TRPV6 N-terminus in a region at position 93 − 103. Detailed analysis revealed that this putative CaM binding region consists of an α-helix according to the structural prediction program GORIV (www.expasy.org). A 1-5-10 motif with consensus sequence (FILVW)xxx(FAILVW)xxxx(FILVW) is present in this particular binding region **(Fig. 6B)**. The interaction between TRPV6 C-terminus and CaM was partially abolished when the C-terminus was truncated at position 655, whereas truncations at position 649 and 642 completely abolished CaM binding **(Fig. 6C).** Truncation at position 667 up to 695 had no effect on the interaction with CaM. These findings suggest that CaM binds the TRPV6 C-terminus at position 649 − 667. This putative binding region contains a 1-8-14 motif with consensus sequence (FILVW)xxxxxx(FAILVW)xxxxx(FILVW) and consists of an α-helix **(Fig. 6D)**.
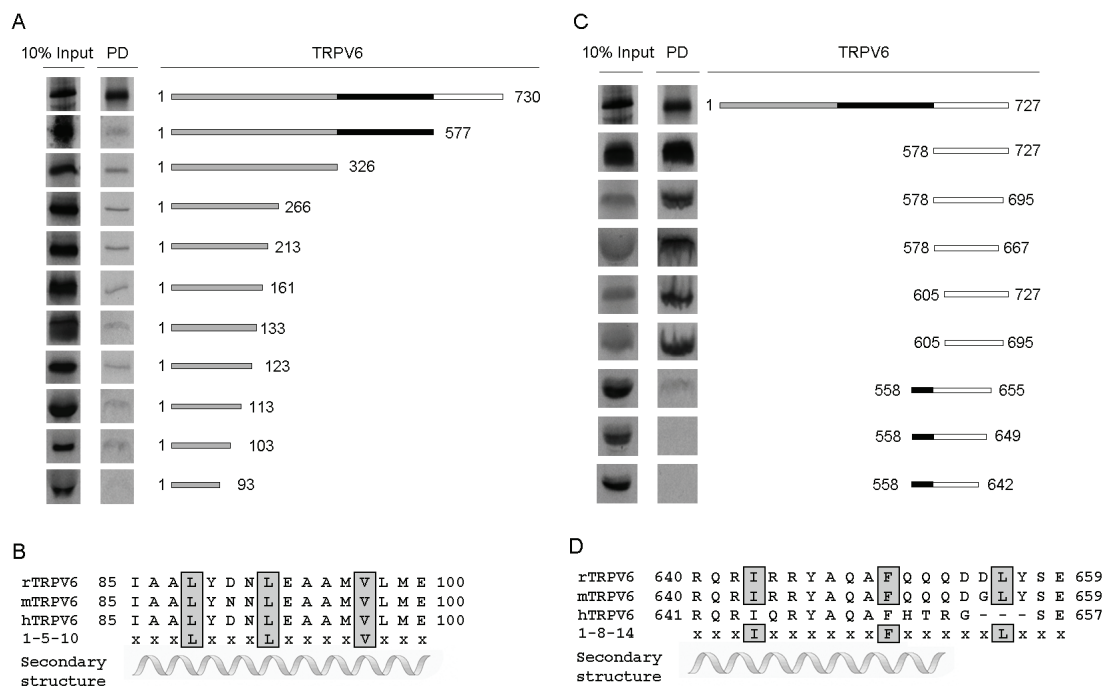
Fig. 6. Mapping of the CaM binding site in the N- and C-terminus of TRPV6. [^{35}S]Methionine labeled *in vitro* translated N- **(A)** or C-termini **(C)** truncates were constructed and incubated with CaM-coupled agarose beads in the presence of 1 mM Ca^{2+}. Input control is 10% of the pull-down input. **(B,D)** Alignment of N- or C-terminal CaM binding motif of different species with consensus CaM binding motifs (boxed). From top to bottom: Rat TRPV6 (AF160798); Mouse TRPV6 (NM022413); Human TRPV6 (NM018646). The structure prediction program GORIV (www.expasy.org) was used to determine whether this region consists of an alpha helix.

CaM binding to TRPV5 and TRPV6 at low Ca^{2+} concentrations

The Ca^{2+}-dependent binding of CaM to TRPV5 and TRPV6 was studied in detail using the TRPV5 and TRPV6 N-termini (TRPV5$^{1-327}$, TRPV6$^{1-326}$) and C-termini (TRPV5$^{578-730}$, TRPV6$^{577-727}$) in the absence or presence of increasing amounts of Ca^{2+} **(Fig. 7)**. Both the TRPV5 N- and C-termini bound CaM at a Ca^{2+}-concentration of 30 nM or higher, whereas binding is lost in the absence of Ca^{2+} (Fig. 7A). Similar observations were made for TRPV6 **(Fig. 7B)**, thus CaM is bound to both TRPV5 and TRPV6 at Ca^{2+}-concentrations as low as 30 nM.

Discussion

The present study identified CaM as a Ca^{2+}-sensor specifically regulating TRPV6 activity. This is based on the following observations. First, electrophysiological measurements of HEK293 cells heterologously expressing TRPV5 or TRPV6 and CaM mutants revealed that

TRPV6, but not TRPV5, is regulated by CaM although both channels bind CaM in a Ca^{2+}-dependent fashion. Second, the effect of CaM is mediated by the high Ca^{2+} affinity EF-hand structures 3 and 4 present in the C-terminus of CaM. Third, binding studies indicated that CaM binds in a Ca^{2+}-dependent fashion to both the TRPV5 and TRPV6 N-termini ($TRPV5^{1-327}$, $TRPV6^{1-326}$) and C-termini ($TRPV5^{578-730}$, $TRPV6^{577-727}$) and to the TRPV6 transmembrane domain ($TRPV6^{327-577}$). Fourth, co-transfection of CaM_{34} and various TRPV5/6 chimeras revealed that the effect of CaM is mediated via the identified CaM-binding domains in TRPV6.
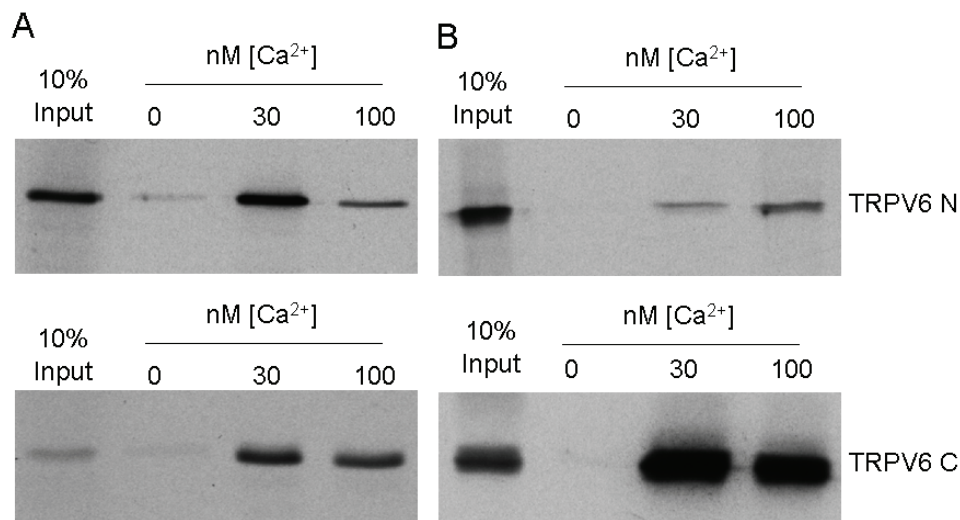

Fig. 7. CaM binding to TRPV5 and TRPV6 at low Ca^{2+} concentrations. [^{35}S]Methionine labeled *in vitro* translated TRPV5 **(A)** and TRPV6 **(B)** N- and C-termini were incubated with CaM coupled agarose beads in the absence (5 mM EGTA) or presence of increasing concentrations of Ca^{2+} (30 or 100 nm). Input control is 10% of the pull-down input. The figure shown is a representative blot of 3 independent experiments.

Previously, it has been shown that TRPV5 and TRPV6 activity is negatively regulated by the intracellular Ca^{2+} concentration and the ubiquitously expressed CaM could potentially play a regulatory role in this process (10,11,25). Interestingly, CaM is involved in Ca^{2+}-dependent regulation of TRPV6 only, since CaM_{1234} significantly reduced the Ca^{2+} and Na^+ current density in TRPV6 expressing HEK293 cells, whereas TRPV5-mediated currents were not significantly altered. This latter finding is remarkable given the high homology between both channels, similar Ca^{2+} dependent regulation of channel activity and binding of CaM to both channels. The effect of CaM_{1234} was localized to the high Ca^{2+} affinity EF-hand structures in the CaM C-terminus (EF hand 3 and 4). Overexpression of CaM_{34}, the CaM mutant that lacks high affinity Ca^{2+}-binding, reduced the TRPV6 current density to the same extent as CaM_{1234}, whereas CaM_{12} did not effect TRPV6 currents. The effect of CaM_{34} on TRPV6 is not restricted to the Ca^{2+} current since also the Na^+ current density was inhibited when CaM_{34} is

co-expressed. Together these results imply that CaM positively affects TRPV6 activity at basal Ca^{2+} concentrations via either structural changes in TRPV6 leading to an increased open probability, or via accumulation of active channels on the plasma membrane. However, to date several studies on voltage-operated Ca^{2+} channels indicated that CaM can regulate channel activity on the plasma membrane, whereas little evidence has been presented for effects on the routing of the channels (6,7,26-29).

The association of CaM with TRPV5 was localized to the N-terminus (TRPV5$^{1-327}$) and C-terminus (TRPV5$^{578-730}$). The association of CaM with TRPV6 was localized to consensus CaM binding motifs in α-helical structures present in the N- and C-terminus and to the transmembrane part (TRPV6$^{327-577}$) of TRPV6, where CaM binds in a Ca^{2+}-dependent fashion. The N-terminal binding is localized to a consensus 1-5-10 motif (position 88-92-97) that is identical among different TRPV6 species. A 1-5-10 motif is a classical region for binding of Ca^{2+}-CaM, which fits with the Ca^{2+}-dependent binding of CaM to the TRPV6 N-terminus. The C-terminal binding is localized to a consensus 1-8-14 motif (position 643-650-656) that is identical between mouse and rat TRPV6. However, human TRPV6 does not contain a 1-8-14 motif at this particular position, which might explain the previous observation that CaM binding to human TRPV6 is localized to a different region (10). When mouse TRPV6 is truncated at the position corresponding to the described human binding region (10) it still binds CaM, whereas truncations in the identified 1-8-14 motif virtually abolished CaM binding (this study). The mouse TRPV6 peptide, corresponding to the described human binding region, binds CaM (11), however these results are not in line with our results. Based on the fact that only the TRPV6 activity was inhibited by CaM$_{34}$, despite binding of CaM$_{WT}$ and CaM$_{34}$ to both TRPV5 and TRPV6, suggests that the regulatory effect of CaM is restricted to TRPV6.

TRPV5 and TRPV6 chimeras were used in order to identify the essential domains of TRPV6 for the CaM effect since CaM mutants had no effect on TRPV5 expressing HEK293 cells and TRPV5/6 chimeras give functional channels (18). The TRPV6 domains that bind CaM all contribute to the CaM$_{34}$ effect because chimeras in which the N- and/or C-terminus of TRPV6 were substituted by that of TRPV5, revealed a significant decrease in both the Ca^{2+} and Na^+ current density when CaM$_{34}$ was co-expressed. Comparison of current amplitudes of the different chimeras suggests that the TRPV6 N-terminus contributes predominantly to the inhibitory effect of CaM$_{34}$, because the CaM$_{34}$-induced decrease is maximally diminished when the TRPV6 N-terminus is substituted by that of TRPV5.

The dominant negative effect of CaM mutants on TRPV6 activity suggests a constant tethering of CaM to the channel complex, since overexpression of Ca^{2+}-insensitive CaM would otherwise not interfere appreciably with currents of TRPV6 expressing HEK293 cells

containing endogenous wild-type CaM. Like described for Cav channels (29) we suggest a tight and constitutive interaction between TRPV6 and CaM. The fact that CaM inhibitors do not affect TRPV6 activity (data not shown) supports the tight and constitutive interaction, as described previously for L-type Cav channels (29). The CaM binding to the TRPV6 N- and C- terminus at a Ca^{2+} concentration as low as 30 nM suggests that CaM is tethered to TRPV6 at Ca^{2+}-concentrations normally present in resting cells (60 – 100 nm). Thus, it is likely that CaM is constitutively tethered to the TRPV6 channel complex.

In conclusion, our data demonstrate a regulatory role of CaM in TRPV6-mediated Ca^{2+} influx. The elucidated molecular mechanism possibly involves constitutively tethering of CaM to the TRPV6 channel complex. Upon Ca^{2+} sensing of the CaM C-terminus, TRPV6 activity is positively affected via combined actions at the N- and C-terminus and transmembrane domain of the channel.

References

1. Montell, C., Birnbaumer, L., Flockerzi, V., Bindels, R. J., Bruford, E. A., Caterina, M. J., Clapham, D. E., Harteneck, C., Heller, S., Julius, D., Kojima, I., Mori, Y., Penner, R., Prawitt, D., Scharenberg, A. M., Schultz, G., Shimizu, N., and Zhu, M. X. (2002) *Mol Cell* **9**, 229-231
2. Hoenderop, J. G., Nilius, B., and Bindels, R. J. (2002) *Ann Rev Physiol* **64**, 529-549
3. Hoenderop, J. G., van Leeuwen, J. P., van der Eerden, B. C., Kersten, F. F., van der Kemp, A. W., Merillat, A. M., Waarsing, J. H., Rossier, B. C., Vallon, V., Hummler, E., and Bindels, R. J. (2003) *J Clin Invest* **112**, 1906-1914
4. Hoenderop, J. G., Vennekens, R., Muller, D., Prenen, J., Droogmans, G., Bindels, R. J., and Nilius, B. (2001) *J Physiol* **537**, 747-761
5. Hoenderop, J. G., Voets, T., Hoefs, S., Weidema, F., Prenen, J., Nilius, B., and Bindels, R. J. (2003) *Embo J* **22**, 776-785
6. Zuhlke, R. D., Pitt, G. S., Deisseroth, K., Tsien, R. W., and Reuter, H. (1999) *Nature* **399**, 159-162
7. DeMaria, C. D., Soong, T. W., Alseikhan, B. A., Alvania, R. S., and Yue, D. T. (2001) *Nature* **411**, 484-489
8. Wang, C. L. (1985) *Biochem Biophys Res Commun* **130**, 426-430
9. Rhoads, A. R., and Friedberg, F. (1997) *Faseb J* **11**, 331-340
10. Niemeyer, B. A., Bergs, C., Wissenbach, U., Flockerzi, V., and Trost, C. (2001) *Proc Natl Acad Sci U S A* **98**, 3600-3605
11. Hirnet, D., Olausson, J., Fecher-Trost, C., Bodding, M., Nastainczyk, W., Wissenbach, U., Flockerzi, V., and Freichel, M. (2003) *Cell Calcium* **33**, 509-518
12. Numazaki, M., Tominaga, T., Takeuchi, K., Murayama, N., Toyooka, H., and Tominaga, M. (2003) *Proc Natl Acad Sci U S A* **100**, 8002-8006
13. Tang, J., Lin, Y., Zhang, Z., Tikunova, S., Birnbaumer, L., and Zhu, M. X. (2001) *J Biol Chem* **276**, 21303-21310
14. Boulay, G. (2002) *Cell Calcium* **32**, 201-207
15. Singh, B. B., Liu, X., Tang, J., Zhu, M. X., and Ambudkar, I. S. (2002) *Mol Cell* **9**, 739-750
16. Xia, X. M., Fakler, B., Rivard, A., Wayman, G., Johnson-Pais, T., Keen, J. E., Ishii, T., Hirschberg, B., Bond, C. T., Lutsenko, S., Maylie, J., and Adelman, J. P. (1998) *Nature* **395**, 503-507
17. Vennekens, R., Hoenderop, J. G., Prenen, J., Stuiver, M., Willems, P. H., Droogmans, G., Nilius, B., and Bindels, R. J. (2000) *J Biol Chem* **275**, 3963-3969
18. Nilius, B., Prenen, J., Hoenderop, J. G., Vennekens, R., Hoefs, S., Weidema, A. F., Droogmans, G., and Bindels, R. J. (2002) *J Biol Chem* **277**, 30852-30858
19. Wei, X., Neely, A., Olcese, R., Lang, W., Stefani, E., and Birnbaumer, L. (1996) *Receptors Channels* **4**, 205-215
20. Nilius, B., Prenen, J., Vennekens, R., Hoenderop, J. G., Bindels, R. J., and Droogmans, G. (2001) *Cell Calcium* **29**, 417-428.
21. van de Graaf, S. F., Hoenderop, J. G., Gkika, D., Lamers, D., Prenen, J., Rescher, U., Gerke, V., Staub, O., Nilius, B., and Bindels, R. J. (2003) *Embo J* **22**, 1478-1487
22. Hoenderop, J. G., van der Kemp, A. W., Hartog, A., van de Graaf, S. F., van Os, C. H., Willems, P. H., and Bindels, R. J. (1999) *J Biol Chem* **274**, 8375-8378
23. Hoenderop, J. G., Voets, T., Hoefs, S., Weidema, A. F., Prenen, J., Nilius, B., and Bindels, R. J. (2003) *Embo J* **in press**
24. Qin, N., Olcese, R., Bransby, M., Lin, T., and Birnbaumer, L. (1999) *Proc Natl Acad Sci U S A* **96**, 2435-2438
25. Hoenderop, J. G., van der Kemp, A. W., Hartog, A., van Os, C. H., Willems, P. H., and Bindels, R. J. (1999) *Biochem Biophys Res Commun* **261**, 488-492
26. Schumacher, M. A., Rivard, A. F., Bachinger, H. P., and Adelman, J. P. (2001) *Nature* **410**, 1120-1124
27. Fanger, C. M., Ghanshani, S., Logsdon, N. J., Rauer, H., Kalman, K., Zhou, J., Beckingham, K., Chandy, K. G., Cahalan, M. D., and Aiyar, J. (1999) *J Biol Chem* **274**, 5746-5754
28. Peng, C., Rich, E. D., Thor, C. A., and Varnum, M. D. (2003) *J Biol Chem* **278**, 24617-24623
29. Liang, H., DeMaria, C. D., Erickson, M. G., Mori, M. X., Alseikhan, B. A., and Yue, D. T. (2003) *Neuron* **39**, 951-960

CHAPTER IV

Calbindin-D$_{28K}$ Dynamically Controls TRPV5-Mediated Ca^{2+} Transport

[1]**Lambers T.T.**, [3]Mahieu F., [4]Oancea E., [1]Hoofd L., [2]de Lande F., [1]Mensenkamp A.R., [3]Voets T., [3]Nilius B., [4]Clapham D.E., [1]Hoenderop J.G., [1]Bindels R.J.

[1]Department of Physiology and [2]Celbiology, Nijmegen Centre for Molecular Life Sciences, Radboud University Nijmegen Medical Centre, The Netherlands
[3]Department of physiology, KU Leuven, Campus Gasthuisberg, Leuven, Belgium
[4]Department of Cardiology, Howard Hughes Medical Institute, Children's Hospital Boston, Harvard Medical School, USA

Abstract

In Ca^{2+}-transporting epithelia, calbindin-D_{28K} ($CaBP_{28K}$) facilitates Ca^{2+} diffusion from the luminal Ca^{2+} entry side of the cell to the basolateral side, where Ca^{2+} is extruded into the extracellular compartment. Simultaneously, $CaBP_{28K}$ provides protection against toxic high Ca^{2+} levels by buffering the cytosolic Ca^{2+} concentration ($[Ca^{2+}]_i$) during high Ca^{2+} influx. $CaBP_{28K}$ consistently co-localizes with the epithelial Ca^{2+} channel TRPV5, which constitutes the apical entry step in renal Ca^{2+}-transporting epithelial cells. Here, we demonstrate using protein-binding analysis, subcellular fractionation and evanescence-field microscopy that $CaBP_{28K}$ translocates towards the plasma membrane and directly associates with TRPV5 at a low $[Ca^{2+}]_i$. $^{45}Ca^{2+}$ uptake measurements, electrophysiological recordings, and transcellular Ca^{2+} transport assays of lentivirus infected primary rabbit connecting tubule / distal convolute tubule cells revealed that associated $CaBP_{28K}$ tightly buffers the flux of Ca^{2+} entering the cell via TRPV5 facilitating high Ca^{2+} transport rates by preventing channel inactivation. In summary, $CaBP_{28K}$ acts in Ca^{2+}-transporting epithelia as a dynamic Ca^{2+} buffer, regulating $[Ca^{2+}]$ in close vicinity to the TRPV5 pore by direct association with the channel.

Introduction

The vitamin D-dependent Ca^{2+}-binding proteins, named calbindins (CaBPs), are expressed in cells that are challenged by a high Ca^{2+} influx such as in brain, bone, teeth, inner ear, placenta, mammary gland, kidney and intestine. In these tissues, CaBPs (i.e. $CaBP_{9K}$ and $CaBP_{28K}$) are widely regarded as a key component in cellular Ca^{2+} handling. In Ca^{2+}-transporting epithelial cells, CaBPs display the potential to facilitate multiple steps in the process of transcellular Ca^{2+} transport. First, Ca^{2+} influx in these cells is mediated by the epithelial Ca^{2+} channels TRPV5 and TRPV6, which are distinct members of the Transient Receptor Potential (TRP) family (1) acting as gatekeepers facilitating cellular Ca^{2+} entry due to a steep inward electrochemical gradient across the luminal membrane of epithelial cells (2). The activity of these highly Ca^{2+}-selective channels is tightly regulated by the Ca^{2+} concentration in close vicinity to the channel mouth (3). Thus, adequate buffering of Ca^{2+} is essential for a continuous influx of Ca^{2+} through these channels. Second, during high rates of transcellular Ca^{2+} transport, strict regulation of the intracellular Ca^{2+} concentration ($[Ca^{2+}]_i$) is crucial in protecting the cell against the cytotoxic high levels of Ca^{2+} (4). Buffering of Ca^{2+} by specialized Ca^{2+}-binding proteins is, therefore, required (5-7). Third, Ca^{2+} entering at the luminal side of the cell has to diffuse, without affecting other intracellular processes, to the basolateral side, where the Na^{+}/Ca^{2+}-exchanger (NCX1) and/or the plasma membrane ATPase (PMCA1b) extrude Ca^{2+} into the extracellular compartment. In transepithelial Ca^{2+} transport, CaBPs have been implicated in facilitated diffusion of Ca^{2+} from the luminal membrane to the basolateral surface by increasing the diffusional range of Ca^{2+} (8, 9). Moreover, the

importance of CaBPs in Ca^{2+}-transporting epithelial cells is underlined by the consistent co-expression with the Ca^{2+} transport proteins including TRPV5, TRPV6, NCX1 and PMCA1b (10).

Negative feedback regulation of channel activity by an increased $[Ca^{2+}]_i$ is not restricted to the epithelial Ca^{2+} channels. A broad range of both voltage and non-voltage-operated ion channels are regulated by $[Ca^{2+}]_i$ (11, 12). Ion channels that are negatively regulated by Ca^{2+} inactivate upon a local rise in $[Ca^{2+}]$ in close proximity to the channel pore. Previous studies indicated that the Ca^{2+} sensor calmodulin is responsible for the Ca^{2+}-dependent regulation of particularly voltage-operated Ca^{2+} channels (13, 14). However, how $[Ca^{2+}]$ near a channel pore is regulated is not well defined. Several studies implicate CaBPs in facilitated diffusion of Ca^{2+}. However, other than mathematical models (15) and coordinated regulation of renal Ca^{2+} transport proteins (16), limited experimental data is available to substantiate these hypotheses.

In addition, previous studies indicated that CaBP$_{28K}$ acts as a cytosolic Ca^{2+} buffer to protect neurons against large fluctuations in $[Ca^{2+}]_i$ (6, 17, 18). Here, the buffer capacity of CaBP$_{28K}$ affects the shape of the postsynaptic Ca^{2+} signals and may underlie paired pulse facilitation of synapses (19-21). Recently, it was shown in cerebellar Purkinje neurons that CaBP$_{28K}$ directly interacts with membrane-targeted inositol-1,4,5-trisphosphate and acts as a Ca^{2+} sensor to regulate the degradation of inositol messengers in an activity-dependent manner (22). Thus, CaBP$_{28K}$ displays several properties that imply an important role in Ca^{2+}-induced signal transmission and hence may function not only as a Ca^{2+} buffer, but also as a Ca^{2+} sensor affecting downstream processes in the cell.

A key biochemical property specifying a Ca^{2+} sensor is the presence of EF-hand motifs that undergo a conformational change upon Ca^{2+} binding. CaBP$_{28K}$ is equipped with 6 EF-hand motifs that bind Ca^{2+} in a highly cooperative fashion. First, Ca^{2+} binds to the high affinity EF-hand site 1, followed by EF-hands 4 and 5 and finally EF-hand 3 is loaded with Ca^{2+}, in contrast to EF-hands 2 and 6 which do not bind Ca^{2+} (23). Although the crystal structure of CaBP$_{28K}$ has not been determined, structural analysis measured by nuclear magnetic resonance indicated that conformational changes occur in CaBP$_{28K}$ upon Ca^{2+} binding (24, 25).

The aim of the present study was to determine how CaBPs contribute to the regulation of TRPV5 channel activity, intracellular Ca^{2+} handling and transcellular Ca^{2+} transport in epithelial cells. By a comprehensive approach using protein-binding analysis, life cell imaging and functional assays, this study reveals a crucial role of CaBP$_{28K}$ in TRPV5-mediated transepithelial Ca^{2+} transport in kidney. Here, we show that CaBP$_{28K}$ acts as a dynamic Ca^{2+} buffer regulating the local $[Ca^{2+}]$ in close vicinity to the TRPV5 pore by direct association with the channel.

Materials and methods

Molecular biology

TRPV4, 5, and 6 N- and C-termini were cloned into the pGEX6p-2 vector (Amersham Pharmacia Biotech, Roosendaal, The Netherlands). TRPV5 was cloned into the pCINeo/IRES-EGFP expression vector as described (26) and fused to the C-terminus of EGFP or ECFP by subcloning into pEGFP-C1 and pECFP (Clontech, Palo Alto, CA, USA). $CaBP_{28K}$ was cloned into the *Xenopus laevis* oocyte expression vector pT7Ts and pEBG (27), pGEX6p-2 and pCINeo/IRES-EGFP expression vectors using PCR. An EYFP-$CaBP_{28K}$ fusion construct was generated by cloning $CaBP_{28K}$ into pEYFP-C1 (Clontech, Palo Alto, CA, USA) and a Ca^{2+}-insensitive $CaBP_{28K}$ mutant ($CaBP_{28K}\Delta EF$) was constructed by mutating the EF-hand motifs (EF1: D24A, D26A; EF2: D69A, D70A; EF3: D111A, D113A, E119A, E121A, E122A; EF4: D155A, D159A, E163A, E166A EF5: D212A, D217A, E220A; EF6: D251A). All constructs were verified by sequence analysis and the integrity of the fusion constructs was investigated by western blot analysis using a rabbit anti-GFP antibody.

Cell culture

HEK293, HEK293T, HeLa and MDCK cells were grown and transfected as described (28). MDCK cells stably expressing both EGFP-TRPV5 and $CaBP_{28K}$ were constructed similar as previously described (29) and maintained in medium containing 800 μg/ml G418/700 μg/ml hygromycine (GIBCO Europe, Breda, The Netherlands). Expression was verified using mouse or rabbit anti-$CaBP_{28K}$ (Sigma-Aldrich, Zwijndrecht, The Netherlands) and rabbit anti-GFP antibodies, respectively. Five cell line clones were pooled to eliminate differences between independent clones. For flow cytometry analysis of EGFP-TRPV5 expression, relative fluorescence intensity was measured on a FACSCalibur™ (BD Biosciences, Amsterdam, The Netherlands). Primary cultures of rabbit CNT/CCD were isolated and transepithelial Ca^{2+} transport was measured as described previously (30).

Protein-binding analysis

GST pull down assays with [^{35}S]Methionine-labeled proteins in TBS-HCl pH 7.4 containing 0.5% (v/v) NP40 and 1 mM Ca^{2+} or 5 mM EDTA, were performed as described (28). For binding competition assays increasing amounts of non-radioactive *in vitro* translated $CaBP_{28K}\Delta EF$ were included during the pull down experiment of $CaBP_{28K}$ and TRPV5.

HEK293 cells were transiently co-transfected with pEBG-$CaBP_{28K}$ and pCINeo-TRPV5-IRES-EGFP. Cells were loaded with or without 50 μM BAPTA-AM for 30 min at 37 ºC and lysed by incubation for 1 h on ice in TBS pH 7.4 containing 0.5% (v/v) NP40, 5 mM EDTA and the protease inhibitors leupeptin (0.01 mg/ml), pepstatin (0.05 mg/ml),

phenylmethylsulfonyl fluoride (1 mM) and aprotinine (5 mg/ml). The lysates were centrifuged for 30 min at 16,000 g and supernatants were incubated with glutathione sepharose beads (Amersham Bioscience, Piscataway, NJ, USA) for 16 h. After extensive washing in lysis buffer co-precipitation was performed by immunoblot analysis using guinea pig anti-TRPV5 (3).

Cell fractionation assay

Primary renal CNT/CCD cultures and transiently CaBP$_{28K}$ and TRPV5-transfected HeLa cells were homogenized in fractionation buffer (300 mM sucrose, 25 mM imidazole-HCl pH 7.4, 5 mM EDTA and protease inhibitors leupeptin (0.01 mg/ml), pepstatin (0.05 mg/ml), phenylmethylsulfonyl fluoride (1 mM) and aprotinine (5 mg/ml)). After 5 min at 4,000 g 4 ºC to remove intact cells, nuclei and mitochondria the supernatant was centrifuged at 16,000 g 4 ºC. The plasma membrane-enriched pellet fraction was subjected to SDS-PAGE and immunoblots were analyzed with rabbit anti-CaBP$_{28K}$ and rabbit anti-Na,K-ATPase (3) antibodies. The intensity of immuno-positive bands were measured and changes in the CaBP$_{28K}$ signal were expressed as a ratio of the internal control Na,K-ATPase.

Confocal, total internal reflection fluorescence microscopy and image analysis

For TRPV5 and CaBP$_{28K}$ co-localization, a Zeiss LSM510meta (Carl Zeiss GmbH, Jena, Germany) confocal laser scanning microscope was used. Images were taken with a PlanApochromatic 63x 1.4 oil immersion DIC lens (Carl Zeiss GmbH, Jena, Germany). The cytosolic localization of CaBP$_{28K}$ was quantified using Image J (NIH) software. Renal epithelial cells were divided in 5 regions (apical, apical-middle, middle, basolateral-middle, and basolateral) and the intensities of the individual regions in 30 renal cells of 6 different tubules were calculated according to the following equation:

Relative intensity = I_x / (I_{apical} + $I_{apical\ middle}$ + I_{middle} + $I_{basolateral\ middle}$ + $I_{basolateral}$)

Where I_x is the intensity of domain X; I_{apical} is the apical intensity; $I_{apical\ middle}$ is the apical middle intensity; I_{middle} is the middle intensity; $I_{basolateral\ middle}$ is the basolateral middle intensity and $I_{basolateral}$ is the basolateral intensity.

To image EYFP-CaBP$_{28K}$ in EYFP-CaBP$_{28K}$ and ECFP-TRPV5-transfected HEK293T cells a custom-built objective-based TIRF microscope was used (31). Briefly, a 488 nm solid-state diode laser (Coherent, Santa Clara, CA, USA) was focused onto a single-mode optical fiber (Newport, Irvine, CA) with a 5-axis fiber-coupler (New Focus, San Jose, CA, USA) and guided through the rear illumination port of an Olympus IX70 fluorescence microscope. The laser light reflected from a specially coated dichroic mirror (Z488RDC; Chroma Technology,

Rockingham, VT, USA) passes through a high-numerical aperture objective (N.A. 1.45, X60, Olympus, Melville, NY, USA) and was totally internally reflected by the glass–water interface ($n = 1.37$). Fluorescence emitted from tagged-proteins passed through an HQ515-30m (Chroma) filter for EGFP/EYFP before being collected by a cooled-CCD (ORCA ER II; Hamamatsu, Bridgewater, NJ). All imaging acquisition was performed with MetaMorph (Universal Imaging, West Chester, PA). Cells grown on glass cover slips were placed in a custom chamber with standard external solution (135 mM NaCl, 5 mM KCl, 1.5 mM MgCl$_2$, 1.5 mM CaCl$_2$, 20 mM HEPES 10 mM D-glucose, pH 7.4 with HCl) and imaged at room temperature. Cells were screened for the expression of ECFP-TRPV5 and EYFP-CaBP$_{28K}$ using the normal light fluorescence setup before switching to TIRF for EYFP imaging. Cells were analyzed for 10 min (1 frame/5 s) to establish a baseline in whole-cell TIRF measurements before 50 µM BAPTA-AM was added. After 15 min, to allow BAPTA loading of the cells, cells were again followed for 10 min (1 frame/5 s). To quantify changes in TIRF, intensities of the regions of interests (ROIs) of several (n = 5-7) cells, with areas between 5-10% of the visible 'footprint' of the cell, were averaged and normalized according to the following equation:

Relative change = I(t) – I(0)

Where I(0) is the intensity at the beginning of the time series and I(t) is the intensity at time point t.

^{45}Ca^{2+} binding and uptake assay

GST-CaBP$_{28K}$ and GST were expressed and purified according to the manufacturers' protocol (Amersham Biosciences, Piscataway, NJ, USA). Blots were washed in overlay-buffer (10 mM imidazole-HCl pH 7.4, 60 mM KCl, 0.5 mM MgCl$_2$) before incubation with ^{45}CaCl$_2$ (1 µCi/ml) in overlay-buffer. After extensive washing in 50% (v/v) ethanol and drying of the blots, bound ^{45}Ca^{2+} was determined by autoradiography. ^{45}Ca^{2+} uptake was determined using confluent layers of MDCK cells as described (32). To block TRPV5-mediated ^{45}Ca^{2+} uptake cells were incubated with 10 µM ruthenium red.

Electrophysiology

Whole-cell currents in HEK293 cells transiently transfected with TRPV5 and CaPB$_{28K}$ were measured using an EPC-9 patch-clamp amplifier and Pulse software (HEKA Elektronik, Lambrecht, Germany). Monovalent cation currents were measured in divalent-free extracellular solution (DVF) containing 150 mM NaCl, 10 mM EDTA and 10 mM HEPES-

NaOH, pH 7.4. The internal (pipette) solution contained 120 mM NaCl, 1 mM CaCl$_2$, 20 mM HEPES-NaOH and 1 mM Fura-2, supplemented with 5 mM 1-(4,5-metoxy-2-nitrophenyl)1,2-aminoethane-N,N,N',N'-tetraacetic acid (DMNP-EDTA). DMNP-EDTA is a Ca^{2+} chelator that exhibits a high affinity for Ca^{2+} ions with an increase in its K$_d$ for Ca^{2+} upon photolysis (K$_d$ rises from 5 nM to 3 mM). All experiments were performed at room temperature. Current-voltage relationships were measured from linear 400-ms voltage ramps, from -100 mV to +100 mV. Ramps were applied every 5 s from a holding potential of +20 mV with a sampling interval of 0.8 ms. All current amplitudes in the dose-response curves were normalized to values of the inward current at -80 mV and a intracellular Ca^{2+} concentration ([Ca^{2+}]$_i$) of 135 nM and subsequently fitted with a Hill function (Origin 7.0 software, OriginLab Corporation, Northampton, MA, USA). For photolytic release of Ca^{2+} and measurement of [Ca^{2+}]$_i$ during patch-clamp Fura-2 was excited with light alternated between 350 and 380 nm using a monochromator (Polychrome IV, TILL Photonics, Planegg, Germany), and the resulting fluorescent signal was measured using a photodiode. The ratio of the fluorescent signal was converted into [Ca^{2+}]$_i$ values according to the Grynkiewicz equation (33). Increases in [Ca^{2+}]$_i$ were achieved by increasing the duration of 350/380 nm illumination from 15 to 150 ms each.

Lentiviral infection of primary rabbit CNT/CCD cultures

Third generation lentiviruses were produced by co-transfection of the packaging vectors pRSV-Rev, pMDL g/p RRE, and pMD2G from Tronolab (Lausanne, Switzerland), containing and the transfer vector into HEK293T cells as described (34). The virus titer was determined by p24 HIV ELISA (Murex Diagnostics, Dartford, UK). Primary rabbit CNT/CCD cultures were infected with lentiviruses containing EGFP or EGFP-CaBP$_{28K}$ΔEF immediately before plating, in the presence of polybrene (8 μg/ml) using 20 virus particles per cell (20 MOI). Virus was removed after 24 h and subsequently transepithelial Ca^{2+} transport was measured 6 days post-infection in the presence of 10 μM forskolin as described previously (30).

Statistical analysis

In all experiments, the data are expressed as mean ± SEM. Overall statistical significance was determined by analysis of variance (ANOVA) followed by Bonferroni to investigate individual significance. P-values below 0.05 were considered significant.

Results

Concomitant regulation of calbindin-D$_{28K}$ and TRPV5 in kidney

In kidney CaBP$_{28K}$ and TRPV5 co-localized in the distal convoluted tubule (DCT) and the connecting tubule (CNT) **(Fig. 1A).** These cells transport Ca^{2+} transcellularly from the pro-urine to the blood compartment (2). To investigate whether there is a correlation between the expression of TRPV5 and CaBP$_{28K}$ the abundance of these proteins was analyzed in different animal models that were treated with calciotropic hormones, exposed to various dietary Ca^{2+} levels or ablated for Ca^{2+} transporting encoding genes **(Fig. 1B)**. Importantly, a highly significant correlation between the TRPV5 expression and CaBP$_{28K}$ abundance was consistently observed. CaBP$_{28K}$ is predominantly localized along the apical side of TRPV5-expressing renal cells **(Fig. 1A)** Therefore, the apical localization of CaBP$_{28K}$ was investigated in kidneys of TRPV5$^{-/-}$ compared to wild-type mice. To this end, the immuno-positive staining of CaBP$_{28K}$ was semi-quantified in five subcellular regions of DCT and CNT cells **(Fig. 1C)**. In TRPV5$^{-/-}$ kidney CaBP$_{28K}$ was equally distributed throughout the tubular cells with no apparent apical localization, whereas CaBP$_{28K}$ was significantly more abundant in the apical region in wild-type kidney cells. This finding further substantiates that the apical localization of CaBP$_{28K}$ is dependent on the presence of TRPV5.

Calbindin-D$_{28K}$ interacts with TRPV5 in a Ca^{2+}-dependent manner

Ion channels in epithelial cells are frequently regulated by associated intracellular protein complexes. A potential interaction between CaBP$_{28K}$ and TRPV5 was investigated using GST pull-down assays. In addition, the interaction of CaBP$_{28K}$ with other TRPV members, including the highly homologous TRPV6 and closely related TRPV4 channels, was studied. CaBP$_{28K}$ bound to both the N- and C-termini of TRPV5 and TRPV6 in the absence of Ca^{2+} (5 mM EDTA), whereas the binding was virtually abolished in the presence of Ca^{2+} (1 mM CaCl$_2$) **(Fig. 1D)**. However, binding between CaBP$_{28K}$ and TRPV4 could not be detected neither in the presence nor absence of Ca^{2+} (data not shown). Subsequently, the interaction of TRPV5 and CaBP$_{28K}$ was evaluated by co-precipitation from GST-CaBP$_{28K}$ and TRPV5-expressing human embryonic kidney (HEK293) cells. The Ca^{2+} dependency of this association was investigated by incubation of the cells with BAPTA-AM to decrease [Ca^{2+}]$_i$. To this end, cell lysates were incubated with glutathione-coupled sepharose beads to precipitate GST-CaBP$_{28K}$ complexes and immunoblots containing the precipitated proteins were analyzed for the presence of TRPV5. TRPV5 co-precipitated with GST-CaBP$_{28K}$ in cells that were treated with BAPTA-AM, whereas the channel was not precipitated from non-treated cells **(Fig. 1E)**. In addition, co-precipitation of TRPV5 could not be detected in GST and TRPV5-expressing cells, demonstrating the specificity of the CaBP$_{28K}$ association.
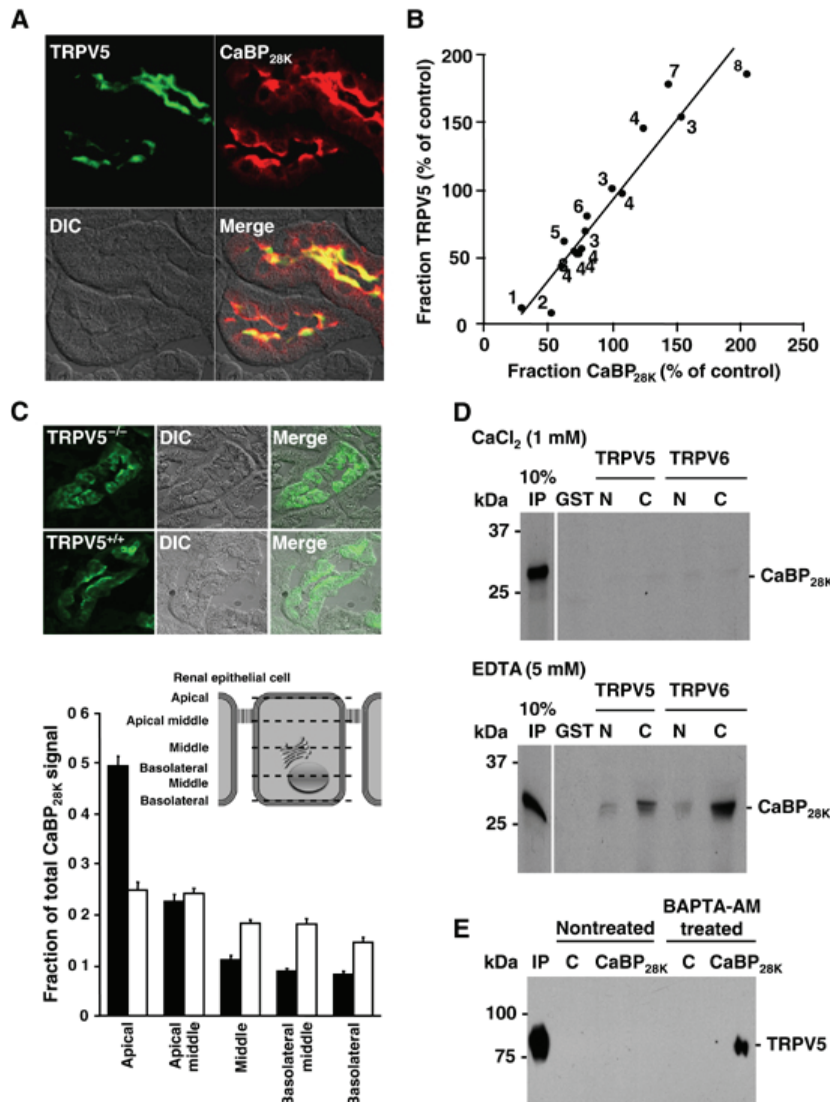
(A) Co-localization of TRPV5 (green) and CaBP$_{28K}$ (red) in the distal convoluted and connecting tubule. **(B)** Correlation in TRPV5 and CaBP$_{28K}$ expression after treatment ([1]parathyroidectomized (16); [2]tacrolimus (35); [3]acidose/alkalose (36); [4]thiazide (35, 37); [5]calcimemetics (16); [6]ovariectomized (16); [7]dexamethasone (37); [8]ovariectomized + vitamine D$_3$ (38)). R^2 = 0.9068. **(C)** Localization of CaBP$_{28K}$ in kidney sections of TRPV5$^{-/-}$ and wild-type mice. The epithelial cells were divided in different regions including apical, apical-middle, middle, basolateral-middle and basolateral as indicated. The immuno-positive CaBP$_{28K}$ staining of these different cellular regions in 30 cells of 6 different tubules was calculated as described in the material and methods. Significant differences in CaBP$_{28K}$ intensities within the group were indicated by an asterisk. **(D)** [^{35}S]Methionine labeled, *in vitro* translated CaBP$_{28K}$ was incubated, either in the presence (1 mM CaCl$_2$) or absence (5 mM EDTA) of Ca^{2+}, with GST or GST fused to the N- or C-terminus of TRPV5 and TRPV6 immobilized on glutathione-Sepharose 4B beads. Input control (IP) represents 10% of the total pull down input. The two TRPV5 immuno-positive bands correspond to the core (lower) and glycosylated forms of the protein. **(E)** Cells were co-transfected with pEBG-CaBP$_{28K}$ (GST-CaBP$_{28K}$) and pCINeo-TRPV5-IRES-EGFP or pEBG (GST) and pCINeo-TRPV5-IRES-EGFP (control, C). To decrease the [Ca^{2+}]$_i$ cells were treated with BAPTA-AM. Lysates were loaded on glutathione-Sepharose 4B beads and after extensive washing co-precipitation was investigated by immunoblotting using the guinea pig anti-TRPV5 antibody (IP = input).

CaBP$_{28K}$ translocates towards the plasma membrane in a Ca^{2+}- and TRPV5-dependent manner

The physiological characteristics of the interaction of CaBP$_{28K}$ with TRPV5 suggests that this Ca^{2+}-binding protein translocates towards the plasma membrane at a low [Ca^{2+}]$_i$. This hypothesis was investigated by the isolation of plasma membrane-enriched fractions of TRPV5 and CaBP$_{28K}$-transfected HeLa cells. As compared to the endogenously expressed Na,K-ATPase, CaBP$_{28K}$ was more abundant (260 ± 105 %, n = 3, p<0.05) in the plasma membrane-enriched fraction of cells that were treated with BAPTA-AM compared to non-treated cells **(Fig. 2A, left panel)**. Importantly, cells lacking TRPV5 did not reveal an elevated expression of CaBP$_{28K}$ in the plasma membrane-enriched fraction after BAPTA-AM treatment **(Fig. 2A, right panel)**. Subsequently, CaBP$_{28K}$ expression in plasma membrane-enriched fractions of primary rabbit CNT / cortical collecting duct (CNT/CCD) cultures endogenously expressing TRPV5 and CaBP$_{28K}$ (2) was evaluated. In line with the experiments using transfected cells, CaBP$_{28K}$ was more abundant (146 ± 6 %, n = 3, p<0.05) in plasma membrane-enriched fractions of BAPTA-AM-treated primary CNT/CCD cultures as compared to non-treated cultures **(Fig. 2B)**.
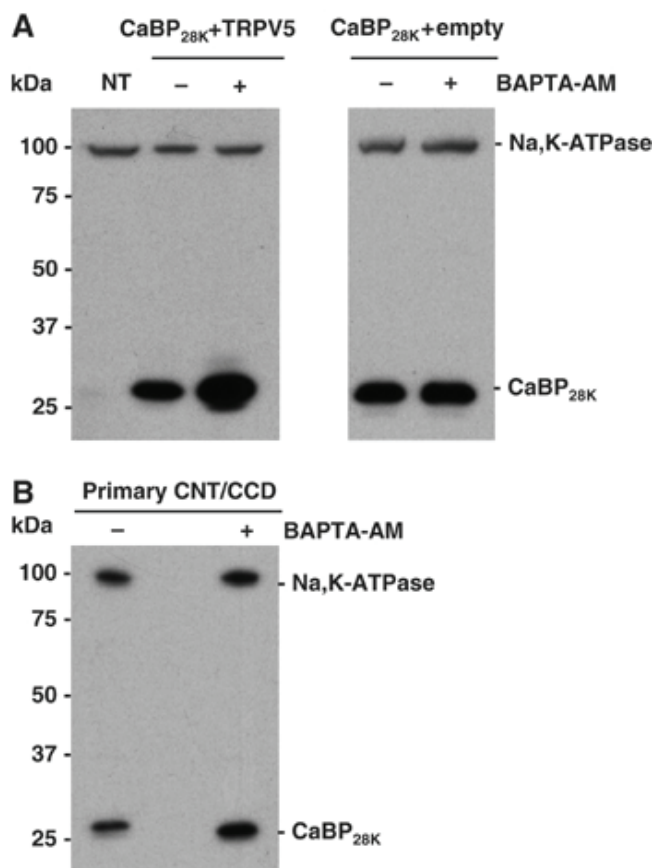

Fig. 2. Subcellular localization of CaBP$_{28K}$ at low intracellular Ca^{2+} concentrations

(A) Cells were transfected with CaBP$_{28K}$ and TRPV5 (left panel) or CaBP$_{28K}$ and empty vector (right panel) and treated with or without BAPTA-AM. Plasma membrane-enriched fractions were probed for the presence of endogenously expressed Na,K-ATPase and exogenously expressed CaBP$_{28K}$ using anti-Na,K-ATPase and anti-CaBP$_{28K}$ antibodies, respectively. NT = non-transfected. **(B)** Plasma membrane-enriched fractions of primary CNT/CCD cultures, either treated with or without BAPTA-AM, were isolated and probed for the presence of endogenously expressed CaBP$_{28K}$ and Na,K-ATPase. Representative blots of 3 independent experiments are shown.

Next, the Ca^{2+}-dependent translocation of $CaBP_{28K}$ towards the plasma membrane in TRPV5-expressing HEK293T cells was investigated by total internal reflection fluorescence (TIRF) or evanescent-field microscopy. TIRF microscopy illuminates fluorophores within 100-200 nm of the plasma membrane-glass cover slip interface, with excitation intensity depending on the relative indices of refraction and the angle of incidence. Light intensity falls exponentially in the axial (z) direction, such that fluorescence output is inversely proportional to the distance from the plasma membrane. TIRF therefore enabled us to study the dynamic process of $CaBP_{28K}$ translocation towards the plasma membrane in a direction vertical to the plasma membrane, without interference of cytosolic $CaBP_{28K}$ fluorescence. The presence of EYFP-$CaBP_{28K}$ in the TIRF signal of cells co-transfected with EYFP-$CaBP_{28K}$ and TRPV5-ECFP was followed in the presence and absence of BAPTA-AM, respectively. After BAPTA-AM treatment, the EYFP-$CaBP_{28K}$ TIRF signal increased in time as compared to non-treated cells **(Fig. 3A and B)**. In line with the cell fractionation experiments, this increase of EYFP-$CaBP_{28K}$ TIRF signal was not observed in cells lacking TRPV5 **(Fig. 3C and D)**. Furthermore, the BAPTA-dependent changes in TIRF signal were not detected in cells expressing TRPV5-IRES-EGFP (bicistronic expression of TRPV5 and EGFP) **(Fig. 3E and F)** demonstrating that the observed alterations in EYFP-$CaBP_{28K}$ fluorescence represent a cellular redistribution of $CaBP_{28K}$.

Co-expression of $CaBP_{28K}$ elevates $^{45}Ca^{2+}$ uptake in TRPV5-expressing MDCK cells

In order to investigate the functional role of the Ca^{2+}-binding EF-hand motifs in $CaBP_{28K}$, a Ca^{2+}-insensitive mutant ($CaBP_{28K}\Delta EF$) was constructed and characterized by $^{45}Ca^{2+}$ overlay and pull down experiments. As compared to the negative control (GST), disruption of the EF-hand motifs in GST-$CaBP_{28K}$ resulted in a Ca^{2+}-insensitive $CaBP_{28K}$ mutant whereas wild-type GST-$CaBP_{28K}$ displayed normal $^{45}Ca^{2+}$ binding **(Fig. 4A)**. In addition, pull down analysis demonstrated that $CaBP_{28K}\Delta EF$ binds in the absence (5 mM EDTA) as well as presence (1 mM $CaCl_2$) of Ca^{2+} to the N- and C-terminus of both TRPV5 and TRPV6 **(Fig. 4B)**. To investigate whether $CaBP_{28K}\Delta EF$ competes with wild-type $CaBP_{28K}$ for TRPV5 binding increasing amounts of non-radioactive *in vitro* translated $CaBP_{28K}\Delta EF$ were added during the pull down assay. This resulted in a dose-dependent reduction of $CaBP_{28K}$ binding indicating that $CaBP_{28K}\Delta EF$ competed with wild-type $CaBP_{28K}$ for TRPV5 association **(Fig. 4C)**.
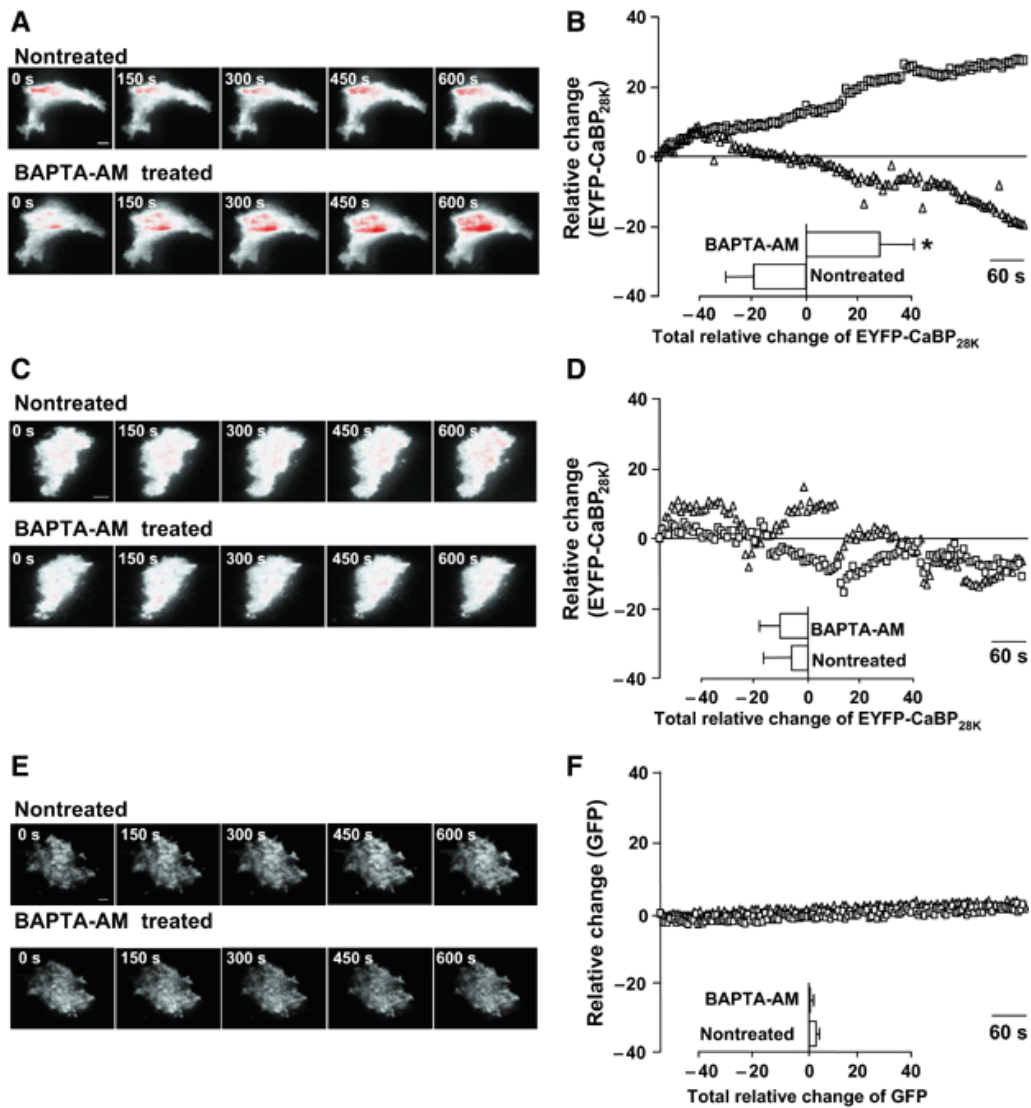
Fig. 3. CaBP$_{28K}$ translocation at low intracellular Ca^{2+} concentrations

(A) TIRF images of a single cell expressing EYFP-CaBP$_{28K}$ and TRPV5-ECFP that was treated with (lower panel) or without (upper panel) BAPTA-AM. Scale bar = 5 μm **(B)** Average time courses of the TIRF signal of EYFP-CaBP$_{28K}$ in EYFP-CaBP$_{28K}$ and TRPV5-ECFP expressing cells that were treated either with (□) or without (Δ) BAPTA-AM (n=7). Significant differences in total EYFP changes after BAPTA-AM treatment (inset) are indicated by an asterisk (p<0.05). **(C)** TIRF images of a single cell expressing EYFP-CaBP$_{28K}$ that was treated with (lower panel) or without (upper panel) BAPTA-AM. Scale bar = 5 μm **(D)** Average time courses of the TIRF signal of EYFP-CaBP$_{28K}$-expressing cells that were treated either with (□) or without (Δ) BAPTA-AM (n=5). **(E)** TIRF images of single cells expressing TRPV5-IRES-EGFP treated with (lower panel) or without (upper panel) BAPTA-AM. Scale bar = 5 μm **(F)** Average time courses of the TIRF signal in TRPV5-IRES-EGFP-expressing cells that were treated either with (□) or without (Δ) BAPTA-AM (n=5). In all images a gradient filter was applied such that saturation of TIRF fluorescence turns red and the intensities were measured between 5–10% of the visible 'footprint' of the cell.
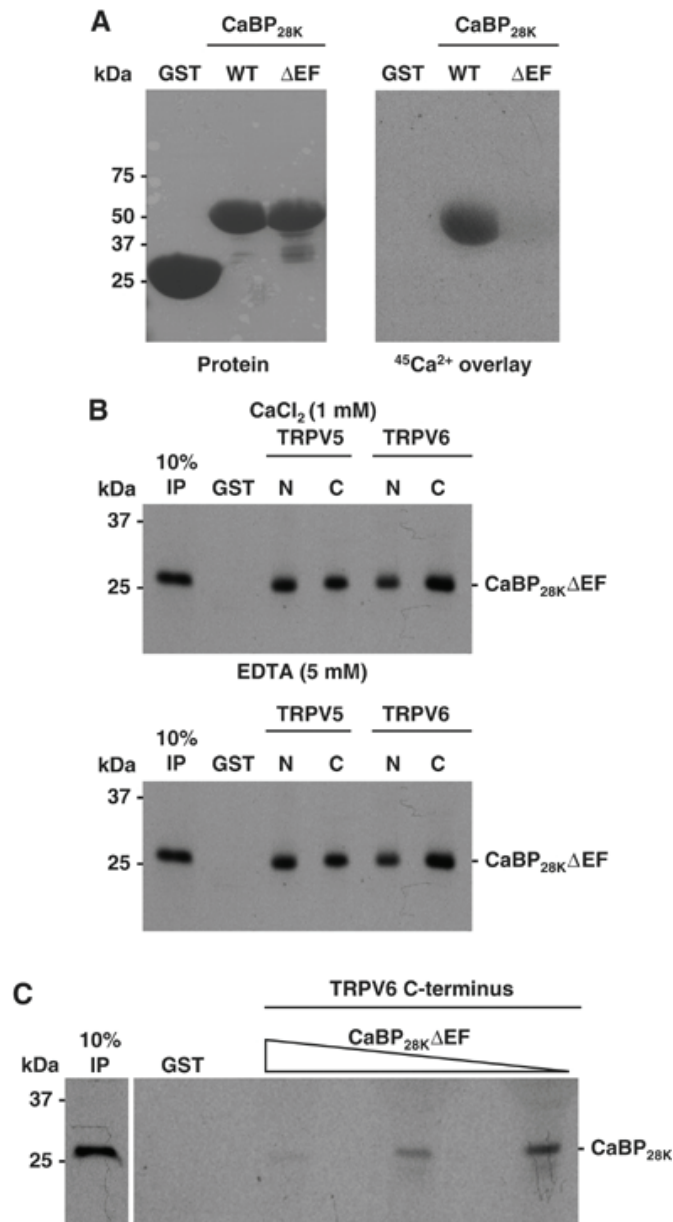
Fig. 4. Characterization of a Ca^{2+}-insensitive $CaBP_{28K}$ mutant

(A) Wild-type $CaBP_{28K}$ and $CaBP_{28K}\Delta EF$ were fused to GST (left panel) and $^{45}Ca^{2+}$-binding was determined (right panel). **(B)** [^{35}S]Methionine labeled, *in vitro* translated $CaBP_{28K}\Delta EF$ was incubated, either in the presence (1 mM $CaCl_2$) or absence (5 mM EDTA) of Ca^{2+}, with GST or GST fused to the N- and C-termini of TRPV5 and TRPV6 immobilized on glutathione-Sepharose 4B beads. Input control (IP) represents 10% of the total pull down input. **(C)** [^{35}S]Methionine-labeled *in vitro* translated $CaBP_{28K}$ was incubated in the presence of increasing amounts of non-radioactive *in vitro* translated $CaBP_{28K}\Delta EF$ with GST or GST fused to C-termini of TRPV5 immobilized on glutathione-Sepharose 4B beads. This pull down experiment was performed in the absence of Ca^{2+} (5 mM EDTA). Input control (IP) represents 10% of the input.

The role of $CaBP_{28K}$ and the Ca^{2+}-binding EF-hand motifs in $CaBP_{28K}$ was assessed on TRPV5-mediated $^{45}Ca^{2+}$ uptake. To this end, stably transfected Madin-Darby Canine Kidney type-I epithelial (MDCK) cell lines were generated that express TRPV5 and $CaBP_{28K}$ or $CaBP_{28K}\Delta EF$. Total expression of EGFP-TRPV5 remained constant in the MDCK-TRPV5, MDCK-TRPV5-$CaBP_{28K}$ and MDCK-TRPV5-$CaBP_{28K}\Delta EF$ cell lines **(Fig. 5A)**. Furthermore, immunoblot analysis demonstrated the integrity of the EGFP-TRPV5 fusion-protein by the protein band of ~100 kDa. In addition, flow cytometry analysis of the EGFP-signal was employed to investigate the percentage of EGFP-TRPV5-positive cells. Importantly, >98% of the cells expressed EGFP-TRPV5, indicating that virtually all cells contribute to $^{45}Ca^{2+}$ uptake in the MDCK-TRPV5, MDCK-TRPV5-$CaBP_{28K}$ and MDCK-TRPV5-$CaBP_{28K}\Delta EF$ cell lines **(Fig. 5B)**. These results demonstrated that differences in $^{45}Ca^{2+}$ uptake are not due to alterations in TRPV5 expression. Stable expression of EGFP-TRPV5 in MDCK cells

(MDCK-TRPV5) resulted in a ~6-fold increase of ruthenium red-sensitive $^{45}Ca^{2+}$ uptake compared to empty vector-transfected cells (mock). Stable expression of $CaBP_{28K}$ in these cells (MDCK-TRPV5-$CaBP_{28K}$) **(Fig. 5C)** further increased the ruthenium red-sensitive $^{45}Ca^{2+}$ uptake by ~2-fold as compared to EGFP-TRPV5 and empty vector-expressing (MDCK-TRPV5-mock) cells **(Fig. 5D)**. Stable expression of $CaBP_{28K}\Delta EF$ in EGFP-TRPV5-expressing cells (MDCK-TRPV5-$CaBP_{28K}\Delta EF$) did not result in an increase of ruthenium red-sensitive $^{45}Ca^{2+}$ uptake, indicating the importance of the Ca^{2+}-binding EF-hand motifs in $CaBP_{28K}$.
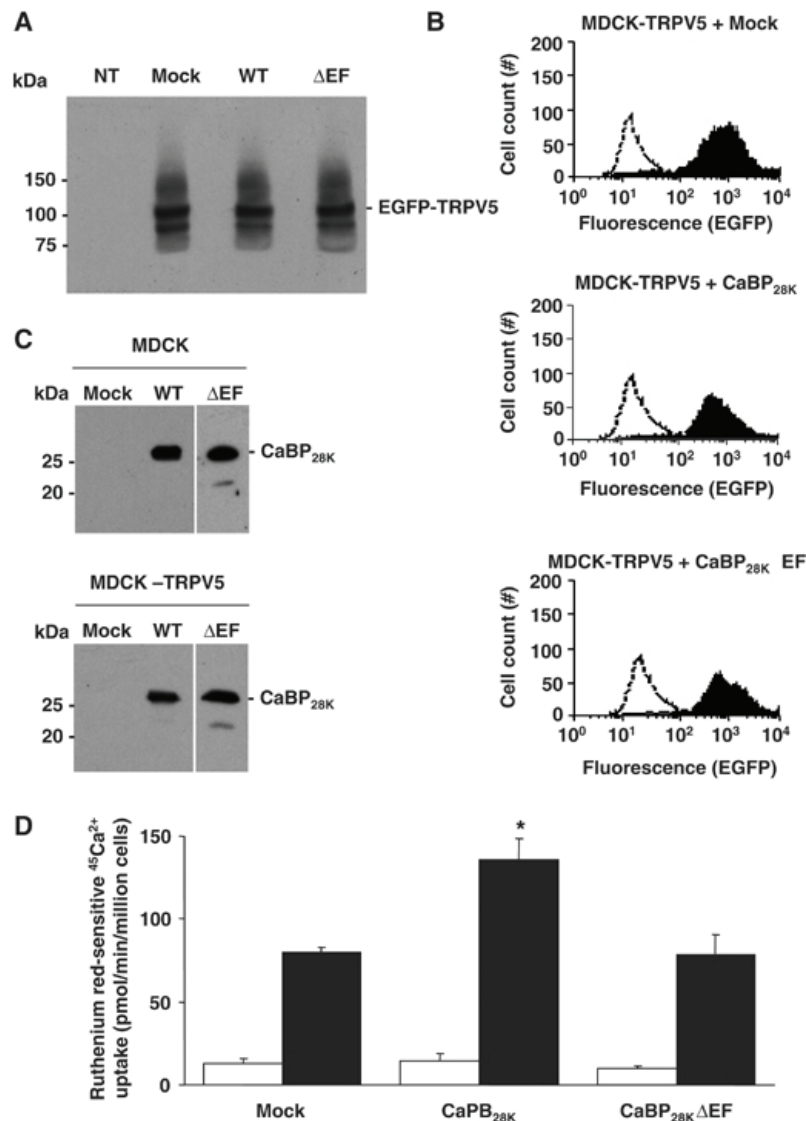

Fig. 5. Role of $CaBP_{28K}$ in TRPV5-mediated $^{45}Ca^{2+}$ uptake EGFP-TRPV5 and $CaBP_{28K}$, $CaBP_{28K}\Delta EF$ or empty vector were stably expressed in MDCK cells. The expression level of EGFP-tagged TRPV5 as determined using rabbit anti-GFP antibody **(A)** or flow cytometry analysis **(B; black peaks)** reveal that the expression of TRPV5 in empty vector and $CaBP_{28K}$ expressing cells equal. The open peak in the three panels indicates background fluorescence in non-transfected cells. The two TRPV5 immuno-positive bands correspond to the core (lower) and glycosylated forms of EGFP-TRPV5. **(C)** The stable expression of $CaBP_{28K}$ and $CaBP_{28K}\Delta EF$ in MDCK or MDCK EGFP-TRPV5-expressing cells was verified using anti-$CaBP_{28K}$ antibodies. **(D)** Ruthenium red-sensitive $^{45}Ca^{2+}$ uptake of MDCK cells stably expressing both (black bars) TRPV5 and $CaBP_{28K}$, $CaBP_{28K}\Delta EF$ or empty vector and MDCK cells stably expressing (open bars) $CaBP_{28K}$, $CaBP_{28K}\Delta EF$ or empty vector. Significant differences in $^{45}Ca^{2+}$ uptake are indicated by an asterisk ($p<0.05$).

CaBP$_{28K}$ has no effect on the current characteristics of TRPV5

Since CaBP$_{28K}$ binds to TRPV5 and posses the ability to regulate downstream cellular processes, CaBP$_{28K}$ could directly affect channel activity. The effect of CaBP$_{28K}$ on the electrophysiological characteristics of TRPV5 was investigated by controlling $[Ca^{2+}]_i$ in a spatially uniform manner using uncaging of Ca^{2+} from the photolysable Ca^{2+}-chelator DMNP-EDTA. TRPV5 activity in the presence and absence of CaBP$_{28K}$ and CaBP$_{28K}\Delta$EF was correlated to $[Ca^{2+}]_i$ (see supplementary data **Fig. S1** for additional information). Regulating $[Ca^{2+}]_i$ enabled us to study the effect of CaBP$_{28K}$ on the characteristics of TRPV5 without the influence of Ca^{2+} buffering by CaBP$_{28K}$. Neither CaBP$_{28K}$ nor CaBP$_{28K}\Delta$EF modulated the Ca^{2+} sensitivity of TRPV5 when $[Ca^{2+}]_i$ was gradually increased from 100 to 600 nM **(Fig. 6A and B).**
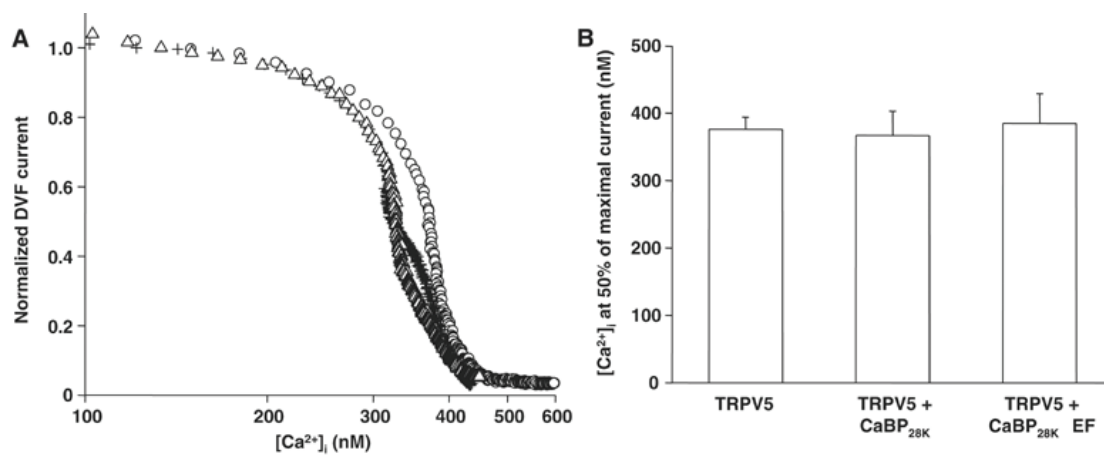

Fig. 6. Direct Influence of CaBP$_{28K}$ on the characteristics of TRPV5

(A) Dose-response curves showing the effect of an increasing $[Ca^{2+}]_i$ on the normalized Na^+ inward current in divalent-free extracellular solution (DVF) of TRPV5 (O, n=9), TRPV5 and CaBP$_{28K}$ (+, n=11) or TRPV5 and CaBP$_{28K}\Delta$EF (Δ, n=12) expressing cells. **(B)** Averaged IC$_{50}$ for each of the transfections and recordings shown in panel A.

CaBP$_{28K}\Delta$EF dominant negatively inhibits transcellular Ca^{2+} transport in primary rabbit CNT/CCD cultures

If the translocation of CaBP$_{28K}$ towards and subsequent interaction with TRPV5 is of any physiological relevance, disruption of the CaBP$_{28K}$-TRPV5 association will result in a decreased Ca^{2+} buffering at the entry gate and coherent impairment of transcellular Ca^{2+} transport. This hypothesis was experimentally evaluated by using the lentiviral expression system to express EGFP-CaBP$_{28K}\Delta$EF in primary rabbit CNT/CCD cultures and subsequent Ca^{2+} transport measurements across these infected confluent cell monolayers. Viral expression of EGFP-CaBP$_{28K}\Delta$EF resulted in a dominant negative effect on transcellular Ca^{2+} transport

across primary CNT/CCD cultures **(Fig. 7A)**. As compared to non-infected cultures, viral expression of only EGFP did not influence transcellular Ca^{2+} transport. Viral infection with efficiencies of ~ 50% **(Fig. S2)** did not affect the transepithelial resistance in any of the conditions tested, confirming the integrity of the CNT/CCD monolayer and (data not shown). Importantly, only half of the CNT/CCD cells expressed the $CaBP_{28K}\Delta EF$ mutant indicating that the observed inhibition is significantly underestimated. To investigate whether $CaBP_{28K}\Delta EF$ inhibited TRPV5-mediated transcellular Ca^{2+} transport in primary CNT/CCD cultures the potent TRPV5 channel blocker ruthenium red was included during the Ca^{2+} transport assay. Addition of 10 μM ruthenium red to the apical side of the cell monolayer abolished transcellular Ca^{2+} transport in the absence or presence of exogenous $CaBP_{28K}\Delta EF$ **(Fig. 7A)**.

Next, we measured expression of wild-type $CaBP_{28K}$ and $EGFP$-$CaBP_{28K}\Delta EF$ in these primary renal cell cultures **(Fig. 7B)**. No differences in wild-type $CaBP_{28K}$ expression was detected between EGFP and $EGFP$-$CaBP_{28K}\Delta EF$-infected cells as compared to the endogenously expressed Na,K-ATPase, indicating that the observed effects were not due to down-regulation of endogenous $CaBP_{28K}$.
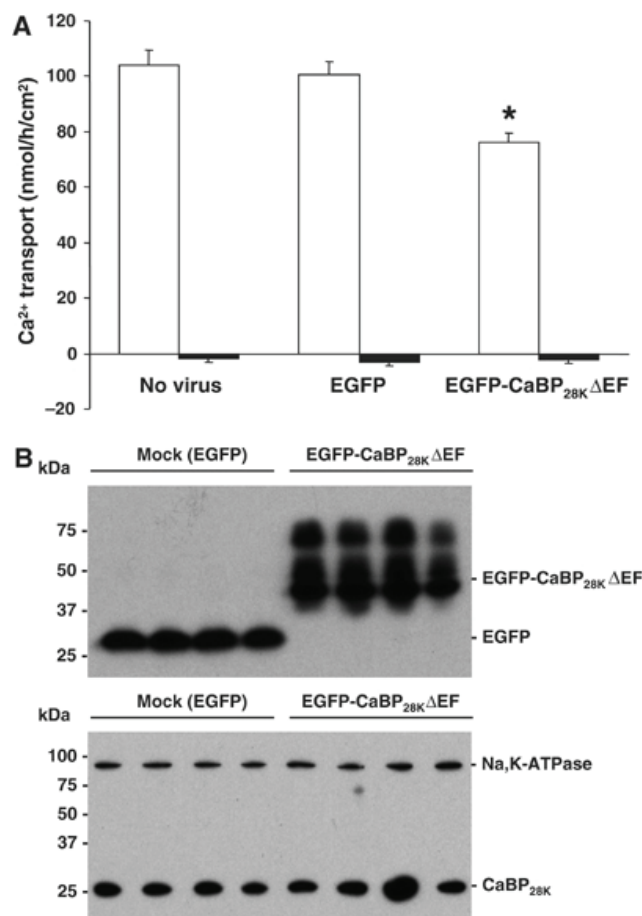

Fig. 7. Effect of $CaBP_{28K}\Delta EF$ on transcellular Ca^{2+} transport

(A) Effect of lentivirus-mediated overexpression of GFP and GFP-$CaBP_{28K}\Delta EF$ on transcellular Ca^{2+} transport in primary rabbit CNT/CCD cells. Averaged transcellular Ca^{2+} transport for each infection, expressed as mean ± SEM. 10 μM ruthenium red was added to the apical side of the cell monolayer during the transport assay to estimate the TRPV5-mediated Ca^{2+} transport. Significant differences as compared to mock infected cells are indicated by an asterisk ($p<0.05$) **(B)** The expression of GFP and GFP-$CaBP_{28K}\Delta EF$ (upper panel) was assessed with immunoblotting using rabbit anti-GFP antibody and the expression of endogenous $CaBP_{28K}$ was checked with monoclonal anti-$CaBP_{28K}$ antibody that does not recognize GFP-$CaBP_{28K}\Delta EF$ (lower panel). To check for equal loading the expression of the endogenously expressed Na,K-ATPase was measured (lower panel).

Discussion

The present study identified CaBP$_{28K}$ as a dynamic Ca^{2+} buffer facilitating TRPV5-mediated Ca^{2+} transport by buffering [Ca^{2+}] in close vicinity to the channel mouth. This conclusion is based on the following observations. First, CaBP$_{28K}$ translocates towards TRPV5-containing plasma membranes upon a decrease in [Ca^{2+}]$_i$. Second, CaBP$_{28K}$ directly associates with TRPV5 at a low [Ca^{2+}]$_i$. Third, expression of CaBP$_{28K}$ in TRPV5-expressing cells increases TRPV5-mediated Ca^{2+} influx, while inactivation of the EF-hand motifs in CaBP$_{28K}$ abolishes this stimulatory effect. Fourth, the Ca^{2+}-insensitive CaBP$_{28K}$ mutant (CaBP$_{28K}\Delta$EF) competes with wild-type CaBP$_{28K}$ for TRPV5 association resulting in a dominant negative inhibition of transepithelial Ca^{2+} transport in primary rabbit CNT/CCD cultures.

In the past, CaBP$_{28K}$ was identified as a high capacity Ca^{2+} buffer with Ca^{2+} affinities fitting the classical properties of a Ca^{2+} buffer. However, sequential Ca^{2+} binding and conformational changes suggested that CaBP$_{28K}$ can act as a Ca^{2+} sensor controlling downstream cellular processes (24, 25, 39, 40). CaBP$_{28K}$ is highly expressed in Ca^{2+}-transporting epithelia where it co-localizes with TRPV5. This study reveals that the expression of CaBP$_{28K}$ and TRPV5 are positively correlated, suggesting a fundamental role of CaBP$_{28K}$ in the regulation of TRPV5 activity. In various studies exploring the regulatory role of the calciotropic hormones including vitamin D, estrogens, parathyroid hormone and dietary Ca^{2+}, we observed the concomitant regulation of TRPV5 and CaBP$_{28K}$ in kidney (10). Likewise, genetic ablation of TRPV5 in mice resulted in a decreased expression of CaBP$_{28K}$ (41). Blockage of TRPV5 by ruthenium red eliminated parathyroid hormone-stimulated transepithelial Ca^{2+} transport in primary CNT/CCD cultures and simultaneously decreased the expression of CaBP$_{28K}$. The magnitude of the Ca^{2+} influx through TRPV5 predominantly controlled the expression of CaBP$_{28K}$ (16). Interestingly, Arnold and Heintz identified a 40-bp element in the CaBP$_{28K}$ promoter which forms a cell-specific and Ca^{2+}-sensitive transcriptional regulatory mechanism that may play a key role in setting the Ca^{2+} buffering capacity of Purkinje cells (42). Together, these data assure adequate CaBP$_{28K}$ expression to facilitate sufficient buffering of the TRPV5-mediated Ca^{2+} influx.

Here, we demonstrated that in Ca^{2+}-transporting epithelia, CaBP$_{28K}$ also directly associates with TRPV5 in a Ca^{2+}-dependent fashion. In line with this interaction, in kidney cells CaBP$_{28K}$ is found in the cytosol as well as along the apical membrane, where it co-localizes with TRPV5. This apical localization of CaBP$_{28K}$ is significantly disturbed in kidney cells of TRPV5$^{-/-}$ mice where CaBP$_{28K}$ is distributed evenly throughout the cytosol. In addition, both static and dynamic measurements using cells co-expressing CaBP$_{28K}$ and TRPV5 revealed that CaBP$_{28K}$ accumulates at the plasma membrane when [Ca^{2+}]$_i$ is low. Importantly, this translocation only occurs in the presence of TRPV5. Taken together, these data suggest that CaBP$_{28K}$ possesses the ability to specifically target to TRPV5-expressing plasma membranes

at a low $[Ca^{2+}]_i$. $CaBP_{28K}$ translocation is supported by previous findings showing that a fraction of $CaBP_{28K}$ specifically associates with particular subcellular domains (39, 43) and that $CaBP_{28K}$ redistributes after Ca^{2+} sensing (44). Further evidence for targeted $CaBP_{28K}$ mobility has been provided by Schmidt and coworkers who demonstrated a specific association of $CaBP_{28K}$ with membrane associated inositol-1,4,5-triphosphate, but not with cytosolic inositol-1,4,5-triphosphate (22).

In addition to $CaBP_{28K}$ other Ca^{2+}-binding proteins were found to associate with and affect the activity of TRPV5 via distinct mechanisms. Functional expression of TRPV5 requires binding of the S100A10-annexin 2 complex, whereas 80K-H acts as a Ca^{2+} sensor regulating TRPV5 activity (45, 46). Regulation by the ubiquitous calmodulin, however, seems to be restricted to the closely related family member TRPV6 (28). This multifaceted regulation of TRPV5 enables a strict control of transcellular Ca^{2+} transport at the apical entry gate. It is, however, not clear yet how these Ca^{2+} binding proteins integrate in this complex regulatory network to balance TRPV5-mediated Ca^{2+} influx.

Co-expression of $CaBP_{28K}$ in TRPV5-expressing HEK293 cells increased the Ca^{2+} uptake, while inactivation of the EF-hand motifs in $CaBP_{28K}$ blocked this stimulatory effect. $CaBP_{28K}\Delta EF$ was still capable to bind TRPV5, although the Ca^{2+}-dependency of the association was abolished. This implies that binding of $CaBP_{28K}$ to TRPV5 does not directly affect the physiological properties of TRPV5, otherwise the presence of Ca^{2+}-insensitive $CaBP_{28K}$ would also lead to an increase in TRPV5-mediated Ca^{2+} uptake. Furthermore, this emphasizes the importance of the EF-hand motifs in $CaBP_{28K}$. The activity of TRPV5 is tightly regulated by $[Ca^{2+}]_i$ in such a way that Ca^{2+} entering through TRPV5 exerts a negative feedback on channel activity (3). The present data showing Ca^{2+}-dependent association of TRPV5 and $CaBP_{28K}$ and an elevated $^{45}Ca^{2+}$ uptake in TRPV5 and $CaBP_{28K}$ co-expressing cells, suggests that the increase in $^{45}Ca^{2+}$ uptake is due to $CaBP_{28K}$ Ca^{2+} buffering in close vicinity of the channel mouth. The activity of TRPV5 in the presence of $CaBP_{28K}$ or $CaBP_{28K}\Delta EF$ was measured at various, experimentally controlled, $[Ca^{2+}]_i$ to further investigate whether $CaBP_{28K}$ directly affects TRPV5 current characteristics. In response to a gradual increase of $[Ca^{2+}]_i$ by UV-induced uncaging of Ca^{2+}, the activity of TRPV5 decreased, revealing the negative feedback of Ca^{2+} on channel activity. Co-expression of $CaBP_{28K}$ or $CaBP_{28K}\Delta EF$ did not change these observations indicating that $CaBP_{28K}$ does not directly affect channel inactivation characteristics at controlled $[Ca^{2+}]_i$. Thus, $CaBP_{28K}$ associates with TRPV5 and stimulates TRPV5-mediated Ca^{2+}-influx by increasing the buffering of $[Ca^{2+}]$ in close proximity to the channel mouth. This dynamic buffering and association is a unique process in comparison to channel regulation by other Ca^{2+}-binding proteins like calmodulin. Channel-associated calmodulin senses $[Ca^{2+}]_i$ and regulates channel activity by directly affecting channel (in)activation (13, 14).

Association of $CaBP_{28K}$ with TRPV5 and the consequent local buffering of Ca^{2+} is essential to facilitate the process of transcellular Ca^{2+}-transport, which is evident from the dominant negative effect of $CaBP_{28K}\Delta EF$ on transcellular Ca^{2+} transport in primary CNT/CCD cultures. $CaBP_{28K}\Delta EF$ lacks Ca^{2+}-buffering capacity, but competes with endogenous $CaBP_{28K}$ for binding sites on TRPV5 as revealed by the reduction of $CaBP_{28K}$ and TRPV5 association in the presence of $CaBP_{28K}\Delta EF$. This will reduce the local buffering of Ca^{2+} entering the epithelial cell via TRPV5, which subsequently results in inactivation of the channel and reduced transcellular transport rates. Note that addition of ruthenium red abolished transcellular Ca^{2+} transport in the absence or presence of exogenous $CaBP_{28K}\Delta EF$. Thus, these findings demonstrate that $CaBP_{28K}$ regulates TRPV5-mediated Ca^{2+}-transport.

Our previous findings that during transcellular Ca^{2+} transport in renal epithelial cells no apparent changes in the overall $[Ca^{2+}]_i$ could be detected (47) indicates that overall Ca^{2+} buffering is efficiently controlled in these cells. These measurements were, however, not performed on the subcellular level or in close proximity to the channel mouth where $[Ca^{2+}]$ fluctuates during transcellular Ca^{2+} transport. Opening of epithelial Ca^{2+} channels likely elicits Ca^{2+} influx of such a large magnitude that spatial distribution of Ca^{2+} is complicated by insufficient local Ca^{2+} buffers as suggested for voltage-operated Ca^{2+} channels (48). The dominant negative effect of $CaBP_{28K}\Delta EF$ on transcellular Ca^{2+} transport in primary CNT/CCD cultures, however, revealed that a channel-associated Ca^{2+} buffer is of utmost importance for buffering of the Ca^{2+} influx through TRPV5.

Together these findings constitute the first direct evidence that $CaBP_{28K}$ is essential for transepithelial Ca^{2+} transport and elucidates the molecular role of $CaBP_{28K}$ as a dynamic Ca^{2+} buffer. At a low $[Ca^{2+}]_i$, $CaBP_{28K}$ translocates towards the plasma membrane and associates with TRPV5. Here, it buffers Ca^{2+} that enters the cell via TRPV5, thereby counteracting local accumulation of cytosolic free Ca^{2+} and coherent inactivation of the channel. Upon Ca^{2+}-binding, $CaBP_{28K}$ diffuses from TRPV5 and subsequently facilitates transport of Ca^{2+} to the basolateral membrane. Furthermore, this illustrates an intrinsic mechanism of targeted Ca^{2+} buffering by spatial interactions to subcellular domains where local Ca^{2+} levels become detrimental. Probably similar mechanisms occur in brain, bone, teeth, inner ear, placenta and intestine where CaBPs are abundantly expressed and where cells tolerate large fluctuations in $[Ca^{2+}]_i$

References

1.	Montell, C., Birnbaumer, L., Flockerzi, V., Bindels, R. J., Bruford, E. A., Caterina, M. J., Clapham, D. E., Harteneck, C., Heller, S., Julius, D., Kojima, I., Mori, Y., Penner, R., Prawitt, D., Scharenberg, A. M., Schultz, G., Shimizu, N. & Zhu, M. X. (2002) *Mol Cell* **9,** 229-31.
2.	Hoenderop, J. G., Nilius, B. & Bindels, R. J. (2005) *Physiol Rev* **85,** 373-422.
3.	Hoenderop, J. G., van der Kemp, A. W., Hartog, A., van de Graaf, S. F., van Os, C. H., Willems, P. H. & Bindels, R. J. (1999) *J Biol Chem* **274,** 8375-8.
4.	Tymianski, M. (1996) *Adv Neurol* **71,** 85-105.
5.	Pauls, T. L., Cox, J. A. & Berchtold, M. W. (1996) *Biochim Biophys Acta* **1306,** 39-54.
6.	Lukas, W. & Jones, K. A. (1994) *Neuroscience* **61,** 307-16.
7.	Schwaller, B., Meyer, M. & Schiffmann, S. (2002) *Cerebellum* **1,** 241-58.
8.	Bronner, F. (1989) *Am J Physiol* **257,** F707-11.
9.	Bronner, F. & Stein, W. D. (1988) *Am J Physiol* **255,** F558-62.
10.	Lambers, T. T., Bindels, R. J. & Hoenderop, J. G. (2006) *Kidney Int* **69,** 650-4.
11.	Kits, K. S. & Mansvelder, H. D. (1996) *Invert Neurosci* **2,** 9-34.
12.	Jones, L. P., DeMaria, C. D. & Yue, D. T. (1999) *Biophys J* **76,** 2530-52.
13.	Zuhlke, R. D., Pitt, G. S., Deisseroth, K., Tsien, R. W. & Reuter, H. (1999) *Nature* **399,** 159-62.
14.	DeMaria, C. D., Soong, T. W., Alseikhan, B. A., Alvania, R. S. & Yue, D. T. (2001) *Nature* **411,** 484-9.
15.	Feher, J. J., Fullmer, C. S. & Wasserman, R. H. (1992) *Am J Physiol* **262,** C517-26.
16.	van Abel, M., Hoenderop, J. G., van der Kemp, A. W., Friedlaender, M. M., van Leeuwen, J. P. & Bindels, R. J. (2005) *Kidney Int* **68,** 1708-21.
17.	Guo, Q., Christakos, S., Robinson, N. & Mattson, M. P. (1998) *Proc Natl Acad Sci U S A* **95,** 3227-32.
18.	Iacopino, A. M. & Christakos, S. (1990) *J Biol Chem* **265,** 10177-80.
19.	Airaksinen, M. S., Eilers, J., Garaschuk, O., Thoenen, H., Konnerth, A. & Meyer, M. (1997) *Proc Natl Acad Sci U S A* **94,** 1488-93.
20.	Blatow, M., Caputi, A., Burnashev, N., Monyer, H. & Rozov, A. (2003) *Neuron* **38,** 79-88.
21.	Schmidt, H., Stiefel, K. M., Racay, P., Schwaller, B. & Eilers, J. (2003) *J Physiol* **551,** 13-32.
22.	Schmidt, H., Schwaller, B. & Eilers, J. (2005) *Proc Natl Acad Sci U S A* **102,** 5850-5.
23.	Venters, R. A., Benson, L. M., Craig, T. A., Bagu, J., Paul, K. H., Kordys, D. R., Thompson, R., Naylor, S., Kumar, R. & Cavanagh, J. (2003) *Anal Biochem* **317,** 59-66.
24.	Berggard, T., Miron, S., Onnerfjord, P., Thulin, E., Akerfeldt, K. S., Enghild, J. J., Akke, M. & Linse, S. (2002) *J Biol Chem* **277,** 16662-72.
25.	Venyaminov, S. Y., Klimtchuk, E. S., Bajzer, Z. & Craig, T. A. (2004) *Anal Biochem* **334,** 97-105.
26.	Nilius, B., Prenen, J., Hoenderop, J. G., Vennekens, R., Hoefs, S., Weidema, A. F., Droogmans, G. & Bindels, R. J. (2002) *J Biol Chem* **277,** 30852-30858.
27.	Tanaka, M., Gupta, R. & Mayer, B. J. (1995) *Mol Cell Biol* **15,** 6829-37.

28.   Lambers, T. T., Weidema, A. F., Nilius, B., Hoenderop, J. G. & Bindels, R. J. (2004) *J Biol Chem* **279,** 28855-61.
29.   van de Graaf, S. F., Chang, Q., Mensenkamp, A. R., Hoenderop, J. G. & Bindels, R. J. (2006) *Mol Cell Biol* **26,** 303-12.
30.   Hoenderop, J. G., Vaandrager, A. B., Dijkink, L., Smolenski, A., Gambaryan, S., Lohmann, S. M., de Jonge, H. R., Willems, P. H. & Bindels, R. J. (1999) *Proc Natl Acad Sci U S A* **96,** 6084-9.
31.   Bezzerides, V. J., Ramsey, I. S., Kotecha, S., Greka, A. & Clapham, D. E. (2004) *Nat Cell Biol* **6,** 709-20.
32.   den Dekker, E., Schoeber, J., Topala, C. N., van de Graaf, S. F., Hoenderop, J. G. & Bindels, R. J. (2005) *Pflugers Arch* **450,** 236-44.
33.   Grynkiewicz, G., Poenie, M. & Tsien, R. Y. (1985) *J Biol Chem* **260,** 3440-50.
        34.   Dull, T., Zufferey, R., Kelly, M., Mandel, R. J., Nguyen, M., Trono, D. & Naldini, L. (1998) *J Virol* **72,** 8463-71.
35.   Nijenhuis, T., Vallon, V., van der Kemp, A. W., Loffing, J., Hoenderop, J. G. & Bindels, R. J. (2005) *J Clin Invest* **115,** 1651-8.
36.   Nijenhuis, T., Renkema, K. Y., Hoenderop, J. G. & Bindels, R. J. (2006) *J Am Soc Nephrol* **17,** 617-626.
37.   Nijenhuis, T., Hoenderop, J. G. & Bindels, R. J. (2004) *J Am Soc Nephrol* **15,** 549-57.
38.   van Abel, M., Hoenderop, J. G., Dardenne, O., St-Arnaud, R., Van Os, C., van Leeuwen, J. P. & Bindels, R. J. (2002) *J Am Soc Nephrol* **13,** 2102-2109.
39.   Winsky, L. & Kuznicki, J. (1995) *J Neurochem* **65,** 381-8.
40.   Gross, M. D., Nelsestuen, G. L. & Kumar, R. (1987) *J Biol Chem* **262,** 6539-45.
41.   Hoenderop, J. G., van Leeuwen, J. P., van der Eerden, B. C., Kersten, F. F., van der Kemp, A. W., Merillat, A. M., Waarsing, J. H., Rossier, B. C., Vallon, V., Hummler, E. & Bindels, R. J. (2003) *J Clin Invest* **112,** 1906-14.
42.   Arnold, D. B. & Heintz, N. (1997) *Proc Natl Acad Sci U S A* **94,** 8842-7.
43.   Hubbard, M. J. & McHugh, N. J. (1995) *FEBS Lett* **374,** 333-7.
44.   Nemere, I., Leathers, V. L., Thompson, B. S., Luben, R. A. & Norman, A. W. (1991) *Endocrinology* **129,** 2972-84.
45.   van de Graaf, S. F., Hoenderop, J. G., Gkika, D., Lamers, D., Prenen, J., Rescher, U., Gerke, V., Staub, O., Nilius, B. & Bindels, R. J. (2003) *Embo J* **22,** 1478-87.
46.   Gkika, D., Mahieu, F., Nilius, B., Hoenderop, J. G. & Bindels, R. J. (2004) *J Biol Chem* **279,** 26351-7.
47.   Koster, H. P., Hartog, A., Van Os, C. H. & Bindels, R. J. (1995) *Cell Calcium* **18,** 187-96.
48.   Neher, E. (1998) *Neuron* **20,** 389-99.

CHAPTER V

Modeling of Transcellular Ca^{2+} Transport in Kidney Reveals a Fundamental Role for Calbindin-D$_{28K}$

Lambers T.T., Hoenderop J.G., Bindels R.J., Hoofd L.

Department of Physiology, Nijmegen Center for Molecular Life Sciences, University Medical Centre Nijmegen, The Netherlands.

Summary

The epithelial Ca^{2+} channel TRPV5 displays Ca^{2+}-dependent negative feedback regulation of channel activity, which is essential during transcellular Ca^{2+} transport to prevent a cellular Ca^{2+} overload. Here, a model of transcellular Ca^{2+} transport in kidney was developed to provide insight in the contribution of calbindin-D_{28K} to TRPV5 activity and transcellular Ca^{2+} transport. The recent finding that calbindin-D_{28K} directly associates with TRPV5 in a Ca^{2+}-dependent fashion was incorporated to further evaluate our results. Renal Ca^{2+}-transporting cells were modeled as a cylinder in which Ca^{2+} enters at the luminal side via TRPV5 from where Ca^{2+} spreads out evenly. The model indicated that at the luminal side a non-equilibrium zone resides were buffering is essential to prevent Ca^{2+} accumulation. Our model predicts that during transcellular Ca^{2+} transport at least ~100 active TRPV5 channels are present at the cell surface of a renal Ca^{2+}-transporting cell. Two possibilities were considered: (*i*) Ca^{2+} enters the cell and subsequently binds to calbindin-D_{28K}; (*ii*) Ca^{2+} passes TRPV5 and is immediately bound by TRPV5-associated calbindin-D_{28K} such that no free Ca^{2+} enters the cell. Our model indicates that in Ca^{2+}-transporting cells, calbindin-D_{28K} efficiently regulates the intracellular Ca^{2+} concentration by providing spatial Ca^{2+}-buffering in close proximity to the TRPV5 pore.

Introduction

Transcellular Ca^{2+} transport in kidney is of fundamental importance to balance the net amount of Ca^{2+} excretion from the body by reabsorbing Ca^{2+} from the pro-urine. In renal Ca^{2+}-transporting cells the Ca^{2+} influx is mediated by the epithelial Ca^{2+} channel TRPV5, which is a distinct member of the Transient Receptor Potential (TRP) family of ion channels (1). In these cells, TRPV5 operates as gate facilitating cellular Ca^{2+} entry due to a steep inward electrochemical gradient across the luminal membrane (2). The activity of this highly Ca^{2+}-selective channel is tightly regulated by the intracellular Ca^{2+} concentration ($[Ca^{2+}]_i$) in close vicinity to the channel mouth (3). Using electrophysiological recordings in inside-out patches a half-maximal inhibition of TRPV5 currents occurred at ~200 nM Ca^{2+} (4). Thus, adequate intracellular buffering of Ca^{2+} is essential for a continuous influx of Ca^{2+} through this channel. In addition, during high rates of transcellular Ca^{2+} transport strict regulation of $[Ca^{2+}]_i$ is crucial in protecting the cell against cytotoxic high levels of Ca^{2+} (5). Buffering of Ca^{2+} by specialized Ca^{2+}-binding proteins (CaBPs) is, therefore, required (6-8). Ca^{2+} entering at the luminal side of the cell will diffuse as Ca^{2+} bound to CaBP to the basolateral side, thereby not affecting other intracellular processes. Subsequently, the Na^+/Ca^{2+}-exchanger (NCX1) and/or the plasma membrane ATPase (PMCA1b) extrude Ca^{2+} into the extracellular compartment. CaBPs have been implicated in facilitated diffusion of Ca^{2+} from the luminal membrane to the basolateral surface by increasing the diffusional range of Ca^{2+} (9-11). In kidney, calbindin-D_{28K} ($CaBP_{28K}$) is contributing to this process, while calbindin-D_{9K} fulfills this role in the

intestine. In the latter organ a comparable mechanism of transcellular Ca^{2+} transport operates as in kidney. Likewise, the intestinal Ca^{2+} transport machinery consists of TRPV6 as the luminal entry channel, calbindin-D_{9K} (CaBP$_{9K}$) for intracellular Ca^{2+} handling and PMCA1b to extrude Ca^{2+} basolaterally.

Negative feedback regulation of channel activity by $[Ca^{2+}]_i$ is a common mechanism occurring in a diverse range of ion channels including voltage and non-voltage-operated ion channels (12, 13). In general, these channels inactivate upon a local rise in $[Ca^{2+}]_i$ in close proximity to the channel pore. One could envisage that upon opening of Ca^{2+} channels a high concentration of Ca^{2+} will be generated. For voltage-operated Ca^{2+} channels, it has been demonstrated that opening of these channels elicits a large Ca^{2+} influx that generates a micro-domain of Ca^{2+} (14). By modifying the spatial and temporal aspects of $[Ca^{2+}]_i$, Ca^{2+}-binding proteins might influence the Ca^{2+}-dependent activity of these ion channels (15). Indeed, CaBP$_{28K}$ was found to affect the activity of L-type voltage-operated channels contributing to the Ca^{2+}-dependent channel activity by increasing the Ca^{2+} sensitivity of the channel (16). Recently, we showed that CaBP$_{28K}$ dynamically controls TRPV5-mediated Ca^{2+} influx (17). At a low $[Ca^{2+}]_i$ CaBP$_{28K}$ translocates from a cytosolic compartment to the plasma membrane and associates with TRPV5. Here, CaBP$_{28K}$ locally buffers the flux of Ca^{2+} entering the cell via TRPV5 thereby preventing inactivation of the channel.

Primary cultures of rabbit connecting tubule (CNT) and cortical collecting duct (CCD) are a well-defined model for TRPV5-mediated transcellular Ca^{2+} transport endogenously expressing the complete transport machinery (2). These cultures are a valid representation of transcellular Ca^{2+} transport in kidney displaying Ca^{2+} fluxes comparable to those *in vivo* and sensitive to regulation by calciotropic hormones and other factors that determine the Ca^{2+} balance (18). Previously, Ca^{2+} measurements in these cultures revealed that no apparent changes in $[Ca^{2+}]_i$ occurred during transcellular Ca^{2+} transport suggesting that overall Ca^{2+} buffering is efficiently controlled in these cells (19). These measurements were, however, not performed at the subcellular level or in close proximity to the channel mouth where Ca^{2+} levels could strongly fluctuate because opening of TRPV5 might generate a micro domain of Ca^{2+} at the channel mouth. Thus, cellular buffering is essential and potentially well regulated during transcellular Ca^{2+} transport across primary cultures of CNT/CCD cells.

The aim of the present study was to evaluate in detail the contribution of CaBP$_{28K}$ to transcellular Ca^{2+} transport in kidney, including the recent findings of CaBP$_{28K}$-TRPV5 association. To this end, mathematical modeling of transcellular Ca^{2+} transport in primary rabbit cultures of CNT/CCD, as a cell system for Ca^{2+} reabsorption *in vivo,* was employed. Our model predicts the physiological importance of CaBP$_{28K}$ as a localized Ca^{2+} buffer providing efficient intracellular Ca^{2+} handling to maintain high levels of transcellular Ca^{2+} transport.

Glossary

A	Average apical cell surface area of primary CNT/CCD cells.
C_{CaBP}	Total $CaBP_{28K}$ concentration
Ca·CaBP	Concentration of Ca^{2+} bound to $CaBP_{28K}$
B_0, B_1	Integration constants
D_{Ca}	Diffusion constant of Ca^{2+}
D_{CaBP}	Diffusion constant of $CaBP_{28K}$
J	Average, experimentally determined, Ca^{2+} flux over primary CNT/CCD cultures
$J_0()$, $J_1()$, $J_2()$	Zeroth, first and second Bessel functions of the first kind, respectively
K_d	Equilibrium constant
k_{on}, k_{off}	Ca^{2+} binding constants of $CaBP_{28K}$
L	Diffusion distance between apical and basolateral membrane
N	Number of TRPV5 channels
p(...)	Port function
r	Cylindrical coordinate (radius)
r_p	TRPV5 pore size
R	Radius of the pore supply area (modeled as cylinder)
z	Cylindrical coordinate (length)
ΔCa_{pore}	Local Ca^{2+} increase at the pore due to the small pore size
$\Delta Ca·CaBP_{pore}$	Local Ca·CaBP increase at the pore due to the small pore size
λ_{AI}	Characteristic distance of non-equilibrium zone at the apical side for model I
λ_{AII}	Characteristic distance of non-equilibrium zone at the apical side for model II
λ_B	Characteristic distance of non-equilibrium zone at the basolateral side
ξ_i	Zero points of the first Bessel function

Theoretical model

To determine mathematically intracellular Ca^{2+} handling during transcellular Ca^{2+} transport, a model was considered where Ca^{2+} enters the cell at the apical side through TRPV5 with a limited pore size r_p. Ca^{2+} that enters the cell via TRPV5 spreads out evenly over a circular region of radius R towards the basolateral side where we considered Ca^{2+} excretion (i.e. via NCX1 and PMCA1b) to be unrestricted **(Fig. 1)**. All these areas, πR^2, together cover the total apical cell surface A.
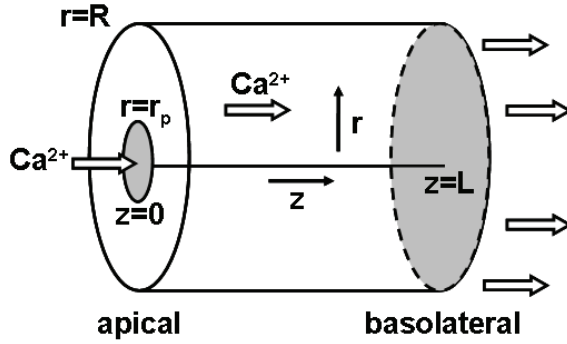
Fig. 1. Model of transcellular Ca^{2+} transport During mathematical modeling of transcellular Ca^{2+} transport from the apical to the basolateral side, a situation was considered where Ca^{2+} enters the cell at the apical side (z=0) through TRPV5 with a limited pore size r_p. Ca^{2+} that enters the cell via TRPV5 spreads out evenly over a circular region of radius R towards the basolateral side where at z=L we considered Ca^{2+} excretion (i.e., via NCX1 and PMCA1b) to be unrestricted.

First, a situation disregarding any Ca^{2+} binding and facilitated diffusion by CaBP$_{28K}$ was considered, as a basic step for the later, more realistic, mathematical treatment incorporating Ca^{2+} binding to CaBP$_{28K}$ and localized CaBP$_{28K}$ buffering by TRPV5 association. In this case, there is only free Ca^{2+} diffusion in the cell, and the steady state diffusion equation for [Ca^{2+}] can be analytically solved in terms of Bessel functions of the cylindrical coordinates r, z[*)]:

$$[Ca^{2+}](r,z) = B_0 - \frac{Jz}{D_{Ca}} + \frac{JR}{D_{Ca}} p(r_p, R; r, z)$$

$$p(r_p, R; r, z) = \sum_{i=1}^{\infty} \frac{2R}{r_p} \frac{J_1(\xi_i r_p / R)}{\xi_i^2 \{J_2(\xi_i)\}^2} J_0(\xi_i r / R) e^{-\xi_i z / R}$$

(1)

Where B_0 is a constant to be determined for the specific calculations (see results), J is the average Ca^{2+} flux, D_{Ca} is the diffusion coefficient of free Ca^{2+}, $J_0()$, $J_1()$ and $J_2()$ are the zeroth, first and second Bessel functions of the first kind respectively, and ξ_i are the zero points of the first Bessel function, $J_1(\xi_i) = 0$. The solution is given in terms of a dimensionless 'port function' p(...) expressing the influence of the small TRPV5 pore size r_p against the 'supply range' R. For the Ca^{2+} flux J we incorporated the average Ca^{2+} flux over primary rabbit CNT/CCD cultures as experimentally determined (100 nmol·h^{-1}·cm^{-2}) **(Fig. 2A)** and the diffusion constant of Ca^{2+} is $0.8*10^{-5}$ cm^2/s (11). Although Bessel functions are mathematically well known, their values must be found from specialized programs or tabulated data impeding a direct insight in the result for the port influence p(...). However, an approximate solution can be found for the TRPV5 location r=z=0, which allows an estimation of the effect of the TRPV5 pore size r_p on the local Ca^{2+} concentration:

[*)] **See supplementary information for details of the mathematical solutions**

$$[Ca^{2+}](0,0) = B_0 + \Delta Ca_{pore}$$

$$\Delta Ca_{pore} = \frac{JR}{D_{Ca}} p(r_p, R; 0, 0) \approx \frac{JR^2}{D_{Ca} r_p} \qquad (2)$$

Where ΔCa_{pore} is the increase due to the small pore size. To obtain insight in the pore architecture, a pore diameter of 5.4 Å was estimated from permeation studies for TRPV6 (20). Because the pore domains of TRPV5 and TRPV6 are highly homologous (2), we assumed the pore size of TRPV5 to be equal to that of TRPV6. If there are N TRPV5 channels over an area A, this implies an average spreading area $\pi R^2 = A/N$ for each TRPV5 and the increase for the average TRPV5 is calculated as:

$$\Delta Ca_{pore} = \frac{JR^2}{D_{Ca}} p(r_p, R; 0, 0) \approx \frac{JA}{\pi D_{Ca} r_p N} \qquad (3)$$

The average apical surface of primary cultures of rabbit CCD/CNT cells, indicative for renal Ca^{2+}-transporting cells *in vivo,* was determined as ~20 μm^2 using confocal imaging of GFP-expressing cells as described previously (17) **(Fig 2B)**.

Next, the effect of Ca^{2+} binding to $CaBP_{28K}$ was considered. In this case, there is additional intracellular Ca^{2+} transport by a diffusing Ca·CaBP complex (facilitated diffusion) such that the solution for the summed concentrations reads:

$$D_{Ca}\left[Ca^{2+}\right] + D_{CaBP}\left[Ca \cdot CaBP\right] = B_1 - Jz + JRp(r_p, R; r, z) \qquad (4)$$

Where again B_1 is a constant to be determined for the specific calculations (see results), D_{CaBP} is the diffusion coefficient of $CaBP_{28K}$ and p(...) is the same function p(...) of eq.(1). The diffusion coefficient of $CaBP_{9K}$ (9 kDa) is determined as $0.12*10^{-5}$ cm^2/s (11). Based on the relation between mass and diffusion coefficient, the diffusion coefficient for $CaBP_{28K}$ (28 kDa) is considered as $0.082*10^{-5}$ cm^2/s. Following the approach of Hoofd and Kreuzer (21), the solution for this facilitated diffusion can be divided into three parts to solve the individual concentrations of Ca^{2+} and Ca·CaBP:

- A luminal side where all Ca^{2+} enters the cell via TRPV5;
- A middle part where both species concentrations (i.e., free Ca^{2+} and Ca^{2+} bound to $CaBP_{28K}$) are close to chemical equilibrium both contributing to the total Ca^{2+} flux;
- A basolateral part where all Ca^{2+} that enters the cell via TRPV5 is transported across the basolateral membrane by NCX1 and PMCA1b.

At this point, we will discern between two possible mechanisms for Ca^{2+} entry:

- **Model I** where Ca^{2+} enters the cell and later binds to $CaBP_{28K}$ for facilitated diffusion to the basolateral membrane;

- **Model II** where, upon entering the cell, Ca^{2+} directly binds to $CaBP_{28K}$ (i.e., no free Ca^{2+} enters at the apical side but is immediately bound by $CaBP_{28K}$) before subsequent facilitated diffusion to the basolateral side. Direct binding of Ca^{2+} to $CaBP_{28K}$ rather then free Ca^{2+}-diffusing before binding $CaBP_{28K}$ was included to further investigate the findings that $CaBP_{28K}$ directly associates with TRPV5 at decreased intracellular Ca^{2+} concentrations (17).

For both models, in the middle part the equilibrium relation between Ca^{2+} and $CaBP_{28K}$ is:

$$[Ca \cdot CaBP] = 4C_{CaBP} \frac{[Ca^{2+}]}{K_d + [Ca^{2+}]} \tag{5}$$

Where C_{CaBP} is the total $CaBP_{28K}$ concentration. Each $CaBP_{28K}$ molecule contains 4 functional binding sites (22), and K_d is the average equilibrium constant. The concentration of $CaBP_{28K}$ in Ca^{2+}-transporting cells in kidney and primary cultures of rabbit CNT/CCD is unknown and variable because of genomic regulation by the calciotropic hormones that determine the Ca^{2+} balance (23). However, Feher *et al.* estimated the concentration of $CaBP_{28K}$ in intestine based upon the concentration of $CaBP_{28K}$ in supernatants from chicken duodenal homogenates (11). According to the same authors, the K_d of $CaBP_{28K}$ is 200 nM. The concentration of $CaBP_{28K}$ in duodenal homogenates in chickens maintained on a normal diet is ~250 μg/ml which translates into ~60 μM, water by weight and given the mucosa is ~70% cytosol. This value is, however, a clear underestimate because $CaBP_{28K}$ is not expressed in all duodenal cells, but merely in enterocytes that results in an overestimation of the volume. Moreover, the expression of $CaBP_{28K}$ in kidney is much higher then the expression in duodenum (24). Since no other values for calbindin concentrations in Ca^{2+}-transporting cells are available and primary cultures of rabbit CNT/CCD cells were maintained under non-stimulated conditions the data from this previous study was used

Equation (5) is sufficient to solve for the individual concentrations in the middle region, however, in the other regions there is no such equilibrium. In the basolateral region where all Ca^{2+} is transported across the basolateral membrane the relation can be calculated as (21):

$$[Ca^{2+}] = \frac{K_d [Ca \cdot CaBP]}{4C_{CaBP} - [Ca \cdot CaBP]} - \frac{J\lambda_B}{D_{Ca}} exp\left(\frac{z - L}{\lambda_B}\right) \tag{6}$$

Where L is the distance between the apical and basolateral membrane which we estimated to be ~20 μm based on confocal laser scanning microscopy of primary rabbit CNT/CCD cultures, indicative for renal Ca^{2+}-transporting cells *in vivo*. The characteristic distance of the non-equilibrium zone at the basolateral side (λ_B) is given by:

$$\lambda_B^{-2} = \frac{k_{on}(4C_{CaBP} - [Ca \cdot CaBP])}{D_{Ca}} + \frac{4k_{off}C_{CaBP}}{D_{CaBP}(4C_{CaBP} - [Ca \cdot CaBP])} \tag{7}$$

Where k_{on} and k_{off} are the Ca^{2+} binding constants for $CaBP_{28K}$. $CaBP_{28K}$ was found to bind Ca^{2+} in at least two distinct kinetic patterns, one arising from high Ca^{2+} affinity sites that bind Ca^{2+} with a k_{on} of $\sim 1*10^7$ $M^{-1}s^{-1}$ and another with lower affinity of $\sim 8*10^7$ $M^{-1}s^{-1}$ (25). For simplification a single averaged k_{on} ($5*10^7$ $M^{-1}s^{-1}$) was used for modeling. Since $K_d = k_{off}/k_{on}$, using the above K_d we find $k_{off} = 10$ s^{-1}.

Equation (7) implies that there is a non-equilibrium zone characterized by the distance λ_B of the equation. The solution can be solved in this form because the flux at the basolateral side is considered uniform, independent of the radial coordinate r.

For the apical side, we can follow the same approach of Hoofd and Kreuzer to calculate a characteristic distance λ_A. However, we have to discern between the two models I and II, leading to different characteristic distances λ_{AI} and λ_{AII}, respectively. For model I, the λ_{AI} is similar to that of equation (7):

$$\lambda_{AI}^{-2} = \frac{k_{on}(4C_{CaBP} - [Ca \cdot CaBP])}{D_{Ca}} + \frac{4k_{off}C_{CaBP}}{D_{CaBP}(4C_{CaBP} - [Ca \cdot CaBP])} \quad (8)$$

Now for the [Ca·CaBP] at the luminal side: For model II, the approach has to be modified accordingly, which leads to a characteristic distance λ_{AII}:

$$\lambda_{AII}^{-2} = \frac{k_{off} + k_{on}[Ca^{2+}]}{D_{CaBP}} + \frac{4k_{on}k_{off}C_{CaBP}}{D_{Ca}(k_{off} + k_{on}[Ca^{2+}])} \quad (9)$$

However, the Ca^{2+} flux is non-uniform and highest at the TRPV5 pore, $r < r_p$, so that no mathematical solution for the concentrations can be found for this region. Nonetheless, an estimate can be made using the characteristic distance formulas since:

- Down to the apical zone, $z \approx \lambda_{AI}$ or λ_{AII}, the solution of the middle, equilibrium, zone can be followed allowing estimates of $[Ca^{2+}]$ and $[Ca \cdot CaBP]$ at $z = \lambda_{AI}$ or λ_{AII}.

- In the apical zone for model I, there are little changes in $[Ca \cdot CaBP]$ since the flux towards the apical membrane is zero ($CaBP_{28K}$ cannot pass through the membrane and does not associate with TRPV5). So, the $[Ca \cdot CaBP]$ at $z = \lambda_{AI}$ can be assumed to be the $[Ca \cdot CaBP]$ in the apical zone.

- In the apical zone for model II, there are little changes in $[Ca^{2+}]$ since the flux towards the apical membrane is zero and $CaBP_{28K}$ immediately buffers the Ca^{2+} (see above). So, the $[Ca^{2+}]$ at $z = \lambda_{AII}$ can be assumed to be the $[Ca^{2+}]$ in the apical zone.

- In turn, knowing either $[Ca \cdot CaBP]$ (model I) or $[Ca^{2+}]$ (model II), the other species concentration $[Ca^{2+}]$ or $[Ca \cdot CaBP]$ follows from equation (4).

Consequently, for model I, the 'port function' p(…) is present only in $[Ca^{2+}]$ and its peak value can be calculated using equations (2) and (3) with an adapted value for B_0: $B_0' = (B_1 - [Ca \cdot CaBP](0,0))/D_{CaBP}$ according to equation (4). For model II, there is no peak in $[Ca^{2+}]$ but

a peak in [Ca·CaBP] because $CaBP_{28K}$ binds TRPV5 determining that equations (2), (3) have to be modified accordingly:

$$[Ca \cdot CaBP](0,0) = B_0'' + \Delta Ca \cdot CaBP_{pore}$$
$$\Delta Ca \cdot CaBP_{pore} = \frac{JR}{D_{CaBP}} p(r_p, R; 0, 0) \tag{10}$$

$$\Delta Ca \cdot CaBP_{pore} \approx \frac{JA}{\pi D_{CaBP} r_p N} \tag{11}$$

Results

Cell model for transcellular Ca^{2+} transport

TRPV5 was originally cloned from primary cultures of rabbit CNT/CCD which is a well studied model for transcellular Ca^{2+} transport in kidney (26). These primary cultures were used to obtain experimentally derived Ca^{2+} transport rates from the apical towards the basolateral compartment as described previous (17). In addition, 10 μM ruthenium red, a potent TRPV5 blocker, was added during the transport assay to establish TRPV5-mediated transcellular Ca^{2+} transport. These cultures displayed a net ruthenium red-sensitive Ca^{2+} flux from apical to the basolateral side of ~100 nmol/h/cm^2 **(Fig. 2A)** and consisted of ~1*10^6 cells/cm^2 as determined after transcellular Ca^{2+} transport measurements. By confocal imaging of GFP-expressing primary rabbit CNT/CCD cultures **(Fig. 2A)** the luminal surface of a single cell was estimated to be ~20 μm^2 and the distance between apical and basolateral membrane ~20 μm (17).
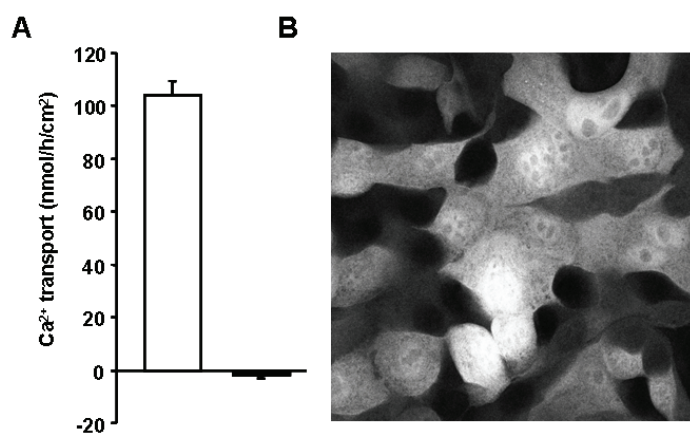
Fig. 2. Transcellular Ca^{2+} transport across primary cultures of rabbit CNT/CCD **(A)** Transcellular Ca^{2+} transport across primary cultures of rabbit CNT/CCD is expressed as mean ± SEM (open bar). 10 μM ruthenium red was added to the apical side of the cell monolayer during the transport measurements to estimate TRPV5-mediated Ca^{2+} transport (closed bar). **(B)** Confocal microscopy image of these cultures expressing EGFP grown to confluence on filter supports. Based on these images an average apical cell surface of ~20 μm^2 and apical to basolateral distance of ~20 μm was estimated.

Recently, we demonstrated a direct interaction between TRPV5 and $CaBP_{28K}$ (17). To further investigate the implication of these data and to establish the role of $CaBP_{28K}$ in intracellular Ca^{2+} handling, transcellular Ca^{2+} transport across primary cultures of rabbit CNT/CCD was modeled primarily focusing on intracellular Ca^{2+} handling. In our calculations $[Ca^{2+}]$ at the basolateral excretion site of the cell was assumed to be zero such that Ca^{2+} entering the cell is transported unrestrictedly across the basolateral membrane (i.e. extruded via NCX1 and PMCA1b). In this case the integration can be calculated by $B_0 = J.L/D_{Ca}$ according to equation (1) (since all the other terms are close to zero at z=L). Similarly, B_1 can be calculated using equation (4). Using the experimentally determined Ca^{2+} flux and cell size $[Ca^{2+}]$ bound to $CaBP_{28K}$ ($[Ca \cdot CaBP]$) and $[Ca^{2+}]$ not buffered by $CaBP_{28K}$ were calculated to obtain an overall estimate of the $[Ca^{2+}]_i$ in primary cultures of rabbit CNT/CCD cells **(Fig. 3A)**. The characteristic size of the basolateral zone λ_B, as calculated using equation (7) is 0.32 µm. This is rather small, but its influence is large as the local $[Ca^{2+}]$ rises to 0.15 µM in this small zone. This in turn implies that $[Ca \cdot CaBP]$ is ~91 µM **(Fig. 3B)**. For the apical zone, the characteristic sizes are $\lambda_{AI} = 0.43$ µm for model I, and $\lambda_{AII} = 0.43$ µm for model II according to equations (8) and (9), respectively.
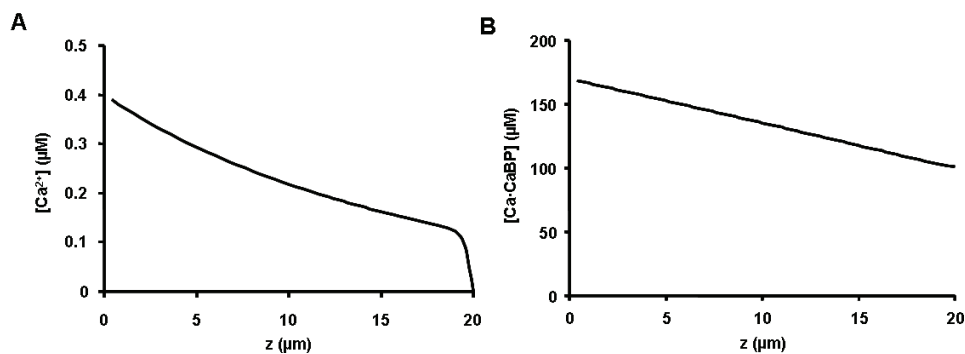
Fig. 3. Intracellular Ca^{2+} profile during transcellular Ca^{2+} transport

Concentration profiles of free Ca^{2+} **(A)** and Ca^{2+} bound to $CaBP_{28K}$ **(B)** in the middle and basolateral zones for both models I and II. Basolateral Ca^{2+} transport (via NCX1 and PMCA1b) was considered to be unrestricted such that all Ca^{2+} entering the cell is excreted at the basolateral side at z=20 µm.

Amount of active TRPV5 channels at the luminal plasma membrane

Overall luminal Ca^{2+} influx is the net result of the amount of channels at the plasma membrane and their single channel activity. Single channel conductance in relation to the total membrane transport capacity is a reliable measurement for the number of channels at the cell surface. *In vivo* TRPV5 conductance is, however, unknown. This makes the estimation of the number of TRPV5 channels contributing to the overall Ca^{2+} transport in primary cultures of

rabbit CNT/CCD not possible via the above-described approach. Therefore, our model was employed to estimate the amount of TRPV5 channels during the process of transcellular Ca^{2+} transport. We postulate that with a given Ca^{2+} flux the local $[Ca^{2+}]$ in close vicinity to the TRPV5 pore is determined by the number of TRPV5 channels in the luminal plasma membrane. This relation is given for the apical domain (r=z=0) according to equations (1) to (3) for model I **(Fig. 4)**. Thus, indicating that the more TRPV5 channels are active at the luminal membrane the lower the $[Ca^{2+}]$ in the TRPV5 pore will be since the flux is divided over the total number of channels.
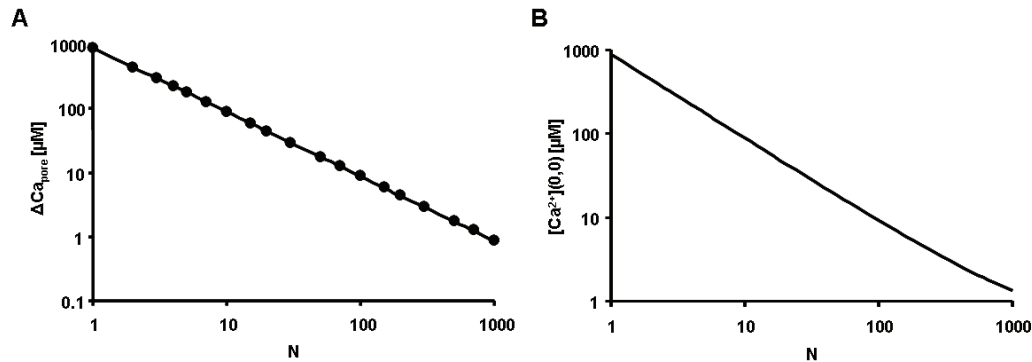

Fig. 4. Relation of apical $[Ca^{2+}]$ and number of channels at the cell surface

Local Ca^{2+} increase ΔCa_{pore} **(A)** and $[Ca^{2+}]$ at the TRPV5 location r=z=0 **(B)**, according to equations (3) (approximation; points in panel A) and equation (2) (using Bessel functions; line in both panels) plotted against the number of TRPV5 channels in the apical plasma membrane, N. Difference between approximation of equation (3) and exact Bessel calculation via equations (1), (2) are negligible.

CaBP$_{28K}$ associates with TRPV5 and thereby prevents channel inactivation because Ca^{2+} that enters the cell via TRPV5 is buffered by CaBP$_{28K}$ (17). To estimate a minimal number of TRPV5 channels contributing to the determined Ca^{2+} flux we assumed that CaBP$_{28K}$ binds all Ca^{2+} entering the cell and that all channels inactivate upon Ca^{2+} saturation of CaBP$_{28K}$. Thus, the total CaBP$_{28K}$ concentration is a measure for the amount of active channels at the cell surface. To this end, the local Ca·CaBP increase (ΔCa·CaBP$_{pore}$) and $[Ca^{2+}]$ bound to CaBP$_{28K}$ ([Ca·CaBP]) at the apical membrane (r=z=0) were plotted against the number of TRPV5 channels at the apical membrane (N) **(Fig. 5)**. Importantly, since one CaBP$_{28K}$ molecule is capable of binding four Ca^{2+} ions (22), [Ca·CaBP] cannot exceed the maximum binding capacity of CaBP$_{28K}$ which is 4 times the total CaBP$_{28K}$ concentration C$_{CaBP}$ (indicated in both figures with broken lines). The point of intersection in the figures indicates the minimal number of TRPV5 channels at the plasma membrane (i.e. ~108). This in turn implies that each TRPV5 channel covers a 'supply area' (πR^2) of 20/108 μm^2 translating into R = 0.24 μm. Knowing the total Ca^{2+} flux per surface area and the size of the apical cell surface, the

estimation of the number of channels during renal transcellular Ca^{2+} transport further indicates that the single channel Ca^{2+} flux of TRPV5 is in the order of $5*10^{-11}$ nmol/s suggesting that $\sim 3*10^{4}\,Ca^{2+}$ ions pass TRPV5 per second (see supplemental data for a detailed description). Thus during renal Ca^{2+} reabsorption at least ~ 100 TRPV5 channels, with a single channel activity in the order of $3*10^{4}\,Ca^{2+}$ ions per second, are in the plasma membrane of a single cell contributing to the Ca^{2+} reabsorption.
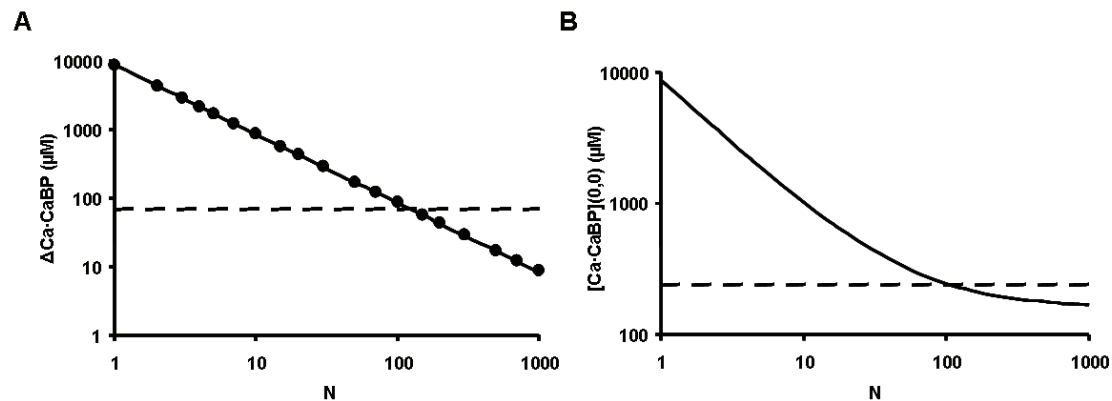

A

B

Fig. 5. Determination of the number of TRPV5 channels at the apical membrane of primary cultures of rabbit CNT/CCD

Local Ca·CaBP increase ΔCa·CaBP$_{pore}$ **(A)** and bound [Ca^{2+}], [Ca·CaBP] at the TRPV5 location r=z=0 **(B)** plotted against the number of TRPV5 channels in the apical plasma membrane, N (point and closed lines). Open lines represent the maximum Ca^{2+} binding capacity of CaBP$_{28K}$, which is 4 times the CaBP$_{28K}$ concentration C$_{CaBP}$. Point of intersection indicates the minimum amount of TRPV5 channels in the apical plasma membrane during transcellular Ca^{2+} transport across primary cultures of rabbit CNT/CCD (N$\approx$108). See text for details.

Role of calbindin-D$_{28K}$ in local Ca^{2+} buffering

To investigate the influence of CaBP$_{28K}$ on the Ca^{2+} buffering capacity within the TRPV5 pore domain the local [Ca^{2+}] was calculated in that area. First, Ca^{2+} influx without any Ca^{2+} binding and facilitated diffusion by CaBP$_{28K}$ (no Ca^{2+} buffering) was considered (equation 1, with R = 0.2 μm originating from the estimation described above, R = 0.24 μm) **(Fig. 6A)**. This resulted in a maximal [Ca^{2+}] in the TRPV5 pore domain and high basal [Ca^{2+}]$_i$ of 7.5 μM. Next, buffering by CaBP$_{28K}$ was considered without CaBP$_{28K}$ binding to TRPV5 (model I) **(Fig. 6B)**. As anticipated, and in line with previous modeling studies (11), this resulted in a decrease of basal [Ca^{2+}]$_i$ to $\sim$0.39 μM. The local [Ca^{2+}] in the TRPV5 pore domain, however, still revealed a maximal [Ca^{2+}] as a result of Ca^{2+} accumulating without sufficient buffering. Subsequently, CaBP$_{28K}$-TRPV5 association was included (model II) which resulted in the disappearance of the local Ca^{2+} peak within the TRPV5 pore domain demonstrating the important contribution of CaBP$_{28K}$ to the local Ca^{2+}-buffering **(Fig. 6C)**.
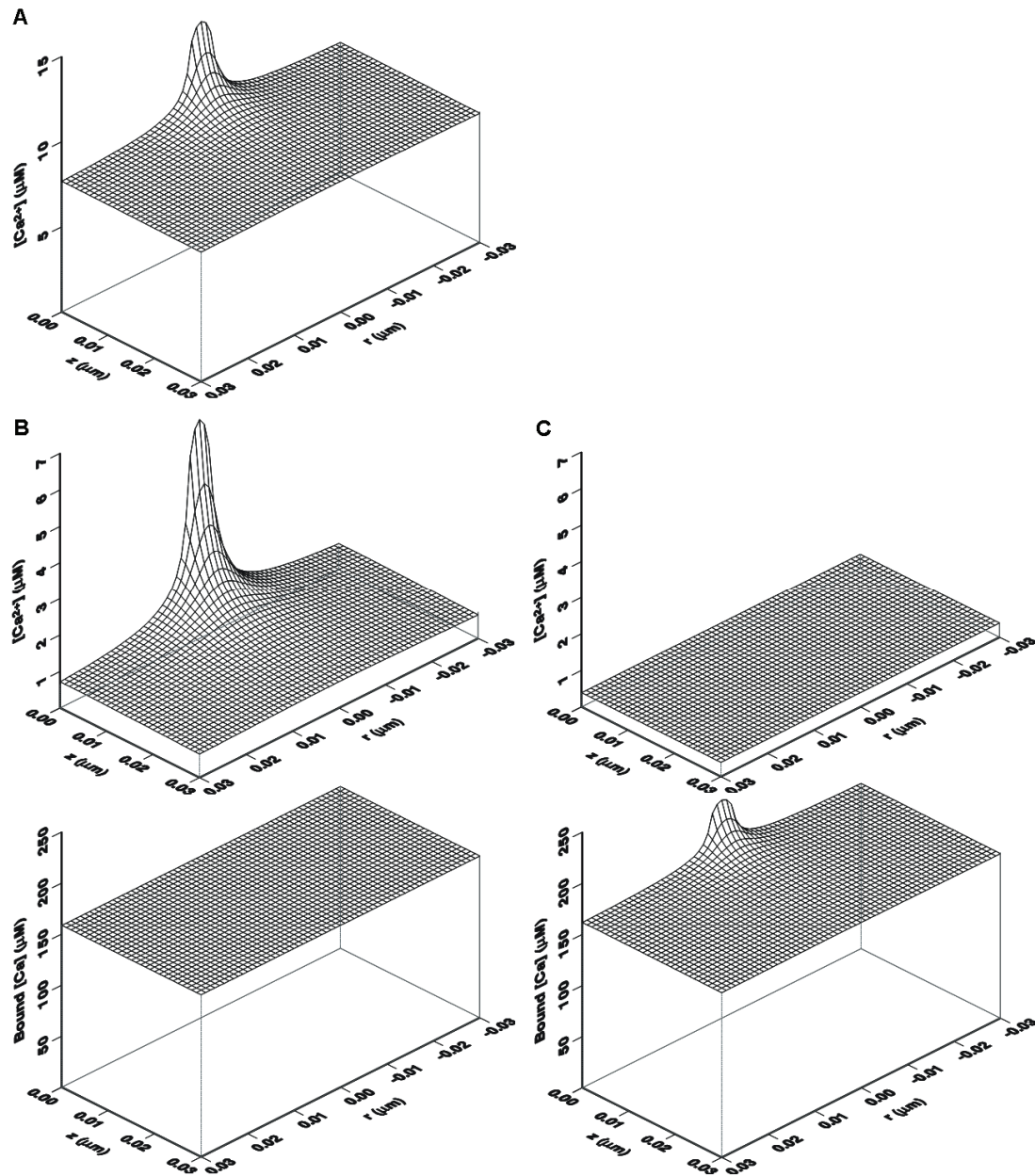
Fig. 6. Role of CaBP$_{28K}$ in maintaining [Ca^{2+}] in the TRPV5 pore

Representation of the Ca^{2+} profile during transcellular Ca^{2+} transport across primary cultures of rabbit CNT/CCD in vicinity of the TRPV5 pore (field sizes of 0.03 µm) **(A)** [Ca^{2+}] in the TRPV5 pore domain for a supply radius R of 0.2 µm in the absence of CaBP$_{28K}$ (no Ca^{2+}-buffering or facilitated diffusion). **(B)** Free [Ca^{2+}] (upper panel) and [Ca^{2+}] bound to CaBP$_{28K}$ (lower panel) in the vicinity of the TRPV5 pore for a supply radius R of 0.2 µm with Ca^{2+}-buffering and facilitated diffusion by CaBP$_{28K}$ but without TRPV5-CaBP$_{28K}$ association (model I). **(C)** Free [Ca^{2+}] (upper panel) and [Ca^{2+}] bound to CaBP$_{28K}$ (lower panel) in the vicinity of the TRPV5 pore for a supply radius R of 0.2 µm with Ca^{2+}-buffering and facilitated diffusion by CaBP$_{28K}$ and with TRPV5-CaBP$_{28K}$ association (model II).

Discussion

In the present study, a mathematical model was developed demonstrating the contribution of $CaBP_{28K}$ to the process of facilitated transcellular Ca^{2+} transport occurring in renal Ca^{2+}-transporting cells. Two versions of the model were developed which may or may not be active simultaneously. These models indicate that *i*) at the luminal side of the epithelial cell a non-equilibrium zone resides where local buffering is essential to prevent accumulation of Ca^{2+}; *ii*) with a given flux $[Ca^{2+}]$ within the TRPV5 pore domain is determined by the number of active TRPV5 channels present at the apical cell surface; *iii*) typically, a minimum of ~100 TRPV5 channels are present at the luminal surface of the Ca^{2+}-transporting epithelial cells; *iv*) association of $CaBP_{28K}$ with TRPV5 prevents a local accumulation of Ca^{2+} within the TRPV5 pore domain, thereby delaying channel inactivation.

Modeling of transcellular Ca^{2+} transport in primary cultures of rabbit CNT/CCD reveals that at the basolateral membrane the non-equilibrium zone is relatively small, however, its influence is high since $[Ca^{2+}]$ within this particular domain increases to ~150 nM (figure 3). Basolateral Ca^{2+} excretion is an interplay between NCX1 and PMCA1b that are both affected by $[Ca^{2+}]$ at the basolateral interior of the cell. At least for NCX1 it has been shown that Ca^{2+} directly binds to the exchanger with an apparent affinity of 140-400 nM which initiates the excretion of Ca^{2+} (27). The activity of PMCA1b is highly dependent on the Ca^{2+} sensor calmodulin which in its Ca^{2+} bound state occupies an auto-inhibitory side, thereby activating PMCA1b (28). The non-equilibrium zone at the basolateral membrane is thus of physiological importance for activation of NCX1 and PMCA1b to extrude Ca^{2+} across the basolateral membrane. Importantly, in our model the basolateral $[Ca^{2+}]$ is in the physiological range essential for NCX1 and PMCA1b activation, substantiating the reliability of our model.

Unlike previous modeling studies that adapted the properties of CaBPs to determine the Ca^{2+} fluxes, our model focuses on the intrinsic mechanism of intracellular Ca^{2+} handling during experimentally derived Ca^{2+} fluxes. Taking into account the physiological Ca^{2+} fluxes and cell properties our model reveals that at the luminal entry side Ca^{2+} accumulates when no adequate Ca^{2+} buffering (and facilitated diffusion of Ca^{2+}) is provided. In this case the determined $[Ca^{2+}]_i$ is beyond the normal physiological range underlining the need for high capacity Ca^{2+} buffering in Ca^{2+}-transporting cells. Importantly, when Ca^{2+} buffering by $CaBP_{28K}$ is included $[Ca^{2+}]_i$ is within the physiological range. This is in line with previous models that suggested an important role for CaBPs in the facilitated diffusion of Ca^{2+} and protection against Ca^{2+} toxicity, thereby allowing high levels of transcellular Ca^{2+} transport (11, 15). The $[Ca^{2+}]$ in the TRPV5 pore domain under these conditions, however, will be high because Ca^{2+} that enters the cell via TRPV5 is not immediately buffered. This would result in preliminary TRPV5

inactivation and insufficient transport of Ca^{2+}. However, when $CaBP_{28K}$-TRPV5 association is included in the model the $[Ca^{2+}]$ peak within the TRPV5 pore domain is abolished, demonstrating the significant effect of localized buffering by $CaBP_{28K}$. The association of TRPV5 and $CaBP_{28K}$ is thus of physiological importance to prevent local accumulation of Ca^{2+} and to facilitate high rates of transcellular Ca^{2+} transport. Importantly, this accumulation is visible in our model and in line with the predominant apical localization of $CaBP_{28K}$ in renal Ca^{2+}-transporting cells, and accumulation at the cell surface upon a decrease in $[Ca^{2+}]_i$ (17). Reflecting the previous results that no apparent changes in the overall $[Ca^{2+}]_i$ are observed during transcellular Ca^{2+} transport this supports our findings that $CaBP_{28K}$ prevents local accumulation by association with TRPV5. In addition, the essential role of $CaBP_{28K}$ in these renal Ca^{2+}-transporting epithelia is underlined by the coordinated expression of $CaBP_{28K}$ and TRPV5 (23). The expression of both proteins, along with the other components of transcellular Ca^{2+} transport, is coupled in such a way that whenever the expression of TRPV5 changes the abundance of the other Ca^{2+} transport proteins follows accordingly. This coordinated control provides for efficient regulation of renal Ca^{2+} reabsorption (23).

A valuable readout in determining ion channel regulation is the single channel conductance that discriminates between regulation of channel activity and cell surface expression. Single channel data of TRPV5-mediated Na^+ currents is available, while no reliable measurements have been made in the presence of extracellular Ca^{2+} (2). The relation between the number of TRPV5 channels and $[Ca^{2+}]$ in the TRPV5 pore with a given influx, however, allows an estimate of the number of channels when the local luminal $[Ca^{2+}]$ is known. Our previous findings that $CaBP_{28K}$ associates with TRPV5 and acts as a dynamic Ca^{2+} buffer controlling TRPV5 activity allows for an alternative approach (17). In our mathematical model of transcellular Ca^{2+} transport, which is supported by experimental evidence (17), Ca^{2+} entering the cell via TRPV5 is directly bound by $CaBP_{28K}$ such that no free Ca^{2+} enters the cell (model II). Since TRPV5 is inhibited upon a rise in the local $[Ca^{2+}]$ this suggests that when $CaBP_{28K}$ is saturated with Ca^{2+} active channels are not present on the cell surface. Thus, with a given flux the total $CaBP_{28K}$ concentration is a measure of the minimal amount of active TRPV5 channels at the plasma membrane. Because each $CaBP_{28K}$ molecule can bind 4 Ca^{2+} ions (22) the effective Ca^{2+} binding capacity reflects four times the $CaBP_{28K}$ concentration which translates in ~100 TRPV5 channels at the plasma membrane. Thus, during renal transcellular Ca^{2+} transport the minimal number of TRPV5 channels at the cell surface that contribute to Ca^{2+} flux is in the order of 100 channels per cell. Adapting this value and knowing the transcellular Ca^{2+} transport rate and the size of the cell surface we estimate that $3*10^4$ Ca^{2+} ions pass each TRPV5 channel per second during renal transcellular Ca^{2+} transport *in vivo* (see supplemental data for calculation).

In conclusion, our mathematical model describes the essential role of CaBPs in preventing local accumulation of Ca^{2+} in micro-domains in close vicinity of TRPV5 during transcellular Ca^{2+} transport. Thus, spatial buffering reduces the apical $[Ca^{2+}]$ and tempers the region in which $[Ca^{2+}]$ exceeds to levels that would cause inactivation of TRPV5.

Acknowledgements

References

1. Montell, C., Birnbaumer, L., Flockerzi, V., Bindels, R. J., Bruford, E. A., Caterina, M. J., Clapham, D. E., Harteneck, C., Heller, S., Julius, D., Kojima, I., Mori, Y., Penner, R., Prawitt, D., Scharenberg, A. M., Schultz, G., Shimizu, N. & Zhu, M. X. (2002) *Mol Cell* **9,** 229-31.
2. Hoenderop, J. G., Nilius, B. & Bindels, R. J. (2005) *Physiol Rev* **85,** 373-422.
3. Hoenderop, J. G., van der Kemp, A. W., Hartog, A., van de Graaf, S. F., van Os, C. H., Willems, P. H. & Bindels, R. J. (1999) *J Biol Chem* **274,** 8375-8.
4. Nilius, B., Prenen, J., Vennekens, R., Hoenderop, J. G., Bindels, R. J. & Droogmans, G. (2001) *Cell Calcium* **29,** 417-28.
5. Tymianski, M. (1996) *Adv Neurol* **71,** 85-105.
6. Pauls, T. L., Cox, J. A. & Berchtold, M. W. (1996) *Biochim Biophys Acta* **1306,** 39-54.
7. Lukas, W. & Jones, K. A. (1994) *Neuroscience* **61,** 307-16.
8. Schwaller, B., Meyer, M. & Schiffmann, S. (2002) *Cerebellum* **1,** 241-58.
9. Bronner, F. (1989) *Am J Physiol* **257,** F707-11.
10. Bronner, F. & Stein, W. D. (1988) *Am J Physiol* **255,** F558-62.
11. Feher, J. J., Fullmer, C. S. & Wasserman, R. H. (1992) *Am J Physiol* **262,** C517-26.
12. Kits, K. S. & Mansvelder, H. D. (1996) *Invert Neurosci* **2,** 9-34.
13. Jones, L. P., DeMaria, C. D. & Yue, D. T. (1999) *Biophys J* **76,** 2530-52.
14. Neher, E. (1998) *Neuron* **20,** 389-99.
15. Roberts, W. M. (1993) *Nature* **363,** 74-6.
16. Lee, D., Obukhov, A. G., Shen, Q., Liu, Y., Dhawan, P., Nowycky, M. C. & Christakos, S. (2006) *Cell Calcium* **39,** 475-85.
17. Lambers, T. T., Mahieu, F., Oancea, E., Hoofd, L., de Lange, F., Mensenkamp, A. R., Voets, T., Nilius, B., Clapham, D. E., Hoenderop, J. G. & Bindels, R. J. (2006) *Embo J* **25,** 2978-88.
18. Bindels, R. J., Hartog, A., Timmermans, J. & Van Os, C. H. (1991) *Am J Physiol* **261,** F799-807.
19. Koster, H. P., Hartog, A., Van Os, C. H. & Bindels, R. J. (1995) *Cell Calcium* **18,** 187-96.
20. Voets, T., Janssens, A., Droogmans, G. & Nilius, B. (2004) *J Biol Chem* **279,** 15223-30.
21. Hoofd, L. & Kreuzer, F. (1979) *J Math Biol* **8,** 1-13.
22. Venters, R. A., Benson, L. M., Craig, T. A., Bagu, J., Paul, K. H., Kordys, D. R., Thompson, R., Naylor, S., Kumar, R. & Cavanagh, J. (2003) *Anal Biochem* **317,** 59-66.
23. Lambers, T. T., Bindels, R. J. & Hoenderop, J. G. (2006) *Kidney Int* **69,** 650-4.
24. Christakos, S., Gill, R., Lee, S. & Li, H. (1992) *J Nutr* **122,** 678-82.
25. Nagerl, U. V., Novo, D., Mody, I. & Vergara, J. L. (2000) *Biophys J* **79,** 3009-18.
26. Abe, J., Nakano, T., Nishii, Y., Matsumoto, T., Ogata, E. & Ikeda, K. (1991) *Endocrinology* **129,** 832-7.
27. Levitsky, D. O., Nicoll, D. A. & Philipson, K. D. (1994) *J Biol Chem* **269,** 22847-52.
28. Strehler, E. E. & Zacharias, D. A. (2001) *Physiol Rev* **81,** 21-50.

Supplemental information: Theory of the model

The model layout

Transepithelial Ca^{2+} transport is modeled in cylindrical coordinates, radial coordinate r and longitudinal coordinate z. Ca^{2+} enters at the apical side, z= 0, through a centrally located circular region of radius r_P, the TRPV5 pore. Transported Ca^{2+} leaves the cell through the basolateral side, z= L, and there is no transport through the cell cylinder side, r= R.
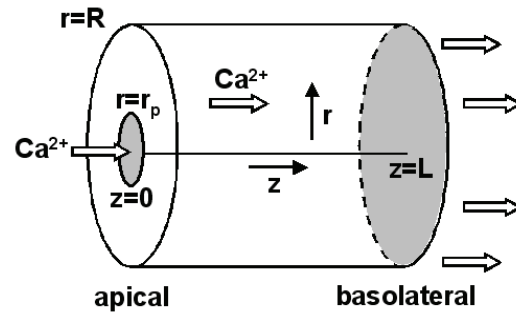
Glossary

C_{CaBP}	Total $CaBP_{28K}$ concentration
$[Ca^{2+}]$	Concentration of Ca^{2+}
$[Ca \cdot CaBP]$	Concentration of Ca^{2+} bound to $CaBP_{28K}$
B_0	Integration constant
D_{Ca}	Diffusion constant of Ca^{2+}
D_{CaBP}	Diffusion constant of $CaBP_{28K}$
$exp()$	Exponential function
$f_{R,i}(r)$, $f_{Z,i}(z)$	Function terms in the separation of variables analysis
$g_I(z)$, $g_{II}(z)$	Function terms in the non-equilibrium models
H_i	Constants in the separation-of-variables solution
J	Total Ca^{2+} flux
$J_0()$, $J_1()$, $J_2()$	Zeroth, first and second Bessel functions of the first kind, respectively
K_d	Equilibrium constant
k_{on}, k_{off}	Ca^{2+} binding constants of $CaBP_{28K}$
L	Diffusion distance between apical and basolateral membrane
p(...)	Port function
r	Cylindrical coordinate (radius)
r_P	TRPV5 pore size
R	Radius of the pore supply area (modelled as cylinder)
t	Integration variable
$Y_0()$	Zeroth Bessel function of the second kind respectively
z	Cylindrical coordinate (length)
λ_{AI}	Characteristic distance of non-equilibrium zone at the apical side for model I

λ_{AII}	Characteristic distance of non-equilibrium zone at the apical side for model II
λ_B	Characteristic distance of non-equilibrium zone at the basolateral side
ρ	Net reaction rate of Ca^{2+} binding to calbindin
ξ_i	Zero points of the first Bessel function

Basic model: no Ca^{2+} binding to $CaBP_{28K}$.

In this case, there is only free Ca^{2+} diffusion, and the steady state concentration $[Ca^{2+}](r,z)$, follows from the diffusion equation:

$$D_{Ca}\nabla^2\left[Ca^{2+}\right](r,z) = 0 \tag{10}$$

where

$$\nabla^2 = \left(\frac{\partial^2}{\partial r^2} + \frac{1}{r}\frac{\partial}{\partial r} + \frac{\partial^2}{\partial z^2}\right) \tag{11}$$

The boundary conditions of this mathematical problem are: no flux through the cylinder side (r= R), since all Ca^{2+} leaves through the basolateral side:

$$D_{Ca}\left(\frac{\partial\left[Ca^{2+}\right]}{\partial r}\right)(R,z) = 0 \quad \text{for any } z \tag{12}$$

and only influx in the central region:

$$D_{Ca}\left(\frac{\partial\left[Ca^{2+}\right]}{\partial z}\right)(r,0) = \begin{cases} -JR^2/r_P{}^2 & r < r_P \\ 0 & r_P < r < R \end{cases} \tag{13}$$

Note that the influx is assumed constant over the TRPV5 pore and that the total incoming flux is $(\pi r_p{}^2)\times(JR^2/r_p{}^2) = \pi R^2 J$, an average flux J over the whole cylinder area πR^2.

Away from the apical side, for increasing z, the Ca^{2+} will spread out evenly and the flux will become uniform, independent of r:

$$D_{Ca}\left(\frac{\partial\left[Ca^{2+}\right]}{\partial z}\right)(r, z \to \infty) = -J \tag{14}$$

with an obvious solution:

$$\left[Ca^{2+}\right](r,z) = B_0 - \frac{Jz}{D_{Ca}} \tag{15}$$

where B_0 is an integration constant. Then, the full solution can be derived as a deviation from this function:

$$\left[Ca^{2+}\right](r,z) = B_0 - \frac{Jz}{D_{Ca}} + \frac{JR}{D_{Ca}}p\left(r_p,R;r,z\right) \tag{16}$$

written here in terms of a dimensionless function p(…) which we shall call 'port function', and constructed by the standard method of separation of variables:

$$p(r_p, R; r, z) = \sum_{i=1}^{\infty} f_{R,i}(r) f_{Z,i}(z) \tag{17}$$

where each term in the summation must obey equation (1):

$$f_{Z,i}(z)\left(\frac{\partial^2}{\partial r^2} + \frac{1}{r}\frac{\partial}{\partial r}\right)f_{R,i}(r) + f_{R,i}(r)\frac{\partial^2}{\partial z^2}f_{Z,i}(z) = 0 \tag{18}$$

This is rewritten in the form

$$-\frac{\left(\frac{\partial^2}{\partial r^2} + \frac{1}{r}\frac{\partial}{\partial r}\right)f_{R,i}(r)}{f_{R,i}(r)} = \frac{\frac{\partial^2}{\partial z^2}f_{Z,i}(z)}{f_{Z,i}(z)} = \frac{\xi_i^2}{R^2} \tag{19}$$

The ξ_i has to be a constant since the first part is independent of z and the second part is independent of r so all parts have to be independent of both variables. Then, textbook mathematics learns that the first part solution is a zero-order Bessel function and the second part solution is an exponential function so that:

$$p(r_p, R; r, z) = \sum_{i=1}^{\infty} H_i \, J_0(\xi_i r / R) \, exp(-\xi_i z / R) \tag{20}$$

where the constants H_i and ξ_i yet have to be determined. Mathematically, also the Bessel function $Y_0(\ldots)$ and the increasing exponential function $exp(+\xi_i z/R)$ are possible as a solution, but the first one is not bounded for r= 0 (approaches infinity) and the second one violates the assumption of approaching equation (15) for large z.

For the ξ_i, we use the boundary condition of no flux through the cylinder side at r=R, equation (12), worked out as:

$$JR\sum_{i=1}^{\infty} H_i \frac{\xi_i}{R} J_1(\xi_i) \, e^{-\xi_i z/R} = 0 \tag{21}$$

which has to be true for any z. This is only possible if

$$J_1(\xi_i) = 0 \tag{22}$$

so that the ξ_i are the intersection points of the first Bessel function with its horizontal axis. This solution has to obey boundary condition (13), but that is easier worked out for the derivative of equation (13):

$$D_{Ca}\left(\frac{\partial^2[Ca^{2+}]}{\partial r\partial z}\right)(r,0) = \frac{JR^2}{r_p^2}\delta(r - r_P) \tag{23}$$

where $\delta(\ldots)$ is the Dirac delta function. This leads to:

$$JR\sum_{i=1}^{\infty} H_i \frac{\xi_i^2}{R^2} J_1(\xi_i r / R) = \frac{JR^2}{r_p^2}\delta(r - r_p) \tag{24}$$

Both sides of this identity can be multiplied by $rJ_1(\xi_k r/R)/(JR)$ and integrated over r from $0 \rightarrow R$:

$$\int_0^R dr \cdot r\, J_1(\xi_k r / R) \sum_{i=1}^{\infty} H_i \frac{\xi_i^2}{R^2} J_1(\xi_i r / R) = \int_0^R dr \cdot r\, J_1(\xi_k r / R) \frac{R}{r_p^2} \delta(r - r_p) \tag{25}$$

where the left side can be rewritten as, defining t= r/R and rearranging:

$$\sum_{i=1}^{\infty} H_i \xi_i^2 \int_0^1 dt \cdot t\, J_1(\xi_k t) J_1(\xi_i t) = \int_0^R dr \cdot r\, J_1(\xi_k r / R) \frac{R}{r_p^2} \delta(r - r_p) \tag{26}$$

so that the orthonormality relation for $J_1()$ can be used:

$$\int_0^1 dt \cdot t\, J_1(\xi_k t) J_1(\xi_i t) = \begin{cases} \frac{1}{2}\{J_2(\xi_k)\}^2 & \text{if } k = i \\ 0 & \text{if } k \neq i \end{cases} \tag{27}$$

to yield, together with the integration over the Dirac delta function:

$$H_k \xi_k^2 \frac{1}{2}\{J_2(\xi_k)\}^2 = r_P\, J_1(\xi_k r_P / R) \frac{R}{r_p^2} \tag{28}$$

from which the terms H_k can be solved as:

$$H_k = \frac{2R\, J_1(\xi_k r_p / R)}{r_p \xi_k^2 \{J_2(\xi_k)\}^2} \quad k = 1,2,\dots \tag{29}$$

which fixes the solution for $p(r_P,R;r,z)$ as:

$$p(r_P,R;r,z) = \sum_{i=1}^{\infty} \frac{2R\, J_1(\xi_i r_p / R)}{r_p \xi_i^2 \{J_2(\xi_i)\}^2} J_0(\xi_i r / R) exp(-\xi_i z / R) \tag{30}$$

To appreciate the effect of TRPV5 on the intracellular Ca^{2+} concentration, it is important to see how this function behaves at the coordinates where the TRPV5 is located, i.e., r=z=0. In the case of a small port radius, $r_P/R \ll 1$, we can derive an approximate solution for $p(r_P,R;0,0)$ by replacing the sum over i by an integral over di:

$$p(r_P,R;0,0) \approx \int_0^{\infty} di \cdot \frac{2R\, J_1(\xi_i r_p / R)}{r_p \xi_i^2 \{J_2(\xi_i)\}^2} \tag{31}$$

Also using the following properties of the Bessel functions:

$$\begin{aligned} \xi_i &\approx \pi(i + \tfrac{1}{4}) \\ J_2(\xi_i) &\approx \pm \sqrt{\frac{2}{\pi \xi_i}} \end{aligned} \tag{32}$$

so that $d\xi_i \approx \pi di$, the summation of equation (30) becomes

$$p(r_P,R;0,0) \approx \int_0^{\infty} \frac{d\xi_i}{\pi} \cdot \frac{\pi R\, J_1(\xi_i r_p / R)}{r_p \xi_i} \tag{33}$$

and, defining t= $\xi_i r_P/R$:

$$p(r_P,R;0,0) \approx \frac{R}{r_p} \int_0^{\infty} dt \cdot \frac{J_1(t)}{t} = \frac{R}{r_p} \tag{34}$$

Note, that in this derivation also an approximation is made for the starting point of the integral, which is kept as zero throughout. A better approximation would be to replace the sum i: $1\rightarrow\infty$ by an integral di: $\frac{1}{2}\rightarrow\infty$ i.e. ξ_i: $\frac{3}{4}\pi\rightarrow\infty$ i.e. t: $\frac{3}{4}\pi r_P/R\rightarrow\infty$, so, the integral t: $0\rightarrow\frac{3}{4}\pi r_P/R$ has to be subtracted. This is easily calculated since for small values of t $J_1(t)\approx\frac{1}{2}t$, and the above solution can be improved to:

$$p(r_P, R; 0,0) \approx \frac{R}{r_p} - \frac{3\pi}{8} \tag{34A}$$

an approximation that turns out to be very close to the exact calculations.

Non-equilibrium, general

When Ca^{2+} is reversibly bound to calbindin, the diffusion rate has to be equal to the reaction rate. This leads to an adapted equation replacing equation (1):

$$D_{Ca}\nabla^2\left[Ca^{2+}\right](r,z) = -D_{CaBP}\nabla^2\left[Ca\cdot CaBP\right](r,z) = \rho \tag{35}$$

where ρ is the net reaction rate of Ca^{2+} binding to calbindin (the (r,z) after the species concentrations is neglected for simplification):

$$\rho = k_{on}\left[Ca^{2+}\right]\left(4C_{CaBP} - \left[Ca\cdot CaBP\right]\right) - k_{off}\left[Ca\cdot CaBP\right] \tag{36}$$

since the on reaction is between Ca^{2+} and the available binding sites, and the off reaction is from the Ca-calbindin complex only; the calbindin can bind 4 Ca^{2+} ions so that the amount of available binding sites equals $(4C_{CaBP} - [Ca\cdot CaBP])$. Note, that the chemical equilibrium follows from equating $\rho= 0$.

The diffusion equation (35) can be rewritten to read:

$$\nabla^2\left[Ca^{2+}\right] = \frac{\rho}{D_{Ca}} \quad ; \quad \nabla^2\left[Ca\cdot CaBP\right] = -\frac{\rho}{D_{CaBP}} \tag{37}$$

or summed to cancel out the reaction rate ρ:

$$D_{Ca}\nabla^2\left[Ca^{2+}\right] + D_{CaBP}\nabla^2\left[Ca\cdot CaBP\right] = 0 \tag{38}$$

which allows for a 'far away' solution, large z, along the same line as with equation (15):

$$D_{Ca}\left[Ca^{2+}\right] + D_{CaBP}\left[Ca\cdot CaBP\right] = B_1 - Jz \tag{39}$$

where B_1 is an integration constant. Again, the full solution can be derived as a deviation from this function:

$$D_{Ca}\left[Ca^{2+}\right] + D_{CaBP}\left[Ca\cdot CaBP\right] = B_1 - Jz + JRp(r_p, R; r, z) \tag{40}$$

Non-equilibrium, model I

The solution method of Hoofd and Kreuzer uses the fact, that one of the species cannot pass the boundary at z= 0 so that its gradient, the first derivative to z, approaches zero there. In model I, this is non-passing species the calbindin complex. The other species is expressed in terms of a deviation $g_I(z)$ from the chemical equilibrium - see equation (6) of the cited paper:

$$\left[Ca^{2+}\right] = \frac{K_d\left[Ca \cdot CaBP\right]}{4C_{CaBP} - \left[Ca \cdot CaBP\right]} + g_I(z) \tag{41}$$

where $K_d = k_{on}/k_{off}$. Note, that there is no coordinate r here since the method is set up as one-dimensional. Then, the reaction rate ρ is, from equation (36):

$$\rho = k_{on}\left(4C_{CaBP} - \left[Ca \cdot CaBP\right]\right)g_I(z) \tag{42}$$

Equation 32 can be differentiated twice, neglecting the first derivative in [Ca·CaBP] that approaches zero towards the boundary:

$$\frac{d^2}{dz^2}\left[Ca^{2+}\right] = \frac{4C_{CaBP}K_d}{\left(4C_{CaBP} - \left[Ca \cdot CaBP\right]\right)^2}\frac{d^2}{dz^2}\left[Ca \cdot CaBP\right] + \frac{d^2}{dz^2}g_I(z) \tag{43}$$

which, using equations (37) and (42), can be worked out as:

$$\frac{d^2}{dz^2}g_I(z) = \lambda_{AI}^{-2}g_I(z) \tag{44}$$

$$\lambda_{AI}^{-2} = \frac{k_{on}\left(4C_{CaBP} - \left[Ca \cdot CaBP\right]\right)}{D_{Ca}} + \frac{4k_{off}C_{CaBP}}{D_{CaBP}\left(4C_{CaBP} - \left[Ca \cdot CaBP\right]\right)} \tag{45}$$

Assuming that in a 3-dimensional case the zone $0 < z < \lambda_{AI}$ can be described having a constant value of [Ca·CaBP], an approximate solution for the $[Ca^{2+}]$ follows from equation (40) as:

$$\left[Ca^{2+}\right] \approx \left[Ca^{2+}\right]\left(r = 0, z = \lambda_{AI}\right) + \frac{J}{D_{Ca}}\left\{Rp\left(r_p, R; r, z\right) + \lambda_{AI} - z\right\} \tag{46}$$

Non-equilibrium, model II

Here, the species that does not pass the membrane is Ca^{2+} and consequently instead of equation 32 expressing $[Ca^{2+}]$ in terms of [Ca·CaBP], an equation has to be used expressing [Ca·CaBP] in terms of $[Ca^{2+}]$:

$$\left[Ca \cdot CaBP\right] = \frac{4C_{CaBP}\left[Ca^{2+}\right]}{K_d + \left[Ca^{2+}\right]} + g_{II}(z) \tag{47}$$

leading to a reaction rate ρ:

$$\rho = -\left(k_{off} + k_{on}\left[Ca^{2+}\right]\right)g_{II}(z) \tag{48}$$

Again, differentiating equation (47) twice leads to:

$$\frac{d^2}{dz^2}\left[Ca \cdot CaBP\right] = \frac{4C_{CaBP}K_d}{\left(K_d + \left[Ca^{2+}\right]\right)^2}\frac{d^2}{dz^2}\left[Ca^{2+}\right] + \frac{d^2}{dz^2}g_{II}(z) \tag{49}$$

which can be worked out again using equation (37) and inserting the ρ for this model II:

$$\frac{d^2}{dz^2} g_{II}(z) = \frac{1}{\lambda_{AII}{}^2} g_{II}(z) \tag{50}$$

$$\lambda_{AII}{}^{-2} = \frac{k_{on}\left(K_d + \left[Ca^{2+}\right]\right)}{D_{CaBP}} + \frac{4k_{off}C_{CaBP}}{D_{Ca}\left(K_d + \left[Ca^{2+}\right]\right)} \tag{51}$$

When assuming that in a 3-dimensional case the zone $0<z<\lambda_{AII}$ can be described having a constant value of $[Ca^{2+}]$, an approximate solution for the $[Ca \cdot CaBP]$ follows from equation (40) as:

$$[Ca \cdot CaBP] \approx [Ca \cdot CaBP]\left(r = 0, z = \lambda_{AII}\right) + \frac{J}{D_{CaBP}}\left\{Rp\left(r_p, R; r, z\right) + \lambda_{AII} - z\right\} \tag{52}$$

Single channel Ca^{2+} flux

Transcellular Ca^{2+} transport rate was experimentally determined as $1*10^{-15}$ mol·h^{-1}·μm^{-2} (100 nmol·h^{-1}·cm^{-2}) and the averaged luminal cell surface as 20 μm^2. This implies that transcellular Ca^{2+} transport over a single cell is $2*10^{-14}$ mol/h. The estimation of the amount of active TRPV5 channels at the apical cell surface (i.e. ~100) then determines that the single channel Ca^{2+} flux is $2*10^{-16}$ mol/h. Applying Avagadro's number ($6.02214*10^{23}$) this thus suggests that the flux of Ca^{2+} through a single active TRPV5 channel complex is in the order of $3*10^4$ Ca^{2+} ions per second.

CHAPTER VI

Identification of Nipsnap1 As a Novel Auxiliary Protein Controlling TRPV5 Activity

Lambers T.T., Schoeber J.P., Topala C.N.,

Hoenderop J.G., Bindels R.J.

Department of Physiology, Nijmegen Centre for Molecular Life Sciences,

Radboud University Nijmegen Medical Centre, The Netherlands

Summary

The Transient Receptor Potential channel Vanilloid 5 (TRPV5) is the most Ca^{2+}-selective channel within the TRP superfamily of ion channels. This distinct member is expressed in Ca^{2+}-transporting epithelia were it acts as a luminal entry gate controlling Ca^{2+} entry. In kidney TRPV5 constitutes the apical influx mechanism during Ca^{2+} reabsorption from the pro-urine. Regulation of TRPV5 activity is thus of utmost importance for determining Ca^{2+} entry and to maintain a normal Ca^{2+} balance. However, little is known about intracellular associated protein partners that affect TRPV5 activity. By a comprehensive approach this study identified Nipsnap1 as a novel factor involved in the control of TRPV5 activity. A combination of GST pull-down and co-immunoprecipitation assays demonstrated that Nipsnap1 associates with TRPV5 in a Ca^{2+}-independent fashion. The binding of Nipsnap1 was apparent at both the amino-terminus (TRPV5$^{77-112}$) and carboxyl-terminus (TRPV5$^{595-601}$) of TRPV5 suggesting a mechanism of regulation involving multiple interaction sides. Electrophysiological recordings and $^{45}Ca^{2+}$ uptake assays revealed that Nipsnap1 significantly reduces TRPV5 activity. Subsequent biotinylation assays showed that TRPV5 plasma membrane expression did not changed in the presence of Nipsnap1 suggesting that TRPV5 inhibition by Nipsnap1 is not caused by reduced channel cell surface expression. In conclusion, this study presents the first physiological function of Nipsnap1 as an associated inhibitory regulator of TRPV5 activity.

Introduction

The highly selective Ca^{2+} channel TRPV5 is a member of the large and functionally diverse family of Transient Receptor Potential (TRP) ion channels. TRPV5 is expressed in Ca^{2+}-transporting epithelia where it acts as gate controlling the entry of Ca^{2+}. Active Ca^{2+} reabsorption in kidney from the luminal compartment (pro-urine) to the basolateral side (blood) comprises a sequence of processes. At the apical side Ca^{2+} enters the renal epithelial cell via TRPV5 due to the steep inward electrochemical gradient across the apical membrane (1). In the cell, Ca^{2+} is rapidly bound to calbindin-D_{28K} that ferries Ca^{2+} from the apical to the basolateral side where the plasma membrane ATPase (PMCA1b) and the Na^+/Ca^{2+}-exchanger (NCX1) extrude Ca^{2+} into the blood compartment. This transcellular process is under tight and coordinated control of the calciotropic hormones that efficiently regulate the above mentioned process via distinct genomic and non-genomic pathways (2). Besides hormonal regulation, the activity of TRPV5 is efficiently controlled by Ca^{2+} itself such that Ca^{2+} entry induces a negative feedback regulation of channel activity which is essential during high levels of Ca^{2+} transport to prevent a Ca^{2+} overload (3). Since TRPV5 lacks conserved Ca^{2+} binding sites that could translate the ambient Ca^{2+} concentration into channel activity,

associated protein complexes are possibly involved in this particular form of TRPV5 regulation.

Basically alterations of TRPV5 activity can be explained by changes in the number of TRPV5 channels at the plasma membrane or by modification of channel activity at the cell surface. The Ca^{2+}-binding proteins calmodulin, calbindin-D_{28K} and 80K-H were previously identified as modulators of the epithelial Ca^{2+} channels affecting the Ca^{2+}-dependent activity of TRPV5 or TRPV6 (4-6). Calbindin-D_{28K} was shown to translocate towards the plasma membrane and associate with TRPV5 upon a decrease in the intracellular Ca^{2+} concentration. Here it locally buffers the flux of Ca^{2+} that enters the cell via TRPV5 thereby preventing channel inactivation. In addition, the Ca^{2+} sensor calmodulin was identified to associate with TRPV5 and, its closely related family member, TRPV6 in a Ca^{2+}-dependent manner although regulation appeared to be confined to TRPV6. Similarly, 80KH was suggested as an associated Ca^{2+} sensor controlling TRPV5 activity. Thus, Ca^{2+}-dependent control of TRPV5 and TRPV6 activity is mediated by a number of factors. The molecular mechanisms that control trafficking of these channels towards the plasma membrane and subsequent activity at the cell surface are, however, poorly understood. Recently, the S100A10-annexin 2 complex and Rab11a were identified to be essential for TRPV5 and TRPV6 cell surface expression (7, 8). S100A10-annexin 2 appeared to be involved in constitutive non-stimulated trafficking of TRPV5, whereas Rab11a was identified as an essential factor of a GTP-dependent mechanism controlling TRPV5 recycling to the plasma membrane.

The aim of the present study was to elucidate the function of a newly identified TRPV5-associated protein Nipsnap1. To this end, GST pull-down and co-immunoprecipitation experiments were performed to investigate Nipsnap1 association and identify the binding domain in TRPV5. $^{45}Ca^{2+}$ uptake assays and electrophysiological recordings of cells co-expressing TRPV5 and Nipsnap1 were established to investigate the role Nipsnap1 in TRPV5 activity. Furthermore, cell surface labeling of these Nipsnap1 and TRPV5 co-expressing cells was carried out to study the ability of Nipsnap1 to control TRPV5 plasma membrane expression.

Materials and methods

Molecular biology and cell culture

TRPV5 N- and C-terminal truncates were inserted into the pGEX6p-2 vector (Amersham Pharmacia Biotech, Roosendaal, The Netherlands) as described (8). TRPV5-pCINeo/IRES-GFP expression vector was constructed as described (9). Nipsnap1 was cloned into the *Xenopus laevis* oocyte expression vector pT7Ts, pCDNA3.1 and pCINeo/IRES-GFP expression vectors using PCR. All constructs were verified by sequence analysis. HEK293

and COS cells were grown and transfected as described (5). HEK293 cells stably expressing HA-TRPV5 were established as previously described for MDCK EGFP-TRPV5 (10) and maintained in medium containing 400 μg/ml G418 (Gibco Europe, Breda, The Netherlands). Expression of HA-TRPV5 was verified using anti-HA and five clones were pooled to eliminate differences between independent cell lines.

Protein-binding analysis

GST pull down assays with [^{35}S]Methionine-labeled proteins in TBS-HCl pH 7.4 containing 0.5% (v/v) NP40 and 1 mM Ca^{2+} or 5 mM EDTA, were performed as described (5). HEK293 cells were transiently co-transfected with pCDNA-Nipsnap1 and pCINeo/IRES-GFP-TRPV5. For co-immunoprecipitations cells were lysed by incubation for 1 h on ice in 50 mM Tris-HCl pH 7.4 containing 0.2% (v/v) Triton-X100, 0.2% (v/v) NP40 and the protease inhibitors leupeptin (0.01 mg/ml), pepstatin (0.05 mg/ml), phenylmethylsulfonyl fluoride (1 mM) and aprotinine (5 mg/ml). The lysates were centrifuged for 30 min at 16,000 g and supernatants were incubated with anti-TRPV5 immobilized on protein A-agarose beads (Kem-En-Tec A/S, Copenhagen, Denmark) for 16 h at 4ºC. After extensive washing in lysis buffer co-immunoprecipitation was investigated by immunoblot analysis using monoclonal anti-Xpress tag (Invitrogen, Breda, The Netherlands).

Electrophysiology and $^{45}Ca^{2+}$ uptake assays

Electrophysiological methods have been described previously in detail (9, 11). Whole cell currents were measured using an EPC-9 amplifier (HEKA, Lambrecht, Germany) using ruptured patches. Electrode resistances were 3-6 MΩ, and capacitance and access resistance was monitored continuously. A ramp protocol, consisting of linear voltage-ramps from -100 to +100 mV within 450 ms, was applied every 2 s from a holding potential of +20 mV. Ca^{2+}-dependent inactivation was studied using a 3 second voltage step to −100 mV from a holding potential of +70 mV. Current densities, expressed per unit of membrane capacitance, were calculated from the current at −80 mV during the ramp protocols (8). The standard extracellular solution ("Krebs") contained 150 mM NaCl, 6 mM CsCl, 1 mM $MgCl_2$, 10 mM HEPES/NaOH pH 7.4 and 10 mM glucose. The Ca^{2+} concentration was varied between 1 and 10 mM. Divalent free solutions did not contain added divalent cations, while trace amounts of divalent cations were removed with 100 μM EDTA. To inhibit monovalent cation currents, 150 mM NaCl was replaced with an equimolar amount of N-methyl-D-glucamine-Cl. The standard internal (pipette) solution contained 20 mM CsCl, 100 mM Cs-aspartate, 1 mM $MgCl_2$, 4 mM Na_2ATP, 10 mM BAPTA, 10 mM HEPES/CsOH pH 7.2. Cells were kept in nominal Ca^{2+}-free medium to prevent Ca^{2+} overload and exposed for maximal 5 min to a

Krebs solution containing 1.5 mM Ca^{2+} before sealing the patch pipette to the cell. All experiments were performed at room temperature (RT). $^{45}Ca^{2+}$ uptake was determined at 37 °C using HEK293 cells as described (12). To block TRPV5-mediated $^{45}Ca^{2+}$ uptake cells were incubated with 10 μM ruthenium red.

Biotinylation

HEK293 cells were transfected with pCINEO/IRES-GFP-HA-TRPV5 and pCINEO/IRES-GFP or pCINEO/IRES-GFP-HA-TRPV5 and pCINEO/IRES-GFP-VSV-Nipsnap1. Proteins that were present on the cell surface were biotinylated at 4 ºC using NHS-LC-LC-biotin (0.5 mg/ml; Pierce, Etten-leur, The Netherlands). Precipitated using neutravidin-coupled beads (Pierce), and analyzed by immunoblot analysis using anti-TRPV5 (1).

Statistical analysis

In all experiments, data are expressed as mean ± SEM. Overall statistical significance was determined by analysis of variance (ANOVA) followed by Bonferroni contrast analysis to investigate individual significance using Instat 3 software for Apple computers (San Diego, CA, USA). P values below 0.05 were considered significant.

Results

Nipsnap1 interaction with TRPV5

To identify novel TRPV5-interacting proteins a GST pull-down assay in combination with proteomics to identify the precipitated proteins was performed. The TRPV5 carboxyl-terminus fused to GST was used as bait and total mouse kidney lysate as substrate. One of the identified proteins was Nipsnap1 that specifically associated with TRPV5 (data not shown). To confirm this interaction, GST pull-down assays were performed using *in vitro* translated Nipsnap1. Nipsnap1 bound to both the amino- and carboxyl-termini of TRPV5, in the presence (1 mM $CaCl_2$) and absence (5mM EDTA) of Ca^{2+} **(Fig. 1A)**. Subsequently, the interaction of TRPV5 and Nipsnap1 was studied by co-immunoprecipitation from TRPV5 and Xpress-tag-Nipsnap1 co-transfected COS cells. To this end, cell lysates were incubated with anti-TRPV5 antibodies coupled to protein-A beads to precipitate the TRPV5 complexes. Immunoblots containing the precipitated proteins were analyzed for the presence of Xpress-tag-Nipsnap1. Nipsnap1 co-precipitated with TRPV5 in cells expressing both TRPV5 and Nipsnap1 **(Fig. 1B),** whereas Nipsnap1 was not co-precipitated from cells expressing Nipsnap1 only, demonstrating the specificity of the co-immunoprecipitation.
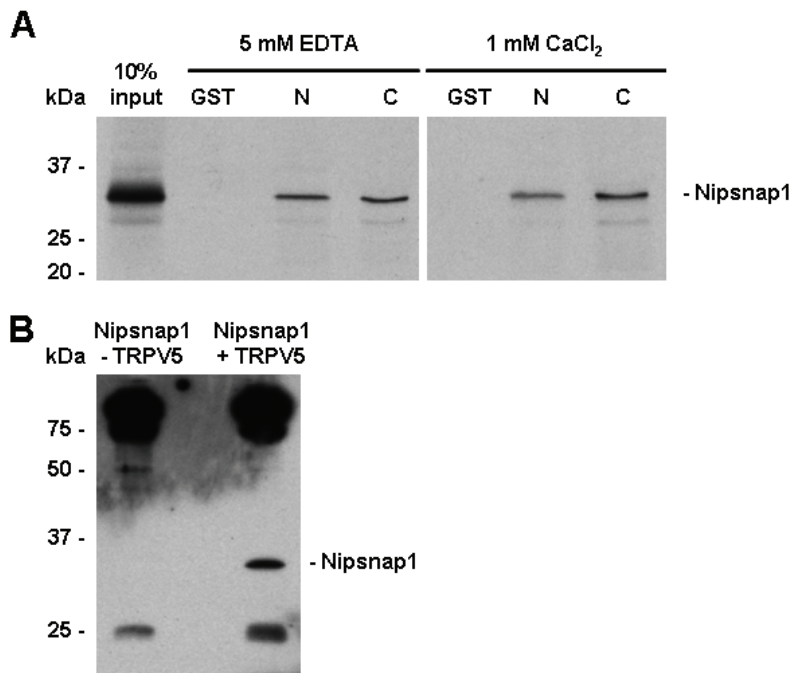
Fig. 1. Nipsnap1 binding to TRPV5 and TRPV6

(A) [^{35}S]Methionine labeled *in vitro* translated Nipsnap1 was incubated with GST or GST fused to the N- or C-terminus of TRPV5 immobilized on glutathione-Sepharose 4B beads either in the presence (1 mM CaCl$_2$) or absence (5 mM EDTA) of Ca^{2+}. Input control represents 10% of the total pull down input. **(B)** Cells were co-transfected with pCDNA3.1-Nipsnap1 and pCINeo/IRES-GFP-TRPV5 or pCDNA3.1-Nipsnap1 and pCNeo/IRES GFP (control). Co-precipitation was investigated by immunoblotting using the Xpress-tag antibody.

Elucidation of the Nipsnap1 binding motif in TRPV5

To further identify the Nipsnap1 binding sites in TRPV5, a series of amino- and carboxyl-terminal deletion mutants were constructed as depicted in **Fig. 2**. Truncated forms of TRPV5 were fused to GST and Nipsnap1 binding was determined by GST pull-down assays as described above. The interaction between TRPV5 amino-terminus and Nipsnap1 was abolished when the amino-terminus was truncated at position 77, whereas truncations at position 112 up to 240 did not disrupt the interaction with Nipsnap1 **(Fig. 2A)**. The association between the carboxyl-terminus of TRPV5 and Nipsnap1 was disrupted when the carboxyl-terminus was truncated at position 596, whereas truncations at position 601 up to 647 did not affect the binding with Nipsnap1 **(Fig. 2B)**.

Tissue distribution of Nipsnap1

TRPV5 is mainly expressed in Ca^{2+}-transporting tissues and to investigate Nipsnap1 co-expression in mice the distribution of this novel protein was assessed in a cDNA tissue panel. Nipsnap1 mRNA was detected in all tissues tested except in spleen **(Fig. 3)**. β-actin expression was established in all tissues demonstrating the integrity of the cDNA.
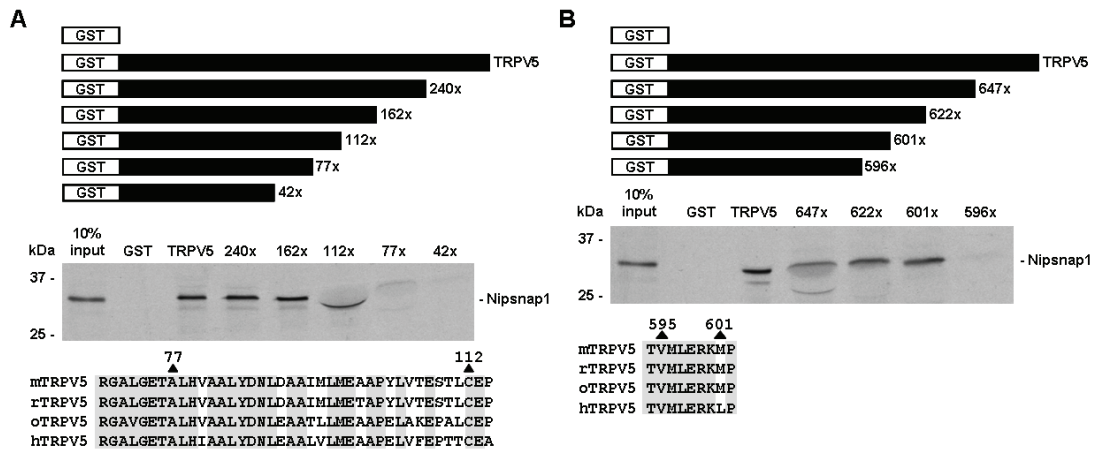
Fig. 2. Nipsnap1 interaction domains in TRPV5

[^{35}S]Methionine labeled *in vitro* translated Nipsnap1 was incubated with GST or GST fused to TRPV5 amino- **(A)** and carboxyl-terminal **(B)** truncations as indicated. Input control represents 10% of the total pull down input.

Effect of Nipsnap1 on TRPV5 activity

To study the potential role of Nipsnap1 in controlling TRPV5, the activity of TRPV5 was determined by whole-cell electrophysiological analysis in HEK293 cells transiently co-expressed with TRPV5 and Nipsnap1. Nipsnap1 significantly reduced the inward Ca^{2+} current in response to a hyperpolarizing voltage step in these HEK293 cells **(Fig. 4A and C)**. Likewise, the Na^+ current was reduced in these Nipsnap1- and TRPV5-coexpressing cells **(Fig. 4B and D)**. Subsequently, the effect of Nipsnap1 on TRPV5 activity was assessed by $^{45}Ca^{2+}$ uptake assays using HEK293 cells stably expressing the channel. Stably TRPV5-expressing HEK293 cells exhibited a ruthenium red sensitive $^{45}Ca^{2+}$ uptake demonstrating the function of TRPV5 in this cell line **(Fig. 4E)**. In line with the patch-clamp results, transient transfection of Nipsnap1 in these stably TRPV5-expressing HEK293 cells significantly reduced $^{45}Ca^{2+}$ uptake as compared to mock transfected stably TRPV5-expressing cells **(Fig. 4E)**. Addition of 10 µM ruthenium red to the stably TRPV5-expressing cells during the assay resulted in a decrease of $^{45}Ca^{2+}$ uptake in both mock and Nipsnap1 transfected cells, demonstrating that the $^{45}Ca^{2+}$ uptake is mediated by TRPV5.
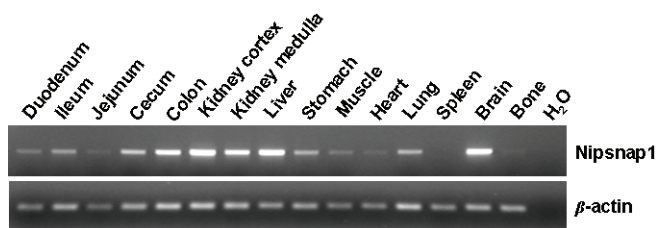

Fig. 3. Tissue distribution of Nipsnap1 mRNA was extracted from several mouse tissues and Nipsnap1 expression was determined by semi quantitative reverse transcriptase PCR. The Nipsnap1 specific band was amplified in all tissues expect in spleen at the expected size of 628 bp. β-actin reverse transcriptase was amplified to check the integrity of the cDNAs.
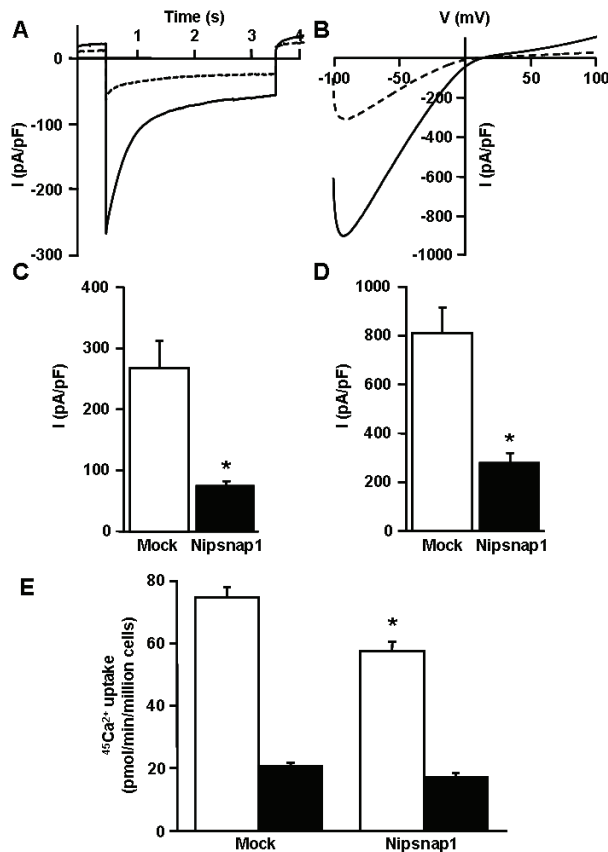
Fig. 4 Nipsnap1 inhibits TRPV5 activity.

(A) Whole cell current voltage relations measured from 400 ms voltage ramps (interval = 5 s) in nominally DVF solution in HEK293 cells transiently transfected with either TRPV5 and mock (solid) or TRPV5 and Nipsnap1 (dotted line). (B) Inward Ca^{2+} currents measured in HEK293 cells transiently transfected with either TRPV5 and mock (solid) or TRPV5 and Nipsnap1 (dotted line) with 10 mM extracellular Ca^{2+} during a 3 s step to –100 mV from a holding potential of + 70 mV. Average peak current density during the voltage step in 10 mM Ca^{2+} (n=10) (C) or average current densities at –80 mV in 10 mM EDTA (n=10) (D) in HEK293 cells transiently transfected with either TRPV5 and mock (open bars) or TRPV5 and Nipsnap1 (closed bars). Significant differences in TRPV5 activity was indicated by an asterisk (p<0.05). (E) $^{45}Ca^{2+}$ uptake of HEK293 cells stably expressing TRPV5 and transiently transfected with empty vector or Nipsnap1 (open bars). 10 µM ruthenium red was included during the uptake to investigate ruthenium red sensitivity (closed bars). Significant differences in $^{45}Ca^{2+}$ uptake compared to all conditions are indicated by an asterisk (p<0.05).

Effect of Nipsnap1 on TRPV5 cell surface expression

A decrease in the TRPV5 activity can in principal be explained by a reduced cell surface expression or altered activity of TRPV5 at the plasma membrane. Therefore, cell surface biotinylation was applied to quantify the number of TRPV5 channels present at the plasma membrane. Co-expression of Nipsnap1 did not change the plasma membrane expression of TRPV5 **(Fig. 5A)**. Analysis of total TRPV5 expression revealed a non-glycosilated and a glycosilated form which is the accessible form to extracellular biotin. As control the expression of Nipsnap1 was confirmed in these cells **(Fig. 5B)**.

Discussion

The present study identified the physiological role of Nipsnap1 as a negative modulator of TRPV5-mediated Ca^{2+} transport. This conclusion is based on the following observations. First, the specific association of Nipsnap1 and TRPV5 was demonstrated in a proteomic assay

to unravel the TRPV5 interactome and subsequently confirmed by GST pull-down analysis and co-immunoprecipitation experiments. Second, Nipsnap1 co-expresses with TRPV5 in Ca^{2+}-transporting tissues like kidney, intestine and bone. Third, Nipsnap1 inhibits TRPV5 activity without affecting the cell surface expression of the epithelial Ca^{2+} channel.
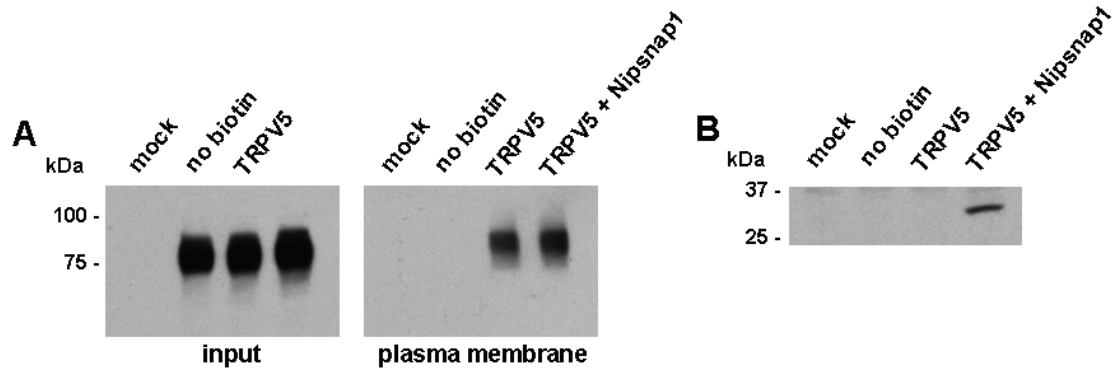

Fig. 5. Nipsnap1 has no effect on cell surface expression of TRPV5

(A) Cell surface expression of TRPV5 as measured by cell surface biotinylation of HEK293 cells transiently expressing TRPV5 and Nipsnap1 or TRPV5 and empty vector. Analysis of total TRPV5 expression revealed a non-glycosilated form (lower band, left panel) and a glycosilated form (upper) which is the band accessible to extracellular biotin (right panel). **(B)** Nipsnap1 expression as assed by anti-Xpress-tag. A representative blot of three independent experiments is shown.

TRPV5 forms the apical entry gate in Ca^{2+}-transporting cells. Its activity is determined by both calciotropic hormones and associated protein partners. Several binding partners including calbindin-D_{28K} and 80K-H directly affect the Ca^{2+}-dependent activity of TRPV5, whereas others such as the S100A10-annexin 2 complex and Rab11a control the TRPV5 cell surface expression. This study demonstrates that Nipsnap1 is co-expressed with TRPV5 in the Ca^{2+}-transporting tissues (i.e., kidney, bone and intestine) which is in line with a function in the regulation of the Ca^{2+} balance. Besides kidney, bone and intestine Nipsnap1 expression was detected in all tested tissues except in spleen. These findings are similar to previous results demonstrating that Nipsnap1 is ubiquitously expressed, although spleen was not included in this latter study (13). Nipsnap1 is a member of an evolutionary conserved gene family with a putative role in vesicular trafficking since NIPSNAP in *C. elegans* localizes in a gene operon encoding SNAP25-like proteins (13). At present only a few studies have provided information about Nipsnap1 and no robust experimental evidence is available indicating that the NIPSNAP family is involved in vesicular trafficking. In line with a role in vesicular trafficking, however, is the punctuate vesicular distribution of GFP-tagged TassC, a NIPSNAP homologue (originally annotated as Nipsnap4). Nipsnap4 was identified in a Yeast two-hybrid screen as a direct interacting partner of the *Salmonella* virulence protein Spic (14).

These authors have named Nipsnap4 as TassC (target for *Salmonella* secreted protein C) since the only established role for Nipsnap4 was its interaction with Spic. Indicated by the survival of a SpiC deficient *Salmonella* strain in Nipsnap4 knockdown macrophages, Nipsnap4 was suggested as a host cell factor in these cells. It was concluded that Nipsnap4 determines vesicular trafficking and postulated that Nipsnap4 is inactivated by *Salmonella* SpiC thereby enabling host cell infection. Thus, although the function of the NIPSNAP family remains elusive, they have been implicated in the process of vesicular trafficking.

Both pull-down assays and co-immunoprecipitations confirmed the potential TRPV5 and Nipsnap1 interaction. Detailed analysis of the interaction domain revealed that Nipsnap1 binds to the TRPV5 amino-terminus (TRPV5$^{77-112}$) and carboxyl-terminus (TRPV5$^{596-601}$) suggesting that Nipsnap1 is part of a mechanism of regulation involving multiple interaction sides. Interestingly, the TRPV5 carboxyl-terminal residues responsible for Nipsnap1 association have previously been demonstrated to be critical for TRPV5 activity, binding of interacting partners 80KH, NHERF4 and Rab11a, and channel multimerization (6, 7, 15, 16). In addition, this domain is conserved throughout evolution underlining the importance of this particular stretch of amino acid residues. Thus, suggesting that this region is either a critical element for the general folding of the carboxyl-terminus of TRPV5 or that several of the associated proteins recognize motifs within this particular region. Nipsnap1-mediated regulation of TRPV5 activity might be an interplay of several associated proteins that affect TRPV5 activity by antagonizing or synergizing each other by competitive association with the channel. In this situation, the occupancy of the binding sites would depend on the relative concentration and affinity of the proteins that, during overexpression of Nipsnap1, is in favor for Nipsnap1. Such a mechanism of ion channel regulation by competitive association for target sites is well defined for G-protein beta gamma subunits (Gβγ) dependent regulation of voltage-operated Ca^{2+} channels. These channels consist of a pore forming α subunit and several associated subunits, such as the intracellularly located β subunit that contributes to the overall functional characteristics of the channel complex (17). Voltage-dependent inhibition of these Ca^{2+} channels is mediated by Gβγ inhibition (18, 19). The binding sites of the Ca^{2+} channel β and Gβγ subunits overlap on the channel α part and functional measurement revealed that these subunits antagonize each other, thereby affecting channel activity (20, 21).

Direct inhibition of TRPV5 activity by Nipsnap1 can theoretically be explained by a reduced cell surface expression of TRPV5 or by a decreased activity at the plasma membrane. The initial characterization of TRPV5 revealed that this channel displays constitutive activity (22). Thus, changes in channel localization at the cells surface are an efficient means to regulate channel activity. The biotinylation experiments, however, demonstrated that TRPV5 cell

surface expression is not affected by Nipsnap1 since the abundance of TRPV5 in the purified plasma membrane fraction is not changed in the presence of co-expressed Nipsnap1. Thus, Nipsnap1 decreased TRPV5 activity of channels present at the cell surface, by a potential competition with other auxiliary proteins for TRPV5 association.

In conclusion, this study demonstrates the first function of the recently identified protein Nipsnap1 in modulating TRPV5-mediated Ca^{2+} transport and thereby affecting the total Ca^{2+} balance of the organism. Nipsnap1 determines the activity of TRPV5 present at the cell surface, thereby providing evidence that the family of NIPSNAP proteins is able to affect physiological processes via mechanisms independent of vesicular trafficking.

References

1. Hoenderop, J. G., van der Kemp, A. W., Hartog, A., van de Graaf, S. F., van Os, C. H., Willems, P. H. & Bindels, R. J. (1999) *J Biol Chem* **274,** 8375-8.
2. Lambers, T. T., Bindels, R. J. & Hoenderop, J. G. (2006) *Kidney Int* **69,** 650-4.
3. Nilius, B., Prenen, J., Vennekens, R., Hoenderop, J. G., Bindels, R. J. & Droogmans, G. (2001) *Cell Calcium* **29,** 417-28.
4. Lambers, T. T., Mahieu, F., Oancea, E., Hoofd, L., de Lange, F., Mensenkamp, A. R., Voets, T., Nilius, B., Clapham, D. E., Hoenderop, J. G. & Bindels, R. J. (2006) *Embo J* **in press**.
5. Lambers, T. T., Weidema, A. F., Nilius, B., Hoenderop, J. G. & Bindels, R. J. (2004) *J Biol Chem* **279,** 28855-61.
6. Gkika, D., Mahieu, F., Nilius, B., Hoenderop, J. G. & Bindels, R. J. (2004) *J Biol Chem* **279,** 26351-7.
7. van de Graaf, S. F., Chang, Q., Mensenkamp, A. R., Hoenderop, J. G. & Bindels, R. J. (2006) *Mol Cell Biol* **26,** 303-12.
8. van de Graaf, S. F., Hoenderop, J. G., Gkika, D., Lamers, D., Prenen, J., Rescher, U., Gerke, V., Staub, O., Nilius, B. & Bindels, R. J. (2003) *Embo J* **22,** 1478-87.
9. Nilius, B., Prenen, J., Hoenderop, J. G., Vennekens, R., Hoefs, S., Weidema, A. F., Droogmans, G. & Bindels, R. J. (2002) *J Biol Chem* **277,** 30852-30858.
10. den Dekker, E., Schoeber, J., Topala, C. N., van de Graaf, S. F., Hoenderop, J. G. & Bindels, R. J. (2005) *Pflugers Arch* **450,** 236-44.
11. Vennekens, R., Hoenderop, J. G., Prenen, J., Stuiver, M., Willems, P. H., Droogmans, G., Nilius, B. & Bindels, R. J. (2000) *J Biol Chem* **275,** 3963-9.
12. Chang, Q., Hoefs, S., van der Kemp, A. W., Topala, C. N., Bindels, R. J. & Hoenderop, J. G. (2005) *Science* **310,** 490-3.
13. Seroussi, E., Pan, H. Q., Kedra, D., Roe, B. A. & Dumanski, J. P. (1998) *Gene* **212,** 13-20.
14. Lee, A. H., Zareei, M. P. & Daefler, S. (2002) *Cell Microbiol* **4,** 739-50.
15. Chang, Q., Gyftogianni, E., van de Graaf, S. F., Hoefs, S., Weidema, F. A., Bindels, R. J. & Hoenderop, J. G. (2004) *J Biol Chem* **279,** 54304-11.
16. van de Graaf, S. F., Hoenderop, J. G., van der Kemp, A. W., Gisler, S. M. & Bindels, R. J. (2006) *Pflugers Arch* **452,** 407-17.
17. Dolphin, A. C. (2003) *J Bioenerg Biomembr* **35,** 599-620.
18. Herlitze, S., Garcia, D. E., Mackie, K., Hille, B., Scheuer, T. & Catterall, W. A. (1996) *Nature* **380,** 258-62.
19. Ikeda, S. R. (1996) *Nature* **380,** 255-8.
20. Dolphin, A. C. (2003) *Pharmacol Rev* **55,** 607-27.
21. Birnbaumer, L., Qin, N., Olcese, R., Tareilus, E., Platano, D., Costantin, J. & Stefani, E. (1998) *J Bioenerg Biomembr* **30,** 357-75.
22. Hoenderop, J. G., Nilius, B. & Bindels, R. J. (2005) *Physiol Rev* **85,** 373-422.

CHAPTER VII

An essential role for the epithelial Ca^{2+} channel TRPV5 in sound perception

[1]**Lambers T.T**., [2]Peters T.A., [2]Beynon A.J., [1]van der Kemp A.W., [4]Corralez E., [3]van der Zee I., [4]Heller S, [2]Curfs J.H., [1]Hoenderop J.G., [1]Bindels R.J.

[1]Physiology, [2]Otorhinolaryngology and [3]Cell Biology, Radboud University Nijmegen Medical Centre,The Netherlands. [4]Otolaryngology and Molecular & Cellular Physiology, Stanford University School of Medicine, Stanford, CA

Abstract

Inner ear physiology is highly homologous to renal physiology since several common transporters and channels are shared by both tissues. A number of Transient Receptor Potential (TRP) ion channels are detected in the inner ear although their precise localization and physiological functions remain elusive. TRPV5 is a unique member of the TRP superfamily of ion channels facilitating apical Ca^{2+} influx in epithelia. Here, we demonstrate using immunohistochemistry, startle response measurements and Auditory Brainstem Response (ABR) recordings that TRPV5, besides its well established function in kidney, fulfills an important role in sound perception. By immunohistochemistry, TRPV5 was localized to the apical membrane of Deiter's supporting cells that are connected to the sensory-motor outer hair cells. Mice lacking TRPV5 displayed a decreased startle pre-pulse inhibition and increased ABR thresholds providing evidence for a critical function of TRPV5 in sound amplification near threshold. In summary, a novel function for the epithelia Ca^{2+} channel TRPV5 as an essential component in inner ear physiology was demonstrated, thereby providing evidence for a direct role of Deiter's supporting cells in sound perception.

Introduction

The inner ear contains the cochlea in which the organ of Corti forms a highly ordered auditory sensory epithelium. This epithelium is composed of an array of sensory hair and non-sensory supporting cell types that are organized in a precise pattern. The mechano-sensitive hair cells are divided along the length of the cochlea from base to apex with a single row of inner hair cells and three evenly spaced rows of outer hair cells. Directly underneath the outer hair cells lay the Deiter's supporting cells of which the function still largely remains elusive. Given the important function of the hair cells as mechanosensory receptors in auditory transduction, it is easily envisaged that hearing deficits could easily occur due to loss or malfunction of hair cell function. However, mutations causing disturbances in the architecture of the organ of corti as a result of defects in supporting cells have also been identified (1, 2). On their apical surface hair cells contain microscopically fine projections, the stereocilia. The displacement of the stereocilia by mechanical forces increases tension in the tip links that connect individual stereocilia leading to opening of mechanotransduction channels and depolarization of the hair cells.

Since several ion transporters and channels that are expressed in transporting epithelia in kidney are localized in the inner ear as well, the characteristics of these epithelia are quite homologous. Genetic disturbance in one of the components may therefore result in both kidney and inner ear malfunction (3, 4). This overlap gained a profound interest since several

key players in inner ear transporting epithelia are unknown but are, however, identified in kidney.

Transient Receptor Potential (TRP) channels constitute a large and functionally versatile superfamily of cation channels that are expressed in many cell types from yeast to mammals (5). Here they fulfill critical functions in processes ranging from sensory physiology, male fertility, vasorelaxation and epithelial Ca^{2+} and Mg^{2+} transport. Although numerous TRPs have been identified their precise physiological function still remains largely unknown. One distinct member of the TRP family, TRPA1 has been identified as part of the mechano-sensitive pathway enabling rapid K^+ and Ca^{2+} entry in hair cell stereocilia (6). However, mice lacking TRPA1 display normal hair cell function and no deficiency in sound detection (7, 8). On the other hand genetic disruption of TRPV4 was found to cause delayed-onset hearing loss and make the cochlea more vulnerable to acoustic trauma (9). Thus, two TRP channels have been detected in the mammalian inner ear although their precise function in hearing remains elusive.

TRPV5 and TRPV6 form the luminal entry gate in Ca^{2+}-transporting epithelia in kidney and intestine, respectively (10). At the cellular level, Ca^{2+} enters the epithelial cells via the highly Ca^{2+}-selective channels TRPV5 and TRPV6 due to a steep inward electrochemical gradient across the luminal membrane. In the cell, Ca^{2+} is bound by calbindin-D_{28K} and -D_{9K} ($CaBP_{28K}$ and $CaBP_{9K}$) that ferry Ca^{2+} from the luminal side to the basolateral side where the Na^+/Ca^{2+}-exchanger (NCX1) and the plasma membrane ATPase (PMCA1b) extrude Ca^{2+} into the blood compartment. Similar as its suggested function in kidney $CaBP_{28K}$ is thought to prevent toxic Ca^{2+} overload of hair cells by increased cytosolic Ca^{2+} buffering and intracellular Ca^{2+} transport (11, 12). However, genetic ablation of $CaBP_{28K}$ in mice does not affect hearing or survival of hair cells in acoustic trauma (13). Compensation may occur by other Ca^{2+} buffer proteins in the outer hair cells such as oncomodulin (prevalbumin-β) and in the inner hair cell calretenin (14). Different PMCA isoforms have been localized to discrete subcellular regions in the hair cells providing for Ca^{2+} excretion and rapid buildup of Ca^{2+} gradients. In analogy with basolateral excretion of Ca^{2+} in kidney, Ca^{2+}-ATPases extrude Ca^{2+} from stereocilia (15). PMCA2a is the predominant isoform present in hair cell bundles, whereas PMCA1b has been detected at the plasma membrane of hair cells and supporting cell somas (16). In addition, NCX1 has been detected in the inner ear epithelia, however, its function is not clear. A spliced isoform of NCX1 is expressed in the cochlear lateral wall and in the organ of Corti, whereas five NCX1 isoforms have been detected in the cochlear modiolus (17). Alternative splicing may therefore provide diverse functions for NCX in the inner ear. The ion-transporting epithelium that is most homologous to the epithelia along the nephron in kidney

is the non-sensory transporting epithelium stria vascularis. In this particular cochlear cell type, ion transport pathways have been detected known from transcellular transport processes in kidney (3, 4). The third part of the cochlea, the spiral ganglion consists of neuronal cells that innervate the hair cells and transduce sound stimuli to the brain.

Several components of transcellular Ca^{2+} transport in kidney are thus expressed in the inner ear where their function could be similar. The localization and function of the apical influx channel TRPV5 in the inner ear is, however, unknown. Recently, TRPV5 transcripts were detected in primary cultures of semicircular canal duct epithelial cells (18). In these cells a similar model for transcellular Ca^{2+} transport, as described in kidney, was suggested with TRPV5 and TRPV6 as apical influx channels, $CaBP_{28K}$ and $CaBP_{9K}$ as intracellular Ca^{2+} transport proteins and NCX and PMCA as extrusion mechanisms. The authors speculated that TRPV5-mediated transcellular Ca^{2+} transport could be essential for the low endolymph Ca^{2+} concentration in the vestibular labyrinth. Interestingly, vitamin D receptors were also detected in these cells and the expression of the Ca^{2+} transport machinery was positively affected by vitamin D as described in kidney cells (10, 18).

The aim of the present study was to investigate the role of TRPV5 in inner ear physiology. By using immunohistochemistry, pre-pulse inhibition and Auditory Brainstem Response (ABR) measurements of TRPV5 knockout mice we provide evidence that TRPV5 fulfills a critical role in sound perception.

Methods

Generation of TRPV5 knockout mice (TRPV5$^{-/-}$)

TRPV5$^{-/-}$ mice were generated by targeted ablation of the TRPV5 gene and genotyped as described previously (19). Wild-type and TRPV5$^{-/-}$ littermates were kept in a light and temperature-controlled room with *ad libitum* access to deionized drinking water and standard pelleted chow (Sniff Spezialdiäten, Soest, the Netherlands). Eight week old TRPV5$^{-/-}$ and wild-type littermates were used for acoustic recordings and subsequently sacrificed for immunohistochemistry.

Acoustic startle reflex

Startle reactivity was measured using a startle response system (SR-LAB, San Diego Instruments, San Diego). The startle chamber consisted of a non-restrictive plexiglas cylinder (4 cm diameter), resting on a plexiglas platform inside the ventilated and sound attenuated chamber. A high-frequency loudspeaker inside the chamber produced both a continuous

background noise of 70 dB and the various acoustic stimuli. Vibrations of the platform, produced by the whole-body startle response of the mouse, were detected and transduced by a piezoelectric accelerometer mounted underneath the platform, connected to an automated system. Each mouse was placed inside the cylinder for 5 min with a background noise of 70 dB to habituate before the first startle stimuli were given. The first block of the testing session consisted of 5 separate 120 dB startle pulse trials. The middle portion of the session consisted of 4 blocks with each block containing: (1) two startle pulse alone trials (120 dB burst), (2) four pre-pulse trials, in which 72, 74, 78, or 86 dB stimuli preceded the 120 dB burst, and (3) a no stimulus trial (only the 70 dB background noise). These 7 trials were presented in a pseudo-random order. The last part of the testing session consisted of a block with 5 separate 120 dB startle pulse trials. Pre-pulse inhibition was calculated and expressed as percentage pre-pulse inhibition according to the following equation:

pre-pulse inhibition (%) = 100 - [100 * (the startle amplitude following a 120 dB pulse preceded by a pre-pulse / the startle amplitude following a 120 dB pulse alone)].

Auditory brainstem response measurements

Auditory Brainstem Response (ABR) measurements were performed in a sound-proof room with low reverberation. Needle electrodes were placed on M1 and M2 (left and right mastoids) and referred to Cz (vertex) to record the auditory-evoked potentials. A ground electrode was placed halfway on the tail of the mice. Interelectrode impedances were measured before and after each measurement (< 8 kOhm). Click stimuli of 100 μs and tone burst stimuli of 8 kHz (1ms rise/fall, 3ms plateau time) were presented in a sound field by placing the loudspeakers 5 cm in front of each ear. The loudness levels at the position of the ear were measured and calibrated with a Bruel and Kjaer 2203 sound pressure level (SPL) meter (Bruel & Kjaer, Nærum, Denmark). All thresholds were corrected afterward for the soundfield setup. Before the measurements were performed, the mice were i.p. injected with ketamine (200 mg/kg) anesthetic. A standard-evoked potential recording system (MedElec Synergy EP, Oxford Instruments Inc, Oxon, U.K.) was used to present 100 μs click stimuli with a fixed stimulation rate of 20 Hz. The analysis time was set at 15 ms from the onset of the click with a 1.5 ms pre-stimulus time to assess baseline levels. The recorded electroencephalography (EEG) signals were high-pass filtered at 100 Hz and low-pass filtered at 3 kHz; an automatic artifact rejection and a 60 Hz notch filter were used to avoid electromyography signals (EMG) or external noise. Auditory brainstem responses were obtained from both contra- and ipsilateral stimulation sites. The EEG signals were averaged for different stimulation levels according to standard audiometrical top-down procedures, starting at 90 dB (SPL), uncorrected for the soundfield. Peaks were identified according to the

Jewett and Williston nomenclature (20). The auditory hearing threshold was defined as the lowest level (in dBSPL) at which at least one reproducible peak was visually recognized in the responses obtained from the ipsilateral measured ear. Additionally, absolute peak and interpeak latencies were analyzed to assess possible conductive and/or retro-cochlear pathology.

Immunohistochemistry

Cochlea's of wild-type and TRPV5^{-/-} littermate mice (p4) were isolated and staining for TRPV5 was performed on cryosections of periodate-lysine-paraformaldehyde fixed cochlear samples using an affinity-purified anti-TRPV5 antibody as described previously (21). Images were taken using a Zeiss LSM510meta confocal laser scanning microscope equipped with a PlanApochromatic 63x 1.4 oil immersion DIC lens (Carl Zeiss GmbH, Jena, Germany).

Statistical analysis

In all experiments, data are expressed as mean ± SEM. Overall statistical significance was determined by analysis of variance (ANOVA) followed by Bonferroni contrast analysis to investigate individual significance using Instat 3 software for Apple computers (San Diego, CA, USA). P values below 0.05 were considered significant.

Results

Localization of TRPV5 in Deiter's cells

The localization of TRPV5 in cochlea of p4 wild-type mice was performed by immunohistochemistry and cochlea of TRPV5^{-/-} littermates were used as a negative control. In wild-type mice TRPV5 immunopositive staining was present in Deiter's supporting cells connecting the outer hair cells in the organ of Corti, whereas no TRPV5 immunopositive staining could be detected in corresponding cells of TRPV5^{-/-} **(Fig. 1B). Fig. 1A** represents an overview of the organ of Corti cell types. Interestingly, TRPV5 immunopositive staining appeared directly at the interface of Dieter's and outer hair cells suggesting apical localization of TRPV5. DIC images revealed that TRPV5^{-/-} and wild-type littermates display normal morphology in the organ of Corti of TRPV5^{-/-} as compared to their wild-type littermates.

Acoustic pre-pulse inhibition startle response is reduced in TRPV5^{-/-} mice

To investigate the contribution of TRPV5 to sound perception, TRPV5^{-/-} and wild-type littermates were analyzed in the acoustic startle reflex setup to asses their immediate reaction to sound stimuli. Both wild-type and TRPV5^{-/-} mice demonstrated a continuous response amplitude of ~40 arbitrary units during the background (70 dB) trails (data not shown). This

response was defined as the basal activity of individual mice. Both groups showed maximal startle amplitude of ~1000 arbitrary units in reaction to the 120 dB startle pulses throughout the protocol (data not shown). Pre-pulse inhibition is defined as the suppression of the 120 dB pulse-induced startle response when this stimulus is preceded by a weak pre-pulse (+2, +4, +8 or + 16 dB above background). The wild-type mice revealed typical pre-pulse inhibition, which was increased by application of elevating pre-pulse intensities **(Fig. 2A)**. The strongest pre-pulse inhibition was shown after the +16 dB pre-pulse. Similarly, TRPV5$^{-/-}$ mice revealed an increased pre-pulse inhibition accompanying elevated pre-pulse intensities. The pre-pulse inhibition was, however, less pronounced as their wild-type littermates with significant differences ($p<0.05$) at +16 dB pre-pulse intensity above background. To investigate potential neuronal conductance alterations the latencies during the startle reflexes were assessed. Latency responses to the startle pulses were equal in both groups throughout the protocol demonstrating the absence of neuronal defects in the TRPV5$^{-/-}$ mice **(Fig. 2B)**.
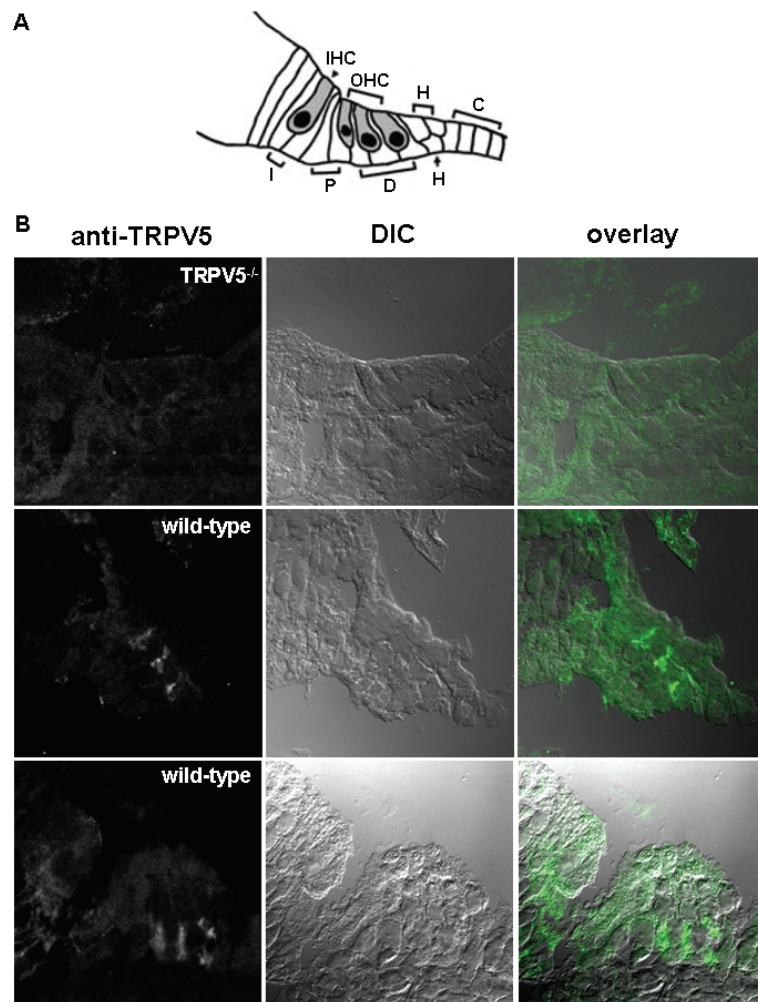
Fig. 1. TRPV5 localizes to the cochlear spiral ganglion

(A) Cartoon representing the sensory epithelium cell types in the organ of Corti. One inner hair cell (IHC) and three outer hair cells (OHC) are surrounded by different supporting cells: interphalangeal cells (I); pillar cells (P); Deiter's cells (D); Hensen's cells (H); and Claudius cells (C). **(B)** Immunohistological detection of TRPV5 in mice Deiter's cells. Sections of cochlea isolated from TRPV5$^{-/-}$ mice were used as negative control in which immunopostive staining was virtually absent.

Fig. 2. Decreased acoustic pre-pulse inhibition startle reflexes in TRPV5$^{-/-}$

(A) Pre-pulse inhibition of the startle response was recorded by offering four successive protocols. Each protocol consisted of four pre-pulse trails, in which a 72, 74, 78, or 86 dB stimulus preceded the 120 dB startle pulse. Pre-pulse inhibition is expressed as percentage inhibition of the pulse response. Wild-type (open bars) mice re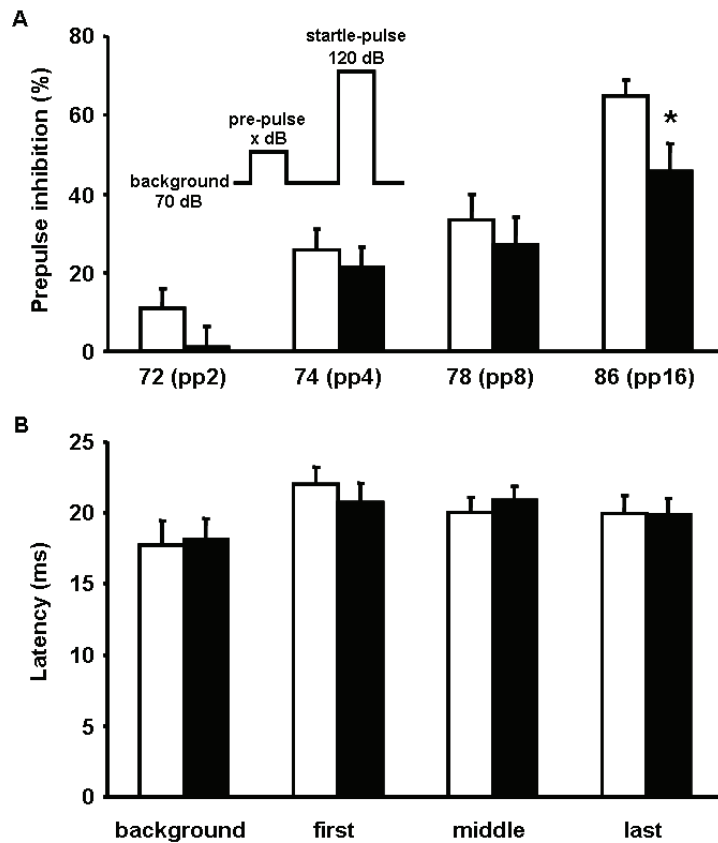veal a clear pre-pulse inhibition that is increased upon elevation of the intensity of the pre-pulse. TRPV5$^{-/-}$ mice (closed bars) reveal a lower pre-pulse inhibition as compared to their wild-type littermates. **(B)** No differences were detected in the latency indicating that the observed decrease is independent from neuronal conductance. Significant differences (P<0.05) between wild-type (n=17) and TRPV5$^{-/-}$ (n=17) littermates are indicated by an asterisk.

Increased auditory thresholds in TRPV5$^{-/-}$ mice

Because TRPV5$^{-/-}$ mice displayed decreased acoustic pre-pulse inhibition startle responses, Acoustic Brainstem Response (ABR) recordings were measured to evaluate the exact hearing capacities of the TRPV5$^{-/-}$ mice. Besides a click ABR (2-3 kHz), a burst protocol (8 kHz) was applied to characterize the auditory thresholds at a higher frequency. In both, wild-type mice and TRPV5$^{-/-}$ littermates consistent and reproducible ABRs at 90 dBSPL were evoked using either click **(Fig. 3A)** or burst **(Fig. 3B)** stimuli. Peaks were subsequently identified according to the Jewett and Williston nomenclature (20) and auditory thresholds were determined by averaging of minimal 500 responses. Mean auditory thresholds were identified for wild-type mice and TRPV5$^{-/-}$ littermates in reaction to click and tone burst stimuli. TRPV5$^{-/-}$ consistently revealed higher thresholds (i.e. no reproducible responses at lower stimulation levels) compared to their wild-type littermates in reaction to both the click and burst stimuli **(Fig. 3C)** suggesting a critical role for TRPV5 in sound perception.
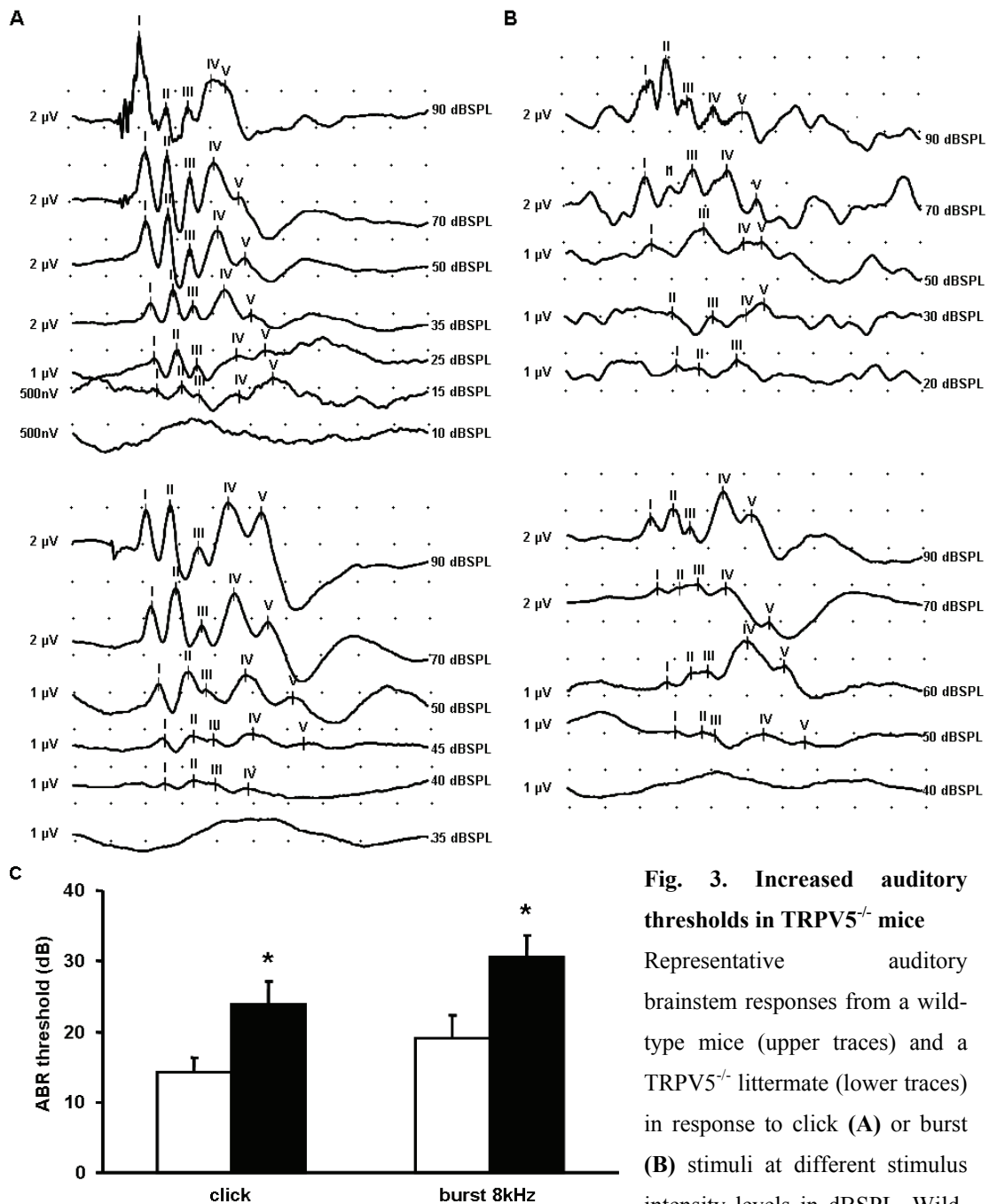
Fig. 3. Increased auditory thresholds in TRPV5$^{-/-}$ mice

Representative auditory brainstem responses from a wild-type mice (upper traces) and a TRPV5$^{-/-}$ littermate (lower traces) in response to click **(A)** or burst **(B)** stimuli at different stimulus intensity levels in dBSPL. Wild-type mice (upper traces) reveal normal brainstem response obtained at different stimulation levels according to standard audiometrical descending top-down procedures until the level where no reproducible responses are recognized (i.e. 15 dBSPL for click and 20 dBSPL for burst stimuli). In contrast to the wild-type mice, the TRPV5$^{-/-}$ littermates (lower traces) show a lack of auditory brainstem responses at lower stimulation levels (i.e. higher hearing threshold at 40 dBSPL for both click and burst stimuli). Horizontal axes: time window of 15 ms (1.5 ms /division); vertical axes: amplitude in microvolt (μV). Stimulus onset at 1.5 ms. **(C)** Mean auditory brainstem thresholds of wild-type mice and TRPV5$^{-/-}$ littermates obtained with click and burst stimuli. Significant differences (p<0.05) between wild-type (n=16) mice and TRPV5$^{-/-}$ littermates (n=18) are indicated by an asterisk.

In order to investigate the neuronal conductivity in TRPV5^{-/-} and wild-type littermate mice, latencies of the click and burst stimuli were analyzed. The mean absolute latencies of peak (JI to JV) and mean interwave intervals (JI-III, JI-IV, JI-V) of the ABR obtained from TRPV5^{-/-} and wild-type mice at 90 dB for clicks **(Fig. 4A)** and tone bursts **(Fig. 4B)** revealed no significant differences between both animal groups suggesting normal neuronal conductivity in TRPV5^{-/-} mice. To investigate neural behavior near threshold levels, input-output functions of latency growth were analyzed for both stimuli. Therefore, the latency of peak V was plotted as a function of the stimulus intensity. The latency shift as a function of stimulus intensity for click **(Fig. 4C)** and burst **(Fig. 4D)** showed the typical latency increase at lower intensities (22) revealing no overall differences between wild-type and TRPV5^{-/-} (p > 0.05).
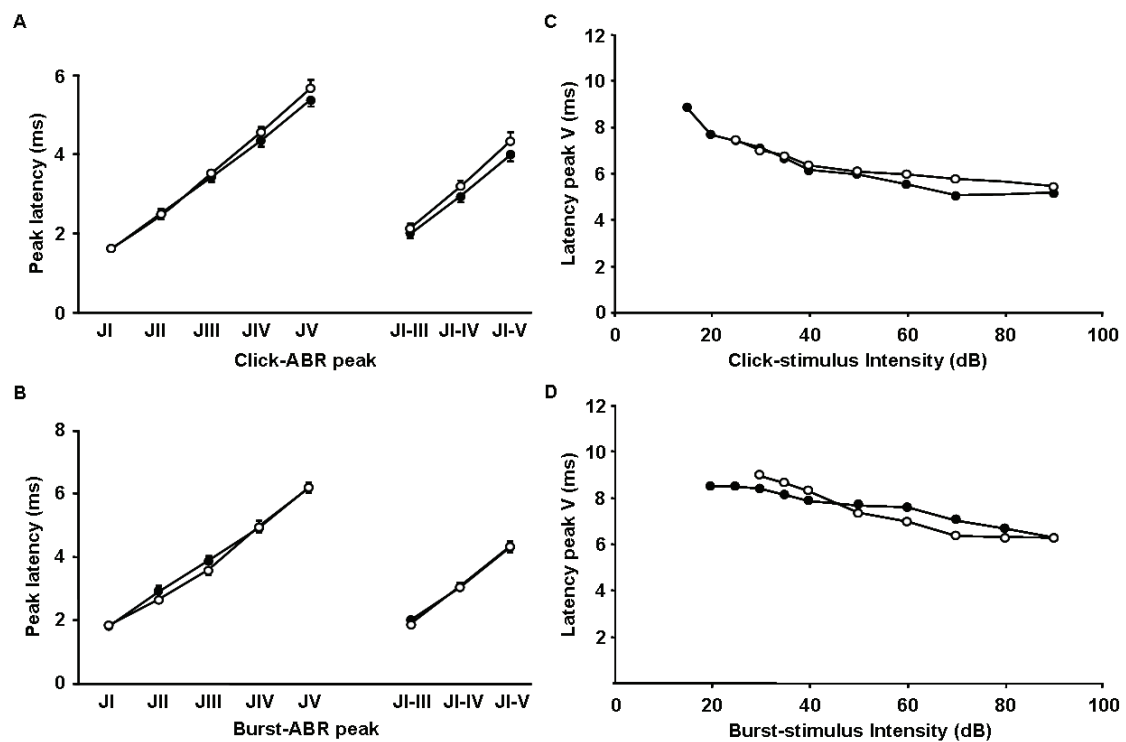
Fig. 4. Normal latencies in TRPV5^{-/-} mice

Mean peak and interpeak latencies (ms) obtained with 90 dB click- **(A)** and tone burst- **(B)** ABR in wild-type (closed symbols) and TRPV5^{-/-} (open symbols) littermates. No differences in latencies in response to either click or burst stimuli indicate a normal neuronal conductivity in TRPV5^{-/-}. Input-output curves of JV latency as a function of stimulus intensity for the click-ABR **(C)** and for tone burst-ABR **(D)**. Mean latencies of peak V decreased with increasing stimulation level and no differences were observed between both groups indicating that neural synchronicity at the brainstem is normal in TRPV5^{-/-} mice.

Discussion

The present study identified TRPV5 as an essential component in Deiter's supporting cells contributing significantly to overall sound perception thresholds. Our conclusion is based on the following experimental observations. First, in cochlea TRPV5 localizes to Deiter's cells at the outer hair cell interface. Second, genetic ablation of TRPV5 decreases the acoustic pre-pulse inhibition while the latencies remained normal. Third, mice lacking TRPV5 display increased thresholds with normal latencies during auditory brainstem recordings.

Mice that lack TRPV5 display renal Ca^{2+} wasting, intestinal hyperabsorption and a reduced bone thickness underlying the important function of TRPV5 in maintaining a normal Ca^{2+} balance (19). Since the Ca^{2+} transport proteins described in transcellular Ca^{2+} reabsorption in kidney are also expressed in the cochlea where they potentially fulfill similar functions we explored the functional aspect of the apical influx channel TRPV5 in sound perception. Recently, TRPV5 transcripts have been detected in primary cultures of semicircular canal duct epithelial cells from neonatal rats (18). The authors speculated that TRPV5 is involved in maintaining the low Ca^{2+} concentration in vestibular endolymph. Here, we localized TRPV5 to the outer hair cell interface of Deiter's supporting cells using wild-type and TRPV5$^{-/-}$ mice. TRPV5 was, however, not detected in the stria vascularis. Like in kidney, TRPV5 localized apically in the Deiter's cells suggesting that TRPV5 could account for apical Ca^{2+} influx.

Acoustic startle responses are specially suited for the investigation of immediate responses to sudden acoustic stimuli resulting in a measurable startle response of the subject (23, 24). Both tested mice strains showed a similar acoustic startle response to the 120 dB startle pulse demonstrating normal detection of the high intensity startle pulses. Startle responses of wild-type mice in reaction to the 120 dB startle pulse preceded by a low intensity pre-pulse revealed a typical reaction such that the startle response decreased when the pre-pulse increased (pre-pulse inhibition). The pre-pulse inhibition in TRPV5$^{-/-}$ littermates was decreased compared to the wild-type mice, suggesting defects in the detection of the pre-pulse. Importantly, no adaptations to the 120 dB startle pulse were detected throughout the protocol indicating that the observed decrease in pre-pulse inhibition is not due to habituation. Furthermore, the time point of the maximal response (Tmax) was comparable demonstrating that the latency is equal in both mice. Besides broadband clicks, higher frequency tone bursts ABRs were recorded since the power spectrum of broadband clicks is merely focused at a relative low frequency range (around 3 kHz). Both click and burst recordings revealed increased thresholds for TRPV5$^{-/-}$ mice as compared to their wild-type littermates further indicating a critical function for TRPV5 in sound perception.

Similar as during the startle response measurements the ABR recordings of TRPV5$^{-/-}$ showed comparable latencies. This suggests that there is no conductive hearing loss or high-frequency cochlear hearing loss, which is normally associated with a total wave delay of the ABR (25).

In addition, the response morphology of the ABR peak latencies does not differ from the control group further demonstrating that TRPV5$^{-/-}$ mice have normal neuronal conductivity. In addition, analysis of the interwave intervals showed that the JI-III and JI-V interwave intervals of the TRPV5$^{-/-}$ mice are similar to the interwave intervals obtained from wild-type littermates confirming the absence of any neuropathology. Tone burst-evoked ABR revealed similar latencies for both wild-type and TRPV5$^{-/-}$ demonstrating that cochlear generation of excitatory postsynaptic potentials are comparable to responses obtained with click stimuli. Moreover, these results reveal the absence of differences in neural conductivity which could potentially explain the higher threshold in the TRPV5$^{-/-}$ mice. Taken together, we found no differences in neural synchronicity at the brainstem or altered neural conductivity between wild-type and TRPV5$^{-/-}$ mice.

Sound detection in TRPV5$^{-/-}$ mice is undisturbed at higher intensity as reflected by the normal startle response at 120 dB and normal ABRs at higher intensities. Since only at low sound intensities hearing of the TRPV5$^{-/-}$ mice is disturbed it is likely that cochlear amplification by the outer hair cells is malfunctioning. TRPV5 localizes to Dieters's cells that are generally not assigned as sensory cells although they can, at least *in vitro*, divide and differentiate into functional hair cells (26). Deiter's cells belong to the organ of Corti non-sensory supporting cells of which the function is not fully understood, while their role in cochlear homeostasis has gained general acceptance. Deiter's cells are in close contact with the apical and basal pole of the outer hair cells. Mutations in both Fibroblast Growth Factor receptor 3 and Sprouty2 were found to cause perturbations in the cytoarchitecture of the organ of Corti leading to a disturbance in the overall sound perception indicating that the architecture of the supporting cells is essential for normal sound perception within the organ of Corti (1, 2). The organ of Corti in TRPV5$^{-/-}$, however, has a normal morphology as compared to their wild-type littermates. Together these results suggest a direct effect, of the Deiter's cells in sound perception, other than merely providing support to the outer hair cells.

In summary, TRPV5 likely plays an essential role in sound perception. In cochlea TRPV5 localizes to the Deiter's cells where the channel contributes to amplification of lower sound intensities thereby determining hearing thresholds. At the outer hair cell interface TRPV5 potentially accounts for apical Ca^{2+} influx in Deiter's cells. Thus, our data provides evidence for a more direct role of Deiter's cells in supporting sound perception near threshold intensities.

References

1.   Shim, K., Minowada, G., Coling, D. E. & Martin, G. R. (2005) *Dev Cell* **8,** 553-64.
2.   Colvin, J. S., Bohne, B. A., Harding, G. W., McEwen, D. G. & Ornitz, D. M. (1996) *Nat Genet* **12,** 390-7.
3.   Peters, T. A., Monnens, L. A., Cremers, C. W. & Curfs, J. H. (2004) *Pediatr Nephrol* **19,** 1194-201.
4.   Jentsch, T. J., Hubner, C. A. & Fuhrmann, J. C. (2004) *Nat Cell Biol* **6,** 1039-47.
5.   Clapham, D. E. (2003) *Nature* **426,** 517-24.
6.   Corey, D. P., Garcia-Anoveros, J., Holt, J. R., Kwan, K. Y., Lin, S. Y., Vollrath, M. A., Amalfitano, A., Cheung, E. L., Derfler, B. H., Duggan, A., Geleoc, G. S., Gray, P. A., Hoffman, M. P., Rehm, H. L., Tamasauskas, D. & Zhang, D. S. (2004) *Nature* **432,** 723-30.
7.   Bautista, D. M., Jordt, S. E., Nikai, T., Tsuruda, P. R., Read, A. J., Poblete, J., Yamoah, E. N., Basbaum, A. I. & Julius, D. (2006) *Cell* **124,** 1269-82.
8.   Kwan, K. Y., Allchorne, A. J., Vollrath, M. A., Christensen, A. P., Zhang, D. S., Woolf, C. J. & Corey, D. P. (2006) *Neuron* **50,** 277-89.
9.   Tabuchi, K., Suzuki, M., Mizuno, A. & Hara, A. (2005) *Neurosci Lett* **382,** 304-8.
10. Hoenderop, J. G., Nilius, B. & Bindels, R. J. (2005) *Physiol Rev* **85,** 373-422.
11. Raymond, J., Dechesne, C. J., Desmadryl, G. & Dememes, D. (1993) *Acta Otolaryngol Suppl* **503,** 114-8.
12. Dechesne, C. J. & Thomasset, M. (1988) *Brain Res* **468,** 233-42.
13. Airaksinen, L., Virkkala, J., Aarnisalo, A., Meyer, M., Ylikoski, J. & Airaksinen, M. S. (2000) *ORL J Otorhinolaryngol Relat Spec* **62,** 9-12.
14. Hackney, C. M., Mahendrasingam, S., Penn, A. & Fettiplace, R. (2005) *J Neurosci* **25,** 7867-75.
15. Yamoah, E. N., Lumpkin, E. A., Dumont, R. A., Smith, P. J., Hudspeth, A. J. & Gillespie, P. G. (1998) *J Neurosci* **18,** 610-24.
16. Dumont, R. A., Lins, U., Filoteo, A. G., Penniston, J. T., Kachar, B. & Gillespie, P. G. (2001) *J Neurosci* **21,** 5066-78.
17. Oshima, T., Ikeda, K., Furukawa, M. & Takasaka, T. (1997) *Biochem Biophys Res Commun* **233,** 737-41.
18. Yamauchi, D., Raveendran, N. N., Pondugula, S. R., Kampalli, S. B., Sanneman, J. D., Harbidge, D. G. & Marcus, D. C. (2005) *Biochem Biophys Res Commun* **331,** 1353-7.
19. Hoenderop, J. G., van Leeuwen, J. P., van der Eerden, B. C., Kersten, F. F., van der Kemp, A. W., Merillat, A. M., Waarsing, J. H., Rossier, B. C., Vallon, V., Hummler, E. & Bindels, R. J. (2003) *J Clin Invest* **112,** 1906-14.
20. Jewett, D. L. & Williston, J. S. (1971) *Brain* **94,** 681-96.
21. Hoenderop, J. G., van der Kemp, A. W., Hartog, A., van de Graaf, S. F., van Os, C. H., Willems, P. H. & Bindels, R. J. (1999) *J Biol Chem* **274,** 8375-8.
22. van der Drift, J. F., van Zanten, G. A. & Brocaar, M. P. (1989) *Audiology* **28,** 181-93.
23. Swerdlow, N. R., Geyer, M. A. & Braff, D. L. (2001) *Psychopharmacology (Berl)* **156,** 194-215.
24. Paylor, R. & Crawley, J. N. (1997) *Psychopharmacology (Berl)* **132,** 169-80.
25. Borg, E., Lofqvist, L. & Rosen, S. (1981) *Scand Audiol Suppl* **13,** 95-7.
26. White, P. M., Doetzlhofer, A., Lee, Y. S., Groves, A. K. & Segil, N. (2006) *Nature* **441,** 984-7.

CHAPTER VIII

GENERAL DISCUSSION & SUMMARY

Introduction

To balance the total amount of Ca^{2+} in our body Ca^{2+} is absorbed in the intestine, exchanged from bone and reabsorbed in kidney. The specialized TRP family members TRPV5 and TRPV6 contribute significantly to this process by acting as luminal influx ports in these tissues (1-3). Transcellular Ca^{2+} transport in Ca^{2+}-transporting epithelia constitutes a three-step process (4). First, Ca^{2+} enters the cell at the luminal membrane via TRPV5 and TRPV6. Second, once in the cell Ca^{2+} is bound by calbindins that ferry Ca^{2+} from the luminal membrane towards the basolateral membrane. Finally, Ca^{2+} is excreted by the Na^+/Ca^{2+} exchanger NCX1 and Ca^{2+} ATPase PMCA1b. A detailed insight into the molecular regulation of TRPV5 and TRPV6 is thus pivotal for the general understanding of Ca^{2+} homeostasis. Various mechanisms to regulate the activity of these channels have been identified operating both on the genomic and non-genomic level. The results described in this thesis focused on the intrinsic mechanisms controlling the activity of these channels thereby describing novel perspectives in TRPV5 and TRPV6 physiology. This chapter will summarize and discuss the data of these studies and will integrate the results in our current understanding of TRPV5- and TRPV6-mediated Ca^{2+} transport. Finally, new research questions will be formulated that can be addressed in future studies.

Coordinated genomic control of the renal Ca^{2+} transport machinery

Several studies exploring the regulatory role of $1,25(OH)_2D_3$, PTH, estrogens and dietary Ca^{2+} revealed a concomitant regulation of the renal Ca^{2+} transport proteins. Additional evidence for $1,25(OH)_2D_3$- and PTH-independent regulation of the Ca^{2+} balance was obtained from TRPV5$^{-/-}$ mice. Down-regulation of the vitamin D-dependent Ca^{2+} transport proteins including calbindin-D_{28K} (CaBP$_{28K}$) and NCX1 in kidneys of these mice despite elevated levels of $1,25(OH)_2D_3$ suggests that TRPV5 is primarily involved in the regulation of the Ca^{2+} transport protein expression in kidney independent of $1,25(OH)_2D_3$. An interesting question is how the expression of TRPV5 specifically coordinates the Ca^{2+} transport machinery. Because TRPV5 is the gatekeeper controlling the apical Ca^{2+} influx it is feasible that the magnitude of Ca^{2+} influx through TRPV5 determines the expression of the Ca^{2+} transport proteins. This hypothesis was recently investigated using primary cultures of rabbit connecting tubule (CNT) and cortical collecting duct (CCD) cells (5). Long-term exposure to PTH stimulated transepithelial Ca^{2+} transport in these epithelial cells, and concomitantly elevated the expression of TRPV5, CaBP$_{28K}$ and NCX1. Blockage of TRPV5 channel activity by ruthenium red abolished PTH-stimulated transepithelial Ca^{2+} transport, which was accompanied by a reduction in NCX1 and CaBP$_{28K}$ expression. These findings support the hypothesis that the magnitude of the Ca^{2+} influx through TRPV5 controls the expression of the other Ca^{2+} transport proteins. This implicates an efficient regulation of Ca^{2+} reabsorption

in kidney where Ca^{2+} regulates its own transport activity. Thus, when the expression of TRPV5 changes the complete machinery including $CaBP_{28K}$, NCX1 and PMCA1b follows accordingly. An important question that remains to be answered, however, is how the flux of Ca^{2+} through TRPV5 adjusts the expression of the Ca^{2+} transport proteins. Previous studies have indicated that Ca^{2+} is important for gene transcription (6). A Ca^{2+}-responsive element has been identified in the promoter sequence of $CaBP_{28K}$ that underlies the purkinje cell specific expression of $CaBP_{28K}$ (7). However, It is not known whether this element is active in kidney and/or whether additional intracellular signaling molecules are involved. An established pathway for regulation of gene expression by Ca^{2+}-signaling is via the ubiquitously expressed Ca^{2+} sensor calmodulin (CaM) that can stimulate gene expression via distinct mechanisms. Nuclear CaM-dependent kinase IV (CaMKIV) and the transcription factor CREB (cAMP-response binding protein) are among the CaM-regulated proteins that affect gene expression (8). Besides CaM, the Ca^{2+}-binding protein calcineurin / NFAT (nuclear factor of activated T cells) signaling cascade can also stimulate gene expression upon a rise of intracellular Ca^{2+}. Recently this pathway has been shown to be essential for the expression of the sodium-phosphate co-transporter (NaP_i) in kidney underlying the Ca^{2+}-dependent expression of NaP_i (9). Currently, it is not known whether these mechanisms are involved in the TRPV5-mediated control of the Ca^{2+} transport machinery transcription. However, recent cDNA micro array analysis, to further identify gene products in the kidney which are regulated by high dietary Ca^{2+} and/or $1,25(OH)_2D_3$, performed on kidneys from high dietary Ca^{2+} or $1,25(OH)_2D_3$-treated 1α-OHase$^{-/-}$ mice provided novel insights in the Ca^{2+}-dependent transcriptional regulation of the Ca^{2+} transport machinery. In this study, $1,25(OH)_2D_3$ induced a significant regulation of ~1000 genes, whereas dietary Ca^{2+} supplementation of the 1α-OHase$^{-/-}$ mice revealed ~2000 controlled genes (4). Importantly, Ca^{2+} transport proteins including NCX1 and $CaBP_{28K}$ were among the dietary Ca^{2+}-regulated genes confirming that besides vitamin D, dietary Ca^{2+} determines the expression of the renal Ca^{2+} transporters. Furthermore, intracellular signaling molecules, including CaM, were identified that might be part of the signaling pathway that underlie the Ca^{2+}-regulated expression of the complete Ca^{2+} transport machinery in kidney.

Together these findings contribute to the concept that once the activity of the gatekeeper TRPV5 is altered, the complete Ca^{2+} transport machinery will be affected accordingly, since the magnitude of the Ca^{2+} flux that enters the cell via TRPV5 coordinates the expression of the other Ca^{2+} transport proteins. From a clinical point of view these findings reveal an efficient way to regulate overall renal Ca^{2+} handling by compounds that specifically stimulate or inhibit TRPV5 channel activity. The underlying molecular signaling pathway, however, remains to be identified. Future studies like promoter analysis in the Ca^{2+} transporter genes to identify functional Ca^{2+}-responsive elements, and experiments focusing on the different Ca^{2+}-

dependent signaling pathways and transcription factors will bring further knowledge about the Ca^{2+}-regulated coordinated genomic control of renal Ca^{2+} transporters.

Factors and mechanisms controlling TRPV5 cell surface expression

One of the mechanisms of ion channel regulation is the control of cell surface expression, thereby determining the ion permeability of the plasma membrane. Since TRPV5 and TRPV6 are localized in vesicular structures and these channels display constitutive activity, cell surface expression of TRPV5 and TRPV6 largely controls the Ca^{2+} permeability of Ca^{2+}-transporting epithelia. Several TRPV5-associated proteins were previously identified in controlling channel plasma membrane expression. The S100A10-annexin 2 complex was identified as an essential component of the machinery employed to deliver TRPV5 to the plasma membrane whereas Rab11A is part of a GTP/GDP-dependent recycling mechanism of TRPV5 cell surface expression (10, 11). The key question that remains to be answered is whether both pathways integrate or operate in parallel. TRPV5 plasma membrane expression controlled by Rab11A recycling is clearly dependent on the processing of GTP as reflected by the different observations with Rab11A mutants that resemble constitutive GTP bound or GTP unbound states (10). No stimuli were identified that initiate plasma membrane expression of TRPV5 under the control of the S100A10-annexin 2 complex, suggesting that TRPV5 trafficking by the S100A10-annexin2 complex operates independently from the Rab11A pathway. However, the S100A10-annexin 2 complex has recently been identified to determine the distribution of Rab11-positive endosomes indicating that both pathways might intersect (12). Future experiments focusing on this overlap should elucidate this potential functional link.

The project described in chapter 2 basically started with the fundamental question not answered thus far: "Which factors known to affect the Ca^{2+} balance control TRPV5 plasma membrane expression?". Importantly, these factors most likely not directly activate or gate TRPV5 given the electrophysiological characteristics that the channel operates as a constitutively active ion channel but initiate Ca^{2+} transport by rapidly recruiting the channel towards the cell surface and visa versa. We demonstrated that extracellular pH dynamically determines TRPV5 cell surface expression and coherent channel activity enabling tight and spatial-temporal control of this channel. Upon extracellular alkalinization TRPV5 containing vesicles are recruited to the plasma membrane resulting in a significant increase in TRPV5 activity, whereas extracellular acidification results in retrieval of TRPV5 from the plasma membrane accompanied by a decrease in channel activity. At the cell surface these TRPV5 containing vesicles remain intact and do not completely fuse and collapse at the plasma membrane indicating that TRPV5 accesses the extracellular solution from inside these vesicles. This "kiss and linger" delivery process is unique as compared to previously

identified modes of vesicular trafficking **(Fig. 1)**. The general concept of TRP channel delivery is that these channels are delivered via classical "fuse and collapse" modes of vesicular trafficking. "Fuse and collapse" exocytosis is a well studied process and many components have been identified that underly vesicle docking, fusion and collapsing at the plasma membrane (13). During "fuse and collapse" the vesicle forms a fusion pore at the cell surface that dilates until the membrane of the vesicle is completely collapsed into the plasma membrane **(Fig. 1)**. "Fuse and collapse" delivery, however, operates on a time scale that might be insufficient for rapid regulation of constitutively active ion channels. Thus "kiss and linger" might be a more delicate mechanism underlying tight and spatial-temporal control of constitutively active ion channels. For exocytosis of soluble cargo three modes of vesicular movement have been identified. Besides the classical pathway "fuse and collapse" rapid stimulated exocytosis of soluble cargo is dependent on "kiss and run" which describes that exocytotic vesicles form a transient opening that does not dilate further. Upon release of its cargo, the vesicle rapidly reseals thereby retrieving the secretory vesicle intact from the cell surface (14-16). A third pathway termed, "fuse-pinch-and linger" or "kiss and coat" is sort of an intermediate between full fusion and transient openings. This latter mode of exocytosis entails prolonged maintenance of the transient opening followed by direct retrieval of the emptied vesicle. The latter two modes of exocytosis of soluble compound are thus comparable to "kiss and linger" delivery of TRP channels and potentially similar underlying machineries are employed. Recently "kiss and coat" vesicles were identified to be surrounded by an actin filament (F-actin) after reaching the cell surface followed by prolonged opening of the transient pore and subsequent direct retrieval (14). Thus, potentially the actin filament prevents the integration of recruited vesicles in the membrane which might be a general mechanism for generating local signals via direct membrane fusion. Detailed electron microscopy of TRPV5-expressing cells should provide further knowledge about potential actin based filaments around TRPV5-containing vesicles that form "kiss and linger" interactions with the plasma membrane.

Kiss and linger delivery of TRP channels was previously investigated for TRPC5 although this study could not distinguish between actual vesicle fusion and subsequent diffusion of the channel into the plasma membrane or transient interaction of the vesicles with the plasma membrane (17). The results described in chapter 2, however, reveal that rapid recruitment of constitutively active TRP channels is dependent on vesicles that "kiss and linger" at the plasma membrane. A series of previous studies suggested that recruitment of TRPs to the plasma membrane is an alternative mechanism by which these channels are activated although the precise underlying mechanism remained unknown (18-20). Therefore, the elucidation of "kiss and linger" opens new insights in ion channel regulation in general. Reflecting previous findings in TRPV5 regulation with the knowledge of this newly identified mechanism might

unravel other factors that rapidly increase overall TRPV5 activity via "kiss and linger" delivery. Intracellular Ca^{2+} is an important factor controlling TRPV5 activity although, recent data indicated that a decrease in $[Ca^{2+}]_i$ does not result in the recruitment of TRPV5 to the cell surface as assed by TIRF microscopy (Lambers *et al*, unpublished results). Providing evidence that urinary Ca^{2+} can affect the trafficking of luminal transporters or channels is the mechanism underlying the coupling of hypercalciuria and polyuria (21). High levels of urinary Ca^{2+} were found to antagonize vasopressin-induced trafficking of the water permeable channel, aquaporin 2, suggesting that the urinary Ca^{2+} concentration controls aquaporin 2 cell surface expression on the luminal membrane (21). During hypercalciuria this mechanism might inhibit water reabsorption thereby preventing further concentration of Ca^{2+} and Ca^{2+} stone formation. Potentially, similar mechanisms exist for TRPV5 and TRPV6 where extracellular Ca^{2+} determines the cell surface expression via a "kiss and linger" pathway. In this case the Ca^{2+}-sensing receptor which is expressed on the luminal surface of the distal conculte tubule (DCT) en CNT (22) senses potential changes in the local extracellar Ca^{2+} level which might result in rapid changes in TRPV5 cell surface expression via a "kiss and linger" mechanism.
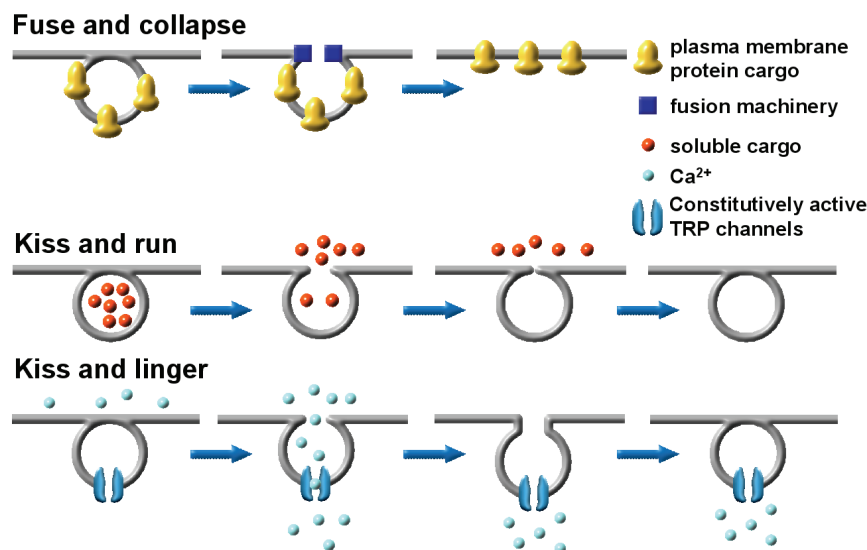
Fig. 1 Modes of vesicular trafficking Activation of constitutively active TRP channels likely depends on rapidly recruited TRP-containing vesicles that remain intact at the plasma membrane interface (process termed "kiss and linger"). Constitutively active TRP channels access the extracellular solutions from inside the vesicle via transient openings in the plasma membrane. Upon removal of the stimulus these vesicles are rapidly retrieved from the plasma membrane, enabling tight spatial-temporal control of the TRPV5 channels. Compared tot the classical vesicular pathway of membrane protein trafficking termed "fuse and collapse", "kiss and linger" is thus a unique mechanism. "kiss and linger" resembles "kiss and run" exocytosis of soluble cargo. This specialized mode of vesicular cargo delivery describes that exocytotic vesicles form transient openings with the plasma membrane, which upon secretion of its cargo, relocate back to the cytosol for reloading.

Ca^{2+}-dependent activity of TRPV5 and TRPV6

Both TRPV5 and TRPV6 display a negative feedback regulation of channel activity by intracellular Ca^{2+}. This is evident from the relation between [Ca^{2+}]$_i$ and channel activity and the immediate decrease in channel activity after a hyperpolarizing pulse even in the presence of high affinity chemical Ca^{2+} buffers (23). TRPV5 inactivation is of physiological importance to prevent a Ca^{2+} overload in the situation where no adequate intracellular Ca^{2+} handling is provided. Both TRPV5 and TRPV6 are thus dependent on the amount and rate of Ca^{2+} they transport and amount of intracellular Ca^{2+}-buffering present. Unlike several other ion channels that contain a functional Ca^{2+}-binding EF-hand motif in their intracellular tail(s) (24-26), TRPV5 and TRPV6 do not have a Ca^{2+}-binding domain. Thus, the stuctural properties of TRPV5 and TRPV6 cannot explain this phenomenon. A potential candidate that translates the local Ca^{2+} concentration in channel activity might be CaM given that a diverse range of both voltage and non-voltage dependent ion channels are regulated by this ubiquitously expressed Ca^{2+} sensor. The results described in chapter 3 reveal that CaM associates with both TRPV5 and TRPV6 although channel regulation appears to be restricted to TRPV6. CaM is constitutively bound to both TRPV5 and TRPV6 at physiological [Ca^{2+}]$_i$ and acts as a Ca^{2+} sensor only controlling TRPV6 activity. The difference in TRPV5 and TRPV6 channel regulation by CaM is rather unique given the high homology of both channels and similar association characteristics with this Ca^{2+} sensor. Detailed electrophysiological analysis revealed that the Ca^{2+}-dependent inactivation kinetics of TRPV5 are, initially after a hyperpolarizing pulse, less pronounced than for TRPV6 although total inactivation is not significantly different. (27). Potentially, CaM is involved in the initial TRPV5 inactivation as suggested from the differences in this particular part of TRPV5 kinetics in the presence of Ca^{2+} insensitive CaM. Since the differences in overall TRPV5 kinetics are not significant, more sensitive measurements focusing on the initial Ca^{2+}-dependent inactivation are needed to establish a potential role of CaM in TRPV5 activity. Previously, CaM was shown to be consistently co-regulated with TRPV5, supporting a potential functional link between these two proteins (28). Taken together these results suggest that CaM only affects the activity of TRPV6. Crucial to the CaM function are the number of CaM molecules regulating each channel. To address this point the stochiometry of the interaction should be known which is in the generally applied *in vitro* binding assays difficult to establish. Recently this important question was answered for L-type voltage-operated channel by creating channel-CaM fusion proteins (29). Using chimeric molecules this study revealed that a single CaM directs channel regulation. Reflecting TRPV6 regulation these results would suggest that a single constitutively associated CaM molecule translates the local Ca^{2+} concentration in TRPV6 channel activity.

In chapter 4 and 5 the role of calbindins in transcellular Ca^{2+} transport is described. $CaBP_{28K}$ is part of the transcellular Ca^{2+} transport machinery in Ca^{2+}-transporting cells and is consistently co-regulated with TRPV5 (30). Previous modeling studies suggested that calbindin-D_{9K} stimulates intestinal Ca^{2+} absorption by increasing the diffusional range of Ca^{2+}, thereby facilitating Ca^{2+} transport from the luminal influx side towards the basolateral membrane where Ca^{2+} is excreted (31, 32). Based on these models a similar role for $CaBP_{28K}$ in renal Ca^{2+}-transporting cells was predicted. In chapter 4 we described $CaBP_{28K}$ as an interacting protein partner of TRPV5 and demonstrated that $CaBP_{28K}$ dynamically regulates TRPV5 channel activity. $CaBP_{28K}$ association does not directly affects the biophysical properties of TRPV5. However, by binding with TRPV5 $CaBP_{28K}$ provides for spatial Ca^{2+}-buffering at the side where Ca^{2+} levels can become detrimental. This prevents a local increase of $[Ca^{2+}]_i$ and preliminary TRPV5 inactivation. Thus, besides facilitating intracellular Ca^{2+} diffusion, $CaBP_{28K}$ enables high levels of transcellular Ca^{2+} transport by preventing a local accumulation of Ca^{2+} in the TRPV5 pore. Probably, similar mechanisms of targeted Ca^{2+}-buffering occur in brain, bone, teeth, inner ear, placenta and intestine where calbindins are abundantly expressed and cells tolerate a large Ca^{2+} influx. In line with this suggestion is the study of Lee and co-workers who found that $CaBP_{28K}$ affects the activity of L-type voltage-operated channels contributing to the Ca^{2+}-dependent activity by increasing the Ca^{2+} sensitivity of the channel (33). Thus for these channels, $CaBP_{28K}$ acts as a Ca^{2+} sensor thereby substantiating previous results that $CaBP_{28K}$ may function not only as a Ca^{2+} buffer, but also as a Ca^{2+} sensor affecting downstream processes (34-36).

Unlike the previous modelling studies that adapted the properties of CaBPs to determine Ca^{2+} fluxes, the model described in chapter 5 focuses on the intrinsic mechanism of intracellular Ca^{2+}-handling during experimentally derived Ca^{2+} fluxes. This enabled us to study in detail the experimental findings described in chapter 4. Renal Ca^{2+}-transporting cells were modelled as a cylinder in which Ca^{2+} enters the cell at the luminal side cell surface via TRPV5 from where Ca^{2+} spreads out evenly. This revealed that spatial buffering of Ca^{2+} by $CaBP_{28K}$-TRPV5 association reduces the apical $[Ca^{2+}]$ and tempers the region in which $[Ca^{2+}]$ exceeds to levels that would cause channel inactivation. During a previous study no changes in $[Ca^{2+}]_i$ were detectable during high levels of transcellular Ca^{2+} transport (37). In line with these findings our model demonstrated that association of $CaBP_{28K}$ with TRPV5 results in the disappearance of the local increase in the TRPV5 pore domain $[Ca^{2+}]$ that originates from the transport of Ca^{2+} via the channel. Compared to other Ca^{2+} channels that generate a micro-domain of high $[Ca^{2+}]$ around their pore to initiate a cascade of signaling processes, TRPV5 possesses a targeted Ca^{2+} buffer that prevents accumulation of Ca^{2+}. In Ca^{2+}-transporting epithelia transcellular Ca^{2+} transport thus operates independently from Ca^{2+}-signaling (37). The underlying mechanism of how $CaBP_{28K}$ discriminates between Ca^{2+}-signaling and Ca^{2+}

transport is likely mediated by spatial buffering via interaction with the channel or plasma membrane. Moreover, the Ca^{2+}-binding properties of $CaBP_{28K}$ are insufficient to prevent Ca^{2+}-signaling. At least for excitable cell it is known that opening of Ca^{2+}-signaling channels generates a Ca^{2+} flux of such a large magnitude that the flux is out of range of any Ca^{2+} buffer. This in turn implicates that $CaBP_{28K}$ continuously binds all Ca^{2+} that enters the cell via TRPV5 and subsequently transports Ca^{2+} to the basolateral membrane. Although the single channel Ca^{2+} conductance of TRPV5 is unknown these findings basically suggest that opening of TRPV5 channels elicits a Ca^{2+} flux that is in range of Ca^{2+}-buffering by $CaBP_{28K}$. Interactions at the side of Ca^{2+} entry further stimulate direct buffering of Ca^{2+} such that no free Ca^{2+} enters the cell but is immediately buffered by $CaBP_{28K}$. This is supported by our findings described in chapter 5 predicting that the single TRPV5 channel Ca^{2+} flux is in the order of 10^4 Ca^{2+} ions per second. This is significantly lower compared to voltage-operated Ca^{2+} channels, contributing to Ca^{2+}-signaling in excitable cells that generate single channel Ca^{2+} fluxes in the order of 10^6 Ca^{2+} ions per second. Thus, Ca^{2+} influx through TRPV5 and subsequent immediate Ca^{2+}-buffering by $CaBP_{28K}$ are processes that are directly coupled and optimized for high levels of transcellular Ca^{2+} transport without initiation of and interference with signaling pathways.

Integration of our current knowledge of Ca^{2+}-dependent regulation of TRPV5 and TRPV6 activity suggests a crucial role for $CaBP_{28K}$ and CaM. In this process, calbindins act as dynamic Ca^{2+} buffers providing adequate intracellular Ca^{2+}-handling, whereas CaM operates as a Ca^{2+} sensor controlling channel activity. Compared to calbindins, the affinity of CaM for Ca^{2+} is relatively high which enables CaM to bind Ca^{2+} even in the presence of submillimolar concentrations of calbindin. This enables CaM to constitutively interact with TRPV5 and TRPV6 at a physiological $[Ca^{2+}]_i$ since Ca^{2+}-CaM associates with these channels under these conditions (35, 38). Thus most likely, both associated proteins operate independently from each other. In addition, the novel EF-hand containing protein 80K-H was identified as a Ca^{2+} sensor controlling TRPV5 activity whereas the role of 80K-H in determining TRPV6 activity is unknown (39). Although 80K-H was shown to bind Ca^{2+}, the Ca^{2+} affinity of the two EF-hand structures remains elusive which makes it difficult to integrate 80K-H in a model of overall Ca^{2+}-dependent activity of these channels. Probably, the Ca^{2+}-binding affinity of the EF-hand structures in 80K-H is comparable with those in the high affinity sites of CaM. Otherwise, 80K-H would not be able to control TRPV5 activity in the presence of the high levels of calbindins in Ca^{2+}-transporting cells. One could envisage that 80K-H is involved in the inactivation of TRPV5 when $CaBP_{28K}$ is saturated with Ca^{2+}. This implicates that inactivation of the EF-hand residues would result in an increased overall TRPV5 activity since the negative feedback inhibition by 80K-H is abolished in this case. The results, however, indicates that inactivation of the EF-hand structures in 80K-H decreases TRPV5

activity. This further substantiates that the affinity of 80K-H is comparable to that of CaM and 80K-H controls TRPV5 activity independently from $CaBP_{28K}$ by acting as a Ca^{2+} sensor. In summary, the effect of CaM on TRPV6 and 80K-H on TRPV5 activity are comparable and implicates that at a physiological $[Ca^{2+}]_i$ these proteins control TRPV5 and TRPV6 function, making them part of the complex regulatory network to balance Ca^{2+} influx in Ca^{2+}-transporting epithelia.

Thus, our findings suggest a comprehensive model for Ca^{2+}-dependent activity of TRPV5 and TRPV6 **(Fig. 2)**. At a physiological $[Ca^{2+}]_i$ these channels are normally transported to the cell surface and 80K-H and CaM associate with TRPV5 and TRPV6, respectively. Here, the channels are active and Ca^{2+} that enters the cell is immediately buffered by recruited calbindins. Subsequently, calbindines transport Ca^{2+} to the basolateral membrane where Ca^{2+} is excreted. Upon saturation of the calbindins the channels inactivate because of a local rise in $[Ca^{2+}]$. The mechanism that translates this local increase in TRPV5 and TRPV6 inhibition, however, remains to be elucidated.
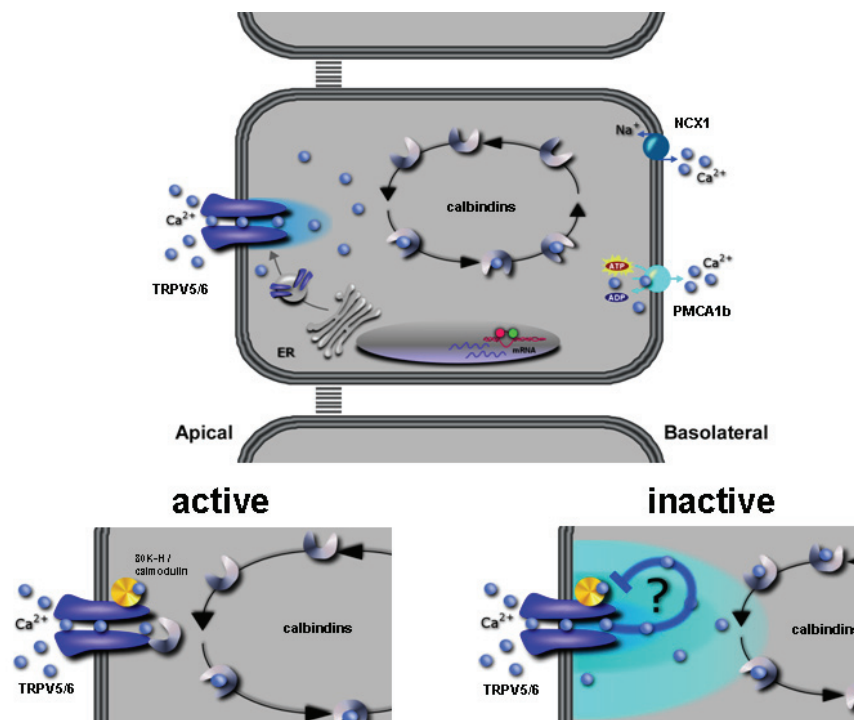
Fig. 2 Regulation of TRPV5 and TRPV6 by Ca^{2+}-binding proteins Overall Ca^{2+}-dependent activity of TRPV5 and TRPV6 is determined by a set of Ca^{2+}-binding proteins. At normal physiological $[Ca^{2+}]_i$ these channels reach the cell surface where 80K-H and CaM associate with TRPV5 and TRPV6, respectively. Here, the channels are active and Ca^{2+} that enters the cell is immediately buffered by recruited $CaBP_{28K}$ (TRPV5) and $CaBP_{9K}$ (TRPV6). Calbindins subsequently ferry Ca^{2+} to the basolateral membrane where Ca^{2+} is excreted by NCX1 and PMCA1b. Upon saturation of the calbindins the channels inactivate due to a local rise in $[Ca^{2+}]$. The mechanism that translates this local increase into TRPV5 and TRPV6 inhibition is, however, still not identified.

TRPV5 regulation at the cell surface

Although the electrophysiological characteristics of both TRPV5 and TRPV6 reveal constitutive activity, these channels appear to be affected by associated proteins via mechanisms other then plasma membrane trafficking (40, 41). The results shown in chapter 6 contribute to this concept by revealing that the recently identified protein Nipsnap1 regulates TRPV5 activity without affecting cell surface expression. Co-expression of Nipsnap1 along with TRPV5 dramatically decreases channel activity. The interaction of Nipsnap1 is localized to the carboxyl-terminus MLERK sequence, previously identified to be essential for 80K-H and Rab11A association, and channel tetramerization (10, 39, 42). These findings suggest that Nipsnap1 competes with other TRPV5-associated proteins for binding to the channel. As evident from the cell surface biotinylation assays this competition does, however, not result in altered TRPV5 plasma membrane expression. Thus, associated proteins like S100A10-annexin 2 and Rab11 are likely not involved in the Nipsnap1-mediated inhibition of TRPV5 activity. Another option is that Nipsnap1 binding results in changes of the TRPV5 structure, which would decrease channel activity. Such a mechanism of structural changes was formulated, at least in part, to explain the pH-sensitivity of the channel (43). Both intra- and extracellular protons were found to affect the position of the TRPV5 pore helix structure such that upon acidification the helix rotates clockwise resulting in narrowing of the channel pore (43). The Nipsnap1-mediated inhibition of channel activity suggests that binding of Nipsnap1 is dynamic, otherwise Nipsnap1 would consistently suppress TRPV5 activity. An obvious candidate factor controlling this dynamic behavior would be Ca^{2+} itself substantiating the negative feedback of Ca^{2+} on TRPV5 activity. However, Ca^{2+} does not affect the binding of Nipsnap1 and TRPV5 given the lack of Ca^{2+} dependence during the binding analysis suggesting that Ca^{2+} is not involved Nipsnap1 regulation. Thus, Nipsnap1 recruitment to TRPV5 at the cell surface might be part of TRPV5 regulation at the cell surface. Further experimental data should finally substantiate this hypothesis.

TRPV5 in other tissues: a critical function in hearing

Over the years TRPV5 research has focused on its regulation and functioning in the maintenance of the Ca^{2+} balance although this channel has also been identified in other tissues generally not implicated in Ca^{2+} homeostasis (4). The results presented in chapter 7 substantiate our knowledge of TRPV5 function by highlighting its presence and physiological role in the inner ear. Besides malfunctioning of the Ca^{2+} balance (44), TRPV5^{-/-} mice display decreased startle pre-pulse inhibition and increased acoustic brainstem response thresholds demonstrating deficits in sound perception. Although many cell types have been identified in the cochlea, the sound perceptive organ in the inner ear, their function still largely remains elusive. Research on hearing loss has traditionally focused on the hair cells, as they are the

first station in the conversion of sound into electrical signals that are conducted by the axons of the spiral ganglion neurons to the brain. Directly underneath the hair cells lay the organ of Corti supporting cells of which the function is unknown. Recently, supporting cells have been suggested to fulfill an active role in the maintenance of the mechano-sensitive hair cell structure and function (45). Our results contribute to this concept by providing evidence for a TRPV5-based pathway in Deiters supporting cells involved in auditory threshold determination. Deiters cells contain a specialized system of endocellular protein filaments which provides them with internal strength important to support the outer hair cells (45). Because outer hair cells are involved in sound amplification near threshold intensities and TRPV5$^{-/-}$ mice display increased hearing thresholds the lack of TRPV5 most likely results in malfunctioning of the outer hair cells. How TRPV5 in Deiters cells contributes to outer hair cell function, however, is not clear. In addition to providing structural support, Deiters cells have been implicated as an ion reservoir salvaging K^+ and avoiding its accumulation in the extracellular solution that might be cytotoxic to hair cells (46). Thus, potentially similar buffering mechanisms exist for the maintenance of $[Ca^{2+}]_e$ such that Deiters cells absorb excess amount of extracellular Ca^{2+}. In analogy to its function in Ca^{2+}-transporting epithelia, TRPV5 accounts for luminal Ca^{2+} influx in these cells.

Glimpse at the future

The novel perspectives in TRPV5 and TRPV6 regulation have significantly contributed to our understanding of the overall control of luminal Ca^{2+} influx in Ca^{2+}-transporting epithelia **(see table 1 for an overview).** While some of these newly identified concepts describe the cell surface expression of these channels, others unravel the Ca^{2+}-dependent channel activity First, the identified pathway of rapid TRPV5 channel delivery to the plasma membrane opens a challenging field of research in TRP regulation. Channeling important questions, like which factors prevent collapsing and fusing during vesicular "kiss and linger" interactions with the plasma membrane, will provide a comprehensive view on the regulation of constitutively active ion channels. In this particular field, knowledge can be gained from research that focuses on "kiss and run" and "kiss and coat" exocytosis that are comparable to "kiss and linger". Second, although several associated proteins are identified to control trafficking of these channels towards the cell surface, we still do not fully understand the mechanisms determining the functional restriction of TRPV5 and TRPV6 to the luminal plasma membrane. Questions like which factors determine apical sorting of TRPV5 and TRPV6 remain unanswered. Since we identified extracellular alkalinization as a stimulus to initiate rapid plasma membrane trafficking of TRPV5 we now have a tool at hand to decipher the routes of apical sorting. Preliminary results adapting this control of TRPV5 cell surface expression, suggest a critical role for syntaxins in this process (Lambers *et al*, unpublished

results) highlighting potential factors controlling "kiss and linger" and apical sorting. Third, our model for transcellular Ca^{2+} transport allows the estimation of the number of TRPV5 channels in the membrane. A more reliable estimation can be obtained when $[Ca^{2+}]$ in the TRPV5 pore has been determined. Future experiments that include fusion of fluorescent Ca^{2+} indicator proteins to the channel complex in combination with total internal reflection microscopy should provide this knowledge. In addition, this approach will provide alternatives to determine Ca^{2+} fluxes through single TRPV5 channels as recently described for other Ca^{2+} channels (47). Finally, besides TRPV5 and TRPV6 function in the tissues that contribute to the Ca^{2+} balance imminent research will spread out to other tissues, including inner ear, where these channels contribute to physiological processes other than the maintenance of the Ca^{2+} balance. In summary, the findings described in this thesis open new perspectives about the physiological function of TRPV5 and TRPV6 and pinpoint to novel associated protein partners controlling apical Ca^{2+} influx in Ca^{2+}-transporting epithelia.

References

1. Hoenderop, J. G., van der Kemp, A. W., Hartog, A., van de Graaf, S. F., van Os, C. H., Willems, P. H. & Bindels, R. J. (1999) *J Biol Chem* **274,** 8375-8.
2. Peng, J. B., Chen, X. Z., Berger, U. V., Vassilev, P. M., Tsukaguchi, H., Brown, E. M. & Hediger, M. A. (1999) *J Biol Chem* **274,** 22739-46.
3. van der Eerden, B. C., Hoenderop, J. G., de Vries, T. J., Schoenmaker, T., Buurman, C. J., Uitterlinden, A. G., Pols, H. A., Bindels, R. J. & van Leeuwen, J. P. (2005) *Proc Natl Acad Sci U S A* **102,** 17507-12.
4. Hoenderop, J. G., Nilius, B. & Bindels, R. J. (2005) *Physiol Rev* **85,** 373-422.
5. van Abel, M., Hoenderop, J. G., van der Kemp, A. W., Friedlaender, M. M., van Leeuwen, J. P. & Bindels, R. J. (2005) *Kidney Int* **68,** 1708-21.
6. Chawla, S. (2002) *Eur J Pharmacol* **447,** 131-40.
7. Arnold, D. B. & Heintz, N. (1997) *Proc Natl Acad Sci U S A* **94,** 8842-7.
8. Ashby, M. C. & Tepikin, A. V. (2002) *Physiol Rev* **82,** 701-34.
9. Moz, Y., Levi, R., Lavi-Moshayoff, V., Cox, K. B., Molkentin, J. D., Silver, J. & Naveh-Many, T. (2004) *J Am Soc Nephrol* **15,** 2972-80.
10. van de Graaf, S. F., Chang, Q., Mensenkamp, A. R., Hoenderop, J. G. & Bindels, R. J. (2006) *Mol Cell Biol* **26,** 303-12.
11. van de Graaf, S. F., Hoenderop, J. G., Gkika, D., Lamers, D., Prenen, J., Rescher, U., Gerke, V., Staub, O., Nilius, B. & Bindels, R. J. (2003) *Embo J* **22,** 1478-1487.
12. Zobiack, N., Rescher, U., Ludwig, C., Zeuschner, D. & Gerke, V. (2003) *Mol Biol Cell* **14,** 4896-908.
13. Rodriguez-Boulan, E., Kreitzer, G. & Musch, A. (2005) *Nat Rev Mol Cell Biol* **6,** 233-47.
14. Sokac, A. M. & Bement, W. M. (2006) *Mol Biol Cell* **17,** 1495-502.
15. Gandhi, S. P. & Stevens, C. F. (2003) *Nature* **423,** 607-13.
16. Ryan, T. A. (2003) *Proc Natl Acad Sci U S A* **100,** 2171-3.
17. Bezzerides, V. J., Ramsey, I. S., Kotecha, S., Greka, A. & Clapham, D. E. (2004) *Nat Cell Biol* **6,** 709-20.
18. Kanzaki, M., Zhang, Y. Q., Mashima, H., Li, L., Shibata, H. & Kojima, I. (1999) *Nat Cell Biol* **1,** 165-70.
19. Bahner, M., Frechter, S., Da Silva, N., Minke, B., Paulsen, R. & Huber, A. (2002) *Neuron* **34,** 83-93.
20. Xu, X. Z. & Sternberg, P. W. (2003) *Cell* **114,** 285-97.
21. Procino, G., Carmosino, M., Tamma, G., Gouraud, S., Laera, A., Riccardi, D., Svelto, M. & Valenti, G. (2004) *Kidney Int* **66,** 2245-55.

22.   Ward, D. T. & Riccardi, D. (2002) *Pflugers Arch* **445,** 169-76.
23.   Nilius, B., Prenen, J., Vennekens, R., Hoenderop, J. G., Bindels, R. J. & Droogmans, G. (2001) *Cell Calcium* **29,** 417-28.
24.   Wingo, T. L., Shah, V. N., Anderson, M. E., Lybrand, T. P., Chazin, W. J. & Balser, J. R. (2004) *Nat Struct Mol Biol* **11,** 219-25.
25.   Xiong, L., Zhang, J. Z., He, R. & Hamilton, S. L. (2006) *Biophys J* **90,** 173-82.
26.   DeMaria, C. D., Soong, T. W., Alseikhan, B. A., Alvania, R. S. & Yue, D. T. (2001) *Nature* **411,** 484-9.
27.   Hoenderop, J. G., Vennekens, R., Muller, D., Prenen, J., Droogmans, G., Bindels, R. J. & Nilius, B. (2001) *J Physiol* **537,** 747-61.
28.   Hoenderop, J. G., Chon, H., Gkika, D., Bluyssen, H. A., Holstege, F. C., St-Arnaud, R., Braam, B. & Bindels, R. J. (2004) *Kidney Int* **65,** 531-539.
29.   Mori, M. X., Erickson, M. G. & Yue, D. T. (2004) *Science* **304,** 432-5.
30.   Lambers, T. T., Bindels, R. J. & Hoenderop, J. G. (2006) *Kidney Int* **69,** 650-4.
31.   Feher, J. J., Fullmer, C. S. & Fritzsch, G. K. (1989) *Cell Calcium* **10,** 189-203.
32.   Feher, J. J., Fullmer, C. S. & Wasserman, R. H. (1992) *Am J Physiol* **262,** C517-26.
33.   Lee, D., Obukhov, A. G., Shen, Q., Liu, Y., Dhawan, P., Nowycky, M. C. & Christakos, S. (2006) *Cell Calcium* **39,** 475-485.
34.   Schmidt, H., Schwaller, B. & Eilers, J. (2005) *Proc Natl Acad Sci U S A* **102,** 5850-5.
35.   Venters, R. A., Benson, L. M., Craig, T. A., Bagu, J., Paul, K. H., Kordys, D. R., Thompson, R., Naylor, S., Kumar, R. & Cavanagh, J. (2003) *Anal Biochem* **317,** 59-66.
36.   Venyaminov, S. Y., Klimtchuk, E. S., Bajzer, Z. & Craig, T. A. (2004) *Anal Biochem* **334,** 97-105.
37.   Koster, H. P., Hartog, A., Van Os, C. H. & Bindels, R. J. (1995) *Cell Calcium* **18,** 187-96.
38.   Wang, C. L. (1985) *Biochem Biophys Res Commun* **130,** 426-30.
39.   Gkika, D., Mahieu, F., Nilius, B., Hoenderop, J. G. & Bindels, R. J. (2004) *J Biol Chem* **279,** 26351-7.
40.   van de Graaf, S. F., van der Kemp, A. W., van den Berg, D., van Oorschot, M., Hoenderop, J. G. & Bindels, R. J. (2006) *J Am Soc Nephrol* **17,** 26-30.
41.   Chang, Q., Hoefs, S., van der Kemp, A. W., Topala, C. N., Bindels, R. J. & Hoenderop, J. G. (2005) *Science* **310,** 490-3.
42.   Chang, Q., Gyftogianni, E., van de Graaf, S. F., Hoefs, S., Weidema, F. A., Bindels, R. J. & Hoenderop, J. G. (2004) *J Biol Chem* **279,** 54304-11.
43.   Yeh, B. I., Kim, Y. K., Jabbar, W. & Huang, C. L. (2005) *Embo J* **24,** 3224-34.
44.   Hoenderop, J. G., van Leeuwen, J. P., van der Eerden, B. C., Kersten, F. F., van der Kemp, A. W., Merillat, A. M., Waarsing, J. H., Rossier, B. C., Vallon, V., Hummler, E. & Bindels, R. J. (2003) *J Clin Invest* **112,** 1906-14.
45.   Ramirez-Camacho, R., Garcia-Berrocal, J. R., Trinidad, A., Gonzalez-Garcia, J. A., Verdaguer, J. M., Ibanez, A., Rodriguez, A. & Sanz, R. (2006) *Med Hypotheses* **67,** 550-5.
46.   Spicer, S. S. & Schulte, B. A. (2002) *Hear Res* **172,** 172-85.
47.   Demuro, A. & Parker, I. (2005) *J Gen Physiol* **126,** 179-92.

Samenvatting

(Summary in Dutch)

Inleiding

Vele vitale functies in ons lichaam zijn afhankelijk van een constante bloed calciumconcentratie. Dit blijkt onder andere uit ziektebeelden die samenhangen met een verstoorde calciumbalans, zoals osteoporose, idiopathische hypercalciurie, nierstenen en rickets. Drie organen spelen een belangrijke rol bij de regulatie van de bloed calciumconcentratie, namelijk de botten, de darm en de nieren die gezamenlijk de calciumbalans handhaven. Het calciumtransport tussen deze organen en het bloed wordt gecontroleerd door de zogenaamde calciotrope hormonen zoals vitamine D en parathyroïdhormoon. Vitamine D stimuleert de actieve calciumabsorptie in de dunne darm en de nieren. Dit transcellulair calciumtransport vindt plaats in de gepolariseerde nier- en darmcellen in drie discrete stappen: (*I*) een calciuminflux via het luminale plasmamembraan, (*II*) cytosolische diffusie van calcium met behulp van calciumbindende eiwitten, (*III*) excretie van calcium over de basolaterale membraan door de natrium-calcium uitwisselaar en de calcium-ATPase. Influx via het luminale plasmamembraan wordt verzorgd door twee epitheliale calciumkanalen, namelijk TRPV5 en TRPV6. Deze eiwitten behoren tot de Transient Receptor Potential (TRP) superfamilie van kationkanalen. Het is uitvoerig bewezen dat TRPV5 en TRPV6 een poortwachtersfunctie vervullen in het calciumabsorptieproces en daarmee een essentiële rol spelen bij de regulatie van de calciumbalans. In diverse muismodellen is aangetoond dat een deficiëntie van TRPV5 of TRPV6 leidt tot ernstige verstoringen van de calciumbalans. Bijvoorbeeld, de TRPV5 knockout muis vertoont een hypercalciurie, hyperabsorptie en een verminderde botdichtheid. Ook muizen die door een genetisch defect geen vitamine D kunnen aanmaken hebben een ernstig fenotype mede doordat TRPV5 en TRPV6 sterk zijn verlaagd. Deze pathologische verschijnselen onderstrepen het fysiologisch belang van deze calciumkanalen. De lokalisatie van TRPV5 en TRPV6 in het luminale plasmamembraan van calciumtransporterende epitheelcellen in de dunne darm en de nieren is in overeenstemming met de gepostuleerde functie als poortwachter van de transcellulaire calciumabsorptie. Deze veronderstelling wordt verder ondersteund door de hormoon-afhankelijke regulatie van de epitheliale calciumkanalen. TRPV5 is met name van belang voor de calciumreabsorptie in de nier, terwijl TRPV6 een rol speelt bij de opname van calcium uit het voedsel. Om de calciumbalans beter te begrijpen dient een gedetailleerde kennis over het functioneren van TRPV5 en TRPV6 verkregen te worden. Het onderwerp van dit proefschrift is derhalve inzicht te verschaffen in de regulatie van deze epitheliale calciumkanalen.

Er zijn diverse regulatiemechanismen die uiteindelijk influx van calcium via TRPV5 en TRPV6 in het apicale membraan bepalen. Ten eerste wordt de hoeveelheid beschikbare kanalen in de cel bepaald via genomische regulatie door de calciotrope hormonen, zoals vitamine D, die de calciumbalans controleren. Ten tweede reguleren gespecialiseerde

processen in de cel het transport van TRPV5 en TRPV6 naar het plasmamembraan. Ten derde wordt de activiteit van TRPV5 en TRPV6 beïnvloed in het plasmamembraan via structuurveranderingen of via geassocieerde eiwitten die door binding aan het kanaalcomplex de influx van calcium reguleren. Tenslotte wordt de recycling en afbraak van beide kanalen bepaald waardoor de influx van calcium via TRPV5 en TRPV6 efficiënt gereguleerd kan worden zonder aanmaak van nieuwe kanalen. Dit hoofdstuk geeft een korte samenvatting van de nieuwe inzichten en de rol van nieuw geïdentificeerde TRPV5 en TRPV6 bindingpartners in de regulatie van TRPV5 en TRPV6, zoals beschreven in dit proefschrift.

Extracellulaire pH reguleert de plasmamembraan expressie van TRPV5

Initiële elektrofysiologische karakterisatie van TRPV5 heeft aangetoond dat dit ionkanaal opereert als een constitutief actief calciumkanaal, wat inhoud dat TRPV5 volledig actief is wanneer het kanaal in het plasmamembraan aanwezig is. In hoofdstuk 2 wordt beschreven dat extracellulaire pH, naast regulatie van de poriestructuur, de expressie van TRPV5 in het plasmamembraan bepaalt via een uniek mechanisme. Gedetailleerde microscopische analyse toonde aan dat TRPV5 lokaliseert in intracellulaire vesicles die na extracellulaire alkalinisatie naar het plasmamembraan transporteren. Eenmaal aangekomen fuseren deze vesicles niet maar blijven intact. In combinatie met de samengaande toename van TRPV5 activiteit en toegankelijkheid voor extracellulaire labeling m.b.v. biotine, suggereren deze resultaten dat TRPV5 toegang verkrijgt tot extracellulair calcium vanuit vesicles via transiënte openingen in het plasmamembraan. Opeenvolgend, resulteerde extracellulaire acidificatie in een translocatie van de vesicles terug naar het cytosol. Dit mechanisme (genaamd "kiss en linger") stelt de cel in staat om de plasmamembraan lokalisatie van TRPV5 snel en efficiënt te reguleren. Uit deze studie blijkt dat constitutieve ionkanalen, aanwezig in vesicles, in contact worden gebracht met het extracellulaire milieu via het "kiss en linger" mechanisme.

Calcium-afhankelijke regulatie van TRPV5 en TRPV6

Elektrofysiologische karakterisatie van TRPV5 en TRPV6 heeft tevens aangetoond dat de activiteit sterk gereguleerd wordt door calcium. Zo heeft calcium wat via TRPV5 en TRPV6 de cel instroomt een sterk negatieve invloed op de activiteit van deze ionkanalen. Het achterliggende moleculaire mechanisme van de calcium-afhankelijke inactivatie is echter nog steeds niet bekend. De regulatie van de lokale calciumconcentratie bij beide kanalen bepaald dus mede de activiteit van de kanalen. Van een groot aantal andere ionkanalen is het bekend dat eiwit-eiwit associaties een belangrijke rol spelen bij de regulatie van de kanaalactiviteit. Uit onderzoek aan diverse ionkanalen is gebleken dat de calciumsensor calmoduline, wanneer geassocieerd met het ionkanaal, een belangrijke rol vervult in de regulatie van de activiteit. In

hoofdstuk 3 is de regulatie van TRPV5 en TRPV6 door calmoduline beschreven. Met behulp van calcium ongevoelige calmoduline mutanten, in verschillende binding en elektrofysiologische studies, is de rol van dit eiwit in de regulatie van TRPV5 en TRPV6 vastgesteld. Dit toonde aan dat regulatie door calmoduline beperkt is tot TRPV6 waar calmoduline functioneert als een calciumsensor die de activiteit van TRPV6 controleert.

Hoofdstuk 4 en 5 beschrijven het belangrijke aspect van regulatie van de lokale calciumconcentratie in de TRPV5 porie. Door de snelle opname van calcium uit de extracellulaire matrix kan calcium accumuleren in het TRPV5 porie domein. Deze ophoping van calcium heeft een negatieve invloed op de activiteit van TRPV5 wat blijkt uit de calcium-afhankelijke activiteit van dit kanaal. In een bindingsanalyse om nieuwe TRPV5-geassocieerde eiwitten te ontdekken bleek dat calbindine-D_{28K} aan TRPV5 bindt. Uit verdere analyses bleek dat, wanneer de intracellulaire calciumconcentratie verlaagt, calbindine-D_{28K} naar de plasma membraan transloceert en associeert met TRPV5. Eerdere studies met primaire niercelkweken, die calcium transporteren vanuit het apicale compartiment naar het basolaterale compartiment, hebben aangetoond dat de verwerking van intracellulair calcium tijdens transcellulair calciumtransport efficiënt is gereguleerd aangezien er geen duidelijke veranderingen in de intracellulaire calciumconcentratie waarneembaar waren. Co-expressie van een calcium ongevoelige calbindin-D_{28K} mutant, die nog wel met TRPV5 associeert, in deze primaire niercelkweken resulteerde in een dominant negatieve inhibitie van het transcellulaire calciumtransport over deze cellen. Deze resultaten tonen dus aan dat de TRPV5-calbindin-D_{28K} associatie van fysiologisch belang is voor transcellulair calciumtransport. Hoofdstuk 5 integreert al deze resultaten in een model voor transcellulair calciumtransport en beschrijft dat calbindine-D_{28K} door binding aan TRPV5 in staat is om lokaal de calciumconcentratie af te stemmen waardoor TRPV5 actief blijft. Wanneer het door TRPV5 instromende calcium aan calbindine-D_{28K} bindt zal calbindine-D_{28K} van TRPV5 dissociëren waardoor er onvoldoende calcium gebufferd wordt, hetgeen resulteert in inactivatie van TRPV5.

Nipsnap1

Hoofdstuk 6 beschrijft de identificatie van Nipsnap1 als nieuw TRPV5-geassocieerd eiwit en zijn rol in de regulatie van TRPV5 kanaalactiviteit. Ook Nipsnap1 kwam naar voren als partner in de bindingsanalyse om nieuwe TRPV5-geassocieerde eiwitten te ontdekken. Uit verdere analyse bleek dat Nipsnap1 binding aan TRPV5 onafhankelijk is van calcium en lokaliseert in de TRPV5 amino- en carboxylterminus. Co-expressie van Nipsnap1 met TRPV5 resulteerde in een drastische vermindering van TRPV5 activiteit. TRPV5-labeling experimenten aan het celoppervlak toonde aan dat NIPSNAP1 geen effect heeft op de

plasmamembraan lokalisatie van het kanaal. Deze studie beschrijft dus als eerste een fysiologische rol voor Nipsnap1 in de regulatie van TRPV5 kanaalactiviteit.

Rol van TRPV5 in het binnenoor

In de afgelopen jaren was het TRPV5 onderzoek met name gericht op de functie in nier en darm. Uit het in dit proefschrift beschreven onderzoek is gebleken dat TRPV5 ook voorkomt in het binnenoor. Iontransporterende cellen in ons lichaam hebben veel overeenkomsten in functie. Zo zijn iontransporterende cellen in nier en binnenoor vergelijkbaar, waardoor de hypothese ontstond dat TRPV5 mogelijk betrokken is in het gehoor. De resultaten in hoofdstuk 7 beschrijven dat TRPV5 inderdaad een rol vervult in het binnenoor. Lokalisatiestudies toonden aan dat TRPV5 tot expressie komt in Dieters cellen. Deiters cellen behoren tot de ondersteunende cellen in het binnenoor die bijdragen aan de structuur en het functioneren van het binnenoor. TRPV5 knockout muizen vertoonden tijdens diverse gehoor testen een verminderde gehoorfunctie vergeleken met muizen uit de controle groep. Deze studie beschrijft dus een nieuwe fysiologische functie voor het epitheliale calciumkanaal TRPV5 als onderdeel van het complexe mechanisme van geluidwaarneming. Welke functie TRPV5 nu vervult in Deiters ondersteunende cellen is nog echter nog niet duidelijk en zou door toekomstig onderzoek uitgezocht moeten worden.

De resultaten beschreven in dit proefschrift dragen bij aan een beter inzicht in de handhaving van de calciumbalans. Naast verder onderzoek naar de calciumafhankelijkheid van TRPV5 en TRPV6 zou toekomstig onderzoek uitsluitsel moeten geven over de factoren die een rol spelen bij de snelle regulatie van beide kanalen via "kiss and linger" mechanismen. Tevens zijn beide kanalen, zoals de resultaten beschreven in dit proefschrift aangeven, naast handhaving van de calciumbalans waarschijnlijk betrokken bij meerdere vitale processen in ons lichaam. Een grote wetenschappelijke uitdaging ligt in het ontrafelen van de functie van TRPV5 en TRPV6 in deze processen.

Dankwoord

(Acknowledgements)

Dankwoord

Nu dan het moment van dankbetuiging aan alle betrokkenen. Terugdenkend aan de afgelopen 4 jaar van proefjes doen, werkbesprekingen, artikelen schrijven en congres- en werkbezoeken in binnen en buitenland gaan mijn gedachten tevens uit naar minder publicabele zaken als borrels, diners, feestjes, reizen e.d. Zo terugdenkend wordt het al snel duidelijk dat dit alles niet op een enkel persoon is terug te voeren. Ik wil dan ook iedereen die op welke manier dan ook een steentje heeft bijgedragen bedanken. Zonder iemand te kort te doen wil ik toch een aantal personen met name noemen.

Allereerst mijn promotor, prof. dr. René Bindels. Beste René, bedankt voor het in mij gestelde vertrouwen, je inzet, de begeleiding en de ruimte die je me hebt gegeven om nieuwe wegen binnen de TRPV5 en TRPV6 fysiologie te verkennen. Hierbij aansluitend mijn co-promotor, dr. Joost Hoenderop. Joost, je kenmerkende en oneindige voorraad energie waren een uitstekend voorbeeld.

The scientific research presented in this thesis was made possible by international collaborations. In this respect I whish to thank the group of prof. dr. Bernd Nilius at Leuven university, Leuven Belgium, in particular drs. Frank Mahieu and dr. Thomas Voets for their contributions to this thesis. In addition, I am grateful to prof. dr. David Clapham and dr. Elena Oancea from Harvard university for their enthusiasm during my working visit to their lab. Furthermore, I thank prof. dr. Stefan Heller and dr. Eduardo Corralez from Stanford university for their participation and interest in the inner ear project.

Tevens wil ik Louis Hoofd bedanken voor zijn hulp bij het calbindine werk. Louis, ik heb enorm veel kunnen leren van je wiskundige kijk op de fysiologie. Door onze samenwerking ben ik van mening, met hoofstuk 5 als bewijs, dat bij het samenvoegen van jouw wiskundige kennis met onze kennis van celbiologie er prachtige modellen ontwikkeld kunnen worden waar bepaalde, voor conventionele methode, onbereikbare aspecten mee onderzocht kunnen worden.

Theo Peters, Jo Curfs en Andy Beynon van afdeling KNO en Ineke van der Zee van afdeling Celbiologie wil ik bedanken voor hun hulp bij de gehoorstudie beschreven in dit proefschrift. Mede door jullie inzet en inspiratie heb ik mijn onderzoeksveld kunnen uitbreiden met het binnenoor.

Of course I thank all colleagues from the Physiology department, including those that left, for their support both professionally and socially. If one would ask me to summarize the environment at the department words like enthusiastic, international and encouraging are particularly suited. In het bijzonder wil ik graag vernoemen Joost S., Catalin, en Arjen voor hun hulp aan de desbetreffende hoofdstukken. Nicole, Jimmy, Sabine en Theun voor hun enorme inzet als studenten. Theun, inmiddels ben je werkzaam op de afdeling als promovendus wat, denk ik, je enthousiasme onderstreept. Ik ben dan ook blij dat je mij wilt bijstaan als paranimf. Annemiete, gedurende mijn onderzoek, met name in de laatste periode, is jouw praktische ondersteuning enorm geweest. Ik ben dan ook blij dat je mij wilt ondersteunen als paranimf.

Vrienden en familie voor jullie deze paragraaf. Wat in dit boekje beschreven staat is dus wat ik daar aan die universiteit in Nijmegen uitvoerde. Pa en Ma, bedankt voor jullie jarenlange steun, hier ligt ie dan. Helaas zonder ex-libris maar wel met een boekenlegger. Ik hoop dat deze een mooi plekje krijgt in jullie collectie.

Tenslotte Kelly, jou bedanken met een zinnetje of pagina zou niet genoeg zijn, vanwaar voor jou deze kreet:

HET IS AF!

Tim

Curriculum vitae

&

List of Publications

Curriculum Vitae

Tim Lambers werd op 25 augustus 1978 geboren te Arnhem. Na het behalen van het eindexamen MAVO in 1995 te Wageningen vervolgde hij zijn studie aan de Middelbare Laboratorium Opleiding te Arnhem. Hier behaalde hij in 1999 het diploma Biologische Laboratoriumtechniek waarna hij aansluitend de Hogere Laboratorium Opleiding Biochemie aan de hogeschool Arnhem/Nijmegen volgde en hier in 2002 afstudeerde. Tijdens deze opleidingen werd stage gelopen op de afdeling Virologie van de Landbouw Universiteit Wageningen onder leiding van Dr. J. van Lent en Prof. Dr. R. Goldbach, RIZA te Lelystad onder leiding van Dr. A. Veen, en op de afdeling Celbiologie van UMC St Radboud onder leiding van Dr. M. Nelen en Prof. Dr. B. Wieringa. In augustus 2002 werd hij als junior onderzoeker aangesteld op de afdeling Fysiologie (UMC St Radboud) op een door NWO-ALW gefinancierd onderzoeksproject. Onder begeleiding van Dr. J. Hoenderop en Prof. Dr. R. Bindels verrichtte hij onderzoek dat beschreven is in dit proefschrift. Door het behalen van een Van Walree stipendium werd een werkbezoek mogelijk aan het laboratorium van Prof. Dr. D. Clapham (Children's Hospital and Harvard Medical School, Boston, USA) en werd door het behalen van een reisbeurs van de American Society for Cell Biology een congresbezoek (ASCB San Francisco, 2005) mogelijk. Tevens werden doctoraal- en HLO-studenten tijdens hun stage begeleid en leverde hij een bijdrage aan het onderwijs van internationale Master studenten aan de Laboratorium Opleiding in Nijmegen. Vanaf 1 september 2006 is hij werkzaam als Scientist bij NIZO food research binnen de afdeling Texture.

Publications related to this thesis

Lambers TT, Weidema AF, Nilius B, Hoenderop JG, Bindels RJ.
Regulation of the mouse epithelial Ca^{2+} channel TRPV6 by the Ca^{2+}-sensor calmodulin.
J Biol Chem. 279: 28855-61, 2004

Lambers TT, Bindels RJ, Hoenderop JG.
Coordinated control of renal Ca^{2+} handling.
Kidney Int. 69: 650-4, 2006

Lambers TT, Mahieu F, Oancea E, Hoofd L, de Lange F, Mensenkamp AR, Voets T, Nilius B, Clapham DE, Hoenderop JG, Bindels RJ.
Calbindin-D_{28K} dynamically controls TRPV5-mediated Ca^{2+} transport.
EMBO J. 25: 2978-88, 2006

Schoeber JP, Topala CN, Wang X, Diepens RJ, **Lambers TT**, Hoenderop JG, Bindels RJ.
RGS2 inhibits the epithelial Ca^{2+} channel TRPV6.
J Biol Chem. 281: 29669-74, 2006

Lambers TT, Oancea E, Hoenderop JG, Bindels RJ.
Extracellular pH dynamically controls cell surface delivery of functional TRPV5 channels.
Mol Cell Biol. 2006, in press

Lambers TT, Hoenderop JG, Bindels RJ, Hoofd L.
Modeling of transcellular Ca^{2+} transport in kidney reveals a fundamental role for calbindin-D_{28K}.
Submitted

Lambers TT, Schoeber JP, Topala CN, Hoenderop JG, Bindels RJ.
Identification of Nipsnap1 as a novel auxiliary protein controlling TRPV5 activity.
In preparation

Lambers TT, Peters TA, Beynon AJ, van der Kemp AW, Corralez E, van der Zee I, Heller S, Curfs JH, Hoenderop JG, Bindels RJ.
An essential role for the epithelial Ca^{2+} channel TRPV5 in sound perception.
In preparation